

Dhand, Aditya (2015). Design of electric vehicle propulsion system incorporating flywheel energy storage. (Unpublished Doctoral thesis, City University London)



**CITY UNIVERSITY
LONDON**

[City Research Online](#)

Original citation: Dhand, Aditya (2015). Design of electric vehicle propulsion system incorporating flywheel energy storage. (Unpublished Doctoral thesis, City University London)

Permanent City Research Online URL: <http://openaccess.city.ac.uk/13699/>

Copyright & reuse

City University London has developed City Research Online so that its users may access the research outputs of City University London's staff. Copyright © and Moral Rights for this paper are retained by the individual author(s) and/ or other copyright holders. All material in City Research Online is checked for eligibility for copyright before being made available in the live archive. URLs from City Research Online may be freely distributed and linked to from other web pages.

Versions of research

The version in City Research Online may differ from the final published version. Users are advised to check the Permanent City Research Online URL above for the status of the paper.

Enquiries

If you have any enquiries about any aspect of City Research Online, or if you wish to make contact with the author(s) of this paper, please email the team at publications@city.ac.uk.



**CITY UNIVERSITY
LONDON**

School of Engineering and Mathematical Sciences

**Design of electric vehicle propulsion system
incorporating flywheel energy storage**

PhD Thesis

Aditya Dhand

**Submitted to City University London in partial fulfilment of the requirements for the
degree of Doctor of Philosophy (PhD)**

May 2015

Abstract

Battery electric vehicles are crucial for moving towards a zero emission transport system. Though battery electric vehicle technology has been rapidly improving, it is still not competitive to the conventional vehicles in terms of both cost and performance. The limited driving range and high cost are significant impediments to the popularity of battery electric vehicles. The battery is the main element which affects the range and cost of the vehicle. The battery has to meet the requirements of sufficient power and energy, quick recharge, safety, low cost and sufficient life. However the battery can either provide high power or high energy but not both. Hybridisation of the energy source is one of the methods to improve the energy efficiency of the vehicle, which would involve combining a high energy battery with a high power source. High power batteries, ultracapacitors and high speed flywheels are the potential high power sources that could be used. Out of these, the high speed flywheel in combination with a mechanical transmission is an attractive high power source for the battery electric vehicle due to its favourable characteristics of high specific power, sufficient high specific energy, high energy efficiency, long cycle life, quick recharge and low cost . This thesis presents and critically assesses a concept of a mechanically connected flywheel assisted battery electric vehicle propulsion system for a modern passenger car application. The main contribution of this thesis is the analysis of the effect of utilizing a mechanically connected flywheel in a hybrid energy storage with Li-ion batteries on the energy efficiency of the electric vehicle.

The starting point of the research was to create a base electric vehicle model based on current technology. An analysis of the battery electric vehicle, its various components and control strategy and various approaches to model it was discussed which led to the creation of the baseline model. Simulations using the baseline model on three real world driving cycles representing urban, extra urban and motorway conditions, showed the potential for improving the energy efficiency of the vehicle by utilizing a power handling device that could transmit power directly to the driveline such as a mechanically connected flywheel. Hybridisation of the energy storage with the incorporation of the mechanically connected flywheel was presented. The flywheel was sized and a road data analysis was performed to support the sizing analysis. To accomplish the integration of the flywheel with the driveline, a fundamental analysis of the mechanical power split continuously variable transmission was conducted which showed various ways of obtaining the desired ratio range for the flywheel operation according to vehicle requirements. The speed ratio, power flow and efficiency were derived for three different types of transmissions. This analysis produced a simple methodology that can be applied to design a transmission for flywheel energy storage to provide any required speed ratio coverage and predict its efficiency in both directions of power flow, which is an important

contribution of the thesis. The hybrid vehicle layout was presented and all its components were discussed.

Further to obtain the maximum potential for improvement in energy consumption with the hybrid vehicle, optimisation of the energy management strategy was conducted. The optimisation problem was complex because of factors such as the small storage capacity of the flywheel, the kinematic constraints and the slipping of clutches. Dynamic programming was used to find optimal energy management strategy on the three real world driving cycles, which was the first instance of its implementation for such a powertrain; another important contribution of the thesis. The results were compared with baseline using a quasi static backward model. There was significant reduction in energy consumption for the more aggressive motorway cycle, less for the extra urban cycle, while there was a small increase in energy consumption for the relatively less aggressive urban cycle. However significant reduction in battery stress was observed for all the cycles which is expected to lead to improvements in battery life and lower operating costs. To provide a further step in implementation, a predictive energy management strategy was applied in the backward model for the hybrid vehicle based on dynamic programming with short computation time and utilizing limited future journey information which showed good performance in comparison to the benchmark simulation results. Finally the control was tested in a forward dynamic simulation to verify its suitability for real life implementation, and showed small deviation in performance compared to the backward simulation.

Acknowledgements

Firstly I would like to thank my supervisor Prof. Keith Pullen for giving me the opportunity to do research in flywheels and guiding me throughout the work. I would also like to thank City University London for awarding me the university doctoral studentship which enabled me to carry out the research without other distractions.

I am extremely grateful to my former colleague Baekhyun Cho, who inspired me to do the PhD in the first place. He gave me plenty of advice about the application process, what the PhD research is like and how to go about it. Throughout my research I had the chance of discussing my work with him and greatly benefited from his advice. I would like to thank Nirav Shah, another former colleague who patiently listened to me on the phone about the technical issues that I was facing during my research and gave valuable advice.

Many thanks also go to Chris Dunn and Alan Walker, former colleagues who provided me with the software tool to help me carry out my simulations.

I am very grateful to Matthew Read, Research fellow at City University London who finished his PhD in flywheels in 2010. Having the chance to discuss with him given his experience in flywheels and transmissions was invaluable.

Finally I would like to thank my lovely wife Otilia for her love and support throughout these years at the university.

Declaration

I confirm hereby to have elaborated this thesis independently under the usual support of the School and have used only the mentioned sources and aids.

I grant powers of discretion to the University Librarian to allow this thesis to be copied in whole or in part without further reference to me. This permission covers only single copies made for study purposes, subject to normal conditions of acknowledgement.

Table of Contents

Abstract.....	2
Acknowledgements.....	4
Declaration.....	5
List of Figures	9
List of Tables	12
Abbreviations.....	13
Nomenclature	15
1 Introduction	18
1.1 Background	18
1.2 Research Question	19
1.3 Objective of the research.....	19
1.4 Methodology.....	20
1.5 Outline of thesis.....	21
2 Literature Review and Background.....	23
2.1 History of BEVs.....	23
2.2 Current batteries for BEVs	24
2.3 Ultracapacitors.....	26
2.4 Flywheels.....	27
2.5 History of flywheels	27
2.6 Flywheels and their characteristics.....	47
2.6.1 Capacity.....	47
2.6.2 Material.....	49
2.6.3 Bearings.....	50
2.6.4 Windage losses.....	50
2.6.5 Safety and Containment	51
2.6.6 Gyroscopic loads	52
2.7 Transmissions.....	54
2.7.1 Hydrostatic transmissions.....	55
2.7.2 Electrical transmissions.....	55
2.7.3 Traction transmissions	57
2.7.4 Planetary gear set	59
2.7.5 Power split CVT	60
2.8 Research direction	60
3 Base Vehicle	62

3.1	Baseline vehicle.....	62
3.2	Battery.....	62
3.3	Battery modelling.....	66
3.4	Vehicle Model	67
3.5	Drive cycle simulation	72
3.6	Real world driving cycles.....	73
4	Hybrid vehicle	79
4.1	Flywheel in Battery Electric Vehicle	79
4.2	Road Data Analysis.....	82
4.3	Transmission Design	88
4.3.1	Kinematics of PSCVT.....	89
4.3.2	Configurations of PSCVT	91
4.3.3	Multi regime PSCVT.....	94
4.3.4	Requirements for FESS.....	95
4.3.5	Design of single regime PSCVT	96
4.3.6	Comparison of Power flow in both cases.....	100
4.3.7	Design of multi regime PSCVT without power recirculation	101
4.3.8	Design of two-regime PSCVT with negative power recirculation	105
4.3.9	Efficiency of PSCVT	108
4.3.10	Power Flow and Efficiency of different designs of PSCVT for the FESS	116
4.3.11	Torque and Speed through the Variator	120
4.3.12	Modelling of Transmission and Flywheel.....	121
4.4	Hybrid Vehicle Layout and Other Components	123
4.4.1	Control strategy	124
5	Benchmark of Energy Management Strategy.....	125
5.1	Dynamic Programming.....	125
5.2	Formulation of the Problem	126
5.3	Component models.....	127
5.3.1	Battery.....	127
5.3.2	Electric Machine.....	127
5.3.3	CVT and Flywheel.....	128
5.3.4	Driveshaft and Vehicle	128
5.4	Hybrid Vehicle Operation.....	129
5.5	Optimisation	130
5.6	Results and Discussion	134

6	Control of the Hybrid Vehicle	138
6.1	Energy Management Strategy	138
6.2	Predictive control for HV.....	139
6.3	DP based Energy management strategy.....	140
6.4	Simulation results	142
6.5	Forward Simulation.....	144
6.6	Simulation process and results	146
7	Conclusions	149
7.1	Summary and Findings.....	149
7.2	Novel Contributions	153
7.3	Assumptions and Limitations.....	153
7.4	Conclusions	154
7.5	Future Work.....	155
7.6	List of Publications	156
	References	158
8	Appendix	171
8.1	Variator only Design.....	171
8.2	Kinematics of dual mode PSCVT	173
8.3	Efficiency and power flow.....	174
8.4	Results and Comparison	175

List of Figures

Figure 1 Ragonne Plot for various ESS [20].....	27
Figure 2 Oerlikon bus [177].....	28
Figure 3 Gyreacta transmission [24]	29
Figure 4 Whitelaw concept [25].....	30
Figure 5 Kugler concept [26]	30
Figure 6 Locker concept [27].....	31
Figure 7 Electromechanical transmission [177]	33
Figure 8 GE concept [37].....	34
Figure 9 US postal service vehicle concept [39].....	34
Figure 10 Garrett FWB concept [41]	35
Figure 11 SAE J227a schedule D drive cycle [178]	36
Figure 12 DOE concept [46]	37
Figure 13 Battelle Columbus Laboratories concept [47]	38
Figure 14 Kumm concept [48].....	39
Figure 15 Garrett Concept [49]	40
Figure 16 Bales-McCoin Inc. concept [50]	41
Figure 17 Comparison of the four concepts [51]	41
Figure 18 Sussex system [54]	42
Figure 19 BMW concept [59]	44
Figure 20 Szumanowski concept [60]	45
Figure 21 Schaible concept [61].....	45
Figure 22 Lundin concept [179]	46
Figure 23 Schematic of angular momentum, angular velocity and precession rate [84].....	53
Figure 24 Schematic showing angle between angular momentum and precession rate vectors, and direction of reaction torque [84]	53
Figure 25 Vehicle axis system and vehicle manoeuvres [84].....	54
Figure 26 Hydrostatic transmission [88]	55
Figure 27 FWB Topologies [89]	57
Figure 28 Types of belt drives [92].....	58
Figure 29 Torotrak design [180].....	59
Figure 30 Schematic of planetary gear set [181]	60
Figure 31 Concept of PSCVT [88]	60
Figure 32 Schematic of BEV powertrain [4]	64
Figure 33 Ragonne plot for various cell chemistries [182]	64
Figure 34 Cell designs (cylindrical, prismatic and pouch) [94].....	65
Figure 35 Battery models (Rint, Thevnin and Dual polarisation) [99]	67
Figure 36 Forces acting on a vehicle [92].....	68
Figure 37 EM characteristics	69
Figure 38 Brake force	71
Figure 39 BEV model	71
Figure 40 Drive cycle comparison	73
Figure 41 RMS acceleration vs. RT battery efficiency	75
Figure 42 Powertrain efficiency	76
Figure 43 AU operating points	77
Figure 44 LA92 operating points	78

Figure 45 US06 operating points	78
Figure 46 Elevation data	82
Figure 47 Average speed distribution	84
Figure 48 Duration distribution	85
Figure 49 Distance distribution	85
Figure 50 Average speed vs. RMS acceleration	86
Figure 51 Average speed vs. RMS gradient.....	86
Figure 52 Ratio of peak to average power vs. Average power	87
Figure 53 Distribution of brake events	87
Figure 54 Maximum change in KE over 11 s vs. Average speed	88
Figure 55 Schematic of PGS (Arrows signify power. Power into the system is taken positive and out of the system as negative).....	90
Figure 56 Input Coupled and Output Coupled PSCVT systems.....	91
Figure 57 Different Power Regimes of PSCVT	92
Figure 58 Graph (a) shows the variation of variator ratio vs. PSCVT ratio. Graph (b) shows the variation of ratio of variator power to input power vs. PSCVT ratio	94
Figure 59 Different types of multi-regime PSCVT systems	95
Figure 60 Schematic of single regime PSCVT with additional gearing to achieve required operation limits.....	97
Figure 61 Ratio of variator power to input power vs. PSCVT ratio for positive and negative power recirculation.....	100
Figure 62 Two-Regime PSCVT without power recirculation	102
Figure 63 Three-Regime PSCVT System without power recirculation.....	103
Figure 64 Two-regime PSCVT system with power recirculation.....	107
Figure 65 PSCVT ratio vs. variator ratio for single, two-regime and three-regime systems.....	108
Figure 66 Power Flow in PGS	109
Figure 67 Cases of Power Flow in PGS of IC PSCVT and OC.....	110
Figure 68 Schematic of OC PSCVT without power recirculation.....	112
Figure 69 Schematic of IC PSCVT with positive power recirculation	113
Figure 70 Schematic of OC PSCVT with positive power recirculation.....	113
Figure 71 Graph (a) shows the ratio of variator power to input power vs. PSCVT ratio for the three systems in both directions. Graph (b) shows the efficiency vs. PSCVT ratio for the three systems in both directions	118
Figure 72 Efficiency vs. ratio with IC PSCVT or OC PSCVT as forward power flow	119
Figure 73 Efficiency vs. PSCVT ratio with IC taken as first or second stage	119
Figure 74 Different positions of variator	120
Figure 75 Schematic of the HV	123
Figure 76 DP process during the mode when vehicle is motoring and clutch A is engaged	131
Figure 77 Cycle charge consumption [Ah] for AU cycle for different initial flywheel SOE	132
Figure 78 Difference [%] cycle charge consumption between EM and flywheel vehicle launch	133
Figure 79 Vehicle speed [kph] and flywheel SOE [%] during drive cycle	134
Figure 80 Driveshaft torque [Nm] and EM torque [Nm] during drive cycles.....	135
Figure 81 Energy economy [Wh/km] for the drive cycles and difference [%] in energy economy between BEV and HV	136
Figure 82 Computation Time vs. Energy Consumption	141
Figure 83 Benchmark vs. DP EMS results for flywheel SOE	143

Figure 84 Benchmark vs. DP EMS results for EM Torque	144
Figure 85 HV model in AVL Cruise.....	145
Figure 86 Flywheel and Controller Model in Simulink.....	146
Figure 87 Forward vs. backward simulation for flywheel SOE.....	147
Figure 88 Forward vs. backward simulation for EM Torque.....	148
Figure 89 Variator only design	171
Figure 90 Dual mode PSCVT design	173
Figure 91 CVT ratio vs. Variator ratio for the two designs.....	176

List of Tables

Table 1 Shape factor for different geometries [72]	48
Table 2 Materials for flywheel [72].....	49
Table 3 Reaction torque sense depending on flywheel orientation [77]	54
Table 4 Base BEV parameters	68
Table 5 Results for homologation drive cycles	72
Table 6 Real world drive cycles results	74
Table 7 Average power results	74
Table 8 HV parameters	81
Table 9 Conditions for different power modes of PSCVT to occur	93
Table 10 Definitions of basic ratio of the PGS depending on branch connections.....	98
Table 11 Values of fixed gear ratios to achieve required PSCVT ratio limits in case of positive power recirculation.....	99
Table 12 Values of fixed gear ratios to achieve required PSCVT ratio limits in case of negative power recirculation.....	99
Table 13 Values of gear ratio factors to achieve required PSCVT ratio limits in case of three-regime system.....	105
Table 14 Values of fixed gear ratios to achieve required ratio limits for two-regime PSCVT with negative power recirculation.....	107
Table 15 Equations for three-regime IC PSCVT system	114
Table 16 Equations for three-regime OC PSCVT system.....	115
Table 17 Equations for two-regime IC PSCVT system with negative power recirculation	115
Table 18 Equations for two-regime OC PSCVT system with negative power recirculation.....	116
Table 19 Variator power for 0-100 kph operation.....	122
Table 20 Comparison between BEV and HV	137
Table 21 Computation Time.....	141
Table 22 Comparison between DP EMS and Benchmark	142
Table 23 Comparison between FWD and BWD simulation	146
Table 24 Power flow and Efficiency for the two designs.....	175

Abbreviations

AC	Alternating current
AT	Automatic transmission
AU	Artemis urban
BEV	Battery electric vehicle
BMS	Battery monitoring system
BWD	Backward
CVT	Continuously variable transmission
DC	Direct current
DLC	Double layer capacitor
DOE	Department of Energy
DP	Dynamic programming
EC	Equivalent circuit
EM	Electric machine
EMB	Electro-mechanical battery
EMS	Energy management strategy
ERDA	Energy Research and Development Administration
ESS	Energy storage system
EV	Electric vehicle
FESS	Flywheel energy storage system
FG	Fixed gear
FTP	Federal test procedure
FUDC	Federal urban drive cycle
FW	Flywheel
FWB	Flywheel battery
FWBEV	Flywheel battery electric vehicle
FWD	Forward
FWICEHV	Flywheel internal combustion engine hybrid vehicle
FWHV	Flywheel hybrid vehicle
GPS	Global positioning system
HES	Hybrid energy storage
HEV	Hybrid electric vehicle
HV	Hybrid vehicle
IC	Input coupled

ICE	Internal combustion engine
ICEV	Internal combustion engine vehicle
ISOA	Improved state of art
IVT	Infinitely variable transmission
JA1015	Japanese 10 15 cycle
KE	Kinetic energy
KERS	Kinetic energy recovery system
LDV	Light duty vehicle
LFP	Lithium iron phosphate
LMO	Lithium manganese spinel oxide
LTO	Lithium titanate oxide
MG	Motor generator
NCA	Lithium nickel cobalt aluminium
NEDC	New European drive cycle
NMC	Lithium nickel manganese cobalt oxide
NYCC	New York city cycle
OC	Output coupled
OCV	Open circuit voltage
PGS	Planetary gear set
PM	Permanent magnet
PMP	Pontryagin's minimum principle
PMSM	Permanent magnet synchronous machine
PSCVT	Power split continuously variable transmission
RC	Resistance capacitance
RMS	Root mean square
RT	Round trip
SOC	State of charge
SOE	State of energy
SUV	Sports utility vehicle
UDC	Urban drive cycle

Nomenclature

A_{rim}	Surface area of rim of the flywheel
A_s	Surface area of side of the flywheel
A_{veh}	Vehicle acceleration
$A_{r_{veh}}$	Frontal area
C_{bat}	Battery capacity
C_d	Coefficient of discharge
C_{rim}	Drag coefficient for flywheel rim
C_s	Drag coefficient for flywheel side
E_{cap}	Flywheel capacity
E_{FW}	Flywheel energy
E_{max}	Maximum flywheel energy
f_r	Rolling resistance
g	Acceleration due to gravity
G	Fixed gear ratio
H	Angular momentum
i_{bat}	Battery current
J	Inertia
J_{FW}	Flywheel inertia
k	Shape factor
K	Constant for PGS
m	Equivalent mass of vehicle
m_{FW}	Mass of flywheel
m_i	Mass of particle
n	Angular speed
P	Power
P_{aux}	Power of auxiliaries
P_{bat}	Battery power
P_{EM}	EM power
P_i	Input power
P_v	Variator power
r	PSCVT ratio
r_{CVT}	CVT ratio
r_{dyn}	Dynamic wheel radius

r_{FD}	Final drive ratio
r_{FW}	Flywheel radius
r_i	Distance of particle from centre of mass
r_{int}	Internal resistance
r_{max}	Maximum PSCVT ratio
r_{min}	Minimum PSCVT ratio
r_t	Ratio range PSCVT
R	PGS ratio
t	Time
Δt	Time step
T	Torque
T_a	Applied torque
T_{CVT}	CVT torque
T_{drs}	Driveshaft torque
T_{EM}	EM torque
T_{FW}	Flywheel torque
T_{loss}	Flywheel loss torque
T_r	Reaction torque
T_{whl}	Wheel torque
$T_{windage}$	Windage loss torque
V	Variator ratio
V_{bat}	Battery voltage
V_{max}	Maximum variator ratio
V_{min}	Minimum variator ratio
V_{OC}	Open circuit voltage
V_t	Variator ratio range
V_{veh}	Vehicle velocity
Ω	Precession
Θ	Angle between angular momentum and precession vectors
ω	Angular speed
ω_{EM}	Angular speed EM
ω_{FW}	Angular speed flywheel
ω_{max}	Maximum flywheel angular speed
ω_{min}	Minimum flywheel angular speed

η	Efficiency
η_{CVT}	Efficiency CVT
η_{EM}	Efficiency EM
η_{FD}	Efficiency final drive gear
σ_{max}	Tensile strength of material of flywheel
ρ	Density of flywheel material
ρ_g	Density of the environment of the flywheel
ρ_{air}	Density of air

1 Introduction

1.1 Background

The reduction and elimination of greenhouse emissions from transport systems is one of the keys to slowing and possibly reversing global warming. The ever increasing human population and rise of newly industrialized countries such as China and India has drastically increased the number of vehicles plying on roads. This has radically increased the need for more and more fuel efficient means of transport. The growing problem of greenhouse gas emissions led to the implementation of the Kyoto Protocol [1]. In Europe, average specific carbon dioxide emission from new passenger cars sold will be required to reach the 120 g/km target by 2012 and this level is to be reduced to 95 g by 2020 [2]. This increasingly strict legislation has put the car makers world-wide under pressure to develop more efficient vehicles.

In recent decades different vehicle technologies have emerged to tackle this problem. Alternate fuels, engine downsizing, fuel cell vehicles, hybrid electric vehicles (HEV) and electric vehicles (EV) are just some of the technologies being developed by various automotive organisations. Fuel cell vehicles still have major technical limitations that prevent them from being in production in the near future. Though powertrain technologies which feature the internal combustion engine (ICE), such as HEV have a great potential to be more fuel efficient than the conventional vehicles, they cannot achieve zero emissions. These still use carbon-based liquid fuels as their main source of energy. Due to their attractive energy density, these are unlikely to be replaced by alternatives such as hydrogen in the near future. Only EVs provide the possibility of truly achieving zero emission transport. Their greatest advantage is that they offer us fuel flexibility. They can be charged with electricity generated through renewable and clean sources, such that the “well to wheel” emissions are greatly reduced. Their biggest disadvantages are their high cost and insufficient driving range as compared to conventional vehicles.

EVs feature an energy storage system (ESS) and an electric machine (EM) along with the required power electronics. The EM in the electric vehicle is usually a motor generator (MG) and this feature along with energy storage give it the inherent capability to perform regenerative braking; a luxury that the conventional internal combustion engine vehicle (ICEV) does not have. The usual energy storage systems that can be used in EV are batteries, ultracapacitors and high speed flywheels, though typically batteries are the only ones used. The energy storage has to meet the requirements of sufficient energy and power, quick recharging, sufficient life, safety and low cost. Unfortunately none of the energy storage systems can satisfy all the requirements. The current energy storage has the biggest impact on

the high cost and low range of EV. One major source is the high initial cost of the battery plus the likely need for replacement once or twice during vehicle lifetime.

1.2 Research Question

The overall argument of the research is that by employing a hybrid energy storage system comprising of a high specific power storage and a high specific energy storage in an electric vehicle leads to improvement in energy efficiency of the vehicle in comparison when the electric vehicle employs a single energy storage. This can be divided into following research questions:

- What hybridisation strategies would be most suitable for the chosen battery electric vehicle application?
- What are the energy efficiency benefits that can be potentially achieved if a secondary energy storage was to be implemented in the battery electric vehicle?
- How to design and integrate the secondary energy storage?
- What is the minimum energy consumption that can be achieved for the hybrid energy storage on specific drive cycles?
- How to define an optimal energy management strategy for the hybrid energy storage?

1.3 Objective of the research

The overall aim of the research is to design and analyse at system level a hybrid energy storage system for an electrical vehicle powertrain for a modern passenger car application. It would also be referred as a hybrid vehicle (HV) since it has two sources of energy.

The main objectives which stem from the research questions are as follows:

- To investigate the hybridisation strategies of the ESS for EV.
- To analyse the performance of battery electric vehicles (BEV) in homologation cycles and real world cycles using a simulation model in order to investigate the potential for improvement in energy efficiency by using a secondary energy storage.
- To implement the hybridisation of the energy storage by defining the secondary energy storage, its integration to the drivetrain and to construct the complete hybrid vehicle model
- To investigate the maximum potential for improvement in energy consumption for the hybrid vehicle on drive cycles.
- To define an optimal control strategy that is practical to be implemented in real life for the HV in order to maximize the energy economy benefit.

1.4 Methodology

To answer the research questions and accomplish the above mentioned research objectives, the following methodology would be applied. The overall approach is to use longitudinal vehicle dynamics simulation to compare the performance of the base electric vehicle and the hybrid vehicle on specific drive cycles, which are pre determined. This is a widely used and trusted method of dividing the drive cycle into smaller time steps and calculating the characteristics of the vehicle at the end of each time step [107]. The method has two techniques namely forward and backward approach and both would be used as deemed suitable. The required input parameters for the BEV and HV models are planned to be obtained from open literature. In case of unavailability, suitable values would be assumed. The steps in the methodology would be as follows:

- A comprehensive literature review would be conducted to understand the history of BEV and the major current challenges and how these can be addressed by hybridisation. Different candidates for the secondary energy storage would be analysed and the most suitable would be selected. Further the previous research on the application of the selected secondary energy storage in BEV would be assessed to identify gaps in knowledge. Also detailed analysis of the characteristics of the chosen secondary storage would be performed. From this step a clear research direction would emerge.
- A forward longitudinal vehicle dynamics model of the BEV would be created in a suitable simulation environment. Firstly a suitable passenger car application would be taken for the BEV. Further different types of currently employed batteries, their characteristics and modelling techniques would be analysed. The electric machine characteristics, control strategy and other BEV components would be studied. From this analysis, a BEV model would result. Further this model would be used to perform simulations on homologation and carefully selected real world drive cycles. The results would then be analysed to show the potential improvement that can be achieved if a secondary energy storage which can provide power directly to the driveline, is implemented in the BEV.
- In this step the hybridisation of energy storage would be designed. The secondary energy storage would be sized using suitable technique and an analysis of real world road usage data would be performed to provide evidence that the secondary energy storage is adequately sized to perform its intended tasks. Further analysis to integrate the secondary storage into the BEV would be conducted and all other components of the HV would be discussed and implemented.

- An analysis would be conducted to obtain the optimal control trajectory and the minimum attainable energy consumption for the HV on real world drive cycles. This would provide a benchmark for the performance of the HV and provide directions to develop a real sub optimal controller. This analysis would be conducted via dynamic programming which is a powerful tool used to compute global optimal solution to non linear problems. For this purpose a backward quasi static discrete time step longitudinal simulation model of the HV and the base BEV would be created. Dynamic programming would then be applied on the HV model and the results would be compared with those computed using the backward base BEV model. Detailed analysis on the results would be conducted.
- Further a real sub optimal controller would be developed for the HV and the aim would be to get as close as possible to the benchmark simulation results. This controller would be first implemented on the backward HV model and the results compared to the benchmark simulation results. Finally to test the suitability of the control for real life implementation, a forward dynamic simulation model of the HV would be created and simulated on the previously used real world drive cycles. The results of the forward model would be compared with the backward model.

1.5 Outline of thesis

The thesis contains 7 chapters.

Chapter 2 presents a background regarding the history of BEV, their current main challenges, different energy storage systems and the concept of hybridisation of the energy storage. From this review the flywheel emerges as the most suitable candidate for the secondary energy storage in a BEV. Further It includes an extensive literature survey on the application of flywheels to BEV.. It includes a discussion on the main characteristics of flywheel energy storage technology and the related transmissions. From this discussion it is concluded that the flywheel is best used in a mechanical transmission.

Chapter 3 introduces the baseline BEV model and discusses the current batteries being used in EVs, touching on the important battery characteristics and their impact on the EV performance. Also discussed are various existing battery models which lead onto detail of the baseline vehicle model, its component models and the control strategy. Finally the simulation results of the baseline model on homologation cycles and real world driving cycles are presented which are analysed to show the potential improvement which can be achieved by utilizing a secondary storage which can transfer power directly to the vehicle driveline.

Chapter 4 introduces the HV. Firstly the main characteristics of the flywheel are defined supported by a real world road usage data analyses. This is followed by fundamental analysis of continuously variable transmissions for flywheel energy storage systems (FESS). A simple methodology is presented which can be used to design a transmission for flywheels to provide any required speed ratio coverage and predict its efficiency in both directions of power flow. Finally the layout and other components of the hybrid vehicle are presented.

Chapter 5 presents the energy saving potential of the HV using dynamic programming (DP). The optimal energy management strategy (EMS) defining the torque split between the EM and flywheel is obtained on three real world cycles representing urban, extra-urban and motorway conditions. The results of this benchmark simulation are compared with the baseline vehicle simulation and analysed.

Chapter 6 presents optimal EMS for the HV building on the results of the previous chapter. A novel strategy is developed using DP and limited future journey information with short computation time for the HV. This strategy is implemented in a quasi-static backward simulation and its results compared to the benchmark simulation. Finally to test the suitability of the controller for real life implementation, a forward dynamic simulation is performed using co-simulation and the results compared to the backward simulation.

Chapter 7 discusses the conclusion of the work and areas for further research.

2 Literature Review and Background

This chapter is structured as follows. Firstly a brief history of BEVs is presented including the current battery technology. From this section the need for hybridisation of energy storage arises and various options are presented to achieve the hybridisation. The flywheel is compared with other energy storage devices and deemed the most appropriate for this purpose. This is followed by a history of flywheels in ground transportation specifically focusing on FWBEV. Further the characteristics of flywheels and types of transmissions are discussed.

2.1 History of BEVs

The BEV has been there since the early days of the automobiles. The first EV was built in 1834 by Thomas Davenport which was a tricycle powered by non-rechargeable batteries. After the lead acid battery was invented by French physicist Gaston Planté in 1859, David Salomons built a rechargeable BEV in 1874. Gustave Trouvé built an electric tricycle which was exhibited at the 1881 international exhibition electricity in Paris. From around that time till the next 20 years BEV competed with the ICEV. In 1900 out of the total sales of automobiles in the US about 38% were EVs as compared to 22% ICEVs with the rest being steam powered vehicles. During that period there were a number of companies in Europe and US which were producing BEVs. The first commercial EV was produced by Electric Carriage and Wagon Company in the US. This vehicle which was called Morris and Salom's Electrobat, was operated as a taxi in New York City. It was powered by two 1.1 kW motors with a maximum speed of 32 kph and a 40 km range. In England there was the London Electric cab company which was started in 1897. In France Bouquet, Garcin and Schivre produced various types of EVs from 1899 to 1906.

The invention of regenerative braking by Frenchman M. A. Darracq on his 1897 car was one of the greatest developments of that time. It allowed the possibility to capture brake energy and charge the batteries. The first vehicle to cross the 100 kph speed was also an EV called "Jamais Contente". But as ICEVs improved in their performance the demand for EVs started dwindling as their cost was high and they had poor performance. In 1911, the electric starter was invented which added to the attractiveness of the ICEV. When Ford started to mass produce the model T, its price was significantly lower than any of the EV which triggered the beginning of the end. By 1930s the EV had almost disappeared from the scene.

The interest in EVs was revived post the 1973 oil crises. During that time a number of companies in various countries around the world started developing EVs. Towards the end of 1970s the oil prices fell and impetus was driven out of EV development. In 1990 the California air resources board ruled that by 1998 2% of all vehicles sold in California should be zero

emission vehicles. Though it was not realised it did push the development of EVs. In the mid-1990s the US government formed the partnership for a new generation of vehicles with the automakers whose main aim was to produce within 10 years a production prototype of a car with three times the fuel efficiency of the current cars of that time. This further drove development of new technologies including EVs. In the last decade or so global warming has been described as a major threat to the environment therefore stricter legislations to reduce carbon dioxide have been enacted around the world.

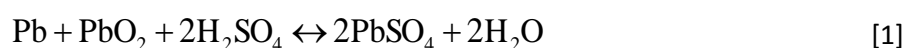
A number of companies around the world had developed EVs in the modern era but they were usually confined to being prototypes or were very small in number. GM built the EV1 in 1996 and produced it till 1999. Toyota built a series of EVs from the EV-10 to the EV40. Ford produced the Ecostar EV between 1992 and 1996. In 1996 PSA launched the 106 Electric which was an EV offered in a number of European countries. BMW launched the E1 in 1991 and E2 in 1992. Nissan produced the EV called FEV II which was powered by lithium ion batteries for the first time. Further details about the history of BEVs can be found in [3-4].

The introduction of production HEVs by Toyota in 1997 and subsequently by Honda in 1999 triggered a number of HEVs to be mass produced by other manufacturers in the 2000s. In the last few years, few production BEVs have entered the market including the Nissan Leaf, the Mitsubishi iMiEV and the Tesla Roadster and many more are in the pipeline. The major advantage of EVs, besides being zero emission vehicles is that they offer fuel flexibility. However their high cost and limited range, relative to ICEVs, are still issues that impede their popularity [5].

2.2 Current batteries for BEVs

At present the most viable batteries for BEVs include the following:

1. Lead-acid batteries: These batteries are the oldest type of rechargeable batteries existing from as far back as the 1800s. Lead-acid batteries consist of spongy lead as the negative cathode, lead dioxide as the positive anode and diluted sulphuric acid as the electrolyte. The cell reaction is shown by the equation 1. During discharging process, lead sulphate is formed at both the electrodes and during charging lead and lead dioxide are reformed. During the overcharge process there is production of hydrogen at the positive electrode, due to which the Lead-acid batteries suffer from water loss. This problem can be reduced by adding distilled water. The valve regulated batteries are maintenance free where the valves allow recombination of hydrogen and oxygen.



Lead-acid batteries are low cost which make them attractive for various applications which are cost sensitive. They were the predominant batteries used for BEVs in the 1970s and 1980s, however their limited specific energy makes them unsuitable for modern long range BEVs. In addition to their limited energy, their cycle life is also limited which would warrant a change in batteries every 2-3 years. Lead-acid batteries commonly have specific energy of about 35 Wh/kg, specific power of about 150 W/kg and cycle life of around 700.

2. Ni-MH batteries: Ni-MH batteries have been popular since 1990s and have been the choice in many HEVs and BEVs since it has relatively high cycle life and specific energy. It uses metal hydride for the negative electrode, nickel oxyhydroxide for the positive electrode and potassium hydroxide solution for the electrolyte. The metal hydride is generally of a rare-earth alloy. There are currently two types of metal alloys being used. They are based on lanthanum nickel, known as an AB₅ alloy, or alloys consisting of titanium and zirconium, known as an AB₂ alloy. During discharging, metal hydride in the negative electrode is oxidized to form metal alloy, and nickel oxyhydroxide in the positive electrode is reduced to nickel hydroxide. The reverse happens during the charging process. The chemical reaction of the battery is shown in the equation 2.



Ni-MH batteries commonly have specific energy of about 70 Wh/kg, specific power of more than 200 W/kg and cycle life of around 1500. The main drawback is their higher cost.

3. Li-Ion batteries: Li-Ion batteries were first announced in 1991 and are considered one of the most promising technologies for BEVs and HEVs. It utilizes lithiated carbon for the negative electrode, lithiated transition metal oxide for the positive electrode and liquid organic solution for the electrolyte. During the discharge process, lithium ions are extracted from the negative electrode and inserted to the positive electrode and the opposite reaction takes place during the charging process. These ions are swinging through the electrolyte between the negative and positive electrodes during the charging and discharging processes, and consequently no metallic lithium will be deposited. The electrochemical reaction is shown below in equation 3.



Their specific energy at around 130 Wh/kg is almost double than that of Ni-MH batteries but they suffer from higher cost. They have typically high specific power of around 250 W/kg and their cycle life is around 1200 which is lower. These are the batteries of choice for current production BEVs. Further details about batteries can be found in [3-4, 6-9].

At present the most important bottleneck in BEVs is the battery itself, which strongly affects the range and cost of the BEV. The batteries offer either high specific power or high specific energy but not both. To provide the BEVs with the characteristic to compete with ICEVs it is beneficial to hybridise the energy storage [10]. The typical strategy would be to combine a high energy battery with another high power source. This would shield the battery from peak currents and improve its capacity and life. The thermal requirements of the battery will also be reduced. A high power battery can be used as a secondary storage device. In this case the battery would suffer from multiple energy conversions during absorbing and release of regenerative energy. Torotrak reports that the round trip efficiency in this case would be around 35% [11]. Besides of using a high power battery as the secondary storage in BEV, the other serious contenders are ultracapacitors and high speed flywheels. The concept of hybridisation is discussed in [12].

2.3 Ultracapacitors

Double layer capacitor (DLC) technology is the major approach to achieve the goals of ultracapacitor. The charge carriers of the electrolyte solution get absorbed at the entire surface of the electrodes when a voltage is applied across the electrodes and form the dielectric of the double-layer capacitor. The electrode material is generally based on activated carbon, structured polymers or noble-metal oxides and the electrolyte solution can be either aqueous or organic.

These have high specific power, high cycle life and are suitable for fast and deep discharges. Its specific energy is quite low and is in the order of a few watt hours per kilogram. Due to this fact it cannot be used as the sole energy source in EVs. However since its specific power can reach 2000 W/kg, which is higher than any battery, it can be a good choice for secondary storage in a hybrid combination with batteries. However its high cost is a major deterrent and like batteries it suffers from the principle of energy conversion during capture and release of regenerative braking energy. A number of authors have discussed the combination of batteries and ultracapacitors [13-19].

2.4 Flywheels

Flywheels have been used to store energy since many years. High speed flywheels have the characteristics of high specific power, adequately high specific energy, long cycle life, high energy efficiency, quick recharge, low cost and environmental friendliness. They do not suffer from temperature dependence and their state of energy (SOE) is most easily determined. One of the common approaches is to couple them with a MG which is termed as a flywheel battery (FWB). The Ragonne plot in Fig. 1 shows the comparison of flywheels with other energy storage devices [20]. Their attractive properties make them an excellent secondary storage device to be used in BEVs. Though the usual application of flywheel in a BEV would incorporate a high speed flywheel coupled with a transmission to the driveline, some authors have suggested using the dead weight of the battery in a flywheel [21-22], though it would be highly impractical.

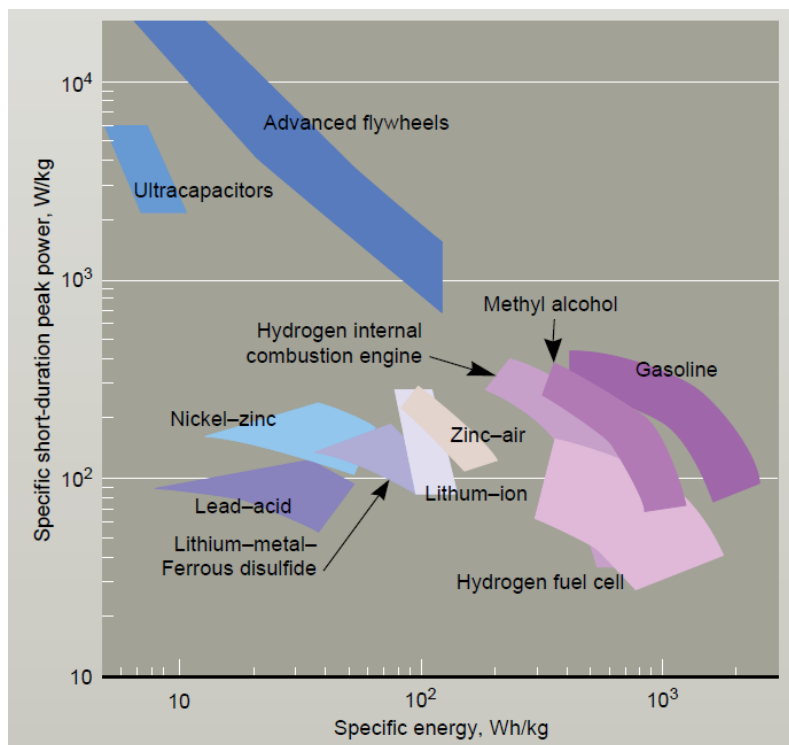


Figure 1 Ragone Plot for various ESS [20]

2.5 History of flywheels

Flywheels have been used in vehicular applications for many years. One of the first major applications was their use in the so called Gyrobus by Oerlikon in Switzerland in the 1950s [23]. Fig. 2 shows the bus. This was a specially designed 35 seater bus which used a 1500 kg, 1.6 m diameter and 32 MJ flywheel as the sole energy source. The bus had three phase overhead contacts which would be charged at the recharging stations placed along the route using 360 V, 50 Hz AC supply. The squirrel cage induction motor attached to the flywheel would spin the

flywheel up to 3000 rpm giving the flywheel enough energy to power the bus for an average distance of 1.2 km till it reached the next charging station. The power was extracted from the flywheel using capacitive excitation by using the motor-generator. This power was then fed to induction type traction motor. During braking the kinetic energy (KE) could be recuperated back to the flywheel through a complex operation by the driver. This bus ran in cities in Europe and Africa for 16 years before it was discontinued in 1969. Few of the drawbacks of this bus included its incapability to be used on gradients, complex operation required by the driver and the fact that it had to be charged frequently.

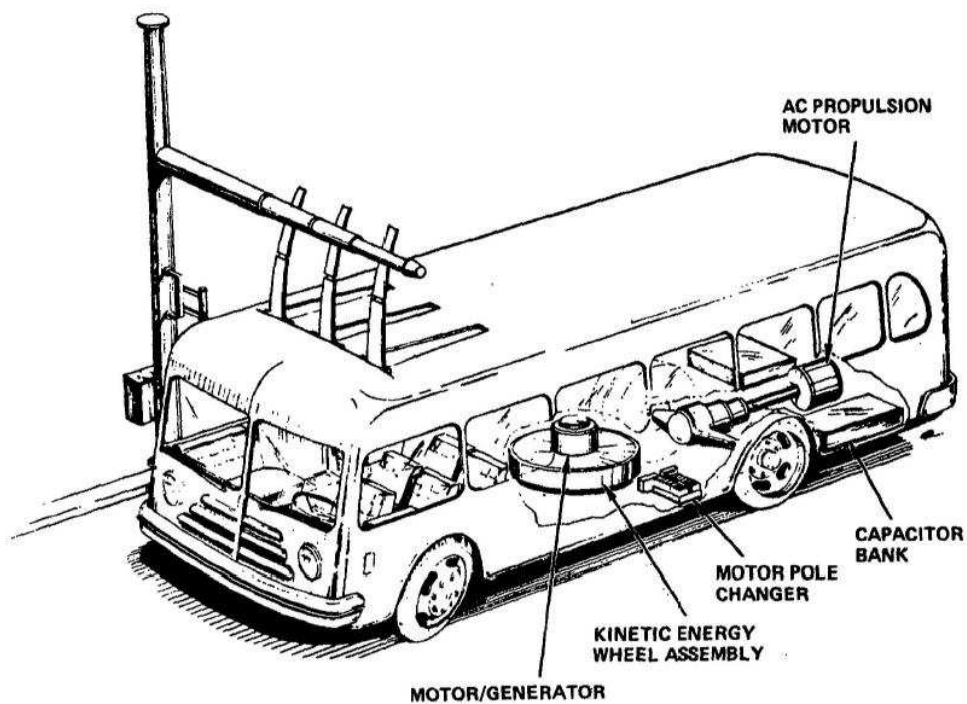


Figure 2 Oerlikon bus [177]

Another of the earlier works on utilization of flywheels in road applications was the Gyreacta and Hydreacta transmissions developed by Clerk [24] in England to be used in a bus and car application respectively. It consisted of a hybrid drive using flywheel and an ICE. The transmission consisted of differentiating and integrating epicyclic gear sets to connect the steel flywheel to the wheels. Fig. 3 shows the transmission. It used the planetary gear set (PGS) as a two degree of freedom device. There were multiple PGSs which were actuated via a clutch. The Hydreacta was a hydromechanical transmission which combined the Gyreacta with parallel geared idling and hydrokinetic datum coupling into the primary epicyclics. In Gyreacta transmission there were stepped datum shifts and there was flywheel speed loss for each shift. The hydro-mechanical transmission was inefficient but smooth whereas the pure mechanical was efficient but stepped. The system was complex and costly though it was the first of its kind.

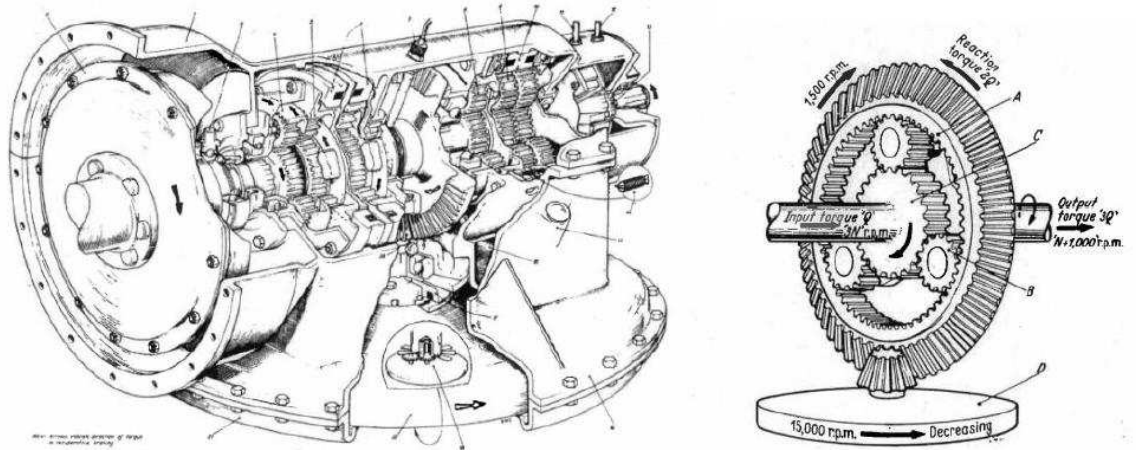


Figure 3 Gyreacta transmission [24]

The further examples will concentrate exclusively on FWBEVs or similar applications.

Whitelaw proposed probably one of the early concepts of a FWBEV [25]. According to the author the case for local duty vehicle (LDV) was strong as most journeys in cities of US were less than 50 miles. The LDV would have an energy storage system, a range of 50 miles and maximum speed 50 mph. Since the BEV was very heavy and the ICEV would burn fuel, a flywheel electric LDV was proposed. A FWB with batteries and DC motor propulsion is shown in Fig. 4. The energy removal rate from FWB would be uniform while the batteries will provide for non-uniform power surges. FWB would be charged at home. The FWB would provide average power and batteries would provide peak power. The author says such a vehicle is possible with current technology. This is a rather unique case as the usual application of flywheel in BEV consists of the flywheel providing the power surges.

Kugler proposed a system in which the flywheel was integrated to reduce peak current in lead acid battery of BEV [26]. Fig. 5 shows the schematic. The goal was to provide an efficient powertrain for lead acid BEV to have the performance to co-exist with ICEVs safely on public roads. The flywheel was coupled to a continuous running electric motor which was designed for efficient operation in a narrow speed range. Once started the motor ran continuously even when the EV was stopped and during these phases it charged the flywheel which acted as a load leveller. The benefits were high power output, mechanical regenerative braking, extended battery life and avoidance of expensive motor controllers. The flywheel rotated at moderate speeds from 5000 to 10000 rpm and the transmission was hydromechanical, which was popular due to its commercial availability. The author mentions that if such a FWBEV is not required to undergo a number of closely spaced consecutive accelerations it would be able to compete with ICEV on performance basis.

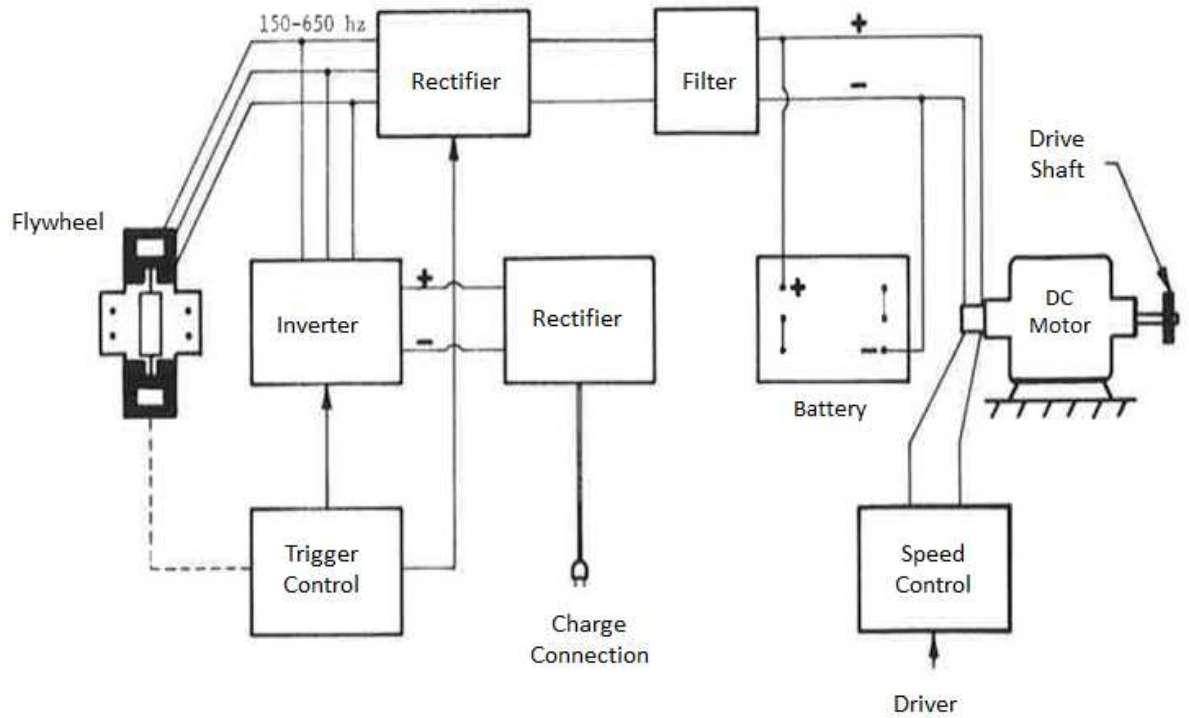


Figure 4 Whitelaw concept [25]

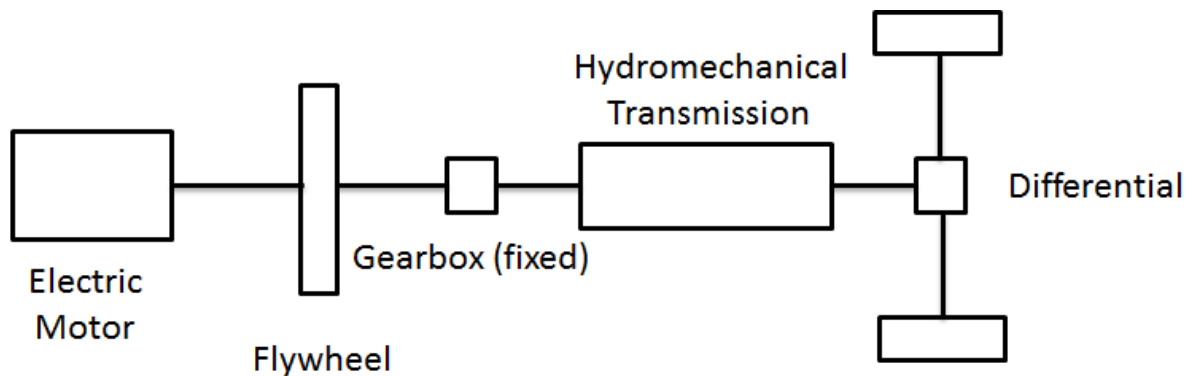


Figure 5 Kugler concept [26]

Locker and Miller [27] developed a FWBEV at the Scientific Research Foundation in Jerusalem. The schematic of the vehicle, which would be an intra-city van or mini bus, is shown in Fig. 6. The flywheel supplies power for acceleration and regeneration and the lead acid battery and electric motor provide average power. Like the Kugler system [26] the FWBEV uses hydromechanical transmission. The author mentions that the hydromechanical CVT is efficient only in a narrow range and thus to improve efficiency the system uses a two regime operation. The maximum speed of the flywheel is 7200 rpm. The control strategy is explained. The principle of the constant total KE of the vehicle and flywheel is used and the battery makes up the losses. However this system has the disadvantage of history dependence and it does not

take into account the other loads on the battery. To overcome this, a delay is introduced in the total KE control principle as long as the battery can provide for all other loads and then the KE of the flywheel would be changed. Vehicle speed is not varied by controlling voltage or current but by varying the transmission ratio depending on the difference between the demanded and actual power. Since the transmission is torque limiting the achievable regeneration has a limit. It mentions that the driver could select the city mode and the maximum flywheel speed would be reduced.

This specific layout of the FWBEV employed in the previous two cases where the flywheel and EM are coupled together upstream of the CVT, gives the possibility that the vehicle could be solely controlled by controlling the CVT, when using certain types of electric machines and no separate machine control is needed [41]. The disadvantage is that the power has to pass through the CVT all the time, which might not be desirable at lower efficiency points. Another is that the flywheel and EM speeds are always coupled together due to which the flywheel cannot be independently controlled.

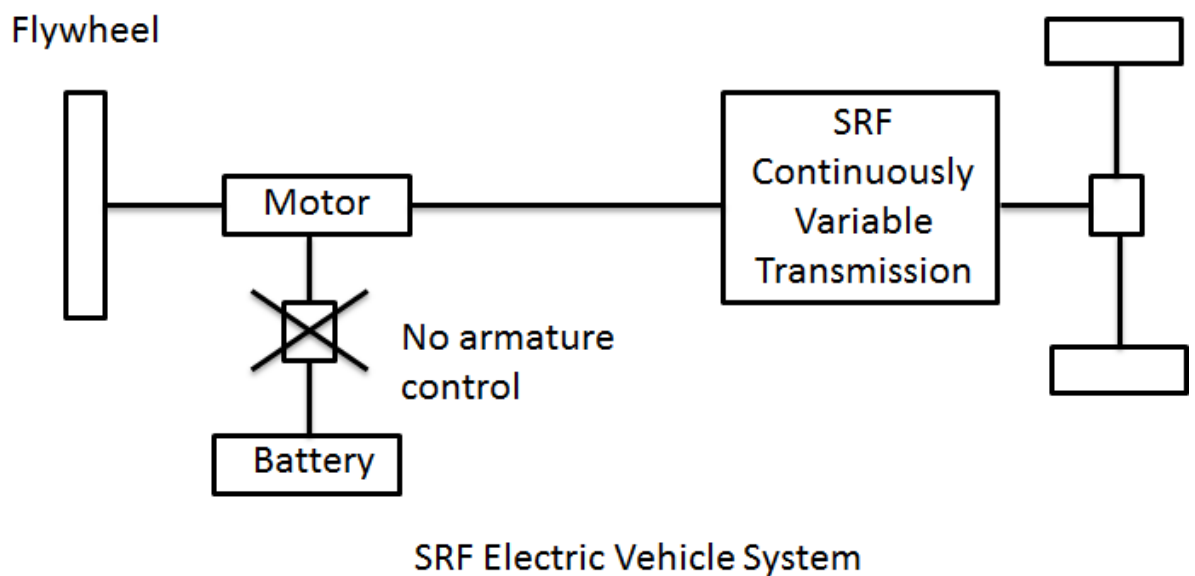


Figure 6 Locker concept [27]

In 1977 Schwarz presented a comparison of three design approaches for BEV – series motor with chopper controller, separately excited motor with field control and FWBEV with v-belt CVT [28]. The range achieved on the SAE J227 a D cycle was highest for the FWBEV but none of the options were able to meet the US Department of Energy (DOE) goals. There is not much information given in the paper.

In 1975 post the 1973 oil crises, DOE (which was the Energy Research and Development Administration (ERDA) at that time) organised the first flywheel technology symposium and

declared its intention to develop flywheel technology [29]. This was after the Rockwell International Corporation conducted a technical and economic feasibility study of the flywheel as an ESS for utilities, transportation, and industry under DOE sponsorship. The findings were presented at the symposium [30]. It was concluded that advanced composite FESS can extend hybrid and all electric transportation application to smaller vehicles. A FWB could also be developed in the near term to be used in a BEV.

In 1976 the US congress enacted the Electric and Hybrid Vehicle Research, Development, and Demonstration Act which authorized a Federal program of research and development to promote electric and hybrid vehicle technologies. From 1976 to 1983 DOE and other federal agencies in the US sponsored many projects related to flywheels which are described below.

In 1976, a patent was filed by Garrett Corporation describing an electromechanical transmission for a FWBEV with lead acid batteries [31]. The project was DOE sponsored and was to contribute to the development of a near term EV [32]. The schematic of the system is shown in the Fig. 7. The flywheel is connected to the sun gear of a PGS and the MG1 is connected to its ring gear. The carrier is connected to the drive shaft on which MG2 is mounted either directly or with suitable gearing. During the acceleration period the flywheel provides power to the vehicle through the direct mechanical link and the MG1 acts as a generator and controls the speed of the flywheel. The MG2 acts as a motor. During Cruise period the MG1 acts as motor to charge the flywheel and the MG2 powers the vehicle. During deceleration part of the vehicle energy directly charges the flywheel and the rest is transferred to the flywheel via the MG1-MG2 circuit. Here the MG1 acts as the motor and MG2 as the generator. The controller modulated the MG1-MG2 circuit to maintain an essentially constant armature current differential between MG1 and MG2 which resulted in almost uniform battery current discharge rates [33]. Another variation of this particular transmission is the MG2 directly on the same shaft as the flywheel which is shown in few patents [34-35]. Stavropoulou (1981) developed a computer model of a similar powertrain for an electric bus [36].

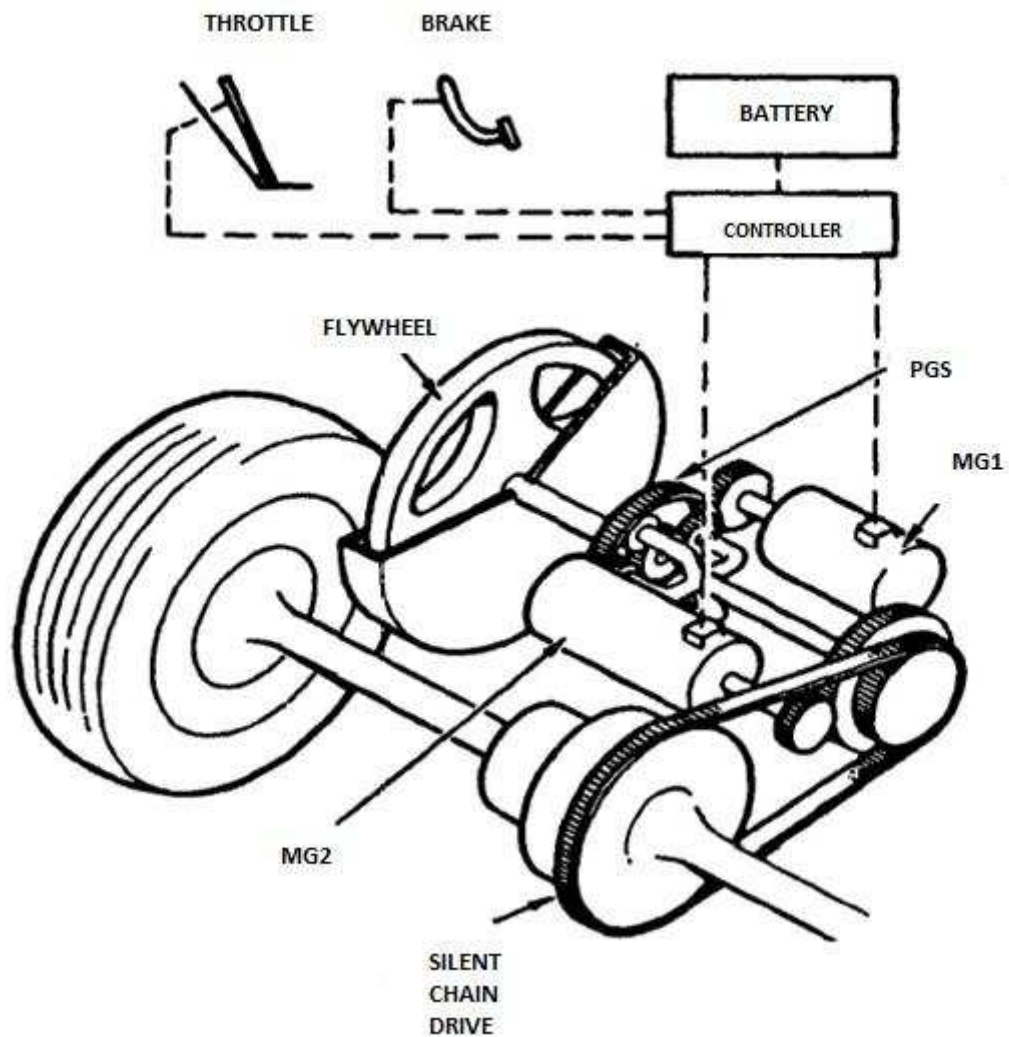


Figure 7 Electromechanical transmission [177]

In 1976 Lustenader et al. from GE introduced the FWB to be used as a load levelling device for a BEV [37]. The concept was first proposed by GE to DOE in 1974 and later GE was contracted to develop the system. Fig. 8 shows the schematic of the proposed vehicle. The steel Flywheel and AC inductor type motor alternator was to be used as a single unit. The FWB was connected electrically to a bidirectional solid state inverter/rectifier. The DC motor is separately excited. Various modes of operation were considered and the load levelling mode in which the FWB would be charged by the battery during idling periods was chosen. During evaluation of the system it was apparent that it suffered from many drawbacks. The performance of the system was highly dependent on the drive cycle and was reduced when operated on low maximum speeds and low stop frequency cycles. This was due to the fact that the vehicle's KE was less and the parasitic losses in the system were high. It was concluded that the system was not suitable for practical implementation and improvements were required [38].

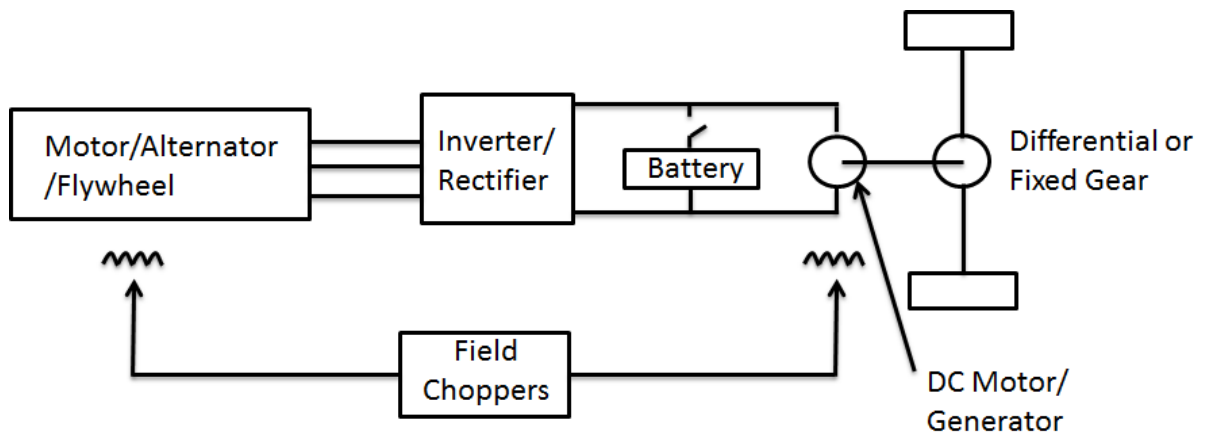


Figure 8 GE concept [37]

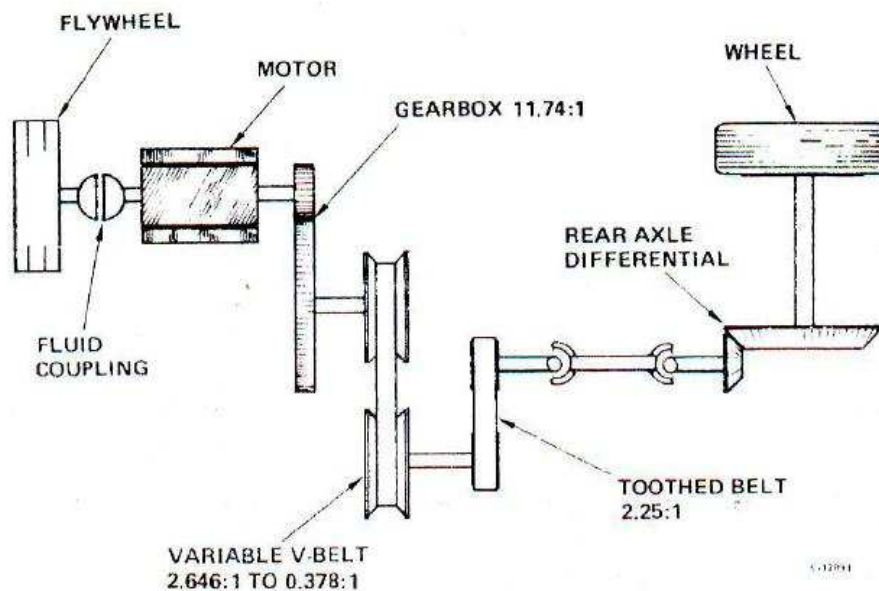


Figure 9 US postal service vehicle concept [39]

The US postal service and DOE jointly developed a flywheel battery electric postal jeep to improve range, stop-start capability and acceleration performance of existing electric postal vehicles [39]. Fig. 9 shows the schematic. The flywheel assists the electric motor in powering the vehicle thereby reducing the peak current on the lead acid batteries. The flywheel is used to power the vehicle from 7 mph to 33 mph, which was its top speed, via the variable v-belt drive. The flywheel was 0.5 MJ, multiple disc type with a top speed of 36000 rpm. The flywheel was able to substantially improve the acceleration (0-30 mph in 12 s) and gradeability (10% @ 20 mph) as compared to the base vehicle's acceleration (0- 30 mph in 24 s) and gradeability (10% @ 14 mph). The drawback of this arrangement was that the vehicle still had to be launched using EM.

Garrett Corporation was also involved in developing a FWB for vehicular use under a DOE contract [40]. The goal of the project was to find out the benefits of a light-weight, hermetically-sealed energy storage unit for vehicular applications. Fig. 10 shows the schematic. The composite flywheel had a speed range from 21000 - 42000 rpm. The MG was a squirrel cage induction type. The peak power was 45 KW and the energy capacity was 250 Wh [41]. The FWB was designed and partially evaluated before the project was discontinued due to electric machine failures and lack of funding [42].

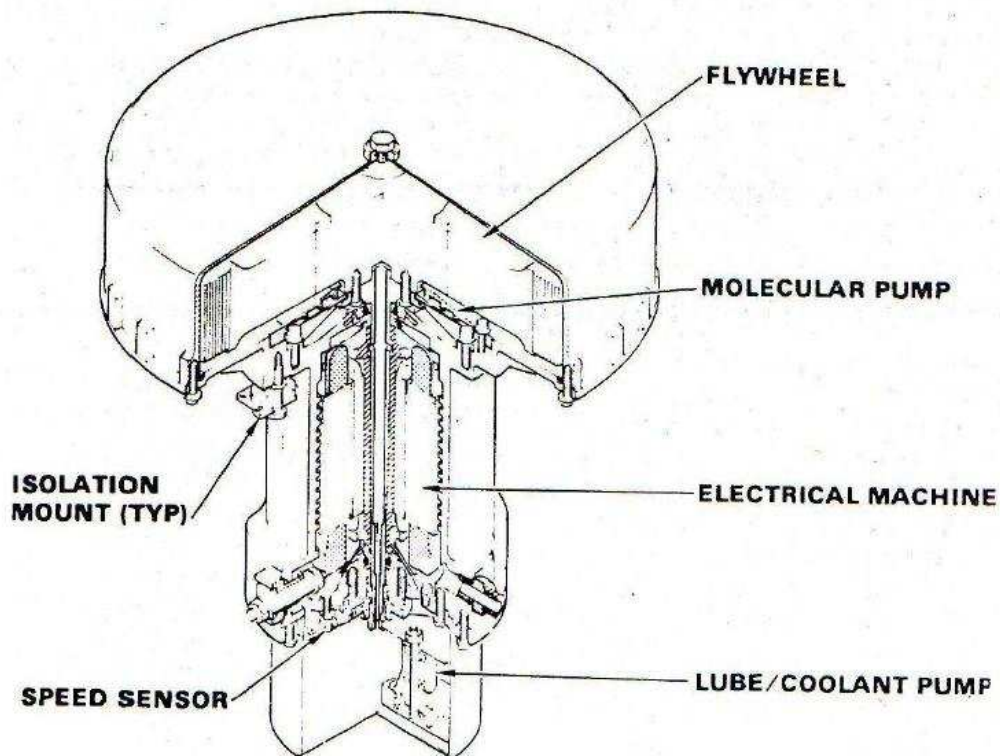


Figure 10 Garrett FWB concept [41]

In 1979 Raynard and Forbes conducted a study on advanced electric propulsion system concept for EV [43]. In this study 17 EV propulsion concepts were evaluated. The systems included basic systems with and without transmissions and with and without flywheels. The evaluation was done through simulation on the SAE J227a schedule D drive cycle (Fig. 11) and considered improved state of the art (ISOA) lead acid and Ni-Zn batteries. For the cases with a flywheel a simple energy management was followed of keeping the total KE constant. Study showed that for driving range of 161 Km on successive SAE J227a schedule D drive cycles, the system with the flywheel would achieve the range with the lowest battery weight. Out of the 17 concepts two were selected for conceptual design. One of the two selected was a flywheel assisted design coupled with double cavity toroidal regenerative CVT.

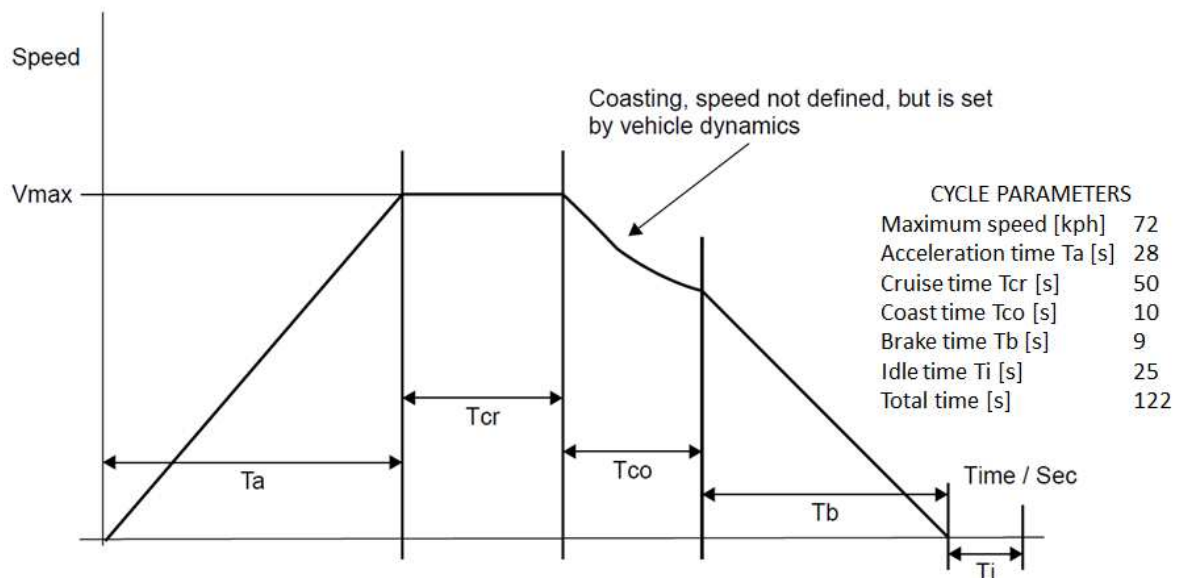


Figure 11 SAE J227a schedule D drive cycle [178]

In 1979 Younger and Lackner conducted a study of advanced electric propulsion systems concept using flywheel for EV [44]. In the study 28 systems were analysed, all incorporating FESS and comparison without FESS was not evaluated. These included different types of components and arrangements and included DC/AC motors with or without multispeed transmissions. They could be grouped in 4 types and included both mechanical and electrical transmissions for the flywheel. Like in the previous study the targeted range was 161 km on the SAE J227a schedule D drive cycle. The batteries considered were mainly ISOA lead acid and some evaluation was carried out on Ni-Zn batteries. It also included an assessment of the technical advancements necessary to achieve the selected drivetrains. Various strategies of dividing power between battery and flywheel during acceleration and deceleration were studied. For the conceptual design stage two of the many analysed designs were selected. These were the AC induction motor with FWB and DC motor with Flywheel/CVT. The two conceptual designs could meet range and performance goals but not the energy consumption targets with lead acid batteries. From the evaluation the greatest technical developmental risk was for the CVT.

In 1979 Schwartz conducted a study to determine the effect of applying flywheels to EVs using advanced batteries [45]. When used with flywheels, the batteries are to have maximized specific energies at the expense of high power capability for optimal performance. The characteristics of FWBEVs are compared to BEVs having the same range and peak-power capability. Different combinations of vehicle power and range are considered and as in the previous studies an SAE J227a schedule D drive cycle is used. Lead/acid, Ni/Fe, Ni/Zn, $ZnCl_2$, $LiAl/FeS_2$, Na/S (cer), and Na/S (glass) are the batteries that have been considered. It

concluded that as the performance requirements of EVs increase the flywheels will be more effective in improving the vehicle's range.

In 1980 as part of the DOE's electric and hybrid vehicle development program 4 CVT concepts were evaluated by various sub-contractors for the flywheel application in EVs [46]. The basic schematic of the vehicle is shown in Fig. 12. The intended application was a 1700 kg vehicle with the flywheel speed varying from 14000 to 28000 rpm and CVT output speed from 0 to 5000 rpm. There was an option to have the minimum CVT output speed as 850 rpm with a slipping clutch to be used at the output in order to attain zero speed. The usual requirements of high efficiency, low cost and weight, high reliability, maintainability, ease of control and low noise were applicable. In this specific layout where the CVT is only linked to the flywheel and the EM is either directly linked on the drive shaft or via some fixed gearing, has the advantage that the flywheel can be independently controlled and it can be integrated easily on an existing system, however the EM needs to be controlled separately.

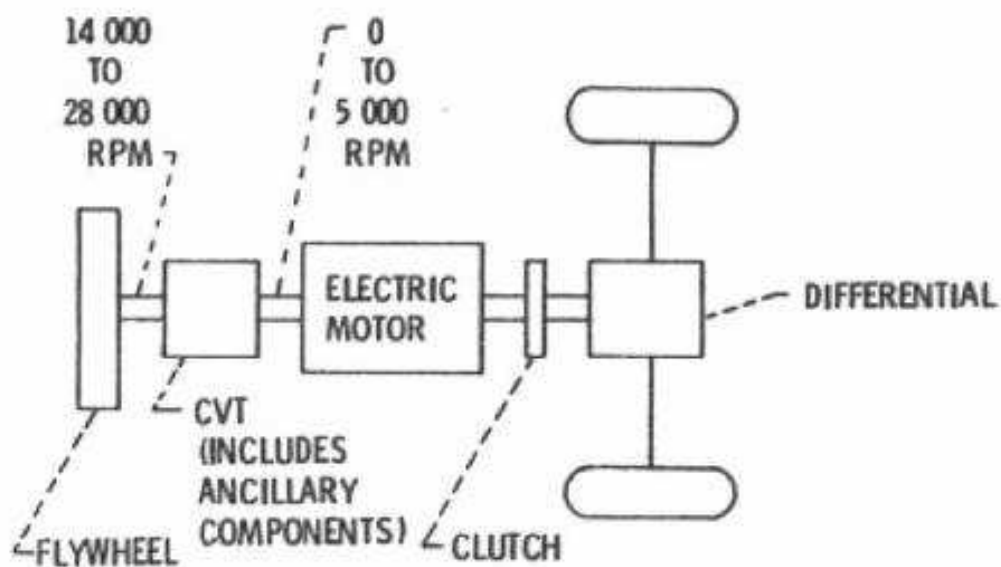


Figure 12 DOE concept [46]

The first of the designs studied was a steel v-belt CVT for the EV by Battelle Columbus Laboratories [47]. The Fig. 13 shows the schematic. The CVT included two steel v-belt elements in series with the necessary clutch and gears. The modulating clutch is used to produce the zero speed requirement on the output. The design of the CVT and the control is described. The belt is composed of a stack of solid cross-struts held together by a set of thin steel bands. It is a compression belt in which the v shaped driver pulley pushes rather than pulls the driven pulley. Since there is sliding movement between the bands over each other and over the struts when the belt moves proper lubrication is necessary. An electrohydraulic control system

controls the belt shifting and regulates the axial clamping force between the pulleys. The vehicle operating modes are described including the start-up, normal operation and shutdown. It is suggested that vehicle controller would provide the driver with some way to set a nominal set point for the flywheel speed depending on the upcoming road conditions and the driving style.

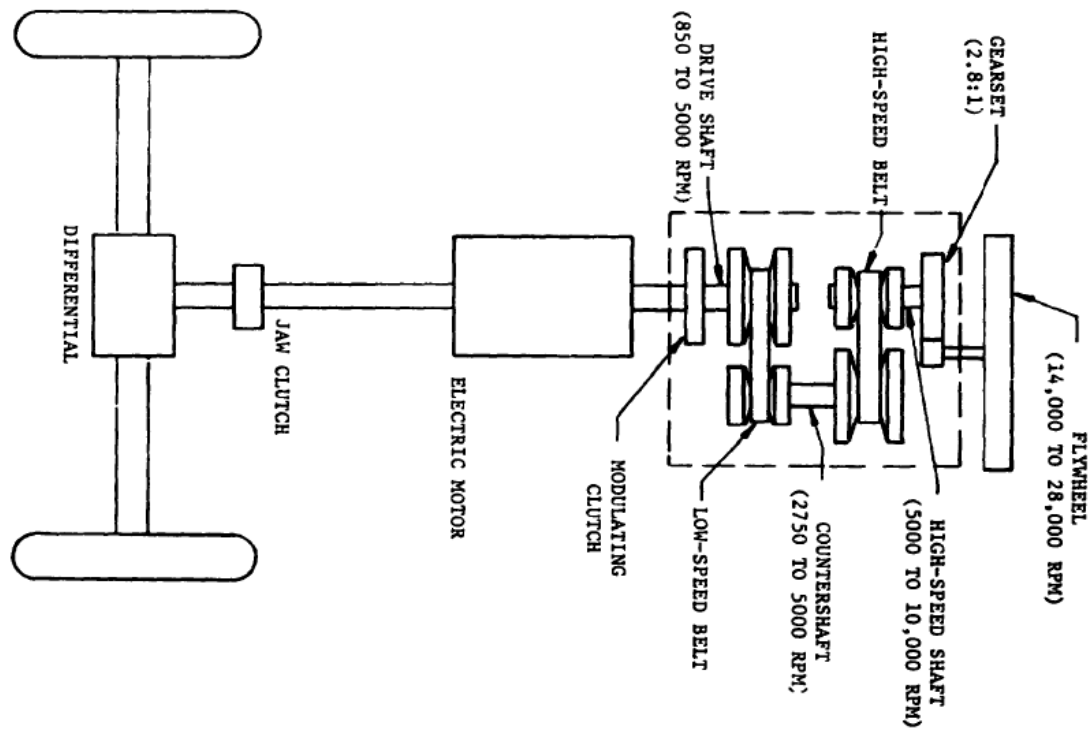


Figure 13 Battelle Columbus Laboratories concept [47]

The next design studied was a flat belt CVT concept by Kumm Industries [48]. The Fig. 14 shows the schematic. The belt is radially positioned between the guideways on the side of the two pulleys and the ratio change is achieved by changing the position of the belt along the guideways. The drive is used in conjunction with planetary gearing which allows the CVT to operate down to zero speed. There are two modes; a low speed and a high speed mode. The power is transmitted through both belt and the planetary gears in low speed mode in regenerative fashion and only through the belt in the high speed mode. The mode shift takes place by synchronous clutching. This design differs from the previous design in that the EM and flywheel are coupled together and all of their power passes through the CVT. The flywheel is coupled to the transmission via an electric clutch. The design of the belt CVT and the control is described. Both direct and differential arrangements for the CVT are examined and the arrangement having the least belt torque and power over the operating range is chosen. The technical requirements for the CVT included the high speed clutch and high speed DC motor which were unavailable at the time of the study.

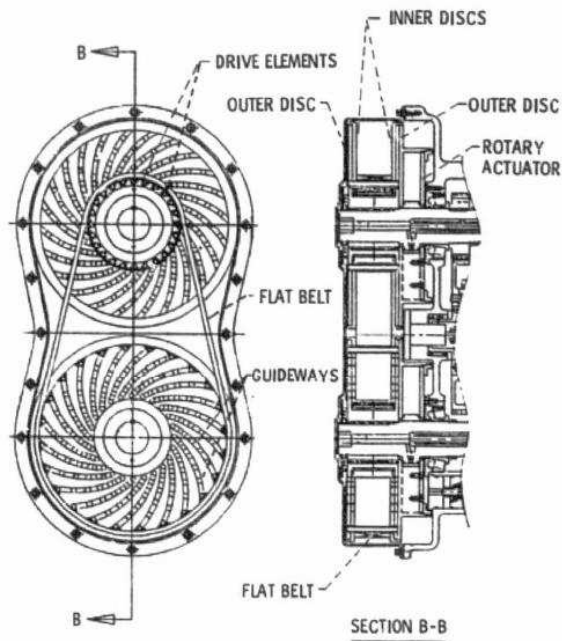


Figure 14 Kumm concept [48]

The third design studied was a toroidal traction CVT by Garrett Corporation [49]. Fig. 15 shows the schematic. The study consisted of designing a preliminary concept for the CVT, identifying the required technical advancements for the development of such a CVT, and determining the suitability of the CVT for alternative applications. Firstly the geometry of the toroids and rollers was selected to achieve high efficiency, low hertz pressure and low energy dissipation. Then five CVT configurations featuring the toroidal traction design were evaluated on efficiency, cost, size, weight, reliability and control. The selected option was the dual cavity full toroidal design with regenerative gearing. The design of the toroidal CVT and the control is described. The CVT is controlled hydraulically by changing the position of the rollers which are clamped in between the toroids. A mechanical loading cam mechanism automatically ensures that there is enough clamping force between the rollers and toroids to prevent slip. Three areas of ratio control, fluid properties and evaluation of traction contact performance were identified to require further technical development.

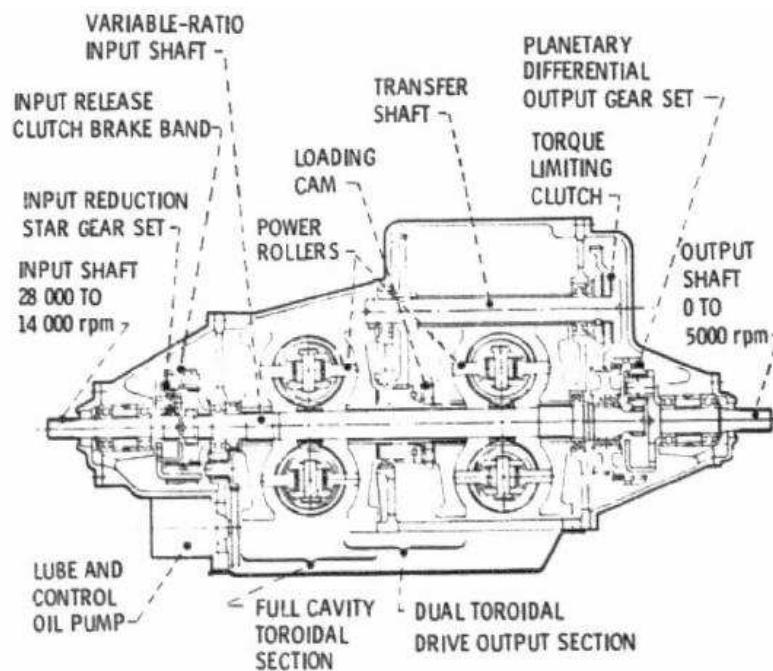


Figure 15 Garrett Concept [49]

The final design studied was a continuously variable roller cone traction CVT by Bales-McCoin Inc. [50]. Fig. 16 shows the schematic. The designed CVT consisted of traction cones and rollers in a regenerative path epicyclic gear differential. The variable ratio traction assembly is connected to output planetary differential through a set of idler gears. The flywheel is connected to the centre shaft through an input epicyclic reduction stage. A modulating clutch controls the ring gear of the input reduction unit. The clutch allows disconnecting of the flywheel at speeds less than 14000 rpm in order to decouple the flywheel when the output speed is below 850 rpm or in reverse mode. There is a central traction roller which is surrounded by four inclined cone rollers whose inner contact surfaces are parallel to axis of the roller. By changing the point of contact between the central roller and the cones the speed ratio is varied. The cones and the roller are loaded against each other hydraulically and the control system monitors the slip between them. The control system maintains optimum traction between the cones and the roller for all operating conditions via slip control feedback.

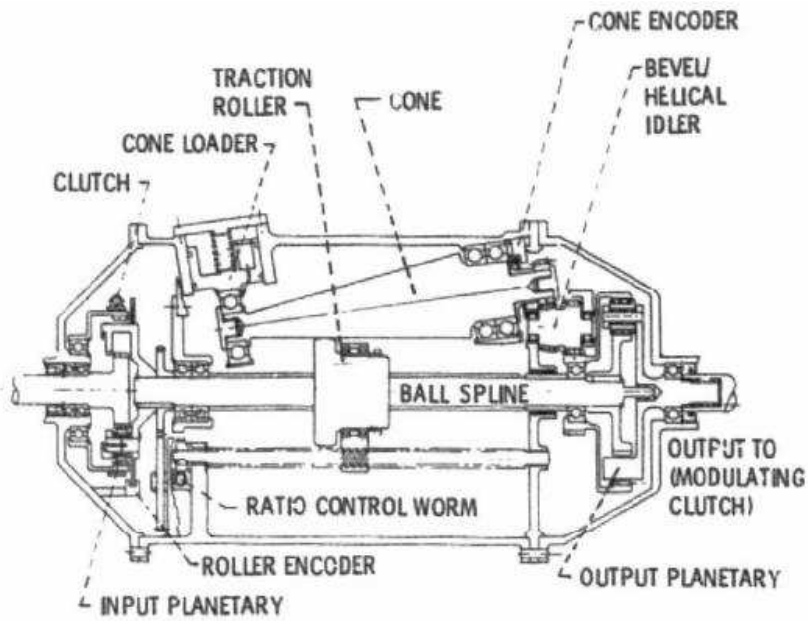


Figure 16 Bales-McCoin Inc. concept [50]

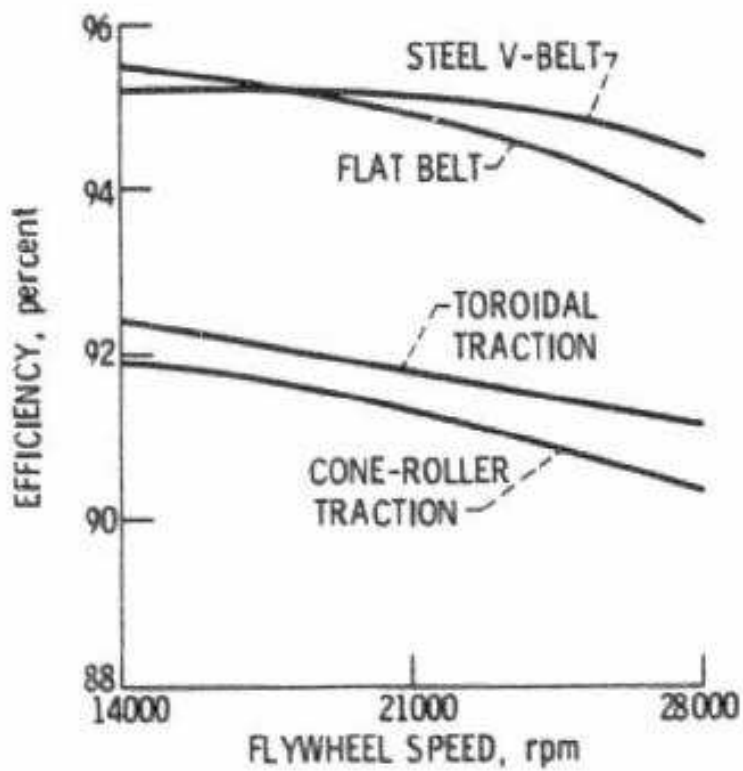


Figure 17 Comparison of the four concepts [51]

These 4 CVTs described above have been compared in [51]. The efficiencies of the CVTs are calculated and compared at nominal weighted averaged power of 16 kW and at an output speed of 3000 rpm for different flywheel speeds. The comparison is shown in Fig. 17. It

seemed that the steel belt CVT was the most efficient under these conditions and in general the efficiencies seemed to differ little over the flywheel speeds.

In 1983 study Secunde et al. discussed the progress in EV propulsion from 1976-1973 under the DOE electric and hybrid vehicle program [52]. Under this study 5 systems were compared having different levels of technology. The first System could have been built in 1976 which has DC motor, chopper and 3 speed auto transmission with torque converter. The second System was the same as the first one but with the latest available and more efficient components from 1982. The third was the DOE ETV-1 [53] which was built by GE and Chrysler. The fourth system was to take the best technology which included both off the shelf one as well as what could have been built at that time. The fifth and final system was a FESS with steel v-belt CVT incorporated in the EV. All the systems were simulated using the same lead acid battery. Results of the range calculations over the SAE J227a schedule D drive cycle showed that required battery energy density for a given range had been reduced by about 40 due to the propulsion system development. The acceleration performance of the flywheel assisted EV was by far the best. The report discusses the current situation, technology needs and the recommends that further development is needed to reduce cost.

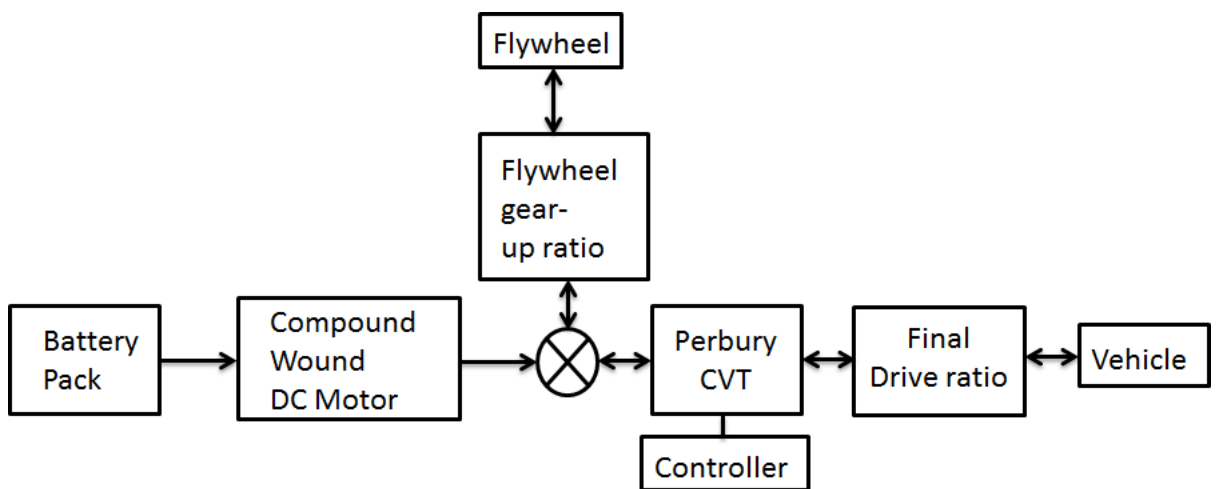


Figure 18 Sussex system [54]

In 1980 a flywheel assisted BEV was developed at Sussex University in the UK using the Perbury transmission [54-55]. The Fig. 18 shows the schematic of the system. The DC compound wound motor is used and is connected to the flywheel via a reduction gear so the flywheel is just an additional inertia on the EM. The CVT is a dual cavity design with power recirculation and is similar to the toroidal traction CVT by Garrett described previously. Ratio change is affected by changing the rollers inclination. There is no external motor control and the only the CVT is torque controlled. The motor automatically produces power depending on

the load it experiences after it is switched on. The system was developed for a 7.5 tonne urban delivery van. The peak torque of the transmission is 880 Nm and the battery is lead acid. The flywheel is 70 kg and runs at 13650 rpm.

During the development of FWBEVs in the 1970s, it was already evident by 1977 that in the near term even with the flywheel assistance the BEVs would not be able to match the ICEV in terms of performance. O'Connell et al. suggested the solution as a quasi-electric drive which was a flywheel BEV augmented by a small ICE [56]. According to Burrows and Barlow the BEVs could meet the standards set by the DOE though they could not meet the Federal Urban Drive Cycle (FUDC) under which the ICEVs were tested [41]. A study by GM in 1982 [57] suggested that GM had postponed its BEV research programs as the BEVs were not competitive due to high cost of vehicle and battery replacement. Though with the flywheel the performance and capacity of the BEV increases but so does the cost and complexity. It also gave the example of the test results of the ETV-2 FWBEV which showed poorer performance than predicted due to poor battery performance and drivetrain losses.

In 1990 Alcan International Limited, in collaboration with Unique Mobility Inc. and the University of Ottawa, had a program to develop an advanced EV utilizing FWB as a power surge unit for load levelling [58]. They used 0.5 kWh flywheel, 40 kW MG and 1000 kg lead acid batteries. The FWB was hermetically sealed, used magnetic bearings and a permanent magnet (PM) MG and had lower parasitic losses. The presented simulation optimisation study showed that the FWBEV could meet the FUDC and that load levelling was accomplished by the flywheel.

In 1991 Braess and Regar presented the BMW EV development trends [59]. BMW built an EV with sodium sulphide batteries in 1990. They proposed another concept to combine a high energy battery with a high power flywheel. The schematic is shown in Fig. 19. It utilized the PGS as a two degree of freedom device connected to a flywheel, the EM and the drive shaft with the necessary brakes and clutch to decouple the flywheel from the system during cruising. The speed and torque of the EM decided the power flow. At vehicle standstill, brake is applied and the MG charges the flywheel. Then flywheel accelerates the vehicle and MG acts as generator till zero speed and then reverses to become motor and gains positive speed and the MG and flywheel both power the vehicle. During cruising the flywheel is decoupled and the reverse happens during deceleration. The system showed improvement in energy consumption with lead acid batteries for the New European Drive Cycle (NEDC) but not for the Federal Test Procedure (FTP) cycle. However for the sodium sulphide batteries the advantage was less pronounced. The disadvantages of such a system are that it is less flexible; flywheel

cannot be charged during vehicle cruising, clutch and brakes have to be controlled which causes loss of efficiency, the MG has to partly absorb braking energy and there are energy conversions.

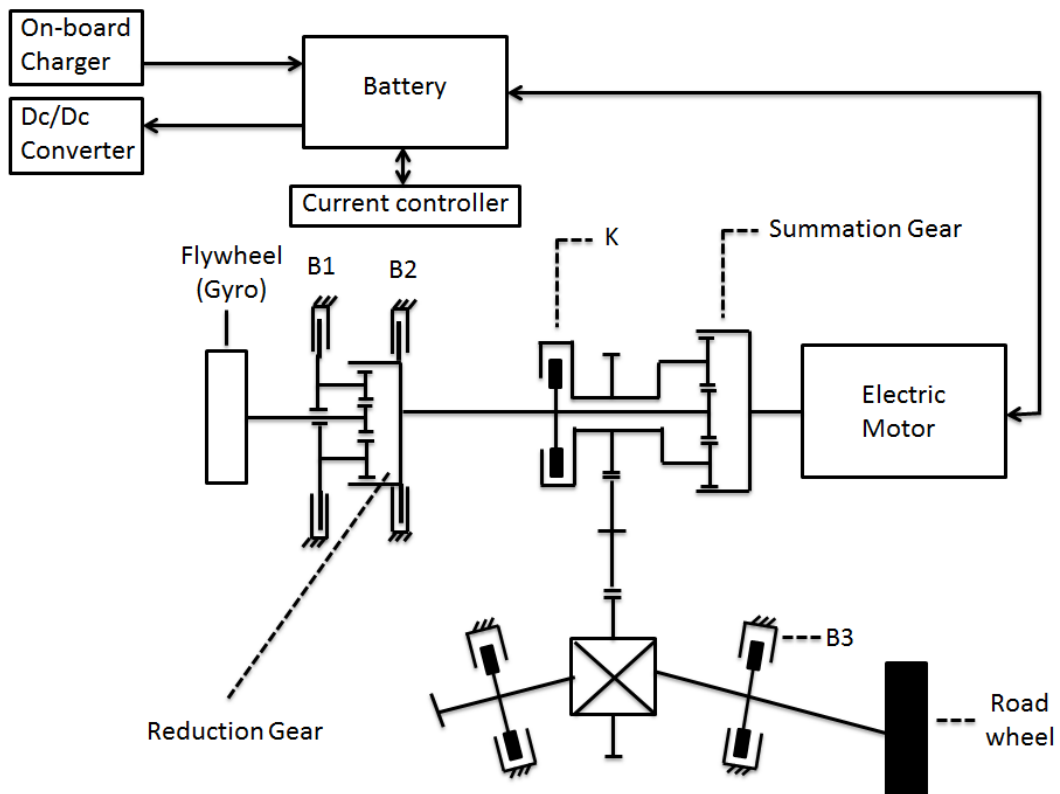


Figure 19 BMW concept [59]

In 1992 Szumanowski and Brusaglino showed a system similar to the BMW system [60]. The schematic is shown in Fig. 20. The PGS is the CVT where the DC MG is connected to ring, flywheel to sun and carrier to wheels. During constant velocity driving flywheel is disconnected using an electromagnetic clutch. The MG is controlled using a DC/DC chopper. Simulations showed improvement in range over the BEV. It would have disadvantages similar to the BMW system.

In 1994 Schaible and Szabados showed an electric drive system incorporating the FWB [61]. The system is shown in the Fig. 21. The FWB consisted of the flywheel coupled to a PM Synchronous machine (PMSM). There is an energy storage tank connected to the PMSM, which is a capacitor bank and acts as a temporary energy storage dump. The author suggests that due to the inertia of the flywheel, the FWB cannot meet the sudden demand in acceleration from the vehicle so the energy storage tank serves that purpose. The torque control of the system is shown.

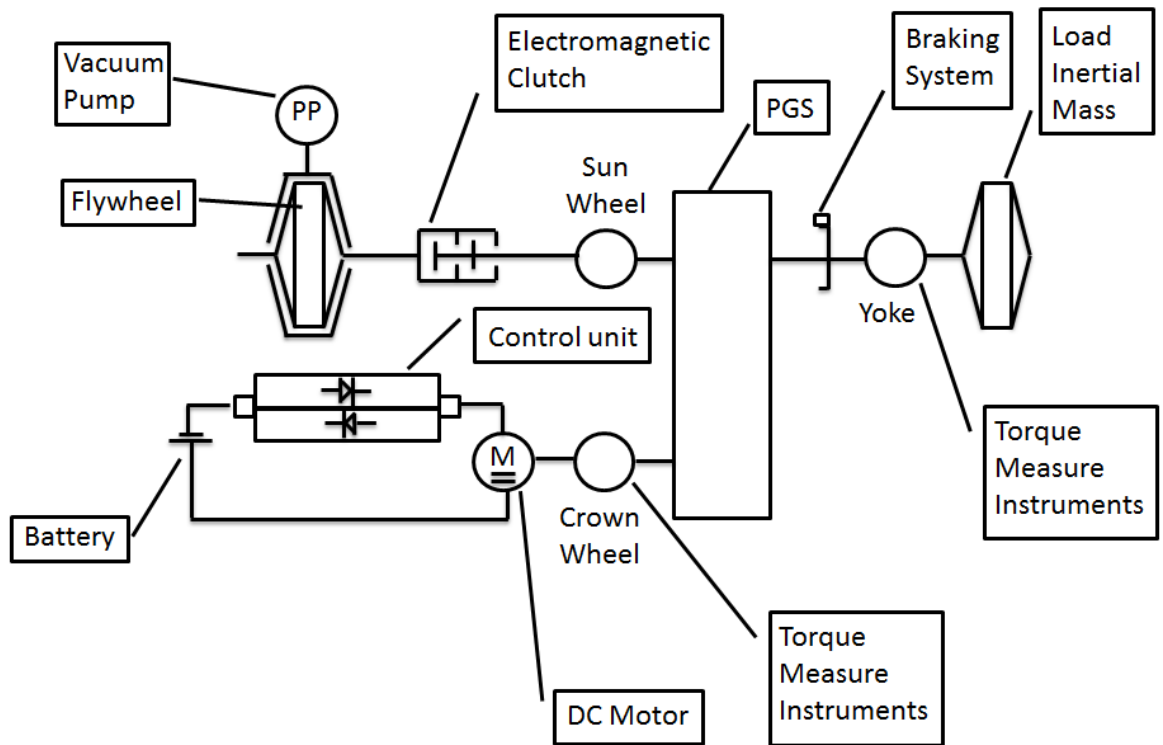


Figure 20 Szumanowski concept [60]

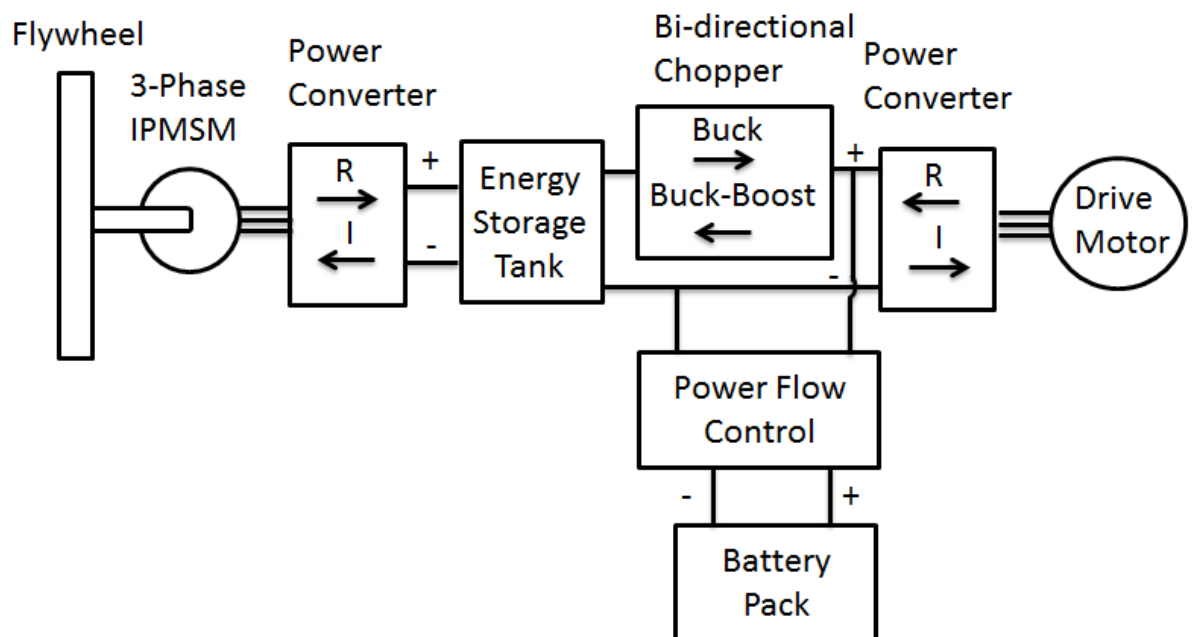


Figure 21 Schaible concept [61]

In 1994 Anerdi et al. showed a study supported by the European Commission evaluating FWB application in BEV [62]. Two cases were studied; one in which the FWB acted as the load leveller to the BEV and another where it was the sole energy source. From simulation results a 20% reduction of energy consumption on the Urban Drive Cycle (UDC) was shown possible by

using FWB as a load levelling device compared to BEV. The FWB under the project was being designed at University of Sheffield [63].

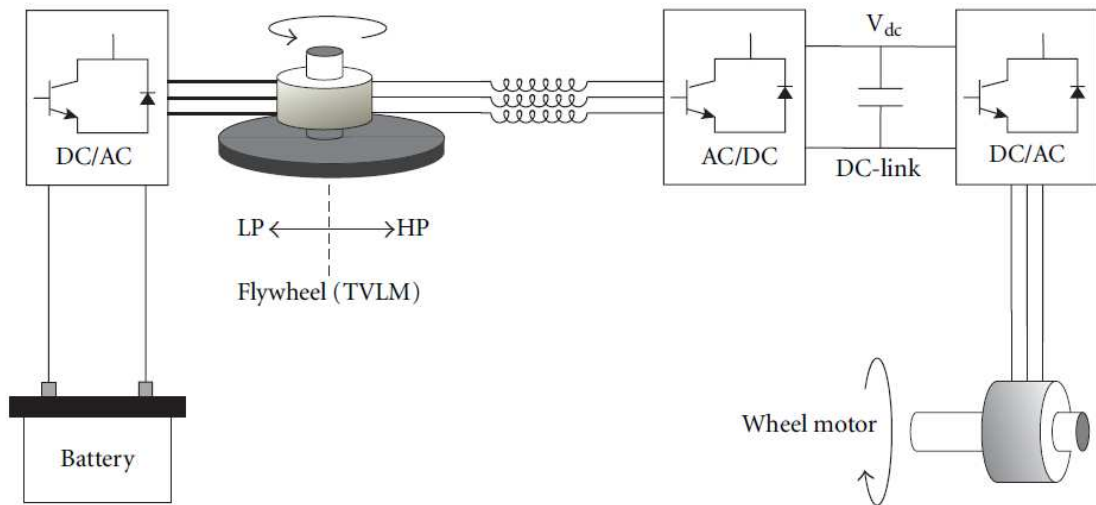


Figure 22 Lundin concept [179]

A number of examples show the use of FWB in an EV. Saitoh et al. studied FWB in an EV and proposed a so called super energy-efficient electric vehicle which consisted of a number of energy sources including Li-Ion batteries, photo voltaic cells and on board generator which could be fuel cell or ICE [64-67]. Xiong Xin Fu et al. described the FWB design and control strategy of charging and discharging the FWB in a BEV [68-69]. Briat et al. showed the application of FWB in a heavy duty EV with discontinuous mission profiles such as a refuse collector [70]. Lundin (2011) used a different design FWB (Fig. 22) in an EV as a secondary storage device [71]. The FWB has double stator windings and is placed between the battery and the drive motor. The low voltage side is connected to the batteries and the high voltage to the drive motor. This allows the FWB to charge or discharge both the drive motor and the batteries at two different voltage levels. A significant decrease in partial charge/discharge cycles, maximum current and battery resistive losses with the flywheel is shown in the results. A common disadvantage in all the layouts presented before which use the FWB is that the design usually includes a number of power converters which cause power losses and are usually high in cost. An important thing to note is that most of the cases discussed above use lead acid as their primary batteries, which is not the preferred choice in current production BEVs.

2.6 Flywheels and their characteristics

The following section provides briefly some key properties that define the FESS.

2.6.1 Capacity

The flywheel in essence is a very simple technology as it is just a rotating mass. The energy stored in the flywheel at any time is given by the simple equation 4.

$$E_{FW} = \frac{1}{2} J_{FW} \omega_{FW}^2 \quad [4]$$

The energy content of the flywheel (E_{FW}) is dependent on the inertia of the flywheel (J_{FW}) as well as its rotational speed (ω_{FW}). The inertia of the body around its principle axis of rotation is given by the mass and its distribution as shown in the equation 5.

$$J = \sum m_i r_i^2 \quad [5]$$

The inertia depends on the shape of the flywheel. The maximum speed of rotation of the flywheel is dependent on the strength of the material it is made of. The ability of the flywheel to withstand centrifugal forces decides the maximum rotation speed. The equation 6 gives the maximum energy (E_{max}) that can be stored in the flywheel at its burst speed where m_{FW} denotes the mass of the flywheel, σ_{max} tensile strength of the material and ρ density of the material of the flywheel respectively.


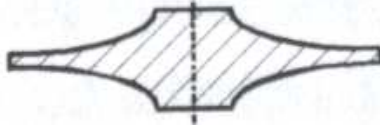

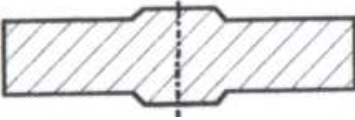
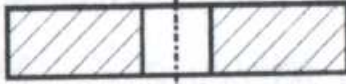

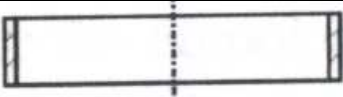

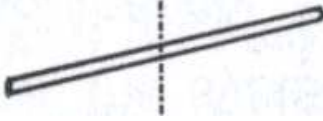
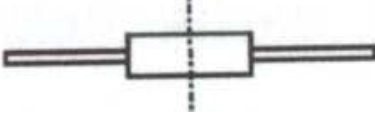
$$E_{max} = \frac{1}{2} m_{FW} \frac{\sigma_{max}}{\rho} \quad [6]$$

The common equation used to describe the specific energy of flywheels is as follows:

$$\frac{E_{FW}}{m_{FW}} = k \frac{\sigma_{max}}{\rho} \quad [7]$$

The symbol k denotes the shape factor. The shape factor describes the tension-moderate utilization of all mass particles in the flywheel [72]. It depends on the geometry of the flywheel. Table 1 shows the factor for different geometries.

Table 1 Shape factor for different geometries [72]

Description	Form	Shape factor 'k'
Disc of equal strength		1
Disc of approximately equal strength (with crown)		0.93
Frustum-disc		0.81
Un-punched plain disc		0.61
Punched plain disc		0.305
Ring with spokes		0.4
Thin ring		0.5
Bar of equal strength		0.5
Bar (thread)		0.33
Radial-brush		0.2-0.3

The energy capacity of the flywheel (E_{cap}) is described by the maximum useful energy that can be extracted or put into the flywheel, which depends on its maximum and minimum operating speed as the energy storage system.

$$E_{\text{cap}} = \frac{1}{2} J_{\text{FW}} (\omega_{\text{FW,max}}^2 - \omega_{\text{FW,min}}^2) = \frac{1}{2} J_{\text{FW}} \omega_{\text{FW,max}}^2 \left(1 - \left(\frac{\omega_{\text{FW,min}}}{\omega_{\text{FW,max}}} \right)^2 \right) \quad [8]$$

The flywheel minimum speed is usually taken as half of the maximum speed which allows the maximum useful energy to be three quarters of the maximum energy of the flywheel.

2.6.2 Material

Different types of materials can be used for flywheels depending on the application and the design constraints. Naturally the choice of the material will play a key role in determining the specific energy of the flywheel. Generally synthetic materials such as carbon fibres provide higher specific energy than steel. The modern high strength composite materials are of the ideal choices for flywheels. These materials have anisotropic properties implying that their characteristics are dependent on the direction. If unidirectional materials are used only certain limited shapes can be realised, however if suitable multidirectional materials are used to increase the strength of the weaker sections of the flywheel, the overall maximum strength is reduced [73].

Table 2 Materials for flywheel [72]

Material	Density	Strength	Theoretical specific energy
	[kg/m ³]	[MPa]	[Wh/kg]
High strength steel	7800	2500	90
Glass fibre	2600	2400	250
GFK (fibre in matrix)	2100	1500	200
Aramide fibre	1450	2800	540
AFK (fibre in matrix)	1400	1800	360
Carbon fibre	1800	7050	1090
CFK (fibre in matrix)	1500	4500	830

Some of the choices for composites include plastic materials reinforced with glass, carbon or aramid fibres, and fibreglass. Other materials include steel and aluminium which are cheaper than composites. Table 2 gives some of the common flywheel materials and their properties [72]. One of the main contributors to the interest in flywheels being rekindled in the 1970s was

the fact that it could be made to store large amounts of energy using composite materials. Rabenhorst (1969) termed these as superflywheels [74].

2.6.3 Bearings

Different types of bearings can be used in flywheels. One of the main differences with conventional applications is that in the case of flywheels they have to operate in at least partial vacuum and are exposed to gyroscopic loads. The bearings must have high load capacity, long life, stability at high speeds, and have low frictional losses. The frictional losses are very important as they form one of the main parasitic loads on the FESS. The choice of bearings will depend on the application and the design requirements.

Usually in case of FWB magnetic bearings are used, which can be active magnetic bearings [75] or a combination of active and passive magnetic bearings, the so called hybrid bearing system [76]. In most cases mechanical bearings are used as a back-up in case the magnetic bearing system fails. Magnetic bearings have the advantage of no friction as they are contactless and there is no need for lubrication, however they are expensive and require complex controls.

In case of mechanical hybrids the usual choice is angular contact bearings or a combination of rolling bearings which provide the support for axial and radial loads [77]. Since they have to operate in reduced environment, grease lubrication is usually used.

2.6.4 Windage losses

The windage losses are probably the most important parasitic losses in high speed flywheels. To keep the self-discharge rate of the flywheel low, it is important to reduce the windage losses. The most common way to reduce windage losses is to operate the flywheel in vacuum. Another way is to use gases such as helium or a mixture of air and helium. The vacuum pump to be used should be energy efficient as it would be unwise if the energy consumption of the pump exceeds the savings from reducing the windage losses. Another aspect is the flywheel temperature. As the pressure inside the containment is reduced to lower the windage losses, the cooling effect of the gas also reduces specially in case of FWB where the MG generates heat. At certain point further reducing the pressure might lead to increase in rotor temperature [78]. The drag torque from the windage losses exists on the rim and the side of the flywheel and is given by the equation [77].

$$T_{\text{windage}} = \rho_g \omega_{\text{FW}}^2 r_{\text{FW}}^3 (C_s A_s + C_{\text{rim}} A_{\text{rim}}) \quad [9]$$

Where ρ_g is the density of the environment; r_{FW} is the flywheel radius; A_s and A_{rim} are the surface areas of the sides and of the rim of the flywheel respectively; C_s and C_{rim} are

non-dimensional drag coefficients that depend (according to the environment in which the flywheel rotates) on other non-dimensional parameters: the Reynolds number, the Mach number and the Knudsen number.

2.6.5 Safety and Containment

Since the flywheel is a rotor spinning at high speeds the issue of safety and containment becomes the biggest technical challenge. For vehicle applications it is essential that the containment is low cost and light weight and is able to withstand the sudden failure of the flywheel. Another approach is to design the flywheel such that full rotor burst failure modes are avoided. The failure modes of metallic flywheels are different to that of composite material flywheels. For composite flywheels the most likely failure scenarios are delamination, burst or transverse epoxy material failure [79]. As an example when a flywheel made of carbon fibre composite, which is a material for choice for many flywheels today, fails the rotor is broken in to fine particles as a result of the impact. These particles behave like a fluid moving inside the containment which causes large axial loads on the containment [80].

Hansen suggests that the safety issue of flywheels should be tackled during the design phases of the development process [80]. The safety risk can be reduced by using various design approaches.

1. One of the approaches is to design the flywheel with a large margin between operating stress and ultimate stress. This can also lead to long life of the flywheel but penalty would be higher weight and volume.
2. Another one is that the rotor be designed that the outer portion operates at a higher stress than the inner portion. Due to this reason, the outer portion is likely to fail first and the containment can be designed to contain the small failure resulting from this and in this was the remainder of the flywheel can be saved from failure.
3. The third approach suggested is to instrument the flywheel with sensors such as acceleration pick-ups which can detect the anomalies and this method can be used along with other methods.
4. If the risk of rotor burst cannot be reduced to a sufficient level, it would be prudent to design the containment which is custom made for the flywheel. An example of this was shown by University of Texas-Austin [81]. They successfully showed in an experiment that by using a free-floating containment structure the major loads from the flywheel burst event were dissipated, and it significantly reduced the loads that were transmitted through the stator structure to its attachments.

Another approach is to use a laminated sheet type structure, laminated axially such that only a small fraction of the rotor can burst at any one instant; the probability of two or more failing at the same time being negligible [82].

2.6.6 Gyroscopic loads

Whenever there is a change in the spin axis of a rotating object, it experiences gyrodynamic forces and flywheels in cars are a perfect example. As the car manoeuvres, the axis of the flywheel will change its direction which will depend on the manoeuvre itself and the orientation of the flywheel. Otaki [83] and McDonald [84] have analysed the gyrodynamic forces of the flywheel in a vehicle. The basic equations of the gyrodynamic forces are shown below. The angular momentum of the flywheel depends on the flywheel inertia and its speed of rotation.

$$H = J_{FW} \omega_{FW} \quad [10]$$

Since the angular momentum is a vector it has both magnitude and inertia. From the equation it can be seen that flywheel of a given inertia will have the greatest angular momentum at its maximum speed so the torque reactions at this point would be most significant. When a torque (T_a) is applied to the flywheel its angular momentum (H) will change according to the equation 11.

$$T_a = \frac{dH}{dt} \quad [11]$$

And the reaction torque (T_r) exerted by the flywheel in response to applied torque will be as shown in equation 12.

$$T_r = -T_a = \frac{dH}{dt} \quad [12]$$

The rate of rotation imposed on the flywheel when the vehicle manoeuvres is called precession rate (Ω), which causes the change in the angular momentum as is shown in Fig. 23. The rate of change of angular momentum is thus given as shown in equation 13.

$$\frac{dH}{dt} = H \times \Omega \quad [13]$$

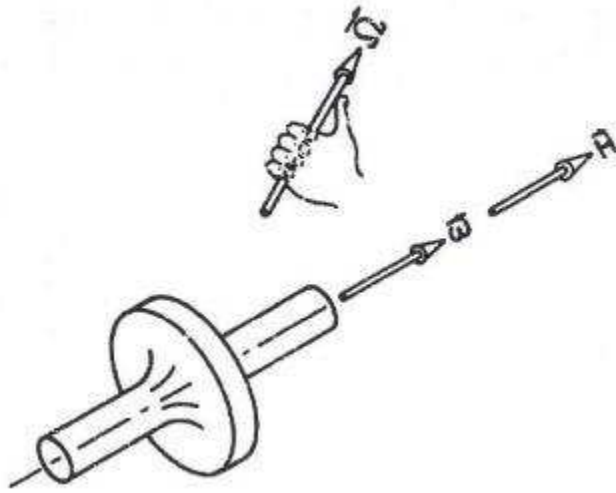


Figure 23 Schematic of angular momentum, angular velocity and precession rate [84]

Looking at equations above it results that the reaction torque is equal to this cross product.

$$T_r = H \times \Omega = H\Omega \sin(\theta) \quad [14]$$

where θ is the angle between the two vectors and is shown in Fig. 24. From the Fig. 24 it can be clearly seen that the reaction torque is perpendicular to the plane containing H and Ω vectors. The reaction torque is the greatest when both are also perpendicular to each other.

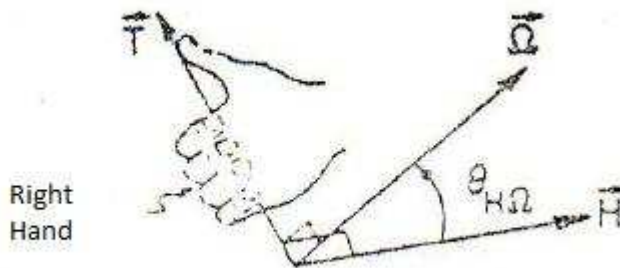


Figure 24 Schematic showing angle between angular momentum and precession rate vectors, and direction of reaction torque [84]

The vehicle manoeuvres can be in three directions. The longitudinal manoeuvre would be roll, lateral one would be pitch and the vertical one would be yaw, as shown in Fig. 25. Depending on whether the orientation of the flywheel is longitudinal, lateral or vertical the Table 3 shows the direction of the corresponding reaction torque.

Table 3 Reaction torque sense depending on flywheel orientation [77]

Flywheel orientation	Direction of precession		
	+Yaw	+Roll	+Pitch
+Vertical	None	-Pitch	+Roll
+Longitudinal	+Pitch	None	-Yaw
+Lateral	-Roll	+Yaw	None

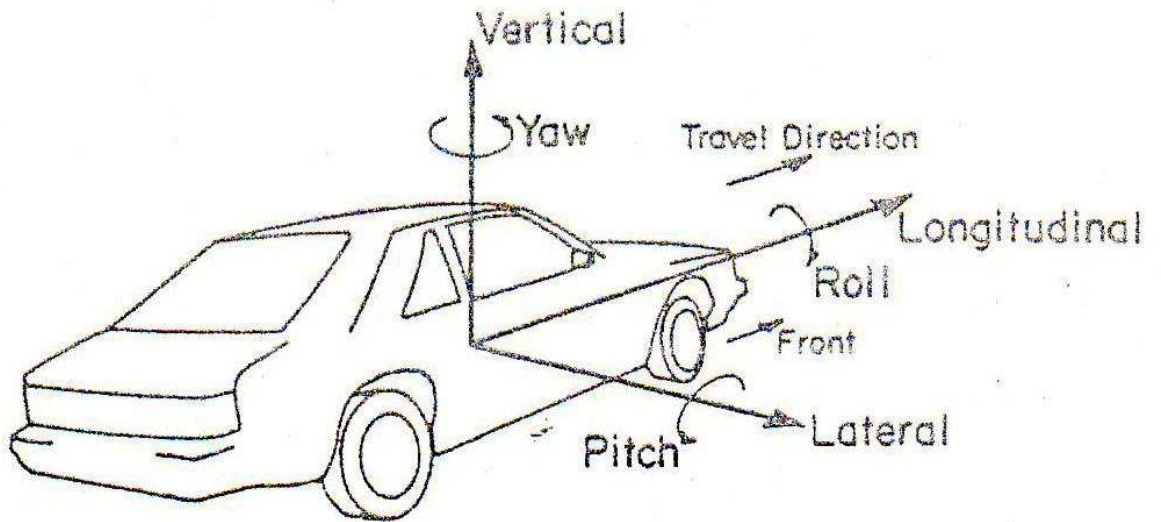


Figure 25 Vehicle axis system and vehicle manoeuvres [84]

In case of conventional vehicles, the track is relatively shorter than the wheelbase so torque reactions that tend to pitch or yaw the vehicle are relatively not significant compared to roll which does not occur under normal vehicle conditions. It has been shown by both Otaki [83] and McDonald [84] that gyroscopic reactions are relatively small for the flywheel size used in cars under normal conditions. However in situations involving accidents, all possibilities need to be looked at.

2.7 Transmissions

The flywheel needs to be connected to the driveline in a manner that allows the flywheel to change its speed independently of the velocity of the vehicle. As the flywheel usually gains speed when the vehicle is slowing down and loses speed when the vehicle is accelerating, the transmission has to be continuously variable in nature. There have been a number of different types of transmissions which will be discussed in the following section. Although changing the speed of the flywheel is the most usual method of varying its energy content, some authors

have suggested using a variable inertia flywheel [85-87]; however its design and control would be complex.

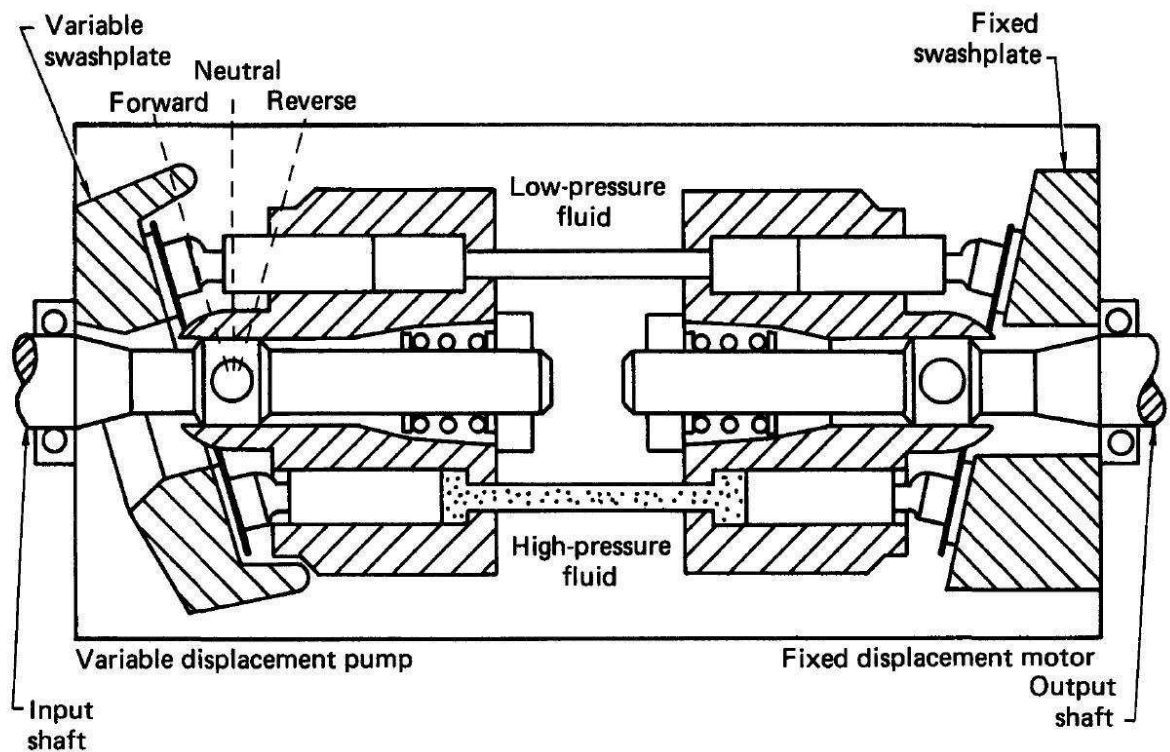


Figure 26 Hydrostatic transmission [88]

2.7.1 Hydrostatic transmissions

In case of hydrostatic transmissions there is a variable displacement pump which is connected to a hydraulic motor via hydraulic lines along with the other necessary components. The pump converts the mechanical power into hydraulic power which is reconverted at the motor. In the reverse direction the pump acts as a motor and the motor behaves like the pump. The hydrostatic transmission will usually be an infinitely variable transmission (IVT). The stroke of the pump can be reversed so the transmission can rotate in both directions. The Fig. 26 shows a typical hydraulic transmission [88]. During the 1970s these transmissions were popular due to their wide availability [55]. They usually tend to be noisy and bulky which makes them less suitable for a passenger car.

2.7.2 Electrical transmissions

The electrical transmission consists of a two MGs which are electrically linked together and necessary power electronics needed. During power transmission one machine acts as generator to convert mechanical power into electrical power and the other as motor to do the reversion. These have been widely used for FESS since the early days and usually employ magnetic bearings. They add flexibility to the system; however they tend to be expensive as

firstly the machines are sized bigger, since the whole power has to be transmitted via them, and secondly these usually include a number of power inverters, and further have the disadvantage of energy conversion. The FWB or electromechanical battery (EMB), which was used probably for first time in 1953 in the Gyrobus, is a popular choice for BEVs and HEVs. There are three topologies defined for the FWB [89] and shown in Fig. 27.

1. Fully integrated: In this case the flywheel and the MG are one unit and usually but not always the inside out configuration is used, which means that the flywheel forms part of the outer rotor with the stator inside. In this case the design is highly compact. Since the containment is under vacuum the only way to remove heat is via radiation, so machine cooling poses a technical challenge. Another advantage of such a structure is that it can be hermitically sealed and it needs only electrical connections.
2. Partially integrated: In this case usually the rotor is inside the containment and the stator is outside the containment. The problem of rotor cooling remains though it is improved by the stator being outside the containment. It has good design adaptability and the available MG technology can be used.
3. Non-integrated: The flywheel and the MG are separate units mounted on the same shafts. It is bigger and simpler than the other topologies. The problem of cooling is avoided; potential to maximize the use of available technology, but a mechanical seal is required and the MG will suffer windage losses continually.

There have been a number of FWBs constructed by various organisations such as the University of Texas-Austin [89], Technical University Eindhoven [90] and Lawrence Livermore Laboratory [20].

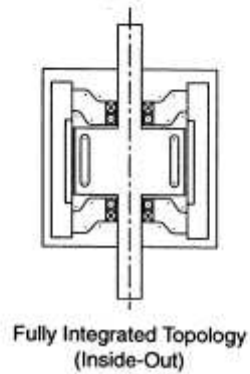
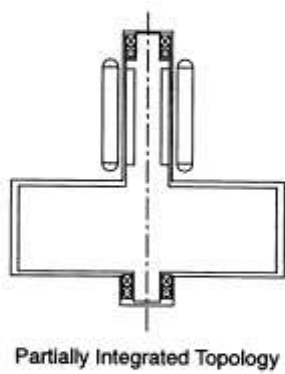
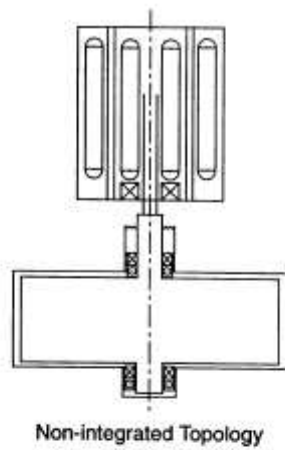


Figure 27 FWB Topologies [89]

2.7.3 Traction transmissions

In the traction drive, power is transmitted between two loaded objects through adhesive friction. The speed ratio is changed by varying the point of action of forces. The two popular transmissions in this category are the belt drives and the rolling contact traction drives. Current traction CVTs are deemed a mature, low-cost and fuel-efficient technology [91].

2.7.3.1 Belt drives

In this type power is transmitted over a belt, chain or band clamped between two pulleys. The speed ratio is varied by varying the axial clamping forces for the two halves of the pulleys thereby changing the rolling radii on the pulleys. The clamping forces are usually controlled via hydraulics. One of the common designs is the Van Doorne steel v-belt in which steel segments are held by a steel band, which was one of the first commercially successful CVTs. In this case the driver pulley usually pushes the driven pulley so it is a compression belt.

Another one is the PIV-Antriebe Werners Reimers design in which a tension loaded chain is used for transmitting power. The single chain's shackle packages are connected with each other by compression parts guided by metallic clips that enclose them. The advantage of this design is that the chain whistle noise can be avoided. The Kumm Industries flat rubber belt design is another one in this category which was explained previously. Fig. 28 shows the various designs [92].

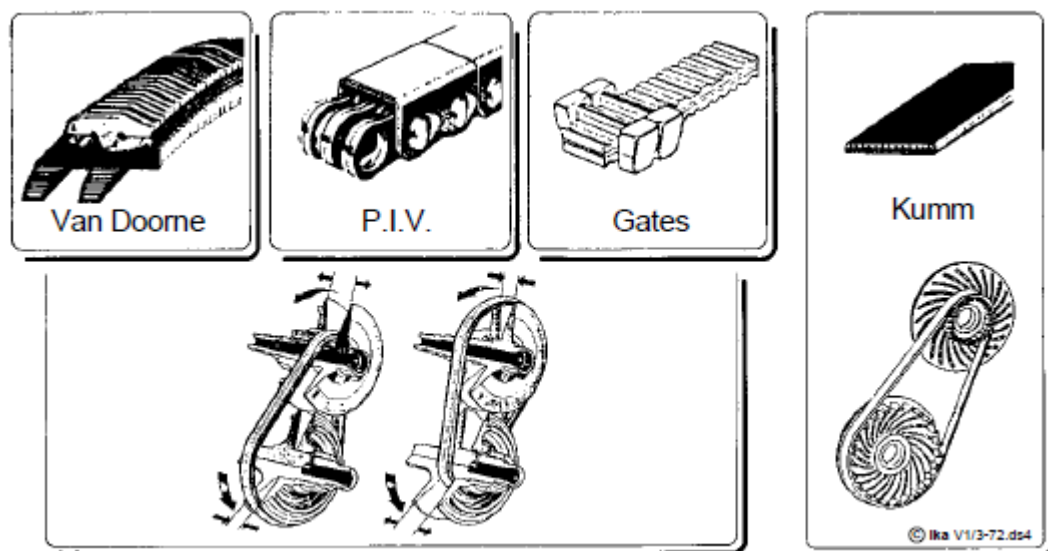


Figure 28 Types of belt drives [92]

2.7.3.2 Rolling contact traction drives

The two popular designs are the toroidal traction drive and the roller cone traction drive. The power is transmitted between two rolling elements separated by lubricant film. In the toroidal drive the inclination of the roller disc in the toroidal cavity is changed to vary the ratio. The required system torque is set by applying a force to the roller hydraulically which allows the roller to follow the ratio automatically, thus the drive is torque controlled. The Perbury transmission in the Sussex propulsion system [55] and the Flybrid-Torotrak system [11] used in Formula 1 Kinetic Energy Recovery System (KERS) employ such a toroidal transmission. Fig. 29 shows the Flybrid-Torotrak drive.

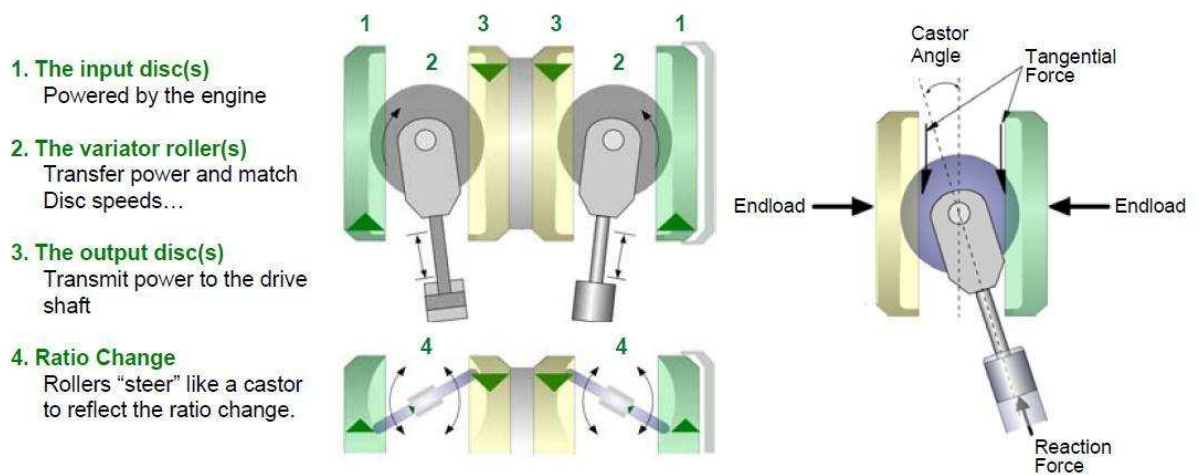


Figure 29 Torotrak design [180]

2.7.4 Planetary gear set

The PGS (Fig. 30) is a speed coupling device commonly used in automatic transmissions (AT) in conventional cars. It gives the advantage of having multiple ratios in a compact space. In the conventional AT case usually one of the arms of the PGS is brakes and the other two act as input and output. However to be used as a CVT it has to be used as a two degree of freedom device implying that all the branches should be free to rotate. As a speed coupling device it has the property that speeds of two branches can be independently controlled and the speed of the third one is dependent on the other two.

$$n_3 = K_1 n_1 + K_2 n_2 \quad [15]$$

The coefficients K_1 and K_2 are constants which are dependent on the geometry and structure of the device [4]. Due to the power equilibrium torque of the three branches are related to each other, in which one torque determines the other two.

$$T_3 = \frac{T_1}{K_1} = \frac{T_2}{K_2} \quad [16]$$

The PGS will be analysed in greater detail in the Chapter 4. In the BMW [59] and Fiat systems [60], the single PGS is used as a CVT.

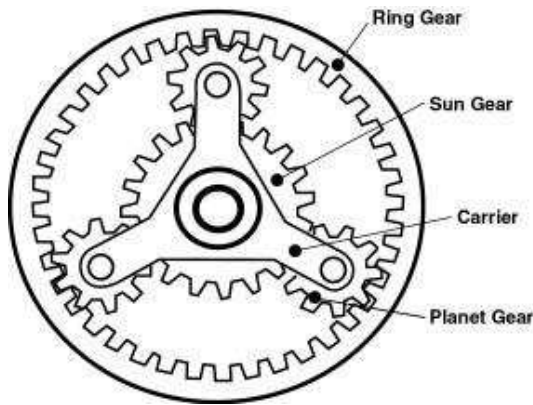


Figure 30 Schematic of planetary gear set [181]

2.7.5 Power split CVT

The power split CVT (PSCVT) is used to avoid the low efficiency of the variator only transmission. For the sake of clarity the previously mentioned transmissions will be referred as variator. The idea of a PSCVT is that part of the power is transmitted through the highly efficient direct mechanical linkage and the rest is transmitted through variator. The common disadvantage is that the speed ratio range is usually smaller than that of the variator itself, which can be altered by various means which will be discussed in the Chapter 4. The common PSCVTs employed in flywheel hybrid vehicles (FHWV) are electromechanical, hydromechanical and various traction drive PSCVTs. Fig. 31 shows the principle of PSCVT.

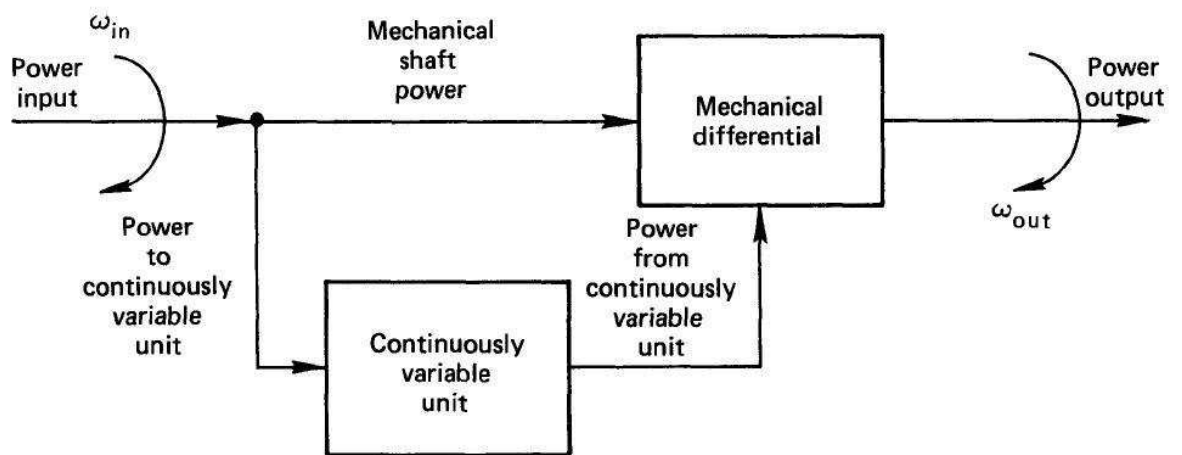


Figure 31 Concept of PSCVT [88]

2.8 Research direction

The development of BEV has to continue to lead us towards a zero emission transport system. The fuel flexibility of the BEV has the greatest potential to utilize power from renewable or low emission sources to be used in the transport system. The greatest limitation of the BEV is the battery itself and hybridisation of the energy sources of the BEV is one of the methods to improve the BEV. The FESS is an ideal secondary storage system for the BEV and is best utilized

in a mechanical CVT to avoid energy conversion and lower the cost. The use of mechanical CVT based FESS also offers the potential to reduce the size of the main prime mover. As the chapter shows, limited research had been attempted in this area mostly in the 1970s which was not successful due to poor technology of that period and the lack of optimal design concepts and energy management. With the advent of production BEVs in the last few years and advancements in flywheel and CVT technology, there is a need for research into optimal design concepts with optimal energy management for a mechanical CVT based FWBEV powertrain. This study will focus on designing a mechanically connected FWBEV powertrain concept for a passenger car application including a fundamental analysis of the transmissions and online predictive energy management using simulation.

3 Base Vehicle

This chapter is divided as follows. First the fundamentals of BEV are explained along with its components. This is followed by the description of the baseline vehicle model and analysis of cycle energy consumption results which demonstrate the potential to improve the energy efficiency of the BEV by employing a power handling device, which could transmit power directly to the driveshaft.

3.1 Baseline vehicle

The configuration of a modern BEV is shown in Fig. 32. It consists of an energy storage device which is a rechargeable battery in most cases powering one or more EM connected to the driveline. The EM might be connected to driveline directly as wheel hub machines or using a single speed or multi speed transmission. There is usually a power converter for AC/DC conversion as most BEV electric machines are AC machines. The primary energy source is usually a high voltage battery and the auxiliary power source is the standard 12 V battery. Most auxiliary loads are electric in nature unlike the conventional vehicle where they are mechanical. The BEVs also have an on board charger which is used to charge the high voltage battery. The vehicle controller and energy management system control the flow of energy. An inherent advantage of BEVs is that they can perform regenerative braking unlike conventional vehicles.

3.2 Battery

The most important element in the BEV is the battery. The battery in a BEV is constituted of a number of modules in series or parallel to achieve the desired voltage and current. The modules are in turn formed by connecting a number of cells in series or parallel. The cell is the smallest element of the battery.

An introduction to the general terminology related to cells that will be used is as follows [93]:

- State of charge (SOC): it is defined as the current cell capacity as a percentage of the maximum capacity. It is usually calculated by integrating the current used over time.
- Nominal voltage: it is defined as the reference voltage of the cell.
- Open circuit voltage (OCV): it is the voltage of the cell when no load is acting on it. It usually increases with SOC.
- Internal resistance: it is defined as the resistance of the cell which causes power loss when load is applied on it. It depends on the SOC and the temperature of the cell and is different for charging and discharging.

- Nominal capacity: the nominal capacity of the cell is defined as the total number of amp-hours available when the cell is discharged at a specific constant current (C-rate) from 100% SOC to the cut off voltage that defines the empty state of the cell. Capacity is usually calculated by the product of the C-rate and discharge time and decreases with increasing C-rate.
- Nominal energy: it is defined as the total energy in watt-hours available when the cell is discharged at a specific constant current rate (C-rate) from 100% SOC to the cut off voltage. It is calculated by the product of discharge power and discharge time and decreases with increasing C-rate.
- C-rate: The C-rate defines the rate at which a cell is discharged relative to its own maximum capacity. A 1 C-rate defines the discharge current that would discharge the cell in 1 hour.
- Specific energy: it is the nominal energy per unit mass of the cell.
- Specific power: it is the maximum available power per unit mass of the cell.
- Energy density: it is the nominal energy per unit volume of the cell.
- Power density: it is the maximum power per unit volume of the cell.
- Maximum continuous discharge current: it is defined as maximum current that can be used to discharge the cell continuously.
- Maximum pulse discharge current: it is defined as the maximum current that can be used to discharge the cell for a short duration.

The terms described above are general and are not always standard. As described in the Chapter 2 there are different types of cell chemistries and the most popular for a modern BEV is the Li-ion. However Li-ion is really a group of chemistries in which the anode is usually a lithium metal oxide and there are a variety of different compounds that can be used. Some of the important chemistries are described below [94]:

- Lithium iron phosphate (LFP)
- Lithium nickel manganese cobalt oxide (NMC)
- Lithium nickel cobalt aluminium (NCA)
- Lithium titanate oxide (LTO)
- Lithium manganese spinel oxide (LMO)

Some of the important properties of cells are specific energy, specific power, life, safety and cost. Safety is linked to the thermal and chemical stability of the cell. The different chemistries have their different properties. LFP and LTO are considered to have high safety and life than Nickel-Cobalt chemistries but the latter usually have higher specific energy [95]. As with

various technologies there are trade-offs. Another important aspect is the specific power which is usually a trade off with specific energy. As indicated by Burke and Miller [95], any specific power can be achieved for all chemistries by sacrificing specific energy. Fig. 33 shows the Ragone plot for various cell chemistries.

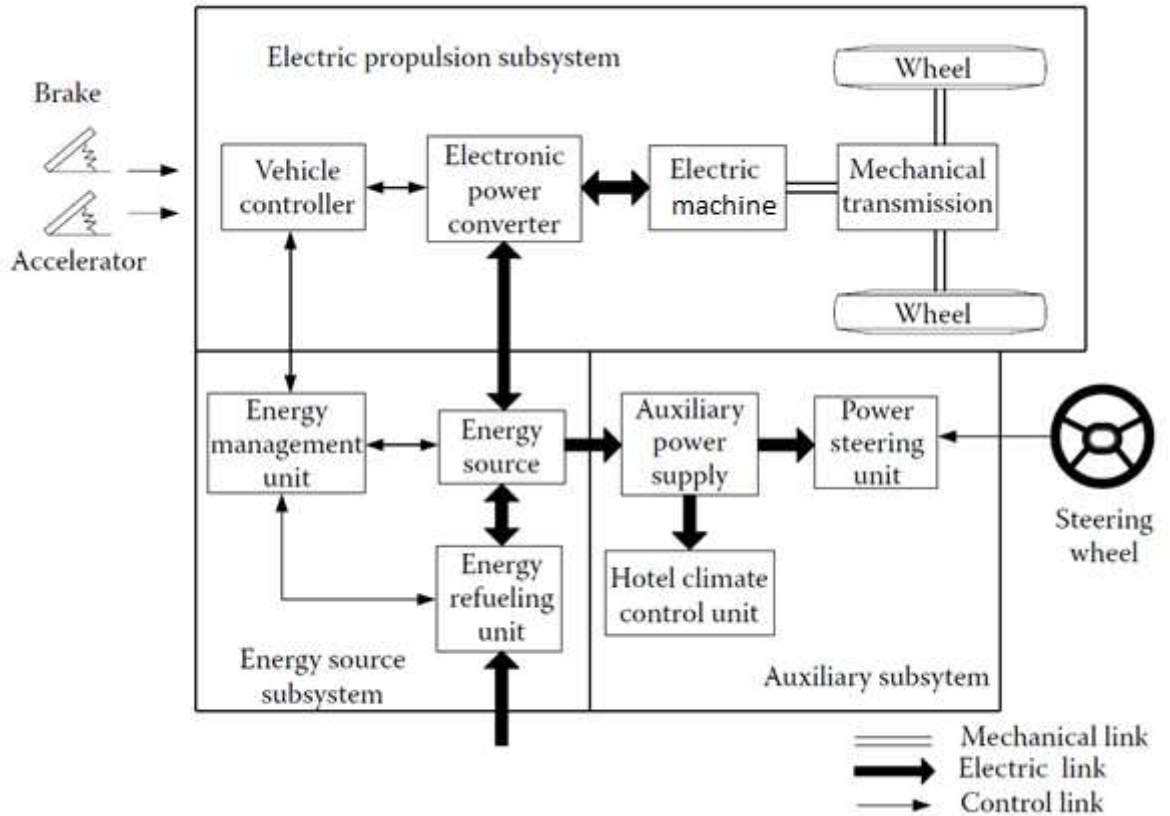


Figure 32 Schematic of BEV powertrain [4]

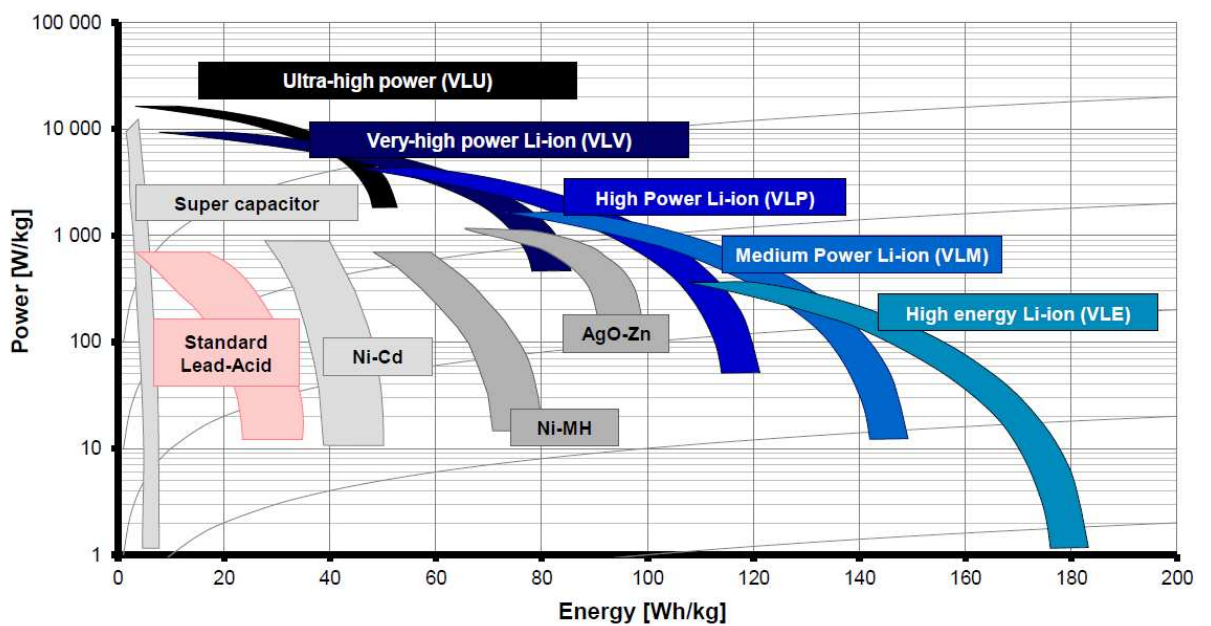


Figure 33 Ragone plot for various cell chemistries [182]

From the Fig. 33 it can be seen that the Li-ion chemistry can be designed from very high power to high energy. The energy in very high power cells is about 35% the energy of high energy cells [18]. Usually for the BEV a high energy cell is more useful as compared to a HEV where high power is more essential. Not only is the chemistry of the cell important in deciding the properties, also the shape of the cell has significant effect in deciding the specific energy and specific power. Currently the cells are shaped into cylindrical, prismatic or pouch shapes which are shown in the Fig. 34. The shape of the cell decides the surface area and volume of the cell. While for high power a bigger surface area is essential so that the lithium ions can be ionized in the electrolyte, transferred from one electrode and intercalated into another, a high energy cell requires a higher volume to store more charge [94]. It can therefore be said that the surface area to volume ratio of the cell is a significant parameter for design. A cell with thin electrodes will provide for bigger surface area whereas a thicker electrode will provide more volume. As the resistance of the cell is inversely proportional to the surface area and directly proportional to the thickness, the high energy cells have higher internal resistance than high power cell and consequently lower energy efficiency. The high energy cell will have higher power losses at high loads as compared to high power cells.



Figure 34 Cell designs (cylindrical, prismatic and pouch) [94]

The cells are connected in series or parallel to create battery packs for BEV. There can be either a large number of small cells or fewer large cells. According to Pesaran et al. [96], using smaller cells has the benefit of lower cost (commodity market), improved safety and high quality production but they suffer from higher integration costs, complicated assembly, a large number of interconnects, lower weight and volume efficiency, lower reliability and costly electrical management. The larger cells have the benefit of lower assembly cost, higher weight and volume efficiency, better reliability though they have higher cell cost, lower quality and difficult thermal management. These are design trade-offs which need to be considered for particular applications. According to Cluzel and Douglas [97], the cell size in the range 40-60 Ah are of good quality currently. They are appropriate for vehicle application.

3.3 Battery modelling

The modern batteries can be modelled in various ways and there are three main types of modelling techniques. The electrochemical model is one of the techniques which describe the dynamic process of chemical reactions occurring on the electrodes based on mathematical method, which can integrally reflect dynamic characteristics of the battery [98]. They consist of partial differential equations with a large number of unknown parameters and do require detailed understanding of the battery design. One such model is the Shepherd model which is a simplified electrochemical model [99].

Another type of battery model is the data driven neural network model [100]. In this case a data set is used for training the model to identify the non-linear battery characteristics during charging and discharging. However the disadvantage of this model is that it requires large amount of data for training and validation.

The third type and one of the more popular one is the equivalent circuit (EC) model. In this case the battery is modelled as a network of resistances and capacitances (RC) to characterize their non-linear behaviour. They usually consist of a voltage source connected with RC elements. The voltage source typically models the open circuit voltage of the battery whereas the rest of the elements model the internal resistance along with other dynamic effects such as polarisation. The EC models are accurate to predict the dynamic behaviour of the battery however they require precise experimental results to parameterize the model. Different authors have used different methodologies to build these models. Zhang et al. [98] use Extended Kalman Filter technique to parameterize the EC model whereas Rahmoun and Biechl [101] use non-linear least squares algorithm.

Among the EC models there are different types with varying complexity. The simplest one is the so called Rint model where there is an open circuit voltage source connected in series with an internal resistance. The open circuit voltage and internal resistance can be specified as function of SOC, temperature and charging or discharging process. According to Rahmoun and Biechl [101] this model is not suitable for any dynamic operation as it does not represent the transient behaviour of Li-ion cells. Another type is the one RC model in which the Rint model is connected in series with a parallel RC network to model the transient behaviour of the cell. This is called the Thevnin model or One Time Constant model. This allows the modelling of one time constant for charging and discharging. Antaloae et al. [102] observe that Li-ion cells exhibit a second longer time constant in practice which reduces the modelling error in longer discharge cycles. This is modelled by adding another RC network to the Thevnin model and is called dual polarisation model or Two Time Constant model. The Fig. 35 shows the circuit of

the three models. According to He et al. [99] and Rahmoun and Biechl [101] the dual polarisation model is the most accurate one for dynamic operations. It is decided to use this type of model in the present analysis.

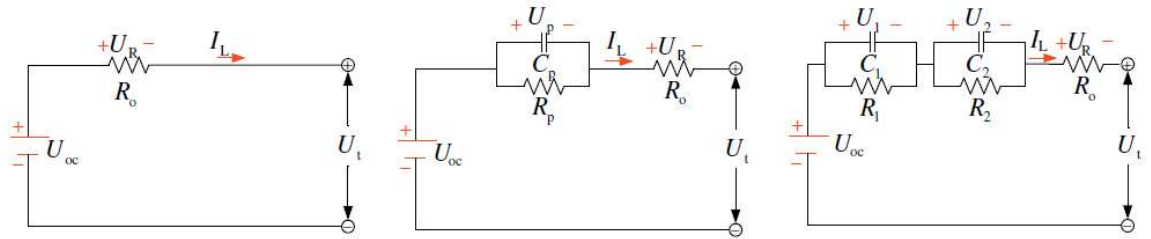
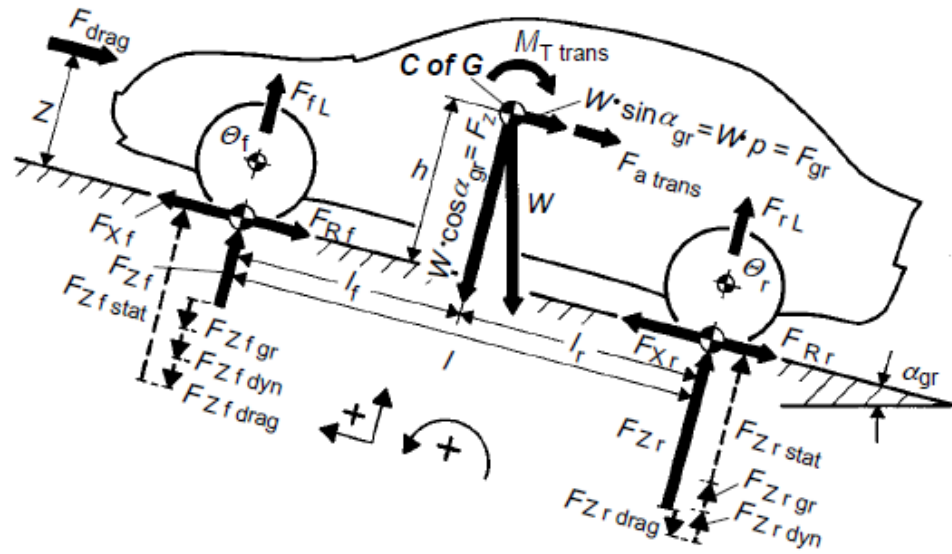


Figure 35 Battery models (Rint, Thevenin and Dual polarisation) [99]

Another important aspect of battery model is the calculation of SOC. The most common method is called coulomb counting where the current is integrated over time to calculate the SOC. For real life application in a battery monitoring system (BMS), this method can introduce errors due to uncertainty over the start SOC and the error can accumulate over time. Another method is the voltage based SOC correction which is again not suitable for BMS application. Other methods which treat the OCV as an internal variable and estimate SOC from the battery model have been developed which are suitable for BMS applications [103]. However for the present analysis the simple coulomb counting method is deemed sufficient as it is a comparative analysis using simulation.

3.4 Vehicle Model

The present analysis deals with the longitudinal dynamics of the vehicle and these are sufficiently and accurately represented by empirical map based models. This type of models can be constructed in Simulink like ADVISOR [104] or PSAT [105]. However there are commercial packages available such as AVL Cruise which can be used to construct them with relative ease [106]. The modular structure of AVL Cruise offers the flexibility in modelling and can perform a variety of tasks such as cycle run, full load performance and climbing performance. It offers the option of both forward and backward simulation and can be linked up with other tools such as Simulink which are more suitable for control system modelling. In the forward modelling approach a driver model is necessary which tries to control the vehicle via pedal movement to achieve the target vehicle velocity. However in the backward approach the calculation is done from wheel to the powertrain. The forward approach is more realistic though the backward approach is faster to run. For this analysis the forward approach is taken. The difference between forward and backward approach is explained in detail [107]. Fig. 36 shows the various forces acting on the vehicle.



W	wight-force vehicle	$F_{Zr drag}$	aerodynamic share, RA
F_{Zf}	axle load front	$F_{Zr dyn}$	dynamic share, RA
$F_{Zf stat}$	statistic share, FA	$F_{Xf(r)}$	traction force, front (rear)
$F_{Zf gr}$	upgrade share, FA	$F_{Rf(r)}$	rolling resistance force, front (rear)
$F_{Zf drag}$	aerodyn. share, FA	$F_{f(r)L}$	lift force, front (rear)
$F_{Zf dyn}$	dynamic share, FA	F_{drag}	air resistance force
F_{Zr}	axle load rear	$F_{a trans}$	inertia force
$F_{Zr stat}$	statistic share, RA	$\theta_{f(r)}$	red. inertia moment FA (RA)
$F_{Zr gr}$	upgrade share, RA	α_{gr}	angle of gradient

Figure 36 Forces acting on a vehicle [92]

A c-segment passenger car is taken as the base vehicle for this study as this is the one of most common mode of private transport especially in Europe. The vehicle is a 5 door hatchback front wheel drive with a kerb weight of 1445 kg. The particulars of the vehicle are mentioned in the Table 4.

Table 4 Base BEV parameters

Parameters	Value
Kerb mass	1445 kg
Gross mass	1884 kg
Frontal area	2.29 m ²
Drag coefficient	0.29
Wheel radius	301 mm
Rolling resistance	0.009

The two time constant model is preferred for the battery and the Li-ion polymer cell modelled in [101] is used for this analysis. The specific energy of the cell is mentioned as 163 Wh/kg by the manufacturer which would classify it as a high energy cell suitable for BEV. It is taken to construct a pack of 98 cells in series giving a nominal voltage of 362.6 V for the base vehicle. This would constitute a battery pack with capacity of 53 Ah and energy of 19.2 kWh, which is similar to the ones used in modern BEVs. The cell model parameters are mentioned at 25° C and that is taken as the working temperature of the pack. The peak pulse current discharge limit is 260 A. Some parameters such as mass of the cell are taken from the manufacturer's website [108]. The mass of the battery pack is modern BEVs is about double the total mass of the cells and similar assumption is used to constitute the battery pack mass for the base vehicle which amounts to be about 225 kg. The auxiliary loads are taken to be 300 W which is a reasonable assumption for the average power consumption related to power requirements for vehicle house-keeping: similar to that stated in [109]. This does not include heating, ventilation and air-conditioning loads. This load is directly added to the EM load at the battery terminals.

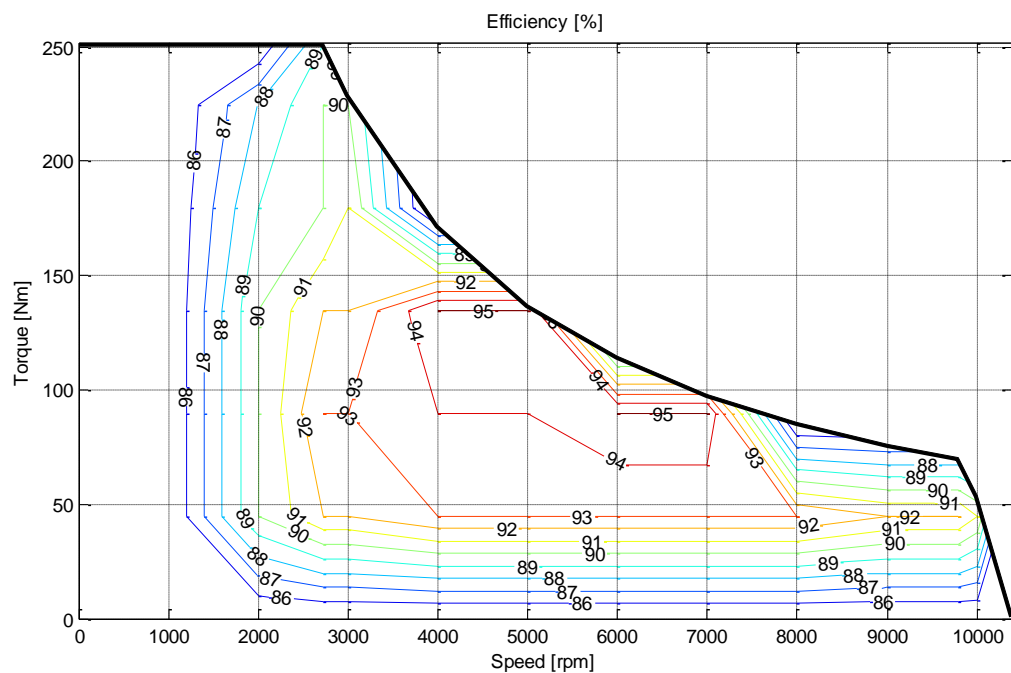


Figure 37 EM characteristics

The EM is a 72 kW machine which is scaled down from the 80 kW machine mentioned in [110] to match the peak power of the battery which is about 77 kW. The maximum torque performance and the efficiency of the EM, including the power inverter in motoring mode are illustrated in [110] and the same is assumed for the generating mode. The rotating inertia of the EM is estimated to be 0.0657 kgm² from its dimensions and mass. The scaled down EM has maximum power of 72 kW, maximum torque of 252 Nm and maximum speed of 10,390 rpm.

The EM characteristics are shown in the Fig. 37 and are assumed the same for all voltages. The EM is connected to a single speed transmission of ratio 7.93, which has an efficiency of 98%. The map based modelling approach is commonly used for the EM in BEVs [111].

There are two operating modes in the vehicle, namely motoring and braking. The motoring control is relatively straightforward. For motoring purposes the driver controls the accelerator pedal to match the desired vehicle speed and that is converted to the load signal for the EM which powers the vehicle forward. The braking mode requires a strategy different from the conventional vehicles since there is possibility of regenerative braking. The regenerative braking strategy used is similar to the one mentioned in [112]. The required braking torque is calculated from the brake pressure signal which comes from the brake pedal controlled by the driver to achieve the desired deceleration. This brake torque is compared to the available EM generating torque and the brake torque limit of the front axle. The minimum of the three values is taken as the desired EM torque which is converted into the load signal for the EM. If at all the brake torque requested by the driver is higher than the available EM torque, the rest is provided by the mechanical braking.

In AVL Cruise the brake pressure signal is same for all the four brakes and the brake size for the front and rear brakes, is dependent on the mass distribution of the vehicle. In this case an equal mass distribution for the front and rear axle is assumed. This is a reasonable assumption as the heavy batteries are usually in the rear of the vehicle. The dimensions of the brake are used to compute the brake torque. The model takes into account the change in axle load due to acceleration or deceleration. This front axle load which is a model output, is used to compute the front axle load limit. According to most standard driving cycles, the maximum deceleration is about 0.4g which is easily achievable by braking only the front axle if the standard road conditions, which have an average friction coefficient of 0.8-0.9 [4], are assumed. It can be seen in the Fig. 38, that the maximum brake force demand for various drive cycles which is calculated by using the maximum deceleration rate and neglecting the resistance force, is lower than the front axle brake limit calculated under steady state conditions, for all drive cycles except HYZEM road cycle.

With regenerative braking a few more conditions have to be incorporated to protect the EM and the battery. It is not easy for the EM to generate electricity at low vehicle speed which implies low EM speed, because of the very low electric motive force (voltage) generated at that speed [112]. Therefore the EM is used for regenerative braking above 10 kph. Another factor is the battery SOC. At close to full SOC the battery is protected from over charging by

limiting regenerative braking and to include this effect in the present analysis the regenerative braking is only allowed up to 90% SOC. Fig. 39 shows the model schematic in AVL Cruise.

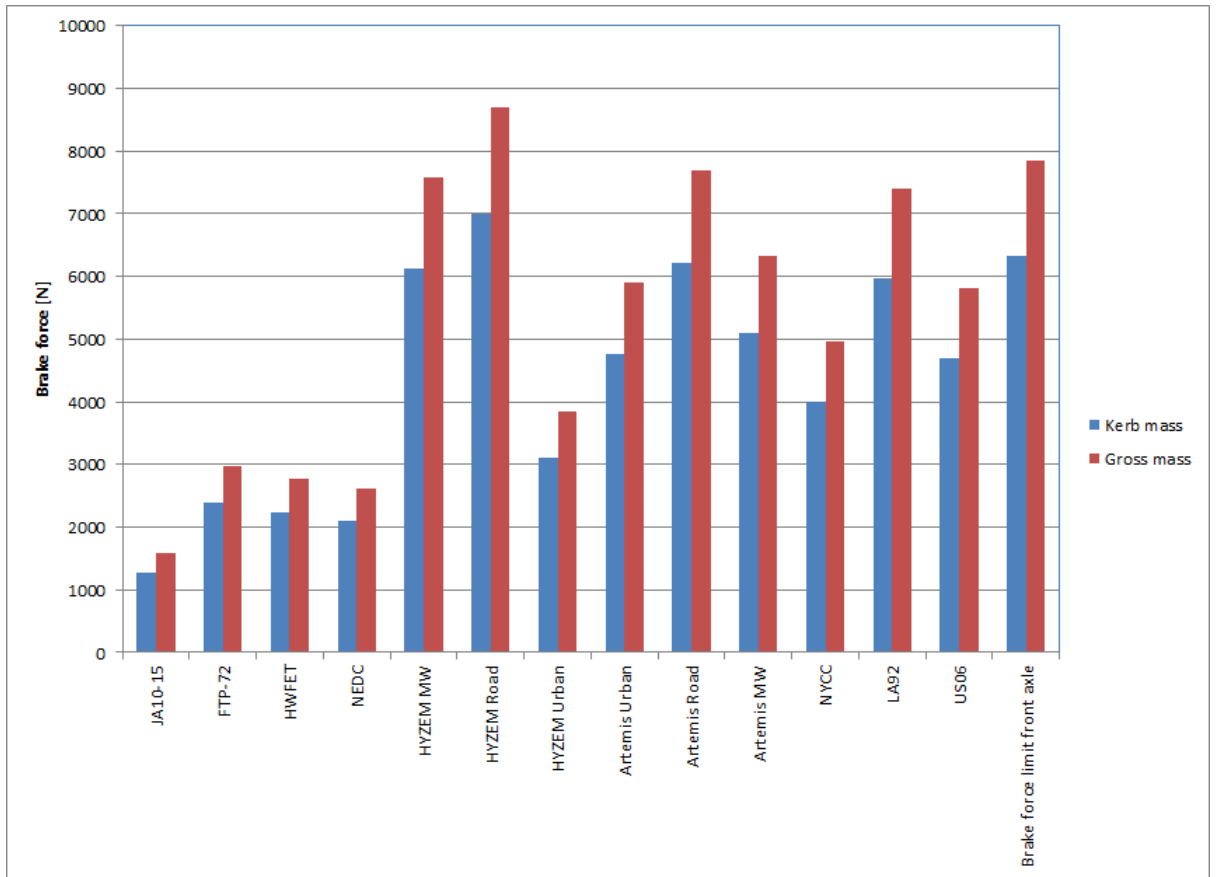


Figure 38 Brake force

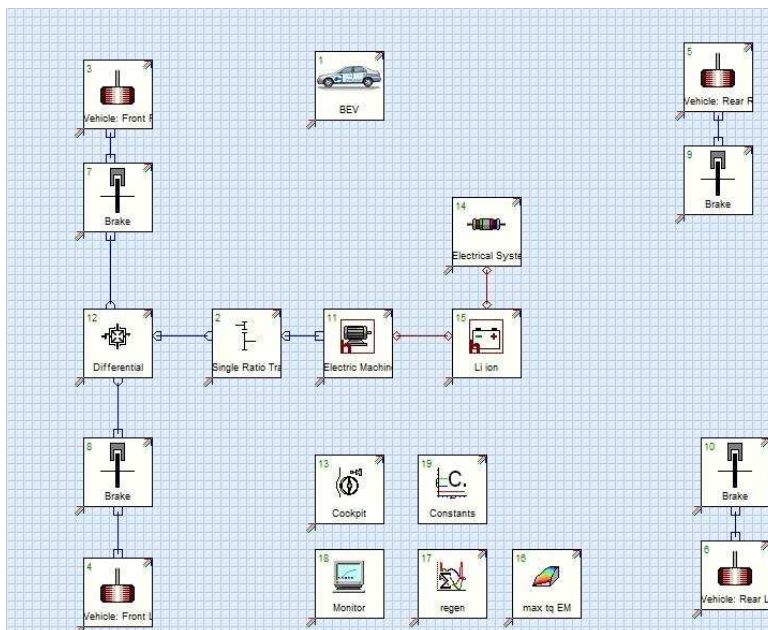


Figure 39 BEV model

3.5 Drive cycle simulation

The standard homologation drive cycles which are used for the fuel consumption simulation include the NEDC, FTP-75, Highway Fuel Economy Test (HWFET) and the Japanese 10-15 (JA1015) drive cycle. As mentioned before the simulations are carried out in the forward simulation mode and at steady state temperature of 25° C. The wheel slip is not considered. The maximum simulation time step is taken to be 10 ms which gives sufficient accuracy. The vehicle test weight during the simulations is taken as the kerb mass plus an additional mass of 75 kg to simulate the driver. The simulations are carried out at initial SOC of 100% and 90% to show the benefit by regenerative braking. Table 5 shows the result of the simulation.

Table 5 Results for homologation drive cycles

	Energy consumed at battery terminals [kWh/km]		Improvement in Energy consumed [%]	Battery Round trip Efficiency [%]
	Start SOC 100%	Start SOC 90%		Start SOC 90%
NEDC	0.1409	0.1083	23.1	90.9
FTP-72	0.1454	0.0963	33.7	89.7
JA1015	0.1438	0.0947	34.1	92.3
HWFET	0.1210	0.1148	5.1	93.9

From the Table 5 the effect of regenerative braking can be easily seen in the energy consumption figures. Considerable improvement is seen in all the cycles where the energy consumption reduces by 23-34% with regenerative braking, except HWFET. The lowest benefit of only 5% is seen in HWFET since it is highway cycle with limited opportunity for regenerative braking.

Another important parameter which is calculated for the cycles is the cycle round trip (RT) battery efficiency. One of the model outputs is the power loss in the battery primarily due to its internal resistance and other factors such as polarisation. Integrating this power loss over the cycle time gives the energy lost in the battery and with the net energy output at the battery terminals known, the round trip battery efficiency is calculated by taking ratio of net energy output to the sum of net energy output and energy lost. It can be seen from Table 5 that the battery gives round trip efficiency of about 90% or more on all the standard drive cycles.

3.6 Real world driving cycles

A problem with the homologation cycles mentioned in the previous section is that they do not represent the real world driving situation. They are made for testing vehicles on the chassis dynamometer and have lower acceleration and deceleration rates than what is encountered in real world driving. This is done to make the testing easier to perform. However in the last 10-15 years a lot of work has been done to create real world driving cycles such as Artemis cycles [113] and HYZEM cycles [114]. Other real world cycles such as US06, LA92 and New York City Cycle (NYCC) have also been created. The US06 is an aggressive highway driving cycle, the LA92 represents the extra-urban driving conditions in California and NYCC represents the urban driving condition in New York. Fig. 40 shows the average velocity and root mean square (RMS) acceleration behaviour for these driving cycles.

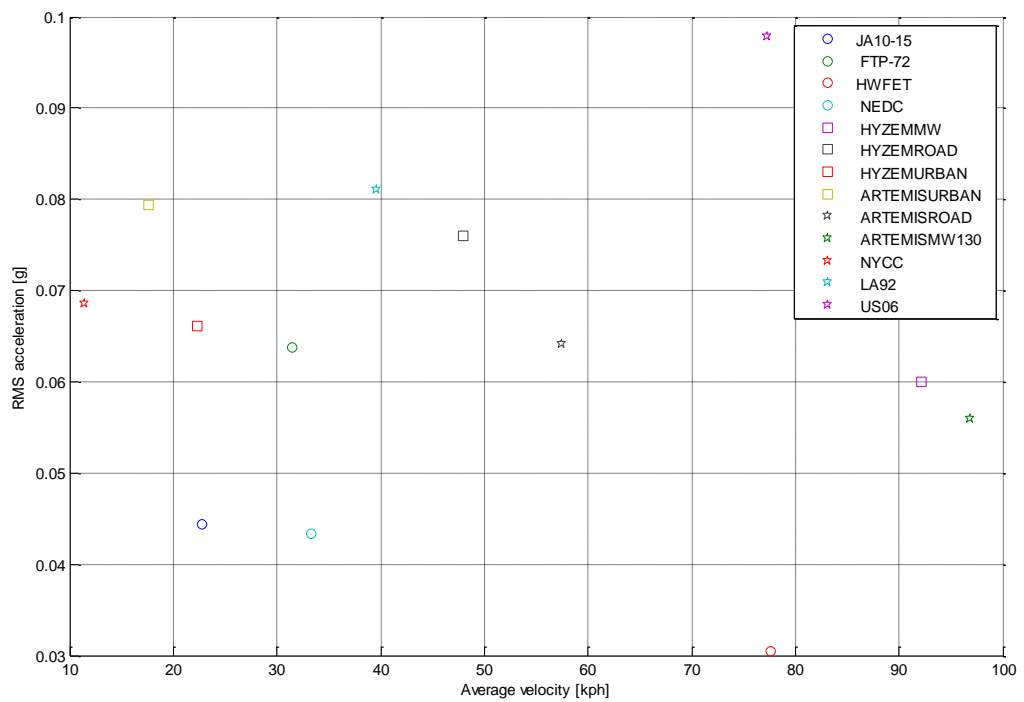


Figure 40 Drive cycle comparison

In the Fig. 40, the results of a statistical analysis of cycles show that the homologation cycles have much lower acceleration than the real world cycles. The US06, LA92 and Artemis urban (AU) cycles seem to have the highest acceleration over the entire speed range. Only the Artemis motorway and HYZEM motorway cycles seem to have higher average velocities than the rest of the cycles. For the present analysis the US06, LA92 and Artemis urban cycles are taken as reference for the real world cycle usage.

Table 6 Real world drive cycles results

	Energy consumed at battery terminals at start SOC 90% [kWh/km]	Battery Round trip Efficiency [%]
US06	0.1546	78.6
LA92	0.1167	82.4
Artemis Urban	0.1100	83.6

Table 6 shows the results of vehicle energy consumption for the US06, LA92 and AU cycle with start SOC 90%. As can be seen the energy consumption of these cycles is higher than most of the homologation cycles though the more interesting result is the overall cycle round trip battery efficiency which is significantly lower. It can be seen that the RT battery efficiency in these real world cycles varies from 78-83% as compared to at least around 90 % for the homologation cycles. The worst case is the US06 cycle where it is about 78%. Fig. 41 shows the trend comparing RMS acceleration of cycles vs. battery RT efficiency. It can be broadly seen that as the RMS acceleration increases the efficiency goes down, hence there is a reasonably good correlation. It is expected that in more demanding terrain such as hills the efficiency could be further reduced. The one way battery efficiency also follows a similar trend.

Table 7 Average power results

	Average Power [kW]	Ratio of peak to average power	Battery round trip efficiency with average power [%]
US06	11.95	5.95	96.2
LA92	4.62	14.7	98.6
Artemis Urban	1.94	23.8	99.4

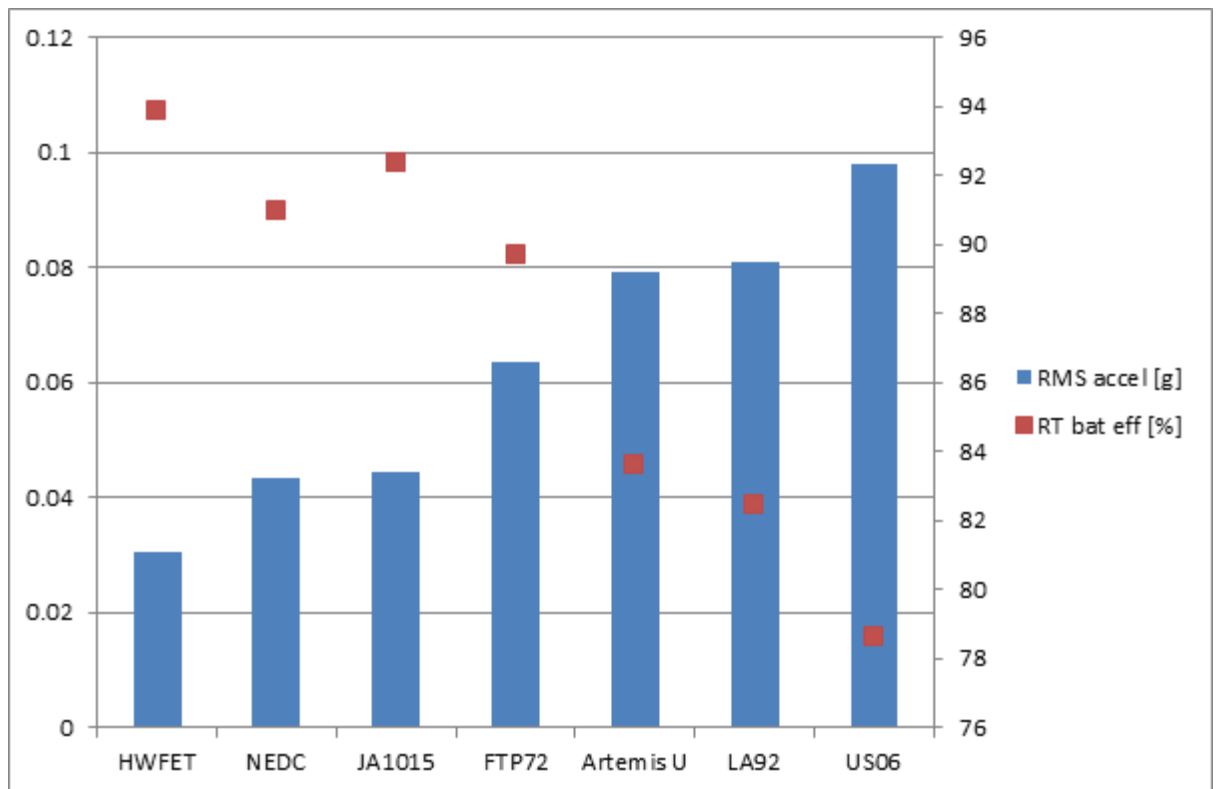


Figure 41 RMS acceleration vs. RT battery efficiency

The average power consumed during these cycles is calculated by dividing the energy consumed by the cycle duration. Table 7 shows the average power consumed during these drive cycles and the simulation results when the battery load is fixed to the average power for the duration of the cycle. The peak power is many times the average power and the worst case is the AU cycle where it is almost 24 times the average power. However when the average power is applied to the battery for the duration of the cycle, the net energy output from the battery terminals is the same as before but the difference is in the cycle roundtrip battery efficiency which is more than 96% for all the cycles. It is more than 99% for the AU cycle and 96.2% for the US06 cycle. Thus it can be seen that the power losses inside the battery can be theoretically reduced significantly if a low constant load is applied instead of the actual dynamic load. This presents a possibility for improving the energy efficiency by utilizing a secondary storage device for power handling.

Another result to observe is the powertrain efficiency which is defined as the ratio of the power at the wheels to the power output of the battery during motoring and reverse during regenerative braking. The powertrain efficiency during motoring is calculated for the cycle by integrating the traction power at the wheels during motoring and dividing that by the energy output from the battery terminals. Similarly the powertrain efficiency during brake regeneration is calculated by taking the energy input at the battery terminals and dividing it by

the integral of the brake power demand at the wheels during brake regeneration. The results show that in cycles with low average speed and low RMS acceleration the positive and negative powertrain efficiencies are lower. Fig. 42 shows the positive powertrain efficiency for various cycles (bubble size represents RMS acceleration [g]).

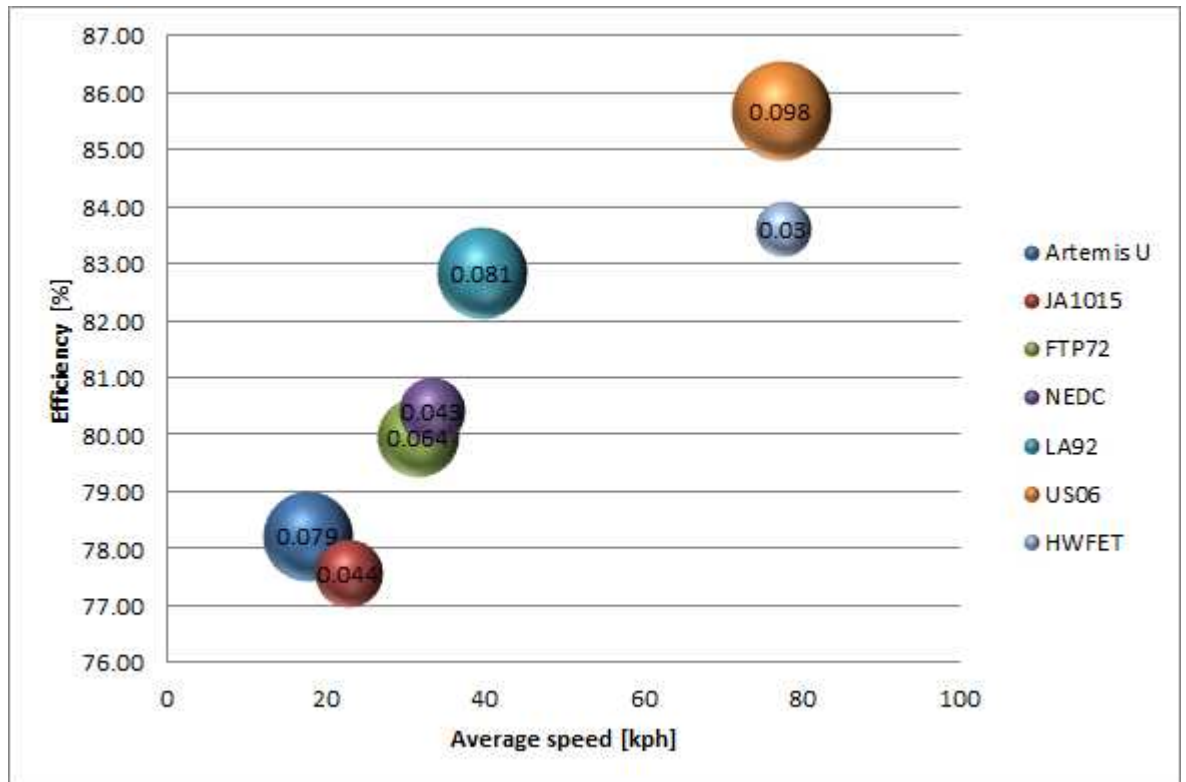


Figure 42 Powertrain efficiency

In the very low average speed cycles such as JA1015 and Artemis Urban, the efficiency seems to be impacted little by average speed and RMS acceleration values. However, in the lower average speed region, say up to 30 kph, the powertrain efficiencies seem to be impacted less by RMS acceleration and more impacted by average speed e.g. in case of JA1015 and NEDC. In the high average speed region, the powertrain efficiencies are affected by RMS acceleration though the impact is smaller e.g. in case of US06 and HWFET. The reason for the higher efficiency values is apparent from the EM efficiency map, which is the major contributor towards powertrain efficiency, where the higher efficiency is observed towards the maximum power region and at lower speeds especially below 1000 rpm the efficiency is relatively low (around 85%) and independent of torque.

The Fig. 43-45 show the time weighted operating points of a drive cycle plotted over the efficiency map of the EM [115] (the bubbles represent the operating points with their size representing their residency in the cycle). It can be seen in the Fig. 43 that for AU cycle, nearly 50% of the time, the EM operates in the below 1000 rpm speed region and in that region the

efficiency is independent of torque. In the higher speed region, they operate in low torque regions and that part of the operation might be benefited by downsized EM.

Looking at the similar Fig. 44 and 45 for LA92 and US06 cycle it is clearly seen that the more points are operating in the higher efficiency regions and higher speed regions as compared to Artemis urban cycle. The higher speed points would benefit from a downsized machine as that would push the high speed and low torque points in the higher efficiency zones. Of course the US06 cycle has more points in the high efficiency region than the LA92. Thus utilizing a power handling device, which is able to transmit power to the driveline directly, would allow the downsizing of the main EM, which would also help to reduce cost. Flywheel connected to the driveline with a mechanical CVT is one such option.

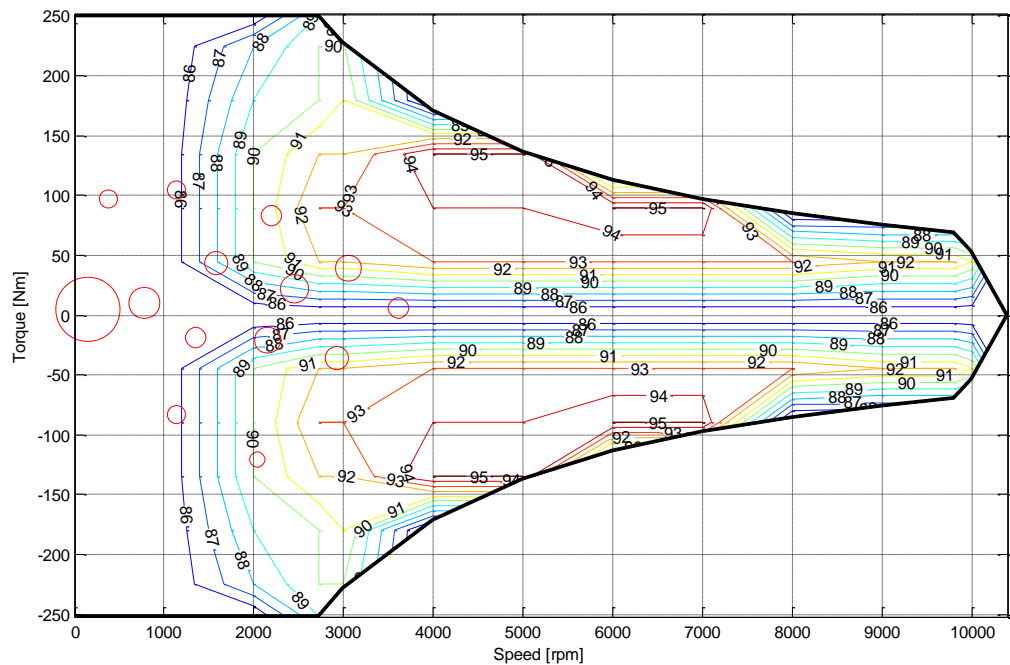


Figure 43 AU operating points

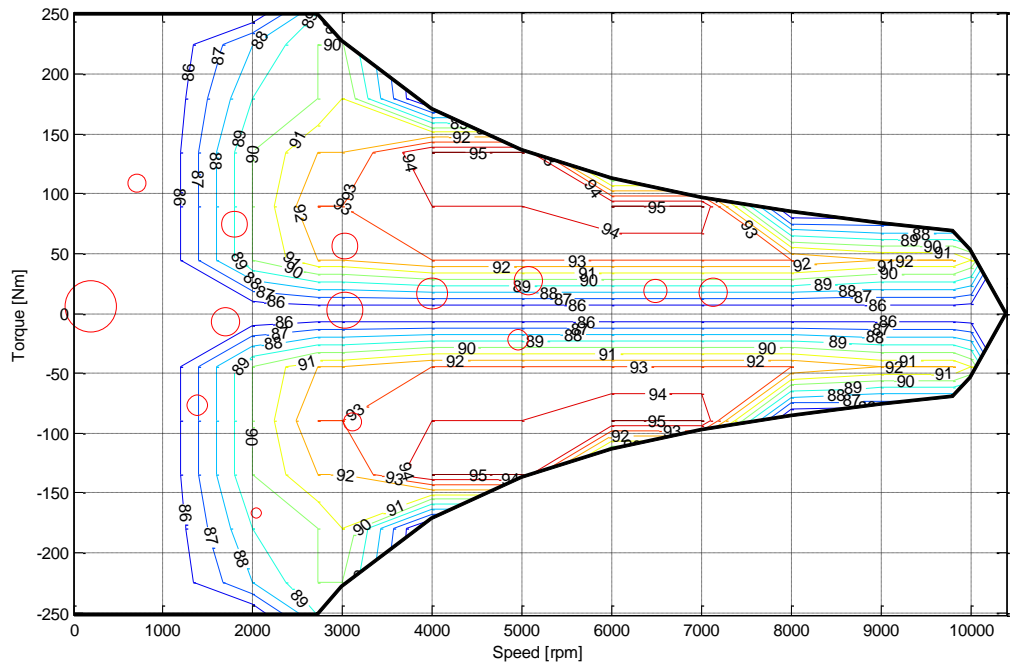


Figure 44 LA92 operating points

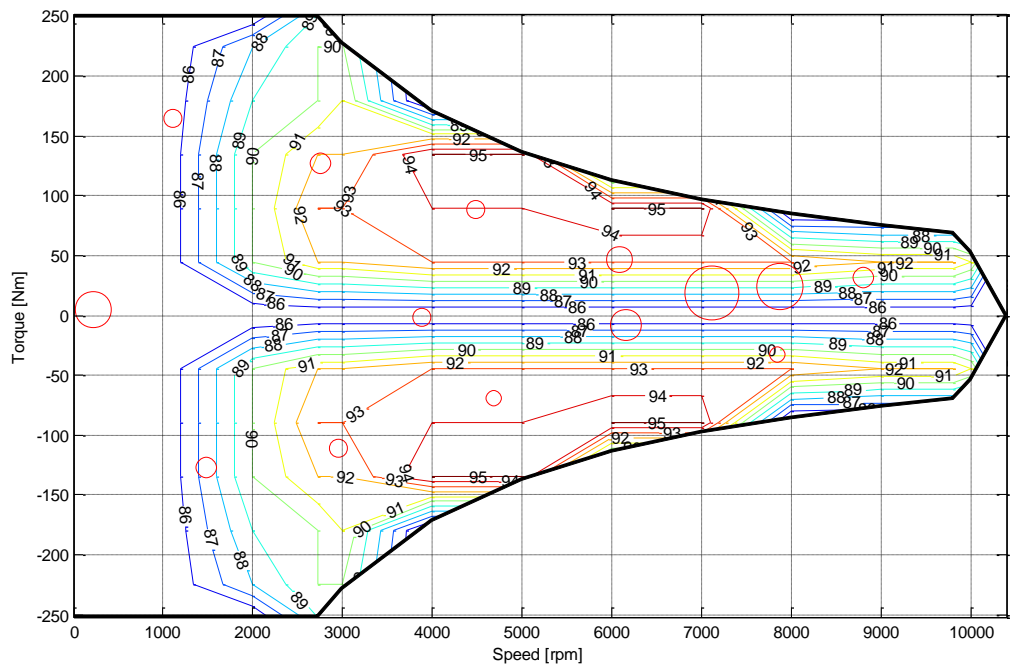


Figure 45 US06 operating points

4 Hybrid vehicle

This chapter is structured as follows. First the sizing of the flywheel is described supported by real world usage data analysis. This is followed by the design of the transmission system which is used to connect the flywheel with the driveline, which includes a fundamental analysis of CVTs for FESS. Finally the HV, its layout, components and various parameters are presented.

4.1 Flywheel in Battery Electric Vehicle

As discussed previously, the most crucial element of the BEV is the battery. The battery is the most expensive and heaviest component of the powertrain. The energy stored in the battery is directly related to the range of the BEV. The battery power is related to the EM power which is usually based on the performance requirements of the vehicle such as the acceleration and gradeability. The performance of the battery strongly depends on its state of charge and operating temperature. Usually the internal resistance is much higher at low and slightly higher at very high SOC implying the battery efficiency is poorer in these regions. The battery is very sensitive to temperature and shows significantly poorer performance at high ($>45^{\circ}\text{C}$) and low ($<-10^{\circ}\text{C}$) temperatures [18]. At these temperatures the effect of peak currents on the battery performance is much worse. Temperature and depth-of-discharge dependent battery aging effects affect the cycle life of the battery and so does the usage pattern. Driving the BEV in heavy traffic can cause significant battery heating and aging [116].

The main benefits of the flywheel in hybrid energy storage (HES) with battery are as follows:

- Improve energy efficiency of the battery by taking care of the peak loads, which would reduce losses in the battery
- Increase life of the battery by reducing number of cycles
- Allow the optimisation of battery as pure energy source such that no trade-off has to be made between energy and power density leading to an increase in driving range
- Reduce the cooling requirements of the battery at high temperature and protecting the battery and associated electronics during vehicle start-up in cold conditions when the battery resistance is high
- The mechanical transmission will allow the downsizing of main EM and inverter
- Allow the powertrain to achieve better regenerative braking efficiency by avoiding energy conversion

The aim of the flywheel is to improve energy efficiency of the battery by taking care of the peak loads, which would reduce losses in the battery and increase range of the BEV. This would also lead to improvement of battery life. This is termed as load levelling whereby the

battery handles the average loads and the flywheel handles the peak loads. The other aim is to perform regenerative braking which could achieve higher efficiency due to absence of energy conversion. A third possibility could be reduction of the main EM size. In a BEV the maximum torque performance of the EM is decided by the vehicle launch and acceleration requirements whereas the lower bound of the design torque limit of the EM decides the hill climbing and top speed ability of the vehicle [117-118]. By utilizing a flywheel in combination with a mechanical CVT these performance requirements might be met completely or partially. Note that this is only possible with a mechanical CVT driven flywheel as with any type of electric transmission the prime mover has to be sized to carry the entire power.

The energy capacity of the flywheel can be sized in a number of different ways. Santiago et al. suggest using particular drive cycles, usually the homologation cycles such as NEDC or FTP to size the flywheel [119]. In this approach they calculate the average power required in FTP cycle and calculate the size of the flywheel based on the delta power between the average and the actual. The battery is providing constant fixed power and the flywheel is taking care of the transients during the cycle. The disadvantage with this approach is that the control strategy is already fixed; the cycles are specific and are assumed to be known at the start. Also these cycles do not represent real world conditions.

In another study, where the battery and DLC constitute the HES for an EV, DP has been used to size the battery and the DLC using real world driving data to minimize the losses in the HES [15]. Two configurations are compared to the battery only EV and both the HES configurations show reduced losses compared to the original BEV. This is an interesting approach though is difficult to adapt to the current study as the losses in the mechanical transmission of the flywheel are unknown at this point.

Gao et al. suggest another way of sizing the flywheel, which is according to the energy needed to accelerate the vehicle from 0 to some final speed like 100 kph which is usually lower than the maximum speed of the vehicle in a specific time [120]. They also state that if the flywheel is sized according to this acceleration requirement, it would meet the requirements of the standard drive cycles as the increase in KE in any period, equal to the 0 to 100 kph acceleration duration, during the cycle is less than the acceleration requirement. This is corroborated by analysis further.

Another way is that the energy stored in the flywheel should be equal to the KE of the vehicle at some specific cruise speed if the flywheel is to be used mainly for regenerative braking [77]. A third way would be sizing the flywheel according to certain deceleration requirement directly. Since in the FWBEV the flywheel would be used for storing regenerative brake energy

and load levelling which might entail charging the flywheel from the battery during low vehicle power demand, the flywheel has been sized according to the energy needed to accelerate the vehicle from 0 to 100 kph.

Using the base vehicle model described in the previous chapter, the vehicle speed profile going from 0-100 kph is calculated. The time take for the vehicle to do this acceleration is 10.99 s. Using the information of the BEV, a simple calculation is done in Simulink to calculate the energy needed to perform the targeted acceleration. The total mass of the HV used for this calculation is taken to be base vehicle mass, which is kerb mass plus one driver mass of 75 kg, and the flywheel and CVT system mass. The assumed mass of the flywheel and the CVT system is taken to be 40 kg which is a good estimation for road cars [121]. Table 8 gives the HV parameters. According to the calculation, for the HV to achieve the same acceleration performance as the base vehicle, the required energy is 0.192 kWh. This is a reasonable estimation of the energy required and assuming a conservative efficiency of 75% for the flywheel and transmission system the energy required to be stored in the flywheel is 0.256 kWh. The peak input power for the system would be around 96 kW for the 0-100 kph operation.

Table 8 HV parameters

Parameters	Value
Target acceleration [0-100 kph]	10.99 s
Vehicle mass	1560 kg
Frontal area	2.29 m ²
Drag coefficient	0.29
Wheel radius	301 mm
Rolling resistance	0.009

This is the maximum useful energy or the energy capacity of the flywheel. Flywheels are normally categorized as high speed with a maximum speed over 20,000 rpm. Maintaining a reasonable flywheel maximum speed of 30,000 rpm, which is much lower than the Flybrid flywheel maximum speed of 64,500 rpm used in Formula 1 KERS [121] and is closer to the maximum flywheel speed taken by others for similar class of vehicle [122], and taking the ratio of maximum to minimum flywheel speed as 2, the minimum flywheel speed comes out to be 15,000 rpm. This gives inertia value of 0.249 kgm² with an energy capacity of 0.256 kWh.

4.2 Road Data Analysis

The road data analysis has been performed to validate the flywheel requirements during real world usage. For this purpose real world car usage data has been downloaded from [123]. The data has been gathered from drivers between 2005 and 2012 from various locations in the US and in Europe and comprises of 420 files. The vehicles covered are mostly passenger cars. The data has been acquired from global positioning system (GPS) of the vehicles and includes the vehicle speed and more crucially the road elevation. The total measured distance is about 23,000 km.

The data has been analysed in Matlab. The data has been cleaned to remove irregularities which come with real world measurements. Trips less than 1 km have been removed. The total number of trips is 746 after data processing. The road elevation data from global positioning system (GPS) is quite noisy. To clean the data, it has been filtered and further it has been assumed that the elevation changes linearly in road span of 100m. The maximum road gradients recommended are in the range of 13% for urban roads [77] and this has been taken as the maximum gradient for the data. Fig. 46 shows the comparison of the data before and after processing.

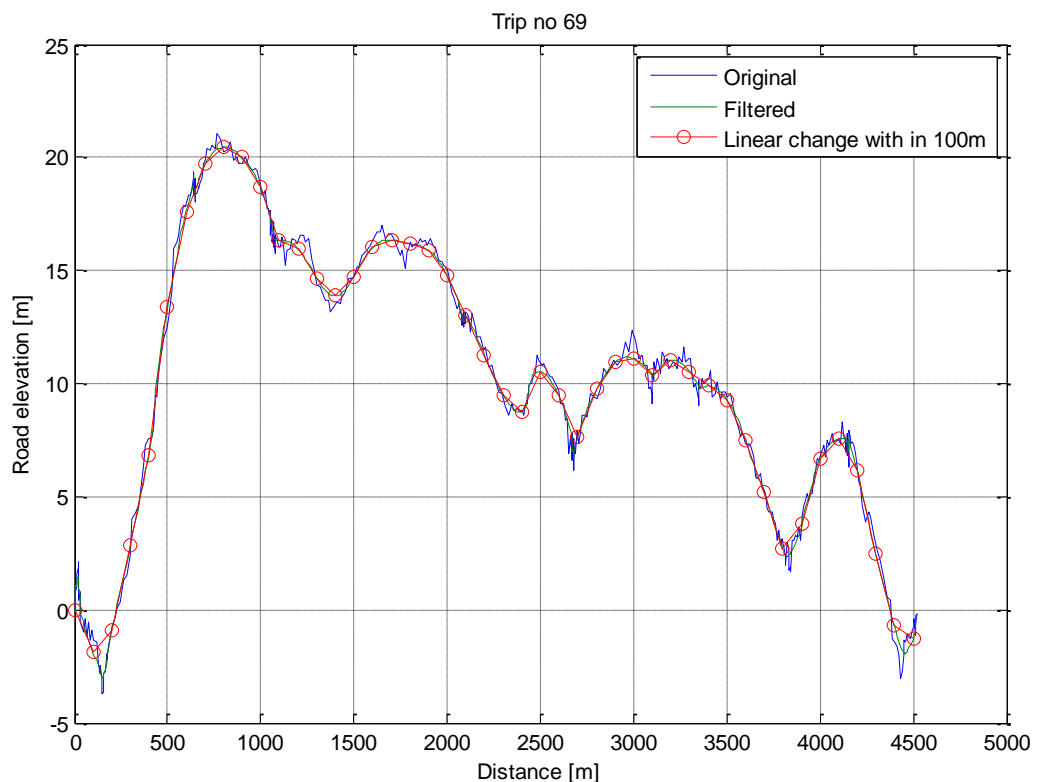


Figure 46 Elevation data

The Fig. 47 shows spread of average speed of the trips. It can be seen that the majority have trips have low average speeds which would indicate that these are urban trips. Further Fig. 48 and 49 show the distribution of trip duration and trip distance. Again it can be noted that most trips are less than 30 min in duration and 20 km in distance travelled. Another interesting comparison is the Fig. 50 showing average velocity and root mean square acceleration. It can be clearly see that majority of trips have the RMS acceleration between 0.05-0.1g, which is the same case for the real world cycles discussed in the previous chapter. Further Fig. 51 shows the RMS gradient vs. average velocity for the trips. Naturally majority of the higher gradient trips occur at lower average velocities. Also more than 44% of the trips have a RMS gradient value of more than 2%.

Further the power demand is calculated using the vehicle information during each trip. Fig. 52 shows the ratio of peak power to average power for the trips. The average power is calculated by integrating the instantaneous power over the entire cycle and dividing the resulting energy by the cycle duration. During the average power calculation, it is assumed that all the brake energy is regenerated. As it can be seen in Fig. 52 the peak power is many times the average power in real world driving which also supports the utilization of a power handling device. Further a negative power demand signifies a braking event for the vehicle. Using this information the braking events in a trip are identified and the energy which would need to be dissipated by brakes is calculated. From this calculation, a total of 69,537 braking events amounting to 746 kWh are found out whose distribution is given in the Fig. 53. Out of these events there are a mere 56 events amounting to 15.7 kWh where the energy dissipated is more than 0.20 kWh per event. Note all the power calculations are done at the wheel.

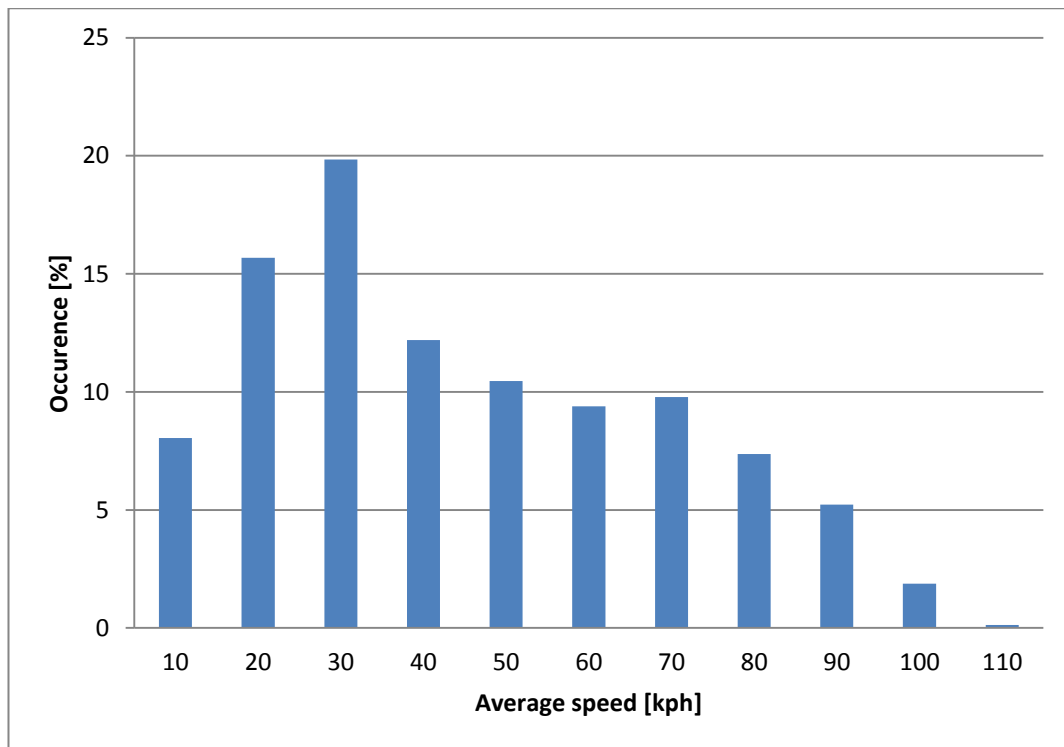


Figure 47 Average speed distribution

The Fig. 53 shows the fact that energy dissipated in most braking events is relatively small. Thus it can be concluded that the flywheel is adequately sized to perform regenerative braking during real world usage. One must note the fact that not all the energy which is dissipated during braking is recoverable. The regenerative braking usually takes place on two wheels rather than four so some energy will be lost. Also the power required during heavy braking events is very high and it is difficult to capture sufficient energy during those events though they occur rather infrequently.

During most real world analysis or cycle analysis the effect of elevation is disregarded. The same analysis was repeated by disregarding the elevation. In this case the total braking events are 67,051 in number which amount to 613.3 kWh of energy. The braking energy is 17.8% less than when gradient is considered. By considering gradient, a downhill slope would give more chance of brake regeneration during deceleration and similarly an uphill slope would give less.

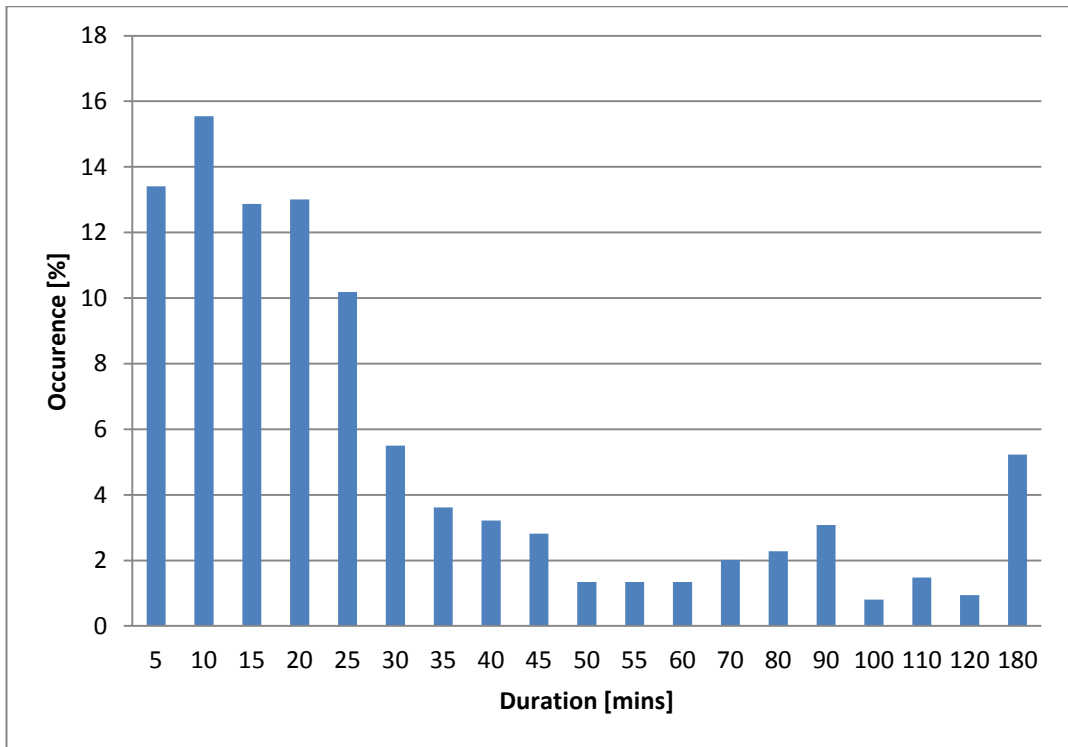


Figure 48 Duration distribution

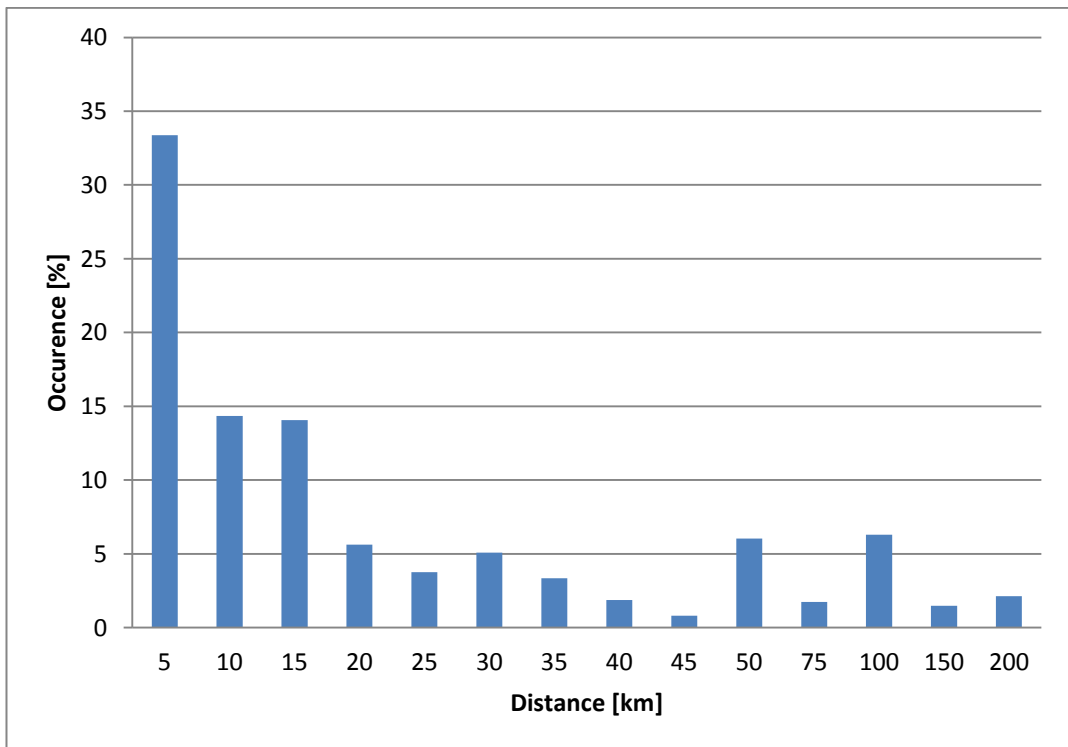


Figure 49 Distance distribution

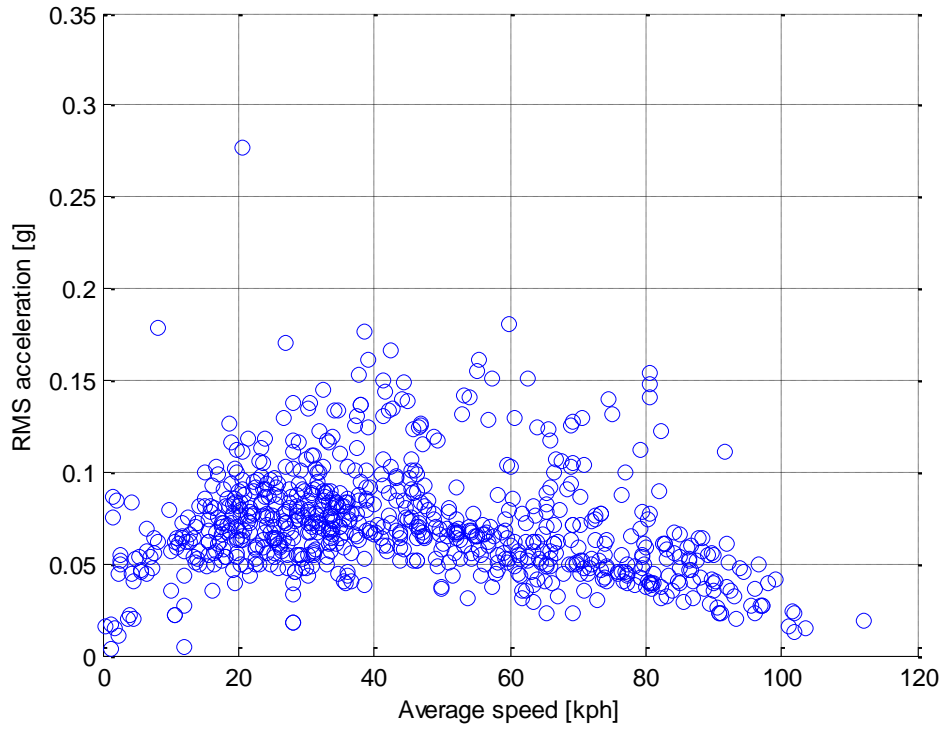


Figure 50 Average speed vs. RMS acceleration

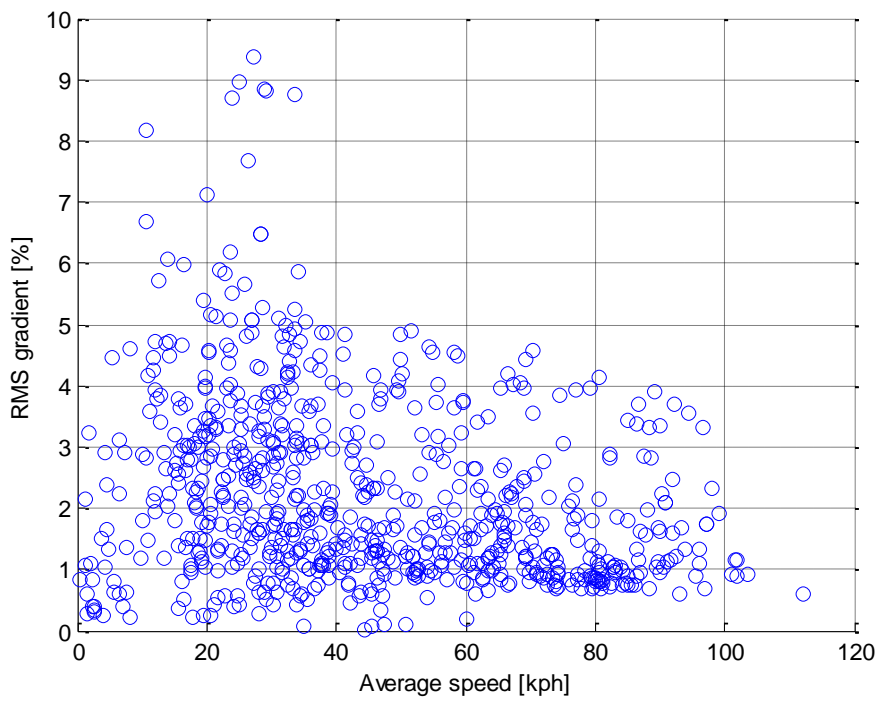


Figure 51 Average speed vs. RMS gradient

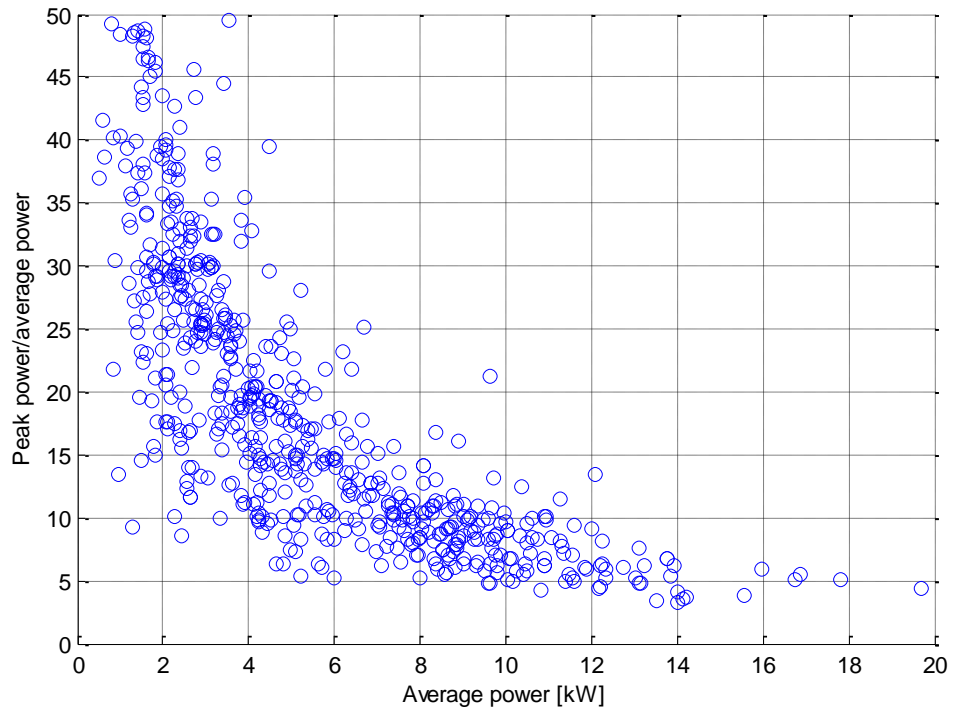


Figure 52 Ratio of peak to average power vs. Average power

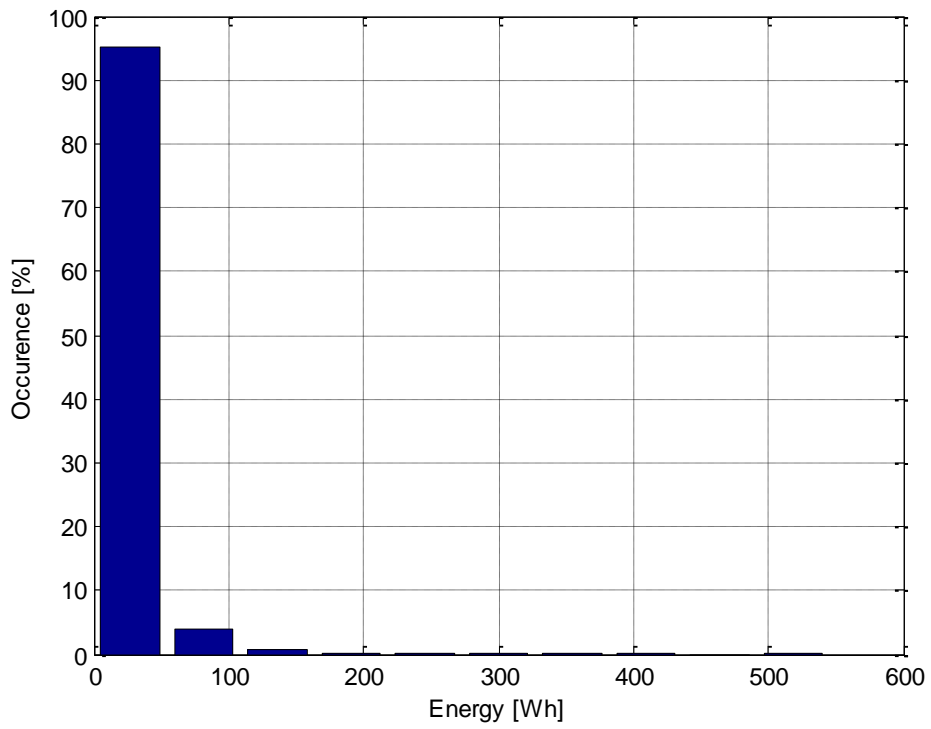


Figure 53 Distribution of brake events

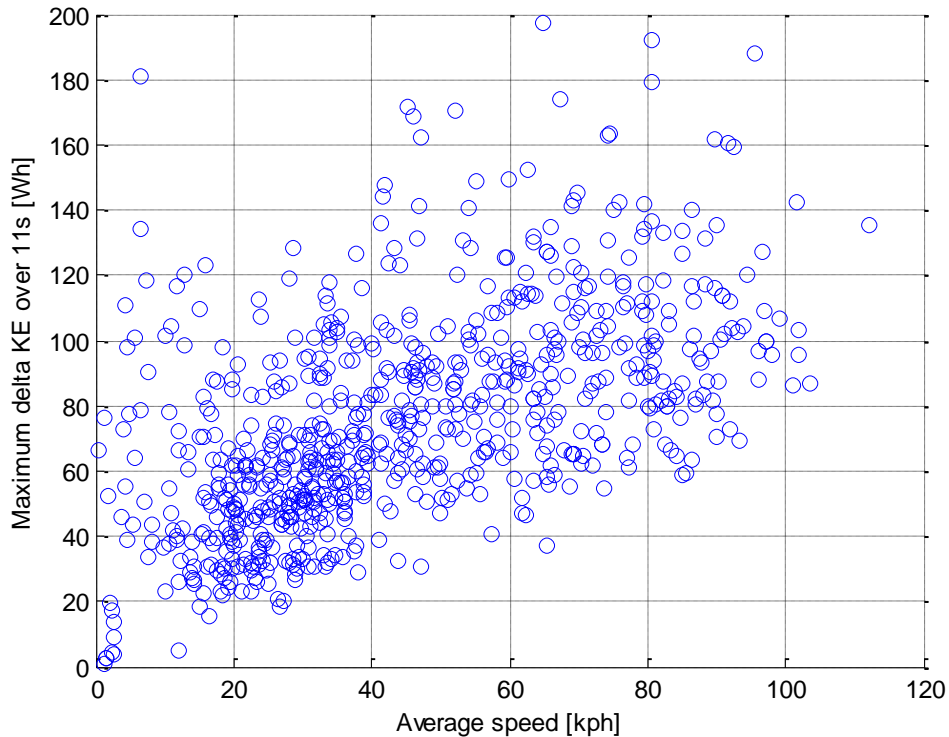


Figure 54 Maximum change in KE over 11 s vs. Average speed

Further Fig. 54 shows the maximum change in the KE of the vehicle calculated at intervals of 11s which is roughly the time taken to accelerate the vehicle from 0-100 kph. The KE in the vehicle at 100 kph is about 167 Wh and that would have been the ideal energy capacity of the flywheel if one was to disregard resistances and inefficiencies. As it can be seen from the Fig. 54, there are hardly any trips where the maximum change in KE over any 11s period is above 167 Wh. Thus it can be said that the flywheel is adequately sized to meet any acceleration requirement during driving. The above analysis supports the flywheel size chosen. The final flywheel capacity is taken to be 256 Wh.

4.3 Transmission Design

In order to connect the flywheel with the vehicle drive line, a suitable means is needed which would allow the flywheel to vary its speed continuously, in other words a CVT is needed. One main difference between the CVT used in conventional vehicle as compared to the ones required for flywheel energy storage system is that they have to be bi-directional and highly efficient in both the directions. Besides the efficiency, the ratio range which is defined as the maximum to minimum speed ratio is a very significant parameter of the CVT.

There are different types of variators and the most common ones used in automotive application are the rolling traction drives and the belt drives. Fuchs et al. [124] and Srivastava and Haque [125] have given a detailed review of the toroidal variator and the belt type

respectively. However the disadvantage for these variators is that their ratio range is very limited. Currently most designs have a ratio span from around 0.4 to 2.4 giving a ratio range of 6, which is generally not sufficient for a flywheel system. Their efficiencies are usually lower than fixed ratio gearing.

The PSCVT has traditionally been used to improve the efficiency of the variator. The essential elements in a PSCVT are variator and PGS. The power flows and kinematics of a lossless PGS have been explained in great detail by White [126]. Further a methodology to create the mechanical efficiency of the two degree of freedom PGS has been described by Pennestri and Freudenstein [127]. The advantage of White's [126] analysis is that it does not assign specific branches of the PGS to its general kinematic equation thereby leading to a set of equations that can be applied to any PGS configuration within the PSCVT.

The PSCVT can be designed to achieve the desired speed ratio range and high efficiency by increasing its complexity. A number of authors have discussed the concept of PSCVT (White [126, 128], Yu and Beachley [129], Hsieh and Yan [130-131], Mangialardi and Mantriota [132-133], Mantriota [134-138], Fussner and Singh [139-140]). Either these have been discussed as lossless systems or as one directional systems. Only a few authors (Beachley et al. [141], Martinez-Gonzales [77], Bottiglione and Mantriota [142]) have partly discussed the PSCVT for a FESS. Martinez-Gonzales [77] applied White's [126] treatment of PGS ratio to the design method for a general single regime input coupled PSCVT presented by Fussner and Singh [133] to design a single regime PSCVT for FESS.

The following section discusses the PSCVT concept for a FESS and the various modes of operation possible including power recirculation and multi-regime mode. The technique used by Martinez-Gonzales [77] is extended to design single as well as multi-regime PSCVTs to meet the desired speed ratio coverage for FESS. An application of the treatise of Pennestri and Freudenstein [127] is used derive equations specifying ratio of variator to input power and efficiency for the PSCVT in both directions of the power flow including the efficiency of the variator, fixed gears and PGS for power recirculating and multi-regime systems. The resulting simple methodology can be applied to design a transmission for FESS to provide any required speed ratio coverage and predict its efficiency in both directions of power flow.

4.3.1 Kinematics of PSCVT

As mentioned before, the power flows and kinematics of the PGS have been explained in great detail by White [126]. For a PGS, the basic ratio R can be defined as the ratio of speeds of any two shafts when the third one is held stationary. With different members being taken as the input, output and the stationary element, six ratios can be defined, though they can be easily

derived from one another. In this analysis, like that of White's [126] the PGS members will not be specifically defined and generalised equations will be created. The Fig. 55 shows the general PGS with three branches labelled as 1, 2 and 3. In Fig. 55 and all the figures describing the PSCVT described in this section and the appendix, the arrows signify power. The sign convention is that power flowing into the system is taken as positive and the power flowing out of the system is taken as negative. Equations 17-18 define the basic ratio. Equation 18 of the basic ratio R is kept the same throughout the paper. The lossless PGS in equilibrium is defined by equations 19-21. In all equations throughout this section and the appendix P , n and T signify power, speed and torque respectively.

$$R = \left(\frac{n_3}{n_1} \right)_{n_2=0} \quad [17]$$

$$R = \frac{(n_3 - n_2)}{(n_1 - n_2)} \quad [18]$$

$$T_1 + T_2 + T_3 = 0 \quad [19]$$

$$T_1 n_1 + T_2 n_2 + T_3 n_3 = 0 \quad [20]$$

$$-T_3 = \frac{T_1}{R} = \frac{T_2}{(1-R)} \quad [21]$$

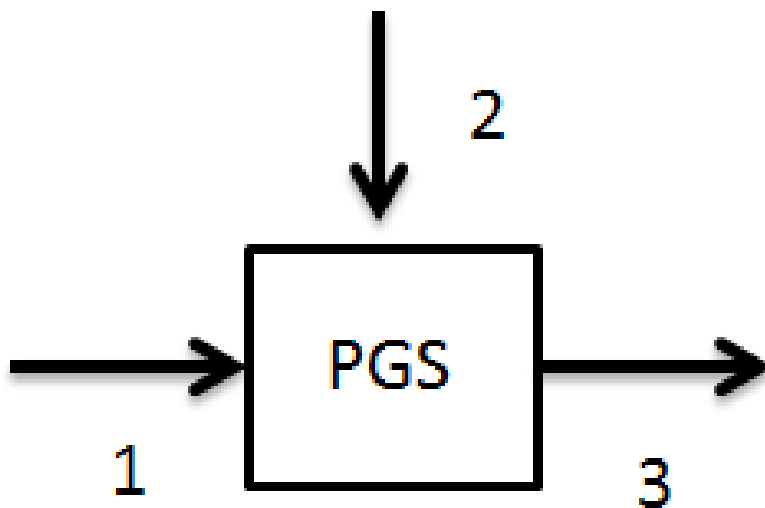


Figure 55 Schematic of PGS (Arrows signify power. Power into the system is taken positive and out of the system as negative)

4.3.2 Configurations of PSCVT

As mentioned previously, the two elements needed to create a PSCVT are variator and PGS. The PGS can be connected to the variator in two ways. The input coupled (IC) system, where the torque is split at the common input shaft, speed remaining the same and the power is recombined via the PGS at the output. The second is the output coupled (OC) where the speed is divided at the input shaft connected to the PGS and the power is recombined at the common output shaft. The Fig. 56 shows the schematic of the two systems. The variator ratio is labelled as V in the Fig. 55. In the IC system power is input at branch 5 and output at branch 3 and in the OC system input at branch 3 and output at branch 5 as shown in Fig. 56.

Considering the IC PSCVT, equations 22-23 define the speed ratio of PSCVT (r) and the speed ratio of the variator (V). Using equation 18 and equations 22-24, equation 25 gives the relationship between r , V and R .

$$r = \frac{n_3}{n_5} \quad [22]$$

$$V = \frac{n_2}{n_4} = \frac{T_4}{T_2} \quad [23]$$

$$n_5 = n_4 = n_1 \quad [24]$$

$$r = R + V \times (1 - R) \quad [25]$$

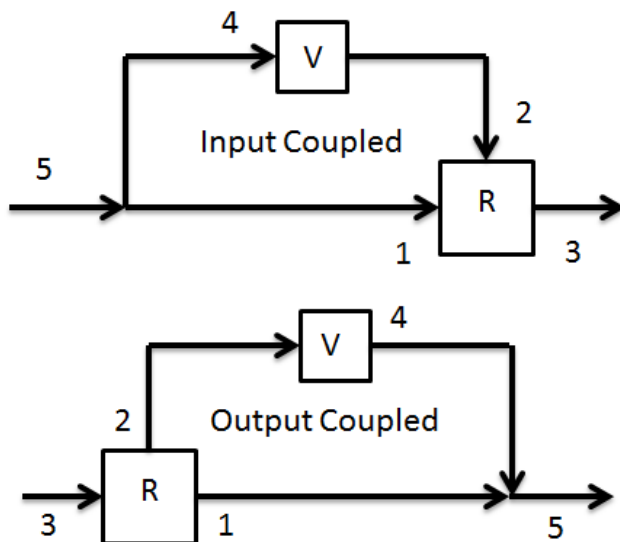


Figure 56 Input Coupled and Output Coupled PSCVT systems

The power flowing in the variator is of special concern as that is usually the least efficient part of the two branches. According to the power flow, three cases are defined for the IC PSCVT (and OC PSCVT), which are shown in Fig. 57. The first case is the no power recirculation case, the second is the case of positive recirculation which is distinguished by the fact that the power going through the variator is in the same direction as the output power and the third case of negative recirculation, in which the power going through the variator is in the opposite direction to that of the output power.

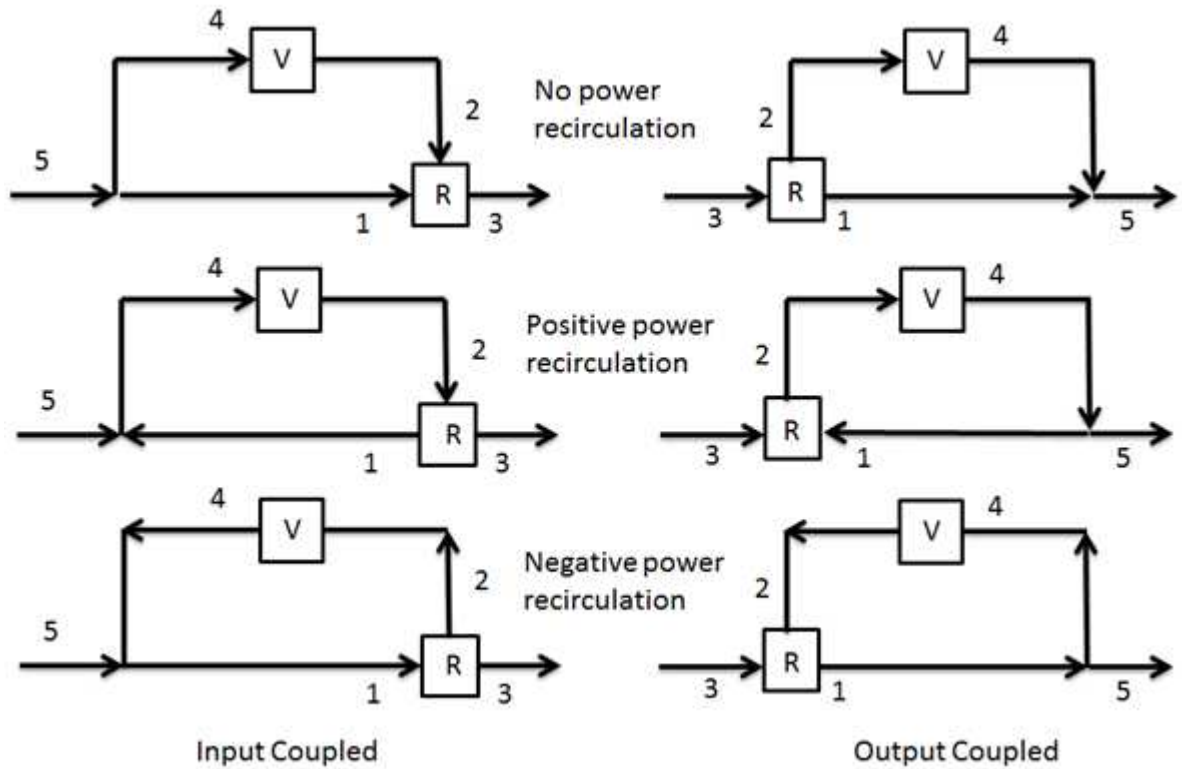


Figure 57 Different Power Regimes of PSCVT

For the case of a lossless IC PSCVT, equation 26 defines the ratio of variator power (P_v) to input power (P_i). Now using equation 21, 23, 25 and 26, equation 27 defines the value of ratio of variator power to input power in terms of R and r .

$$\frac{P_v}{P_i} = \frac{P_4}{P_5} = \frac{P_4}{P_4 + P_1} = \frac{T_4 n_4}{T_4 n_4 + T_1 n_1} = \frac{T_4}{T_4 + T_1} \quad [26]$$

$$\frac{P_v}{P_i} = 1 - \frac{R}{r} \quad [27]$$

Further equations 28-29 define the ratio range of the PSCVT (r_i) and that of the variator (V_i).

$$r_t = \frac{r_{\max}}{r_{\min}} \quad [28]$$

$$V_t = \frac{V_{\max}}{V_{\min}} \quad [29]$$

Now it can be easily derived, as has been shown by White [126], that for $r_t > V_t$, power recirculation has to exist. The important difference is that to have $r_t > V_t$, for the case of negative recirculation r_{\min} will occur at V_{\max} and vice versa, whereas for positive recirculation this condition is r_{\min} at V_{\min} and vice versa. In other words, for positive recirculation or no recirculation, a numerical increase in value of V will result in a numerical increase value of r and the opposite is true for negative recirculation. Table 9 shows the conditions for the three types for IC PSCVT.

Table 9 Conditions for different power modes of PSCVT to occur

Relation between r_t and V_t	Ratio of variator power to input power $\left(\frac{P_v}{P_i}\right)$	PSCVT operating mode
$r_t > V_t$	$\frac{P_v}{P_i} < 0$	Negative recirculation
$r_t < V_t$	$0 < \frac{P_v}{P_i} < 1$	No recirculation
$r_t = V_t$	$\frac{P_v}{P_i} = 1$	Variator only
$r_t > V_t$	$\frac{P_v}{P_i} > 1$	Positive recirculation

Power recirculation also gives the opportunity to create a geared neutral and reversing PSCVT. This can be easily seen from graph (A) in Fig. 58 where for an IC PSCVT, the value of r can go to zero or even negative with positive values of V depending on value of R . However to achieve $r \leq 0$, the power recirculation will be very high as can be seen in graph (B) in Fig. 58.

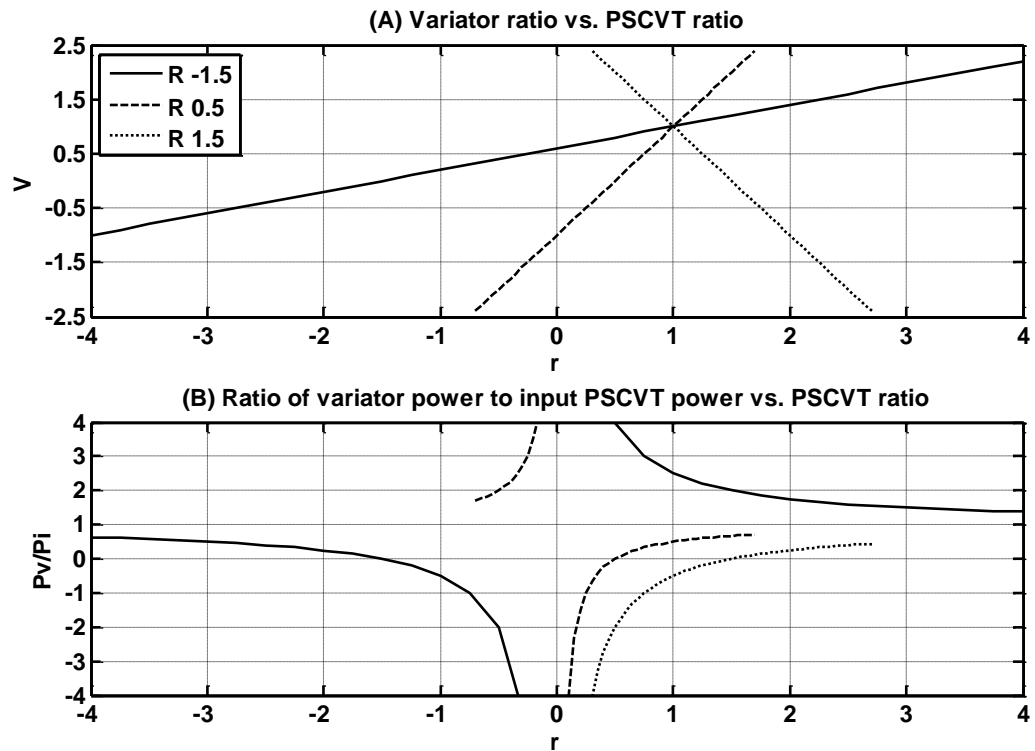


Figure 58 Graph (a) shows the variation of variator ratio vs. PSCVT ratio. Graph (b) shows the variation of ratio of variator power to input power vs. PSCVT ratio

The OC PSCVT looks an inverse of the IC PSCVT; however they have different characteristics. Beachley et al. [141] showed that for a designing a geared neutral and reversing OC PSCVT, the variator should have the ability to achieve zero and reverse ratio respectively. This is not possible by either the toroidal or belt variator as the sign of the speed ratio is fixed by mechanism [143].

4.3.3 Multi regime PSCVT

The disadvantage of increasing the ratio range by using a power recirculating design is that in most cases more power will be flowing through the variator which will reduce the efficiency and the variator would have to be designed bigger and heavier. The other way of increasing the ratio range in a PSCVT without power recirculation is the multi regime synchronous PSCVT which is discussed by White [128] and later by Mantriota [134-136].

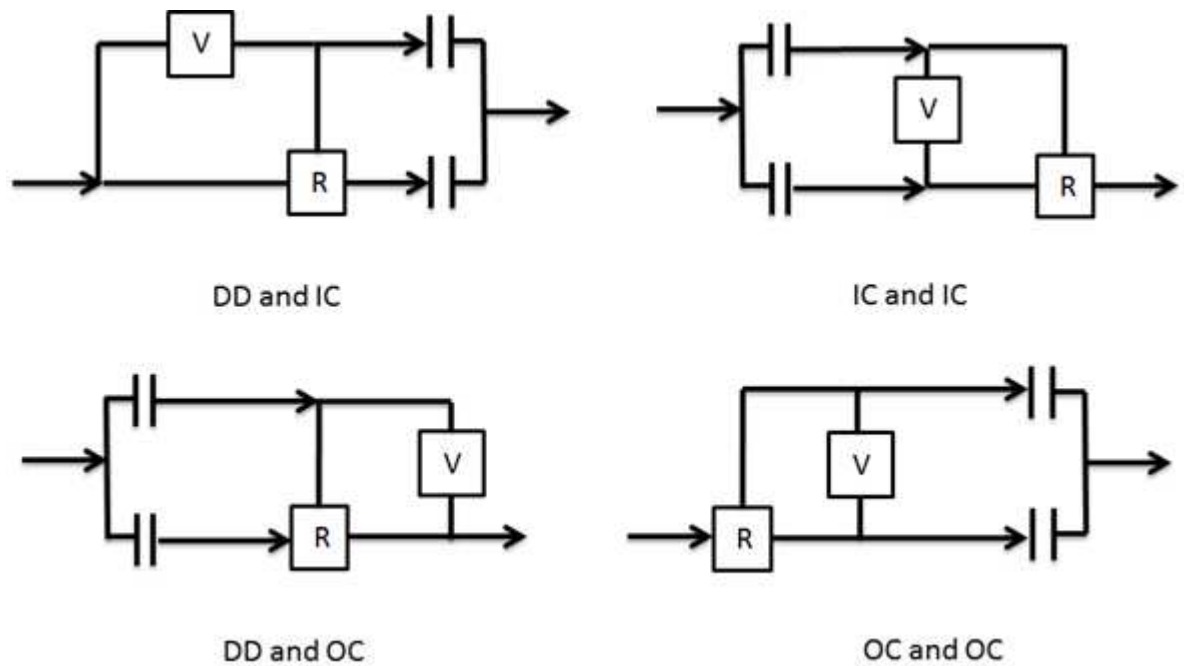


Figure 59 Different types of multi-regime PSCVT systems

White [128] discusses that there are four different types of configuration possible by utilizing two clutches, a variator and PGS. They are the direct drive and input coupled transmission, direct drive and output coupled transmission, two input coupled stages and two output coupled stages, which are shown in the Fig. 59. White [128] also showed that the systems having a direct drive stage will involve negative recirculation. These systems are therefore not useful if one is trying to avoid negative recirculation. That leaves the other two systems which have either two input coupled stages or two output coupled stages. In this case the variator ratio will increase in the first stage along with the PSCVT ratio and in the second stage the variator ratio will decrease while the PSCVT ratio continues to increase. For this to occur in a two IC stage PSCVT, the condition $0 < R < 1$ needs to be satisfied [128].

4.3.4 Requirements for FESS

In case of a FESS, the power will be flowing in both directions of the PSCVT during operation, so the IC PSCVT in the forward direction will behave as the OC PSCVT in the reverse power flow direction. In terms of ratio coverage it is not a problem since the IC PSCVT and the OC PSCVT will have the same coverage in both directions. Additionally if losses are not considered the ratio of variator power to input power will be same in both directions [141]. However if losses are considered then the ratio of variator power to input power will be different and has to be separately analysed. The PSCVT for FESS does not require a speed reversal as the flywheel will only be used during forward motion. Therefore a clutch would be necessary for disconnecting the PSCVT during reverse vehicle motion. The IC PSCVT design can be used to create geared

neutral, as it was shown before, however the power recirculation will be very high. Since a clutch would be present, it would make sense to use it to achieve neutral condition by allowing it to slip.

In our case the operation of the flywheel, as discussed previously is from 15,000 rpm to 30,000 rpm. The outer shaft which is connected to the vehicle driveline operates from 0 rpm to 10,390 rpm. With the help of a slipping clutch the shaft can operate from 1000 rpm to 10,390 rpm. This gives us the conditions for the limits of PSCVT (equations 30-32).

$$r_{\max} = \frac{10390}{15000} = 0.69 \quad [30]$$

$$r_{\min} = \frac{1000}{30000} = 0.033 \quad [31]$$

$$r_t = \frac{r_{\max}}{r_{\min}} = 20.909 \quad [32]$$

The limits of the variator are taken to be as shown in equations 33-35.

$$V_{\max} = 2.4 \quad [33]$$

$$V_{\min} = 0.4 \quad [34]$$

$$V_t = \frac{V_{\max}}{V_{\min}} = 6 \quad [35]$$

4.3.5 Design of single regime PSCVT

For designing the PSCVT to achieve specific limits of operation, additional gearing is necessary, as explained by Fussner and Singh [139]. The Fig. 60 shows the schematic of the PSCVT in consideration. The additional gears are represented by gear ratios G_m and G_v . In this case equations 36-40 define the kinematics of the PSCVT system in the forward power flow direction.

$$r = \frac{n_3}{n_7} \quad [36]$$

$$V = \frac{n_2}{n_4} \quad [37]$$

$$G_v = \frac{n_4}{n_5} \quad [38]$$

$$G_m = \frac{n_1}{n_6} \quad [39]$$

$$n_5 = n_6 = n_7 \quad [40]$$

Now using equation 25 and modifying it for the above system, equation 41 defines the relationships between various ratios.

$$r = RG_m + VG_v(1-R) \quad [41]$$

The other thing to look at is the ratio of variator power to input power to the PSCVT. Equation 42 gives the ratio for a lossless system.

$$\frac{P_v}{P_i} = \frac{G_v V}{G_v V + \frac{RG_m}{(1-R)}} \quad [42]$$

As it is observed in the requirements for the transmission specified previously, $r_t > V_t$, therefore power recirculation would be necessary in any single stage design.

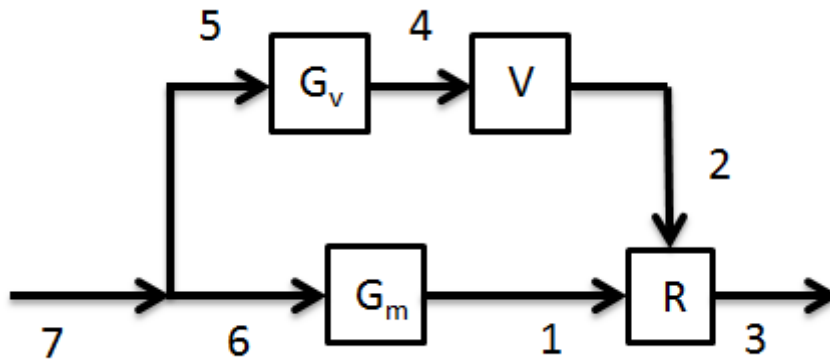


Figure 60 Schematic of single regime PSCVT with additional gearing to achieve required operation limits

4.3.5.1 Case of positive power recirculating design of PSCVT

First the case for positive power recirculation is considered, which implies r_{\min} occurs at V_{\min} and vice versa. Taking a fixed value of R , the values of G_m and G_v can be calculated by simultaneously solving equations 43-44.

$$r_{\max} = RG_m + V_{\max} G_v(1-R) \quad [43]$$

$$r_{\min} = RG_m + V_{\min} G_v (1 - R) \quad [44]$$

Table 10 Definitions of basic ratio of the PGS depending on branch connections

Symbol	Definition	Basic ratio	Value of basic ratio taking $\frac{D_r}{D_s} = 3$
R_1	$\frac{(n_3 - n_2)}{(n_1 - n_2)} = \frac{(n_c - n_r)}{(n_s - n_r)}$	$\frac{D_s}{D_s + D_r}$	0.25
R_2	$\frac{(n_1 - n_2)}{(n_3 - n_2)} = \frac{(n_s - n_r)}{(n_c - n_r)} = \frac{1}{R_1}$	$\frac{D_s + D_r}{D_s}$	4
R_3	$\frac{(n_2 - n_3)}{(n_1 - n_3)} = \frac{(n_r - n_c)}{(n_s - n_c)} = \frac{R_1}{R_1 - 1}$	$-\frac{D_s}{D_r}$	-0.33
R_4	$\frac{(n_1 - n_3)}{(n_2 - n_3)} = \frac{(n_s - n_c)}{(n_r - n_c)} = \frac{R_1 - 1}{R_1}$	$-\frac{D_r}{D_s}$	-3
R_5	$\frac{(n_3 - n_1)}{(n_2 - n_1)} = \frac{(n_c - n_s)}{(n_r - n_s)} = 1 - R_1$	$\frac{D_r}{D_s + D_r}$	0.75
R_6	$\frac{(n_2 - n_1)}{(n_3 - n_1)} = \frac{(n_r - n_s)}{(n_c - n_s)} = \frac{1}{1 - R_1}$	$\frac{D_r + D_s}{D_r}$	1.33

Now the numerical value of R will depend on how branches of the PGS are defined physically, as shown in Table 10. Taking a reasonable value of 3 for ratio of ring gear diameter to sun gear diameter, the last column of Table 10 shows the different numerical values of R . The diameters of the ring and sun gears are labelled as D_r and D_s in Table 10. As can be observed from Table 10, the definition R_1 can be used to derive all the other definitions. In other words each definition can be used to derive the others.

Table 11 Values of fixed gear ratios to achieve required PSCVT ratio limits in case of positive power recirculation

Case	1	2	3	4	5	6
R	0.25	4	-0.33	-3	0.75	1.33
G_m	1: -2.54	1: -40.6	1:3.35	1:30.4	1: -7.62	1: -13.5
G_v	1:2.28	1: -9.13	1:4.04	1:12.18	1.31:1	1: -1.004

Using the numerical values of R from the last column of Table 10, and specific limits of the PSCVT defined in equations (30-35), the corresponding values of G_m and G_v are calculated by using equations 43-44 and are shown in Table 11. As can be seen from the Table 11, G_m and G_v can be defined for any value of R, although some of the values might be impractical like cases 2, 4, 5 and 6.

4.3.5.2 Case of negative power recirculating design of PSCVT

Similarly for the case of negative power recirculation equations 43-44 will become equations 45-46.

$$r_{\min} = RG_m + V_{\max} G_v(1 - R) \quad [45]$$

$$r_{\max} = RG_m + V_{\min} G_v(1 - R) \quad [46]$$

In other words the condition will be that r_{\min} occurs at V_{\max} and vice versa. Again using the above equations 45-46, values of R from Table 10 and limits of the PSCVT defined in equations (30-35) and solving for G_m and G_v , Table 12 shows the corresponding values for negative power recirculation. Similar to the positive power recirculation case, there are some combinations such as cases 2 and 4 which would be impractical.

Table 12 Values of fixed gear ratios to achieve required PSCVT ratio limits in case of negative power recirculation

Case	1	2	3	4	5	6
R	0.25	4	-0.33	-3	0.75	1.33
G_m	3.28:1	1:4.86	-2.46:1	1: -3.65	1.09:1	1:1.62
G_v	1: -2.28	1: 9.13	1: -4.05	1: -12.18	1.31:1	1:1.01

4.3.6 Comparison of Power flow in both cases

Using equation 42, the ratio of variator to input power can be calculated for the case of positive and negative power recirculation as a function of PSCVT ratio. The Fig. 61 shows the ratio of variator power to input power for both positive as well as negative power recirculation in terms of magnitude. It can be seen from the Fig. 61 that at lower ratios the $\frac{P_v}{P_i}$ value can be very high for both cases and especially for the case of negative recirculation. Although it can also be seen that for higher values of r , the ratio $\frac{P_v}{P_i}$ for negative recirculation can be below unity which would mean that less power would be going through the variator. Since the variator has to be sized to carry the power, the negative recirculation case would not be suitable. In the further analysis the case of negative power recirculation will not be considered. Note that the values shown in Fig. 61 for positive power recirculation and negative power recirculation will be the same for any combination of R , G_m and G_v shown in Tables 11 and 12.

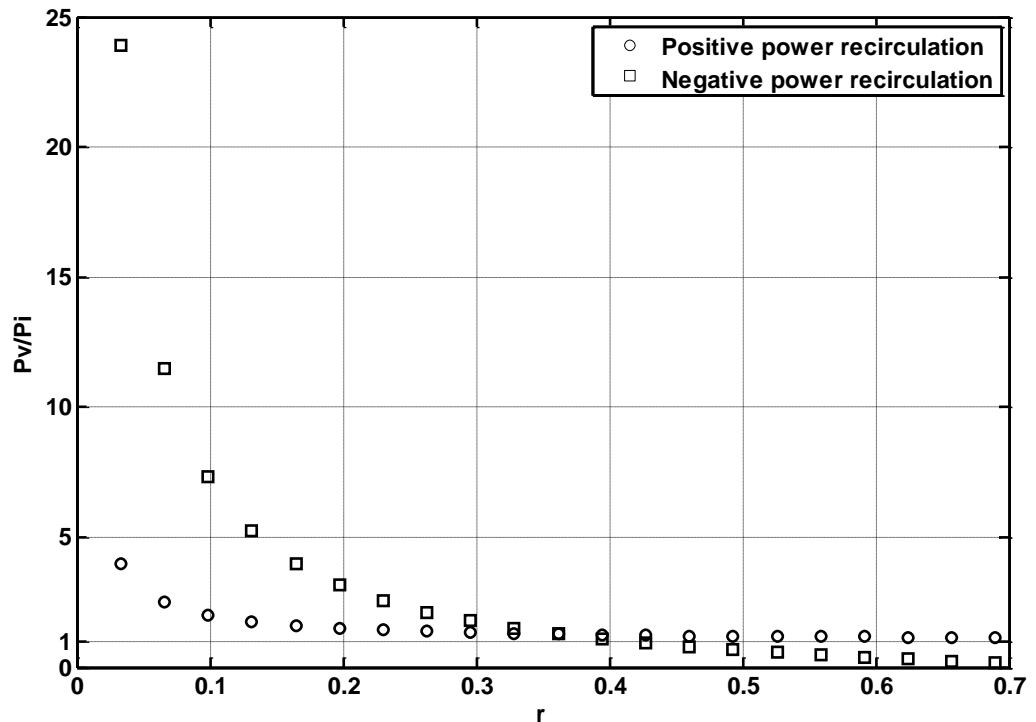


Figure 61 Ratio of variator power to input power vs. PSCVT ratio for positive and negative power recirculation

4.3.7 Design of multi regime PSCVT without power recirculation

The other option of increasing the ratio range without power recirculation is using a multi regime PSCVT.

4.3.7.1 Two-regime PSCVT without power recirculation

Fig. 62 shows a two-regime PSCVT. There are two clutches used for synchronous shift between the two regimes and are labelled as A and B in Fig. 62. Also G_1 , G_2 and G_3 are gear ratios of additional gears necessary to achieve the required ratio range. Equations 47-51 are used to define the ratio range for the two-regime PSCVT. Equations 47-49 are common for the PSCVT, while equations 50-51 give the PSCVT ratio for stage 1 and stage 2.

$$r = \frac{n_3}{n_8} \quad [47]$$

$$V = \frac{n_4}{n_5} \quad [48]$$

$$n_8 = n_6 = n_7 \quad [49]$$

$$r = (1-R)G_2 + RVG_1 \quad [50]$$

$$r = RG_1G_3 + \frac{G_2G_3(1-R)}{V} \quad [51]$$

In the first stage, clutch A will be closed and clutch B will be open. The variator ratio V will go from V_{\min} to V_{\max} and at the end of the first stage the speed n_4 will be equal to $V_{\max} \times n_7$. For the synchronization to happen to shift from stage 1 to stage 2, the equation 52 should be true.

$$G_3 = V_{\max} \quad [52]$$

During synchronisation, clutch A will be opened and clutch B will be closed. In this second stage, V will go from V_{\max} to V_{\min} and r will keep on increasing till it reaches r_{\max} .

Now it can be easily shown that for two-regime system r_i will be equal to V_i . Using equations 50-51, equations 53-54 define the end conditions for the system.

$$r_{\min} = (1-R)G_2 + RV_{\min}G_1 \quad [53]$$

$$r_{\max} = RG_1G_3 + \frac{G_2G_3(1-R)}{V_{\min}} \quad [54]$$

Using equations 52, 53 and 54, equation 55 can be reached.

$$r_t = \frac{r_{\max}}{r_{\min}} = \frac{G_3}{V_{\min}} = \frac{V_{\max}}{V_{\min}} = V_t \quad [55]$$

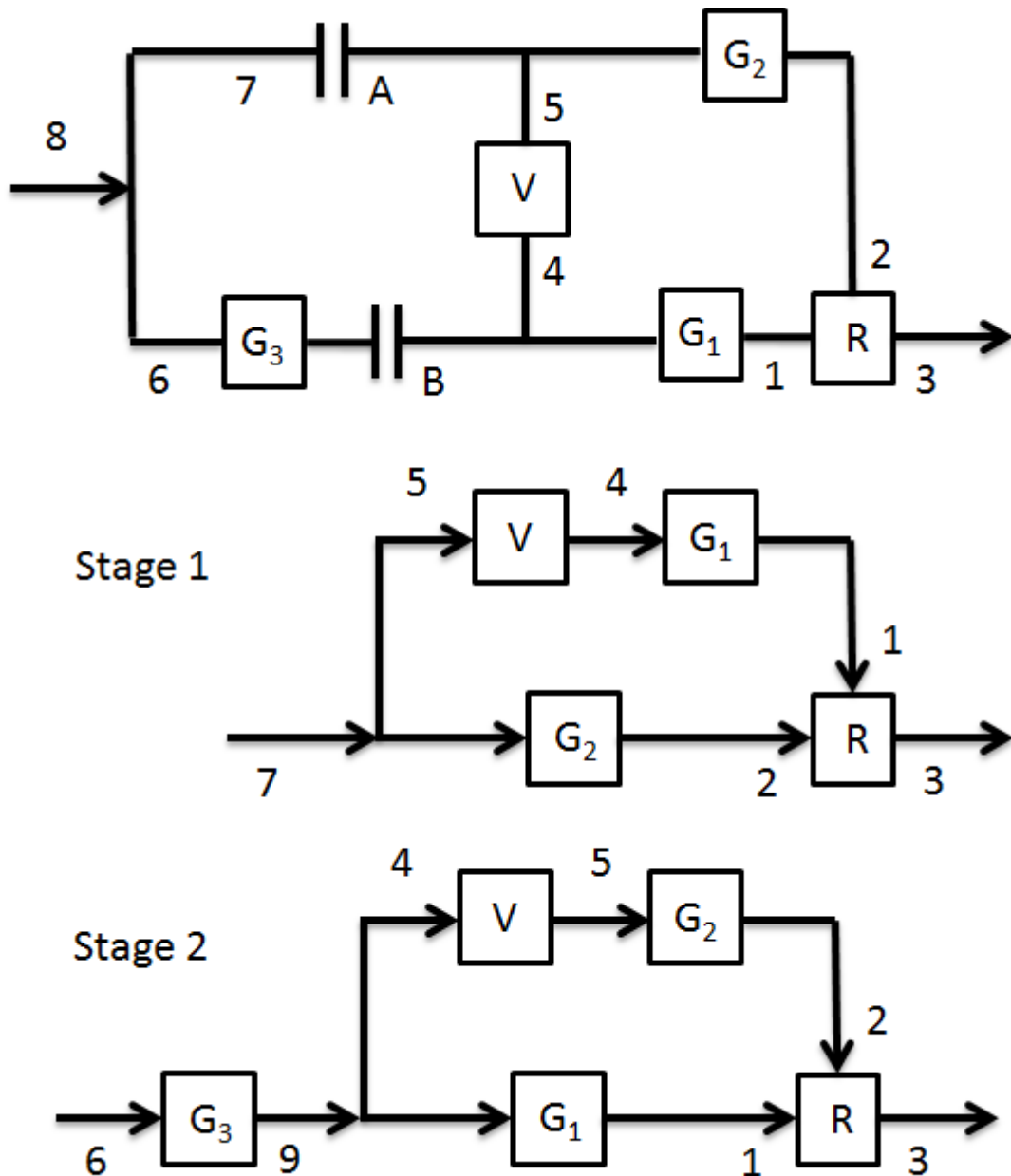


Figure 62 Two-Regime PSCVT without power recirculation

From equation 55, it can thus be concluded that a two-regime PSCVT (without power recirculation) cannot be used to increase the ratio range of the PSCVT beyond the ratio range of the variator. Although this conclusion isn't new, the simple derivation of this condition has not been presented previously. Mantriota [136] mentioned that the ratio range for a 4-regime PSCVT is equal to V_t^2 . For the present case where the required ratio range is around 21, the system most suitable would be a three-regime PSCVT which will be discussed further.

4.3.7.2 Three-regime PSCVT without power recirculation

Fig. 63 shows the general 3-regime PSCVT. Again clutches A, B and C are labelled in Fig. 63, which are needed for synchronous shifts. Also G_1 , G_2 , G_3 , G_4 and G_5 are gear ratios of additional gears necessary to achieve the required speed ratio range. Equations 56-62, give the general definitions for the PSCVT.

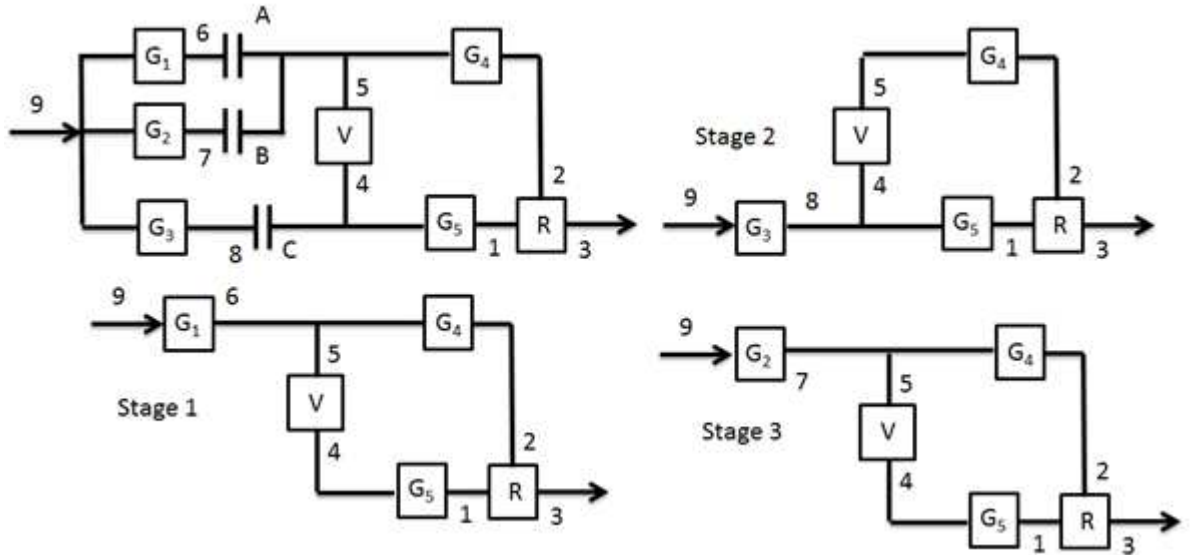


Figure 63 Three-Regime PSCVT System without power recirculation

$$r = \frac{n_3}{n_9} \quad [56]$$

$$V = \frac{n_4}{n_5} \quad [57]$$

$$G_1 = \frac{n_6}{n_9} \quad [58]$$

$$G_2 = \frac{n_7}{n_9} \quad [59]$$

$$G_3 = \frac{n_8}{n_9} \quad [60]$$

$$G_4 = \frac{n_2}{n_5} \quad [61]$$

$$G_5 = \frac{n_1}{n_4} \quad [62]$$

For stage 1, the clutch A will be closed and clutches B and C will be open. Equation 63 gives the ratio for PSCVT in stage 1.

$$r = RVG_1G_5 + G_1G_4(1 - R) \quad [63]$$

In this stage the variator ratio V will go from V_{\min} to V_{\max} and at the end of the first stage the speed n_4 will be equal to $V_{\max} \times n_9 \times G_1$. Now if the equation 64 is satisfied, synchronisation will take place.

$$G_3 = V_{\max} G_1 \quad [64]$$

For stage 2, the clutch C will be closed and clutches A and B will be open. Equation 65 gives the PSCVT ratio for stage 2.

$$r = RG_3G_5 + \frac{G_4G_3(1 - R)}{V} \quad [65]$$

Now following the same procedure for stage 3, clutch B will be closed and clutches A and C will be open. In this case equation 66 gives the synchronisation condition, which can also be written in terms of G_1 using equation 64. Equation 67 gives the PSCVT ratio.

$$G_2 = \frac{G_3}{V_{\min}} = \frac{V_{\max}}{V_{\min}} G_1 = V_t G_1 \quad [66]$$

$$r = RVG_2G_5 + G_2G_4(1 - R) \quad [67]$$

As in the case of power recirculation, the values of G_1 , G_4 and G_5 can be computed for a given value of R to achieve the end conditions of PSCVT ratio. In this case two parameters to compute are given by equations 68-69.

$$G_{15} = G_1 \times G_5 \quad [68]$$

$$G_{14} = G_1 \times G_4 \quad [69]$$

Now using equations 63, 67, 68 and 69, the equations for PSCVT ratio end conditions are given by equations 70-71 as follows.

$$r_{\min} = RV_{\min} G_{15} + G_{14}(1 - R) \quad [70]$$

$$r_{\max} = RV_{\max} V_t G_{15} + G_{14} V_t(1 - R) \quad [71]$$

Again using the numerical values of R from the last column of Table 10, and specific limits of the PSCVT defined in equations (30-35), the corresponding values of G_{14} and G_{15} are calculated by using equations 70-71 and are shown in Table 13.

Table 13 Values of gear ratio factors to achieve required PSCVT ratio limits in case of three-regime system

Case	1	2	3	4	5	6
R	0.25	4	-0.33	-3	0.75	1.33
G_{14}	0.0221	-0.0055	0.0125	0.0042	0.0664	-0.0498
G_{15}	0.164	0.0103	-0.123	-0.0137	0.0547	0.0308

Using the values of G_{14} and G_{15} from the Table 13, equations 68-69 and assuming suitable value for G_1 , the values of G_4 and G_5 can be computed. Although it might seem that G_1 is redundant, its importance can be gauged from the Table 13. If G_1 is taken to be unity, then G_4 and G_5 will have highly impractical values.

Though the three-regime system is beneficial in terms of the ratio of variator power to input power, which will be always less than unity, it increases the complexity of the system. Another option which is a compromise between the single regime system and three-regime system is the two-regime system with negative power recirculation as was briefly mentioned in before.

4.3.8 Design of two-regime PSCVT with negative power recirculation

The third option would be a two stage system with negative power recirculation. As mentioned previously such a system would have one direct stage; the other being an OC or IC stage and this other stage would involve negative power recirculation. Moreover the direct drive stage can either be the first stage or the second stage. Fig. 64 shows this kind of system with the first stage as direct drive and second stage as IC. There are two clutches used for synchronous shift between the two regimes and are labelled as A and B in Fig. 64. Also G_v , G_m and G^* are gear ratios of additional gears necessary to achieve the required ratio range. An example of this design is shown by White [144].

Equations 72-78 define the system.

$$G_v = \frac{n_4}{n_5} \quad [72]$$

$$G_m = \frac{n_1}{n_6} \quad [73]$$

$$V = \frac{n_8}{n_4} \quad [74]$$

$$r = \frac{n_{10}}{n_7} \quad [75]$$

$$G^* = \frac{n_{11}}{n_3} \quad [76]$$

$$n_7 = n_6 = n_5 \quad [77]$$

$$n_9 = n_8 = n_2 \quad [78]$$

For stage 1, clutch A is closed and B is open and equation 79 gives the PSCVT ratio.

$$r = VG_v \quad [79]$$

For stage 2, clutch A is open and B is closed, with the ratio given by equation 80.

$$r = G^* (RG_m + VG_v(1 - R)) \quad [80]$$

For synchronous shift to happen between stage 1 and stage 2, the following condition should be satisfied.

$$G^* = \frac{V_{\max} G_v}{V_{\max} G_v(1 - R) + RG_m} \quad [81]$$

Now using the limits of the variator ratio and the PSCVT ratio, G_v and G_m can be calculated as follows.

$$G_v = \frac{r_{\min}}{V_{\min}} \quad [82]$$

$$G_m = \frac{(1 - R)V_t(r_{\max} - r_{\min})}{R(V_t - r_t)} \quad [83]$$

An interesting point is that in this case unlike others the value of G_v is fixed with the limits and does not change with respect to R . Again using the numerical values of R from the last column of Table 10, and specific limits of the PSCVT defined in equations (30-35), the

corresponding values of G_m and G^* are calculated by using equations 82 and 83, and are shown in Table 14. A variation of this system would be that the stage with power recirculation is the first stage and the direct drive is the second stage. Such a system is used in the Torotrak IVT [145].

Table 14 Values of fixed gear ratios to achieve required ratio limits for two-regime PSCVT with negative power recirculation

Case	1	2	3	4	5	6
R	0.25	4	-0.33	-3	0.75	1.33
G_m	1: -1.26	1:5.04	1.057:1	1:2.83	1: -11.34	1:15.12
G^*	-3.97:1	1:1.006	-2.23:1	1: -1.341	-11.9:1	8.94:1

The Fig. 65 compares the ratio range for the 1, 2 and 3 regime systems using equations described previously. The synchronous shifts can be easily seen.

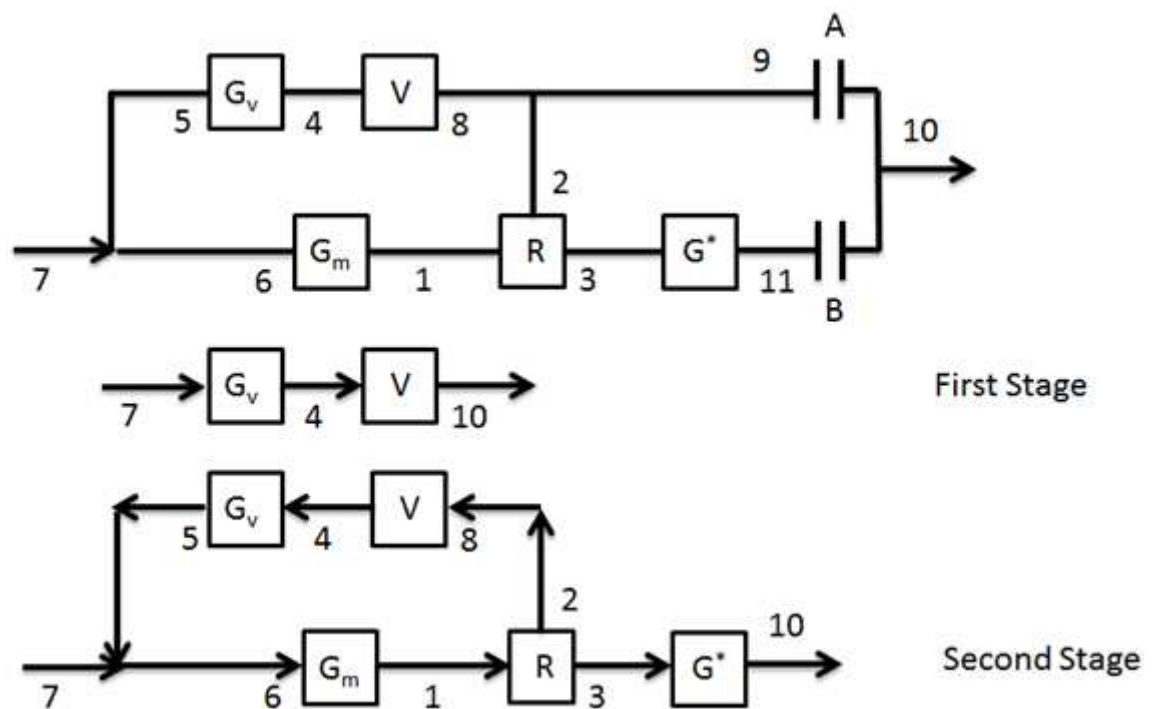


Figure 64 Two-regime PSCVT system with power recirculation

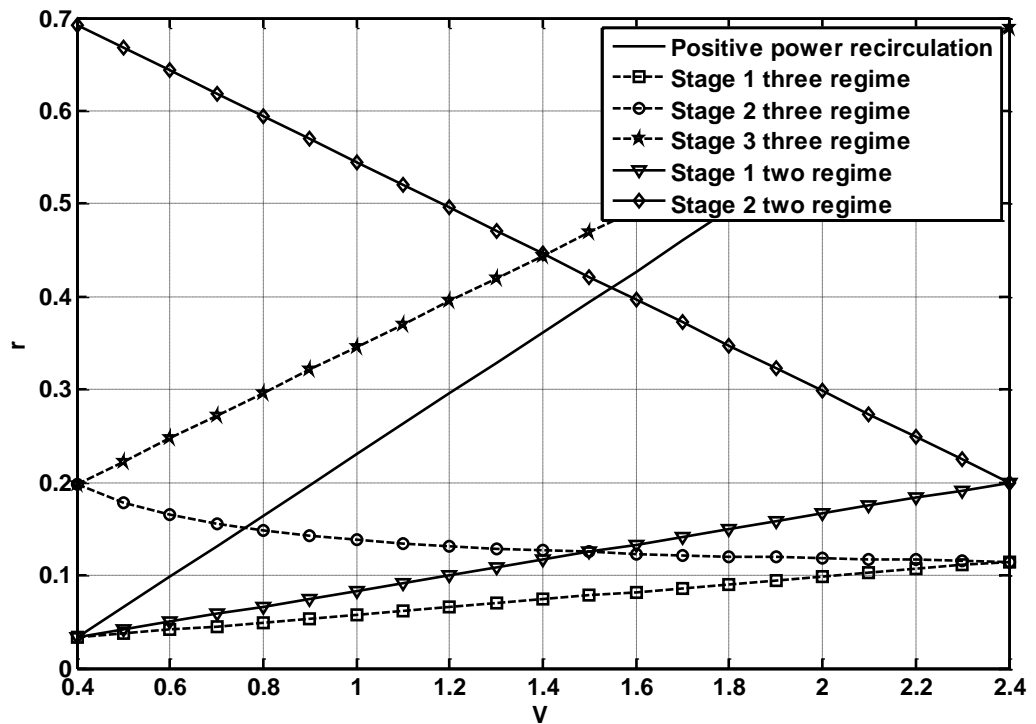


Figure 65 PSCVT ratio vs. variator ratio for single, two-regime and three-regime systems

4.3.9 Efficiency of PSCVT

4.3.9.1 Efficiency of the PGS

Up till now the PSCVT system has been considered to be lossless and equations involving power flow were derived taking into account this assumption. In reality all the mating elements of the PSCVT system will have efficiencies. The next set of equations will take the efficiency into account. Pennestri and Freudenstein [127] derived a methodology to define the mechanical efficiency of the two degree of freedom PGS. The methodology has been used here to create the efficiency of the PGS. Only the meshing losses have been considered in the analysis. Pennestri and Valentini [146] demonstrated the numerical equivalence of the various approaches available in literature to calculate the mechanical efficiency of the PGS.

According to Pennestri and Freudenstein [127], a two degree of freedom PGS can be represented as shown in the Fig. 66. In the Fig. 66 m , n and p are the three branches of a generic PGS.

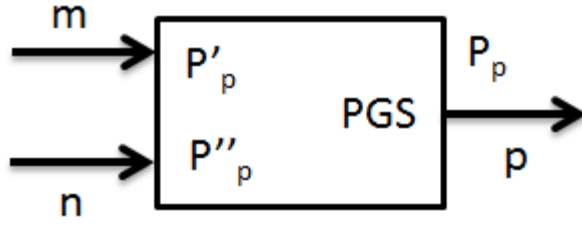


Figure 66 Power Flow in PGS

Now assuming that power is input into the system through branches m and n , and using the principle that there are two power flow paths as shown in the Fig. 66, equations 84-86 can be derived. The symbols η , P , T and n in equations 84-86 represent efficiency, power, torque and speed. Equation 84 represents the speed relationship between different branches of the PGS. Equation 85 represents the efficiency of the PGS. Since the power flows in two different paths represented by P'_p and P''_p , and with their efficiencies represented by η_1 and η_2 , equation 86 represents the power balance in the PGS.

$$n_p = K_1 \times n_m + K_2 \times n_n = n'_p + n''_p \quad [84]$$

$$\eta_{pgs} = \frac{|P_p|}{P_m + P_n} \quad [85]$$

$$P_p = P'_p + P''_p = T_p (n'_p + n''_p) = \eta_1 P_m + \eta_2 P_n \quad [86]$$

K_1 and K_2 are constants which depend on the gear ratios in the PGS. Now combining equations 84-86, the efficiency of the PGS can be defined in terms of η_1 and η_2 as shown in equation 87.

$$\eta_{pgs} = \frac{1}{\frac{1}{\eta_1} \frac{K_1 \times n_m}{n_p} + \frac{1}{\eta_2} \frac{K_2 \times n_n}{n_p}} \quad [87]$$

Now utilizing the principle explained above the efficiency of the PGS can be calculated depending on the direction of power. The efficiency of the individual path in the PGS is defined as $\eta_{m(n-p)}$ where m is the fixed link and the power is flowing from n to p . Two cases (case 1 and case 2) of different power flows are shown below in Fig. 67 which represent the power flows in the PGS of an IC PSCVT and OC PSCVT as shown in Fig. 56.

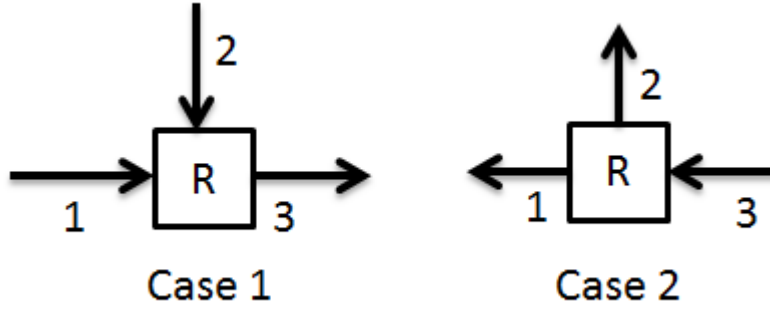


Figure 67 Cases of Power Flow in PGS of IC PSCVT and OC

Using the principle from above, the efficiencies of the case1 and case 2 are defined by equations 88-89 respectively.

$$\eta_{\text{pgs}_1} = \frac{1}{\frac{R}{\eta_{2(1-3)}} \frac{n_1}{n_3} + \frac{(1-R)}{\eta_{1(2-3)}} \frac{n_2}{n_3}} \quad [88]$$

$$\eta_{\text{pgs}_2} = \frac{n_1}{n_3} R \eta_{2(3-1)} + \frac{n_2}{n_3} (1-R) \eta_{1(3-2)} \quad [89]$$

4.3.9.2 Efficiency of the IC PSCVT without power recirculation

Now applying equation 88 to the case shown in Fig. 60 (IC PSCVT, no power recirculation) and using equations 36-40, the efficiency of the PSCVT is defined as follows in equation 90. The symbols η_v , η_{G_m} and η_{G_v} represent the efficiencies of the variator, fixed gears G_m and G_v respectively. It is assumed that these efficiencies are the same in both forward and reverse power flow, though in reality the efficiency especially that of the variator would be different in both directions and can be easily incorporated in the equations.

$$\eta_{\text{PSCVT}} = \frac{r}{\frac{R}{\eta_{2(1-3)}} \frac{G_m}{\eta_{G_m}} + \frac{(1-R)}{\eta_{1(2-3)}} \frac{VG_v}{\eta_{G_v} \eta_v}} \quad [90]$$

As stated before, the ratio of variator power to input power will also depend on the efficiency. Introducing efficiencies in the PGS system, equation 21 will become equation 91.

$$-T_3 = \frac{T_1}{R} \eta_{2(1-3)} = \frac{T_2}{(1-R)} \eta_{1(2-3)} \quad [91]$$

Now using equation 91 and 42, the variator power to input power ratio for the case IC PSCVT and no power recirculation is shown by equation 92.

$$\frac{P_v}{P_i} = \frac{P_4}{P_7} = \frac{P_5 \eta_{Gv}}{P_7} = \eta_{Gv} \frac{\frac{G_v V}{\eta_v \eta_{Gv}}}{\frac{G_v V}{\eta_v \eta_{Gv}} + \frac{R G_m}{(1-R) \eta_{Gm}} \frac{\eta_{1(2-3)}}{\eta_{2(1-3)}}} \quad [92]$$

4.3.9.3 Efficiency of the OC PSCVT without power recirculation

During reverse power flow, the IC PSCVT will behave like an OC PSCVT which is shown in Fig. 68. Equations 93-97 define the OC PSCVT. It is easily seen that the values of r , V , G_v and G_m are just the inverse of IC PSCVT (equations 36-39).

$$r = \frac{n_7}{n_3} \quad [93]$$

$$V = \frac{n_4}{n_2} \quad [94]$$

$$G_v = \frac{n_5}{n_4} \quad [95]$$

$$G_m = \frac{n_6}{n_1} \quad [96]$$

$$n_5 = n_6 = n_7 \quad [97]$$

Now using equation 89 and 93-97, the efficiency for the OC PSCVT can be defined as follows.

$$\eta_{PSCVT} = \frac{r \eta_{Gm}}{G_m} R \eta_{2(3-1)} + \frac{r \eta_v \eta_{Gv}}{V G_v} (1-R) \eta_{1(3-2)} \quad [98]$$

Equation 21 can be re written for this case as follows.

$$-T_3 \eta_{1(3-2)} = \frac{T_2}{(1-R)} \quad [99]$$

Equations 100-101 will describe the ratio of variator power to input power utilizing equations 93-97 and 99.

$$\frac{P_v}{P_i} = \frac{-P_2}{P_3} = \frac{-T_2 n_2}{T_3 n_3} \quad [100]$$

$$\frac{P_v}{P_i} = (1-R) \eta_{1(3-2)} \frac{r}{V G_v} \quad [101]$$

It can be appreciated that equations (92 and 101) describing the ratio of variator power to input power are different for the case of IC PSCVT and OC PSCVT once the efficiencies are considered.

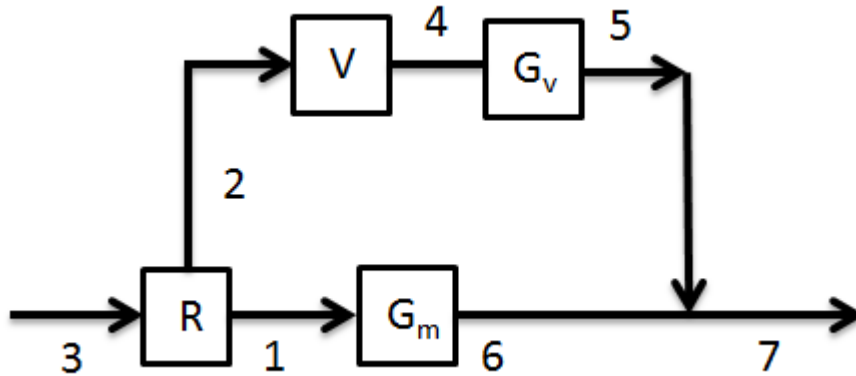


Figure 68 Schematic of OC PSCVT without power recirculation

4.3.9.4 Efficiency of the Single regime PSCVT with positive power recirculation

4.3.9.4.1 Efficiency of the single regime IC PSCVT with positive power recirculation

The Equations derived previously are for the case with no power recirculation. However for the case of positive recirculation with efficiencies different set of equations need to be derived. Considering the case for positive power recirculation for IC PSCVT shown in Fig. 69 and including the efficiencies, equations 102-103 can be derived, using the terminology stated in equations 36-40.

$$\frac{P_v}{P_i} = \frac{P_4}{P_7} = \frac{P_5 \eta_{Gv}}{P_7} = \eta_{Gv} \frac{\frac{G_v V}{\eta_v \eta_{Gv}}}{\frac{G_v V}{\eta_v \eta_{Gv}} + \frac{R G_m \eta_{3(2-1)} \eta_{Gm}}{(1-R)}} \quad [102]$$

$$\eta_{PSCVT} = \frac{r \eta_{1(2-3)}}{R G_m \eta_{Gm} \eta_{3(2-1)} + \frac{V G_v (1-R)}{\eta_{Gv} \eta_v}} \quad [103]$$

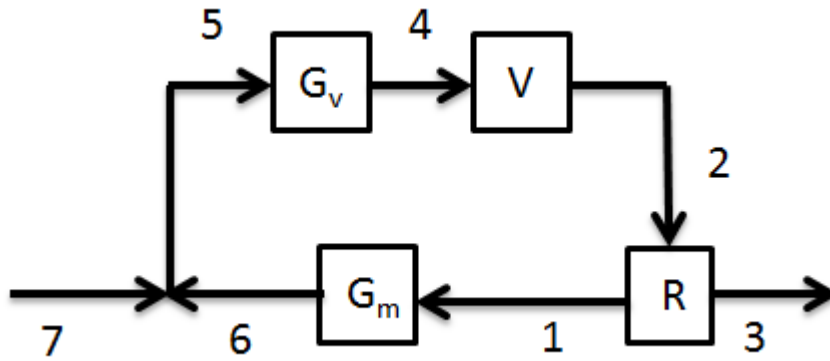


Figure 69 Schematic of IC PSCVT with positive power recirculation

4.3.9.4.2 Efficiency of the single regime OC PSCVT with positive power recirculation

Similarly for the case of OC PSCVT with positive power recirculation as shown in Fig. 70, equations 104-105 can be derived. The terminology used is defined in equations 93-96.

$$\frac{P_v}{P_i} = (1 - R)\eta_{1(3-2)} \frac{r}{VG_v} \quad [104]$$

$$\eta_{PSCVT} = r\eta_{1(3-2)} \left(\frac{R}{G_m\eta_{Gm}\eta_{3(1-2)}} + \frac{\eta_v\eta_{Gv}(1-R)}{VG_v} \right) \quad [105]$$

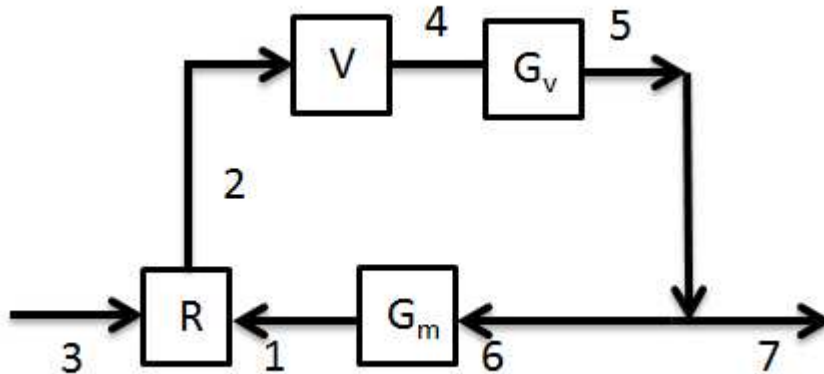


Figure 70 Schematic of OC PSCVT with positive power recirculation

Again it can be seen from equations 92 and 102 that with the inclusion of efficiencies, the ratio of variator power to input power is different for the case of no power recirculation and positive power recirculation. It can therefore be said that when efficiencies are concerned, different cases have to be analysed separately.

4.3.9.5 Efficiency of the Three-regime PSCVT without power recirculation

4.3.9.5.1 Efficiency of the three-regime IC PSCVT without power recirculation

Using the above methodology, the PSCVT efficiency and variator power to input power ratio can be derived for the three-regime PSCVT shown in Fig. 63 in both power flow directions. Losses are only considered in the gears which are in the path of the power flow from input to output of the PSCVT during the individual stages. Table 15 shows the corresponding equations for three-regime IC PSCVT. The terminology used is defined in equations 56-62.

Table 15 Equations for three-regime IC PSCVT system

	$\frac{P_v}{P_i}$	η_{PSCVT}
Stage 1	$1 + \frac{\eta_{G1}}{(1-R)G_4\eta_v\eta_{G5}\eta_{2(1-3)} + R\eta_{1(2-3)}\eta_{G4}VG_5}$	$\frac{r}{\frac{RG_5VG_1}{\eta_{2(1-3)}\eta_v\eta_{G5}\eta_{G1}} + \frac{(1-R)G_4G_1}{\eta_{1(2-3)}\eta_{G4}\eta_{G1}}}$
Stage 2	$1 + \frac{\eta_{G3}}{RG_5V\eta_v\eta_{G4}\eta_{1(2-3)} + (1-R)\eta_{2(1-3)}\eta_{G5}G_4}$	$\frac{r}{\frac{RG_5G_3}{\eta_{2(1-3)}\eta_{G5}\eta_{G3}} + \frac{(1-R)G_4G_3}{\eta_{1(2-3)}\eta_{G4}\eta_{G3}\eta_vV}}$
Stage 3	$1 + \frac{\eta_{G2}}{(1-R)G_4\eta_v\eta_{G5}\eta_{2(1-3)} + R\eta_{1(2-3)}\eta_{G4}VG_5}$	$\frac{r}{\frac{RG_5VG_2}{\eta_{2(1-3)}\eta_v\eta_{G5}\eta_{G2}} + \frac{(1-R)G_4G_2}{\eta_{1(2-3)}\eta_{G4}\eta_{G2}}}$

4.3.9.5.2 Efficiency of the three-regime OC PSCVT without power recirculation

For the reverse power flow direction equations 106-112 define the parameters. As previously for the case of reverse power flow the values of r , V , G_1 , G_2 , G_3 , G_4 and G_5 are inverted.

$$r = \frac{n_9}{n_3} \quad [106]$$

$$V = \frac{n_5}{n_4} \quad [107]$$

$$G_1 = \frac{n_9}{n_6} \quad [108]$$

$$G_2 = \frac{n_9}{n_7} \quad [109]$$

$$G_3 = \frac{n_9}{n_8} \quad [110]$$

$$G_4 = \frac{n_5}{n_2} \quad [111]$$

$$G_5 = \frac{n_4}{n_1} \quad [112]$$

Table 16 shows the corresponding equations for three-regime OC PSCVT.

Table 16 Equations for three-regime OC PSCVT system

	$\frac{P_v}{P_i}$	η_{PSCVT}
Stage 1	$R\eta_{G5}\eta_{2(3-1)} \frac{r}{VG_1G_5}$	$\frac{r\eta_{G1}}{G_1} \left(\frac{R\eta_{2(3-1)}\eta_v\eta_{G5}}{VG_5} + \frac{(1-R)\eta_{1(3-2)}\eta_{G4}}{G_4} \right)$
Stage 2	$(1-R)\eta_{G4}\eta_{1(3-2)} \frac{Vr}{G_4G_3}$	$\frac{r\eta_{G3}}{G_3} \left(\frac{R\eta_{2(3-1)}\eta_{G5}}{G_5} + \frac{(1-R)V\eta_v\eta_{1(3-2)}\eta_{G4}}{G_4} \right)$
Stage 3	$R\eta_{G5}\eta_{2(3-1)} \frac{r}{VG_2G_5}$	$\frac{r\eta_{G2}}{G_2} \left(\frac{R\eta_{2(3-1)}\eta_v\eta_{G5}}{VG_5} + \frac{(1-R)\eta_{1(3-2)}\eta_{G4}}{G_4} \right)$

4.3.9.6 Efficiency of the Two-regime PSCVT with negative power recirculation

4.3.9.6.1 Efficiency of the Two-regime IC PSCVT with negative power recirculation

Similarly for the two-regime system with negative power recirculation, the Table 17 shows equations.

Table 17 Equations for two-regime IC PSCVT system with negative power recirculation

	$\frac{P_v}{P_i}$	η_{PSCVT}
Stage 1	η_{Gv}	$\eta_v\eta_{Gv}$
Stage 2	$\frac{VG_v}{VG_v\eta_v\eta_{Gv} + \frac{RG_m}{(1-R)\eta_{Gm}\eta_{3(1-2)}}$	$\frac{r\eta_{G^*}\eta_{2(1-3)}}{G^*R} \frac{1}{\left(\frac{G_m}{\eta_{Gm}} + \frac{(1-R)\eta_{3(1-2)}VG_v\eta_v\eta_{Gv}}{R} \right)}$

4.3.9.6.2 Efficiency of the Two-regime OC PSCVT with negative power recirculation

For the reverse power flow direction equations 113-117 define the parameters. As was the case previously for reverse power flow, the values of r , V , G_m , G_v and G^* are inverted.

$$G_v = \frac{n_5}{n_4} \quad [113]$$

$$G_m = \frac{n_6}{n_1} \quad [114]$$

$$V = \frac{n_4}{n_8} \quad [115]$$

$$r = \frac{n_7}{n_{10}} \quad [116]$$

$$G^* = \frac{n_3}{n_{11}} \quad [117]$$

Table 18 shows equations for the OC PSCVT system.

Table 18 Equations for two-regime OC PSCVT system with negative power recirculation

	$\frac{P_v}{P_i}$	η_{PSCVT}
Stage 1	1	$\eta_v \eta_{Gv}$
Stage 2	$\frac{\eta_{G^*} r (1-R) \eta_{2(3-1)}}{G^* V G_v \eta_v \eta_{3(2-1)}}$	$\frac{r \eta_{G^*} \eta_{2(3-1)}}{G^*} \left(\frac{(1-R)}{\eta_{3(2-1)} \eta_{Gv} G_v V \eta_v} + \frac{R \eta_{Gm}}{G_m} \right)$

4.3.10 Power Flow and Efficiency of different designs of PSCVT for the FESS

The fixed gear pairs are usually highly efficient; therefore a fixed efficiency value of 99% is taken for them. Similarly a constant efficiency value of 98% is taken for the PGS and it is assumed that the value is same in all directions of power flow. The slightly lower efficiency value reflects the fact that the number of teeth meshing in PGS is higher. The maximum variator efficiency is typically lower than the efficiency of the fixed gears. Yanamoto et al. reported that maximum efficiency of 95% can be reached for half toroidal variator [147]. The efficiency is mainly influenced by input torque and speed ratio, and the dependency on input speed is weak. Kluger and Long reported that the efficiency of the toroid transmission is

around 91% over the majority of the operation [148]. Burke et al. also suggests that for an optimised variator, average efficiency of about 90% is expected [145]. For the present analysis the efficiency of the variator is taken as 90%. This does not include the losses due to the hydraulic control system which is used for variator and clutch operation.

Taking the efficiency values shown in equations 118-120 and applying the formulae derived previously for the different systems, the variator power to input power ratio and the overall efficiency for the example stated before are calculated. The Fig. 71 shows the results in the direction of forward power flow and reverse power flow respectively.

$$\eta_{m(n-p)} = \eta_{pgs} = 0.98 \quad [118]$$

$$\eta_v = 0.9 \quad [119]$$

$$\eta_{FG} = 0.99 \quad [120]$$

The graph (A) in Fig. 71 shows the ratio of variator power to input power for the three systems in both directions of power flow. It can be seen that the single regime system has high ratio of variator power to input power especially towards the lower speed ratios. Also the difference between forward and reverse flow is pronounced in this case towards the lower speed ratios. The three-regime system, of course has this ratio less than unity and the difference between forward and reverse directions is insignificant. For the third system the negative ratio of variator power to input power can be seen for the second stage.

Consequently the effect of the ratio of variator power to input power can be seen on the system efficiency in the graph (B). The three-regime system has the highest efficiency of the three systems except towards higher speed ratios, where the two-regime system shows higher efficiency. The two-regime system has a drop in efficiency towards the start of the second stage, where it even drops below that of the single regime system. At this point the difference in efficiency between the forward and reverse power flow is also pronounced for the two-regime system.

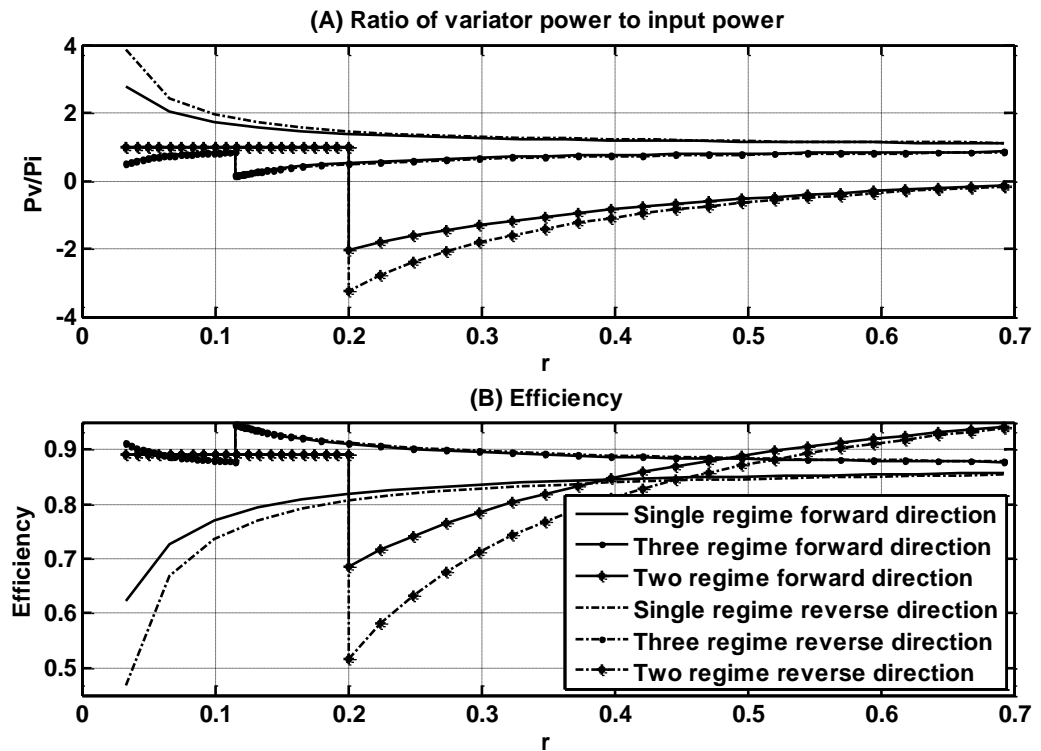


Figure 71 Graph (a) shows the ratio of variator power to input power vs. PSCVT ratio for the three systems in both directions. Graph (b) shows the efficiency vs. PSCVT ratio for the three systems in both directions

Although the efficiency of the three-regime PSCVT is higher than power recirculating PSCVTs, the trade-off is increased complexity. Another thing to note is that up till now, the IC PSCVT has been taken for the forward power flow and consequently the PSCVT behaves as OC for the reverse power flow. However if OC PSCVT is taken for the forward power flow, the values of efficiency and ratio of variator to input power will remain the same for OC and IC. The difference would be that the position of efficiencies versus the PSCVT ratio will be opposite as compared to the previous case and naturally the values of the fixed gear ratios will change. In other words if in previous case the efficiency of the PSCVT was higher towards higher PSCVT ratios, in this case it will be lower towards higher PSCVT ratios. An example is shown in Fig. 72. Similarly in case of the two-regime system, currently the direct drive is the first stage and IC is the second stage. By switching the direct drive to second stage and IC to first stage the position of PSCVT efficiency vs. ratio can be switched as well as is shown in Fig. 73.

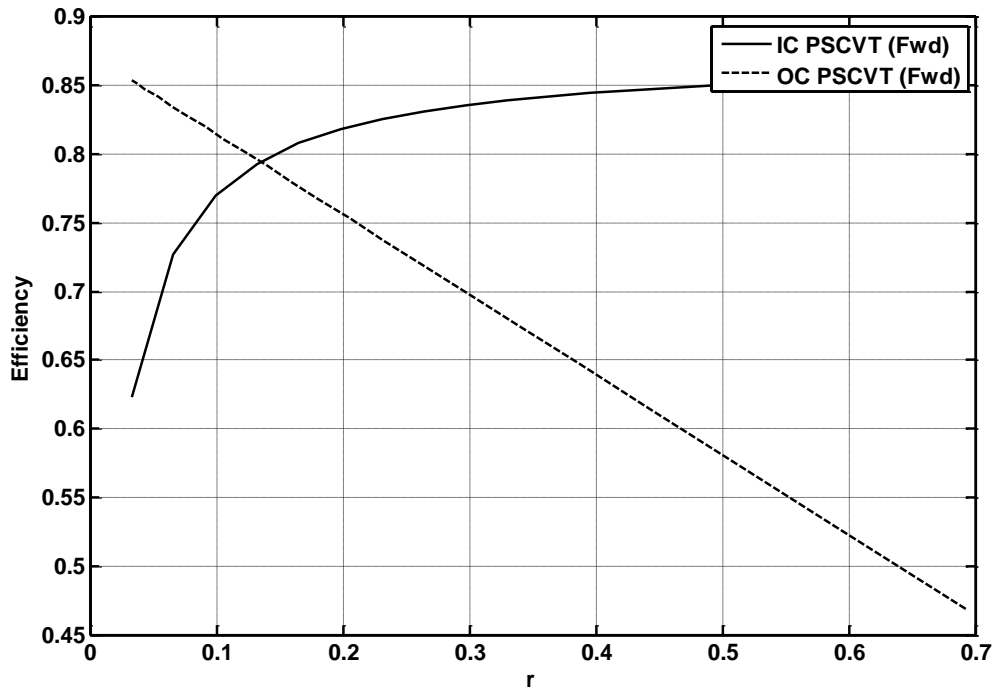


Figure 72 Efficiency vs. ratio with IC PSCVT or OC PSCVT as forward power flow

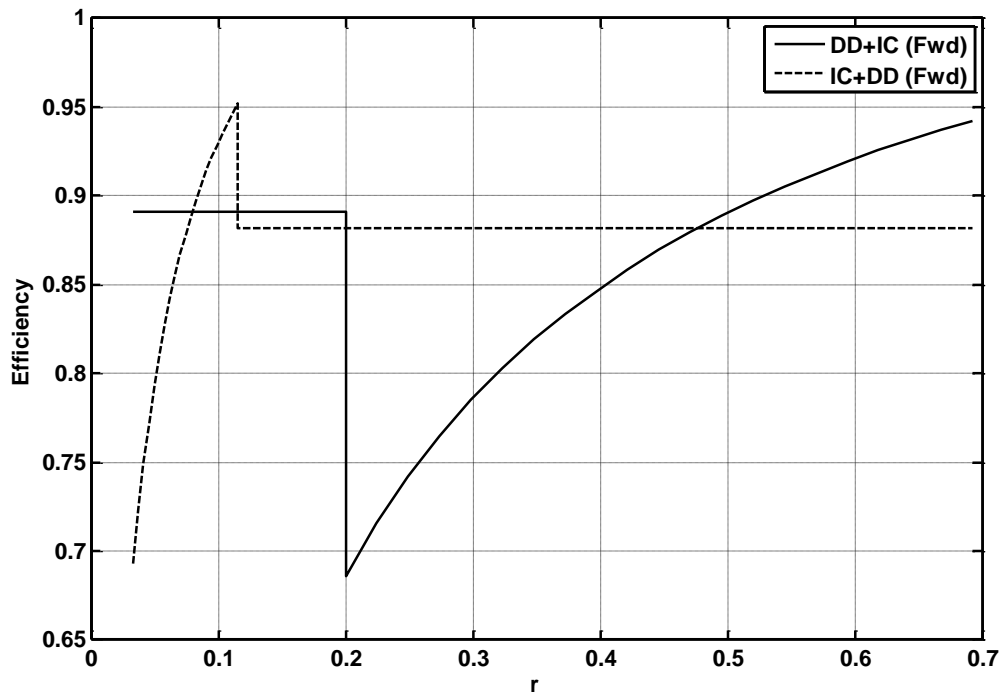


Figure 73 Efficiency vs. PSCVT ratio with IC taken as first or second stage

4.3.11 Torque and Speed through the Variator

Considering the single stage, two stage and three stage systems, all of which satisfy the ratio range requirements, the variator has to be specified as a function of torque, speed and power. The variator is designed for maximum transferrable torque and maximum operating speed over the ratio span. These two factors decide the power capacity of the variator. Martinez-Gonzales [77] explained for a PSCVT that the position of the fixed gear in the variator branch can be used to limit the maximum torque into the variator though this results in higher variator speeds. The Fig. 74 shows the two variations.

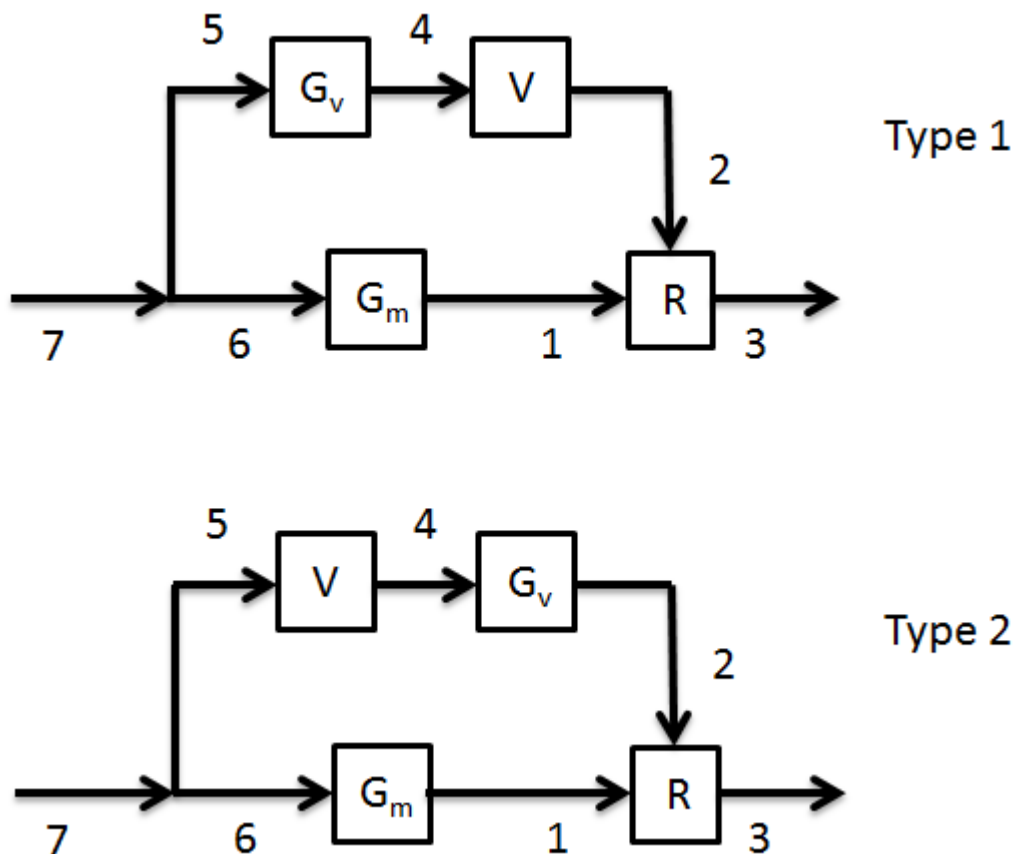


Figure 74 Different positions of variator

For type 1 and type 2, the ratio of variator input torque to PSCVT output torque is given by equation 121-122 respectively.

$$\left| \frac{T_4}{T_3} \right| = \frac{V(1-R)}{\eta_{pgs}\eta_v} \quad [121]$$

$$\left| \frac{T_5}{T_3} \right| = \frac{G_v V(1-R)}{\eta_{pgs}\eta_{G_v}\eta_v} \quad [122]$$

From equations 121-122 it can be seen that the torque input into the variator is reduced by G_v . Since power flowing through the variators is almost the same in both the cases, this reduction in torque will lead to a corresponding increase in variator input speed.

4.3.12 Modelling of Transmission and Flywheel

The power through the variator will be higher in the single regime system than in the multi regime system, which would result in a bigger and heavier variator. The additional weight of the clutches and gears in the multi regime system would be offset by a smaller variator [143], so the mass of the system would be more or less same. A number of authors note that for a well-designed flywheel system the operating losses are 2% per minute [121, 11] and that is taken as the assumption for the HV. For the fuel economy simulation the complete dynamics of the CVT are not required and the CVT will be modelled as a simple variator with a speed ratio range, efficiency and two lumped inertias at the input and output sides which rotate with the flywheel and drive shaft respectively. The idling loss in the CVT is neglected. The inertia value of 0.249 kgm² is the equivalent inertia on the input side which includes flywheel and CVT input lumped inertia. Since there is lack of information about mass and inertia of individual components, the mass of the system used in the sizing of the flywheel is taken as the mass for all systems. Cho [149] uses an output inertia value of 0.1 kgm² for a two regime IVT modelled similarly for a 156 kW engine in a sports utility vehicle (SUV). Since the peak input power for the current system is around 100 kW from the analysis of the sizing of the flywheel, the lumped output inertia value of 0.067 kgm² is taken for the current system.

As mentioned before for the multi regime systems, the efficiency includes only those gear pairs which are in the main power flow path for individual stages. According to the actual physical design, there might be gear pairs which are idling while power flows through the others. These losses are expected to be small and are neglected. For the current analysis, the worst case for PSCVT is taken as the acceleration of the vehicle from 0-100 kph, as it includes the maximum acceleration of 0.41g which is higher than the maximum acceleration or deceleration of any of the drive cycles under consideration. The model of the vehicle acceleration as described previously is taken and is updated with the model parameters. This model is then used to calculate the deceleration of the flywheel. The torque loss of the flywheel due to internal losses is calculated using the equation 123 corresponding to 2% loss per minute, which is similar to the one used in [143].

$$T_{\text{loss}} = 0.5 \times J_{\text{FW}} \times \omega_{\text{FW}} \times \frac{\log(0.98)}{60} \quad [123]$$

Further using the efficiency values of PSCVT and corresponding $\frac{P_v}{P_i}$ values, the input power to the variator is calculated during the vehicle acceleration from 0-100 kph using FESS. The Table 19 shows the variator power for different designs. The two regime IC PSCVT (with direct drive as second stage), three regime IC PSCVT and three regime OC PSCVT designs have reasonable level of power flowing through the variator. These are further tested for variator torque in the same operation and the effect of type 1 and type 2 designs is observed in the case of two regime system. The variator torque in type 1 is much higher than in type 2, though its variator speed is much lower. The torque capacity of current belt variators is of the order of 400 Nm [150] and toroidal variator can be even higher [151]. Further the speeds of the individual components is analysed at fixed vehicle speeds for these three transmissions in both forward and reverse directions. Although the ratio of variator power to input power as well as efficiency will be the same for any combination of PGS ratio and fixed gear ratios from the Tables 11-14 for their respective transmissions, the torque and speed through the variator can be influenced by these parameters to suit the design requirements. These three transmissions will be used further for the HV model.

Table 19 Variator power for 0-100 kph operation

Forward power flow	Regimes	Variation	Maximum variator power [kW]
IC	1		174
IC	2	DD first stage	229
IC	2	DD second stage	86
IC	3		73
OC	1		451
OC	2	DD first stage	153
OC	2	DD second stage	461
OC	3		72

A thing to note is that the variator should be able to traverse its entire range in the required time. The worst case would be for a three regime PSCVT where the variator has to traverse its range three times in the duration when the vehicle accelerates from 0-100 kph. The rate of ratio change depends on hydraulics. Higher rate would cause higher pump loss. Hofman and Dai [111] suggests about 2 s for a conventional CVT to traverse its entire range. Pfiffner et al.

[152] mentions the example of a chain drive CVT having a maximum gear ratio difference of 5.5, which takes around 2 s to go from minimum to maximum gear ratio. Judging by these examples the CVT would have sufficient time to traverse its entire range.

4.4 Hybrid Vehicle Layout and Other Components

The Fig. 75 shows the HV schematic. There are two clutches which are introduced into the system. One clutch is placed between the EM and the final drive, which can be used to charge the flywheel while the vehicle is stationary. The other clutch is for bridging the gap between the CVT output speed and vehicle speed.

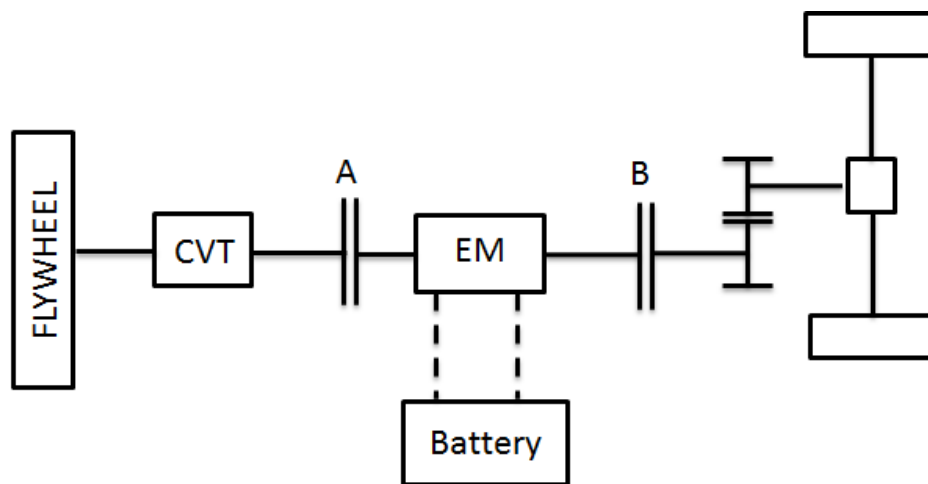


Figure 75 Schematic of the HV

The EM in the original BEV is 72 kW. As mentioned previously the minimum torque of the EM is used for sustained climbing and vehicle top speed. The power required is calculated at the top speed of the vehicle as well as the power required for hill climbing. The performance goals for gradeability are taken from [153]. Accordingly a power of 45 kW is selected for the EM and the machine characteristics are scaled down. The reduction of mass and inertia due to downsizing of the machine would be compensated by the additional clutches in the system.

Another point to consider is the hydraulic control losses due to CVT operation. These losses depend on the pump specification and operation. It is reported that these losses can be from 0.5-1 kW depending on application [11], presumably the lower end would be for passenger car application. In a conventional vehicle, this pump would be driven by the ICE and it would be sized for maximum capacity. Further its operation would be independent of the power requirements. However by controlling the operation of the pump according to requirements these losses can be significantly reduced. It is reported that that the efficiency of the CVT can be improved from 70-80% to 80-86% if the application force is controlled by power requirement [154]. Kluger and Long report that the pump loss is about 67% of the total loss

[148]. One of the ways could be by using an electrical pump which would make sense in an EV [155]. Therefore a reasonable assumption for the pump loss would be around 300 W and that is applied as a constant electric load on the battery. It is assumed that an onboard vacuum pump is not needed to maintain pressure inside the containment which is similar to the case of Flybrid Torotrak system [156].

4.4.1 Control strategy

Control strategy is very important for HV. When hybridising a conventional ICE vehicle there will always be some fuel economy benefit due to engine stop-start and regenerative braking; however in this case it is important to have an optimal strategy as that makes all the difference. There is a wealth of literature on control strategies for HEVs which include ICE and EM, powered by batteries. However, there is lack of literature specifically on control strategies for mechanically integrated high-speed flywheels [157]. This is especially true in case of a mechanical CVT connected FWBEV. Due to this reason, it was important to first find out the global optimal solution to the above control problem which would provide a benchmark for improvement potential and also give ideas to design the controller. This is explored in the next chapter.

5 Benchmark of Energy Management Strategy

In this chapter the energy consumption improvement potential of the HV over the base vehicle in the three real world cycles has been computed. Since the HV layout and most of its components have been fixed in the previous chapter, the only major component left is the control strategy. As mentioned in the previous chapter, it is important to compute the global optimal control strategy which would serve as a benchmark and provide design direction. This would provide the maximum attainable energy consumption benefit that can be achieved by the HV.

5.1 Dynamic Programming

In general the control strategy is one of the most important elements, which decides the energy consumption of the HV. The primary purpose of the supervisory controller is to specify the power distribution between the two sources of energy in the system in order to maximize energy economy while achieving the driver demand. There might be additional requirements such as maintaining SOC of the energy storage and driveability of the vehicle.

The objective of optimal control is to provide a set of control parameters which will cause the system to satisfy certain constraints while minimizing or maximizing certain performance criteria. There are two approaches to optimisation in classical control, one of which is based on the work of Richard Bellman called Dynamic Programming [158] and the other based on the work of Lev Pontryagin called Pontryagin's minimum principle (PMP) [159]. Out of the two approaches, DP guarantees a global optimal.

DP is a very useful tool to find out the optimal solution to non-linear problem with given boundary conditions. It results in global optimum, though it is non-causal in nature and requires that the drive cycle to be known in advance. Further DP takes a lot of computing power and time. Due to these facts it does not offer an online implementable solution, though it can be used to set a benchmark for the performance of other sub optimal control strategies. It also provides insight on how the realistic sub optimal controller should be designed.

DP deals with solving the overall complex problem by dividing it into a series of smaller sub problems. In optimal control theory, DP can be defined as an intelligent brute force method that reduces the computation by seeking to solve each sub problem once. It does that by applying the principle of optimality as defined by Bellman. The principle of optimality states that "An optimal policy has the property that whatever the initial state and the initial decision are; the remaining decisions must constitute an optimal policy with regard to the state resulting from the first decision" [158].

In a DP implementation, the problem is divided into multiple time stages where the implementation of certain control action leads to the transformation of the state variables from their form in one stage to their form in the next stage. With the principle of optimality, given the current state, the optimal control for the remaining states, does not depend on the previous states or control actions. The DP algorithm looks at every stage and computes the minimum cost to go from every stage to the final stage. There exists a recursive relationship that computes the sub problems at each stage using the solutions found for the sub problems of the following stage. The values at the final stage are given by the boundary conditions. The computation time for DP is long and increases with the number of state variables and length of drive cycle.

DP has been extensively applied for the optimisation of energy management of HEV to achieve maximum fuel economy over pre-defined drive cycles [160-162, 149]. However, there are only few cases of DP being applied for flywheel based internal combustion engine hybrid vehicles (FWICEHV) [163-165]. Jamzadeh and Frank applied DP to find the optimal control policy for a FWICEHV on the federal urban drive cycle [163]. In this case the ICE and flywheel are coupled to the CVT and the driver controls the vehicle torque by the CVT and has no control over the engine operation. The only control decision to be made is whether the ICE should be on or off. This simplifies the system control to a great extent. Van Berkel et al. used DP to optimise the fuel economy for a FWICEHV [164]. In this case the ICE and the flywheel are connected using clutches and the CVT is downstream. The speeds of ICE and flywheel are linked and there is no mode of operation where the flywheel and ICE simultaneously motor the vehicle. Dingel et al. used DP to benchmark and compare the fuel savings for an HEV and a FWICEHV [165]. It has been recognised by Van Berkel et al. [164] and Dingel et al. [165] that unlike for an HEV, there is no univocal approach for applying DP to a FWHV and the process is more complex than for an HEV due to many factors including the relatively many kinematic constraints, small energy capacity of the flywheel and slipping clutches. In case of a mechanically connected FWBEV, there is no example in literature showing the application of DP to find optimal EMS. For this application, the optimisation using DP is further complicated due to the fact that both the battery and the flywheel have state variables associated with them and there are more functional options.

5.2 Formulation of the Problem

For the formulation of an optimal control problem, the following three need to be defined.

- A mathematically defined process
- The physical constraints need to be defined

- Performance criteria needs to be specified

In this case, the main criterion is the minimizing of energy consumption during the pre-defined drive cycle and system constraints are defined. DP is used to calculate the optimal torque distribution over the cycle. Additional options such as vehicle launch using slipping clutch and using EM as well as variation of initial flywheel SOE are explored. For the implementation of DP, the model of the HV needs to be defined as discrete step using the backward power flow approach.

5.3 Component models

5.3.1 Battery

The battery here is modelled simply as consisting of an internal resistance and an open source voltage. The primary reason for choosing this model is to reduce complexity and save on computation time. V_{OC} is the open circuit voltage of the battery and r_{int} is the internal resistance which depend on the SOC of the battery. P_{bat} and C_{bat} denote the power and the capacity of the battery. The simulation time step is denoted as Δt . Battery current and voltage are denoted by i_{bat} and V_{bat} respectively.

$$V_{bat} = V_{OC} - r_{int} \times i_{bat} \quad [124]$$

$$P_{bat} = V_{OC} \times i_{bat} - r_{int} \times i_{bat}^2 \quad [125]$$

$$SOC_t = \frac{SOC_{t-1} \times C_{bat} - i_{bat,t} \times \Delta t}{C_{bat}} \quad [126]$$

5.3.2 Electric Machine

The EM is modelled by using a characteristic map specifying efficiency as a function of torque and speed. P_{EM} , T_{EM} , ω_{EM} and η_{EM} describe the power, torque, speed and efficiency of the EM respectively. The auxiliary power (P_{aux}) includes which includes the power required for vehicle housekeeping and pump losses of the transmission.

$$P_{bat} = P_{EM} + P_{aux} \quad [127]$$

$$P_{EM} = \frac{T_{EM} \times \omega_{EM}}{\eta_{EM}} \quad [128]$$

5.3.3 CVT and Flywheel

The CVT is modelled by its efficiency dependent on ratio and lumped input and output inertias. The idling losses of the CVT are neglected. The flywheel and the input inertia of the CVT are modelled as a single inertia. The equations (129-130) describe the torque acting on the flywheel depending on whether it is providing energy or absorbing it. T_{CVT} , r_{CVT} and η_{CVT} give the CVT torque, speed ratio and efficiency of the transmission. T_{FW} , T_{loss} , ω_{FW} , J_{FW} , SOE and E_{FW} are defined as the net flywheel torque, flywheel loss torque, flywheel speed, flywheel inertia, state of energy and energy capacity of flywheel.

In case the flywheel is providing energy, the equation 129 applies

$$T_{FW} = \frac{T_{CVT} \times r_{CVT}}{\eta_{CVT}} + T_{loss} \quad [129]$$

In the case the flywheel is absorbing the energy

$$T_{FW} = T_{CVT} \times r_{CVT} \times \eta_{CVT} + T_{loss} \quad [130]$$

As mentioned previously in equation 123, the loss of the flywheel is defined as the energy loss of 2% per minute.

$$\omega_{FW,t} = \Delta t \times \frac{T_{FW,t}}{J_{FW}} + \omega_{FW,t-1} \quad [131]$$

$$SOE = \frac{1}{2} \times J_{FW} \times \frac{(\omega_{FW}^2 - \omega_{FW,min}^2)}{E_{cap}} \quad [132]$$

5.3.4 Driveshaft and Vehicle

The torque required at the drive shaft (T_{drs}) is the summation of T_{EM} and T_{CVT} .

$$T_{drs} = T_{EM} + T_{CVT} \quad [133]$$

The driveshaft torque is simply derived from the torque at the wheel (T_{whl}) by using the various vehicle resistances, final drive ratio (r_{FD}) and efficiency (η_{FD}) as shown in equation 134 where A_{veh} is the acceleration of the vehicle, m the equivalent mass of the vehicle including the rotating inertias, C_d the discharge coefficient, $A_{r_{veh}}$ the frontal area, ρ_{air}

density, V_{veh} velocity of vehicle, g acceleration due to gravity, f_r rolling resistance and r_{dyn} the rolling radius.

$$T_{whl} = (m \times A_{veh} + 0.5 \times C_d \times A_{veh} \times \rho_{air} \times V_{veh}^2 + m \times g \times f_r) \times r_{dyn} \quad [134]$$

In case of the motoring vehicle, the equation 135 applies.

$$T_{drs} = \frac{T_{whl}}{r_{FD} \times \eta_{FD}} \quad [135]$$

In case of braking vehicle, the equation 136 applies.

$$T_{drs} = \frac{T_{whl} \times \eta_{FD}}{r_{FD}} \quad [136]$$

5.4 Hybrid Vehicle Operation

The torque at the drive shaft is calculated in advance for the pre-defined drive cycle. It is assumed that the flywheel has an initial speed. Following are the various modes of operation.

$$V_{veh} = 0$$

The vehicle is stationary and the clutch A (from Fig. 75) is not engaged. During this mode the speed of the flywheel is decreasing due to the friction losses of the flywheel and the CVT is at its minimum speed ratio. The only electric load is the auxiliary load.

$$T_{whl} > 0 \text{ and } \omega_{EM} < (\omega_{FW} \times r_{CVT, \min})$$

The vehicle is motoring and the clutch A is not engaged. In this mode there are two options, either the EM motors the vehicle till the speed difference between the input and output sides of the clutch is overcome or the flywheel motors the vehicle while the clutch is slipping till the speed difference is overcome and after that the clutch is closed. In the former case, the flywheel is idling and in the latter case the EM is idling. The CVT ratio is maintained at its minimum value. The electric load on the battery is the sum of the auxiliary load and EM load, in case it is used to motor the vehicle.

$$T_{whl} > 0 \text{ and } \omega_{EM} \geq (\omega_{FW} \times r_{CVT, \min})$$

The vehicle is motoring and the clutch A is engaged. During this mode, the torque is split between the EM and the flywheel, though the option of the EM providing torque to the vehicle and charging the flywheel is also there. The CVT ratio changes accordingly. Theoretically the

flywheel could also be used to charge the battery via EM, but that option is not used as that would negate the primary purpose of using the flywheel as the secondary storage device.

$$T_{whl} < 0 \text{ and } \omega_{EM} \geq (\omega_{FW} \times r_{CVT,min})$$

The vehicle is braking and clutch A is engaged. In this case the flywheel is performing regenerative braking and EM is idling. The CVT ratio varies as needed till the minimum ratio is reached and thereafter the clutch is disengaged.

$$T_{whl} < 0 \text{ and } \omega_{EM} < (\omega_{FW} \times r_{CVT,min})$$

The vehicle is braking and clutch A is not engaged. In this case the mechanical brakes are used. This case as well any other case where the clutch A is not engaged, would usually take place at vehicle speeds below 10-15 kph. This situation is similar to the case with the base BEV where the EM does not do brake energy recuperation below 10 kph.

5.5 Optimisation

The target of the optimisation process is to reduce the energy consumed during a drive cycle. For this purpose the control objective taken is to minimize the total charge removed from the battery which is a direct indicator of the energy consumed during the cycle.

$$\min \sum_{t=1}^N i_{bat} \times \Delta t \quad [137]$$

The boundary condition is that the flywheel SOE at the end should be the same as that in the beginning so that there is no net energy stored in the flywheel.

$$SOE(N) = SOE(1) \quad [138]$$

The two state variables are flywheel SOE and battery SOC. The EM torque is the control variable and is used to derive the flywheel state. The constraints are applied on the flywheel speed, CVT ratio, EM torque and battery current. The flywheel and CVT ratio have to be within their minimum and maximum limits. The transmission design limits have been considered during its design, so they are not applied here. The rate of change of CVT ratio is also observed. Further DP requires gridding of the state and control variables. The important thing to make sure is that this grid should be balanced, in other words the action of the control variable on the state variable should change its state from one grid point to another one which is as close as possible to a grid point. This has an important effect on the computation time. A more balanced grid significantly reduces the computation time. Fig. 76 shows the DP procedure to

calculate SOC_t , SOE_t and $i_{bat,t}$ at time t when SOC_{t+1} and SOE_{t+1} are known at time $t + 1$ during the vehicle motoring operation when the clutch A is engaged. The rest of the process is the usual one.

$$\omega_{FW \min} \leq \omega_{FW,t} \leq \omega_{FW \max} \quad [139]$$

$$r_{CVT \min} \leq r_{CVT,t} \leq r_{CVT \max} \quad [140]$$

$$T_{EM,t} \leq T_{EM \max} \quad [141]$$

$$i_{bat,t} \leq i_{bat \max} \quad [142]$$

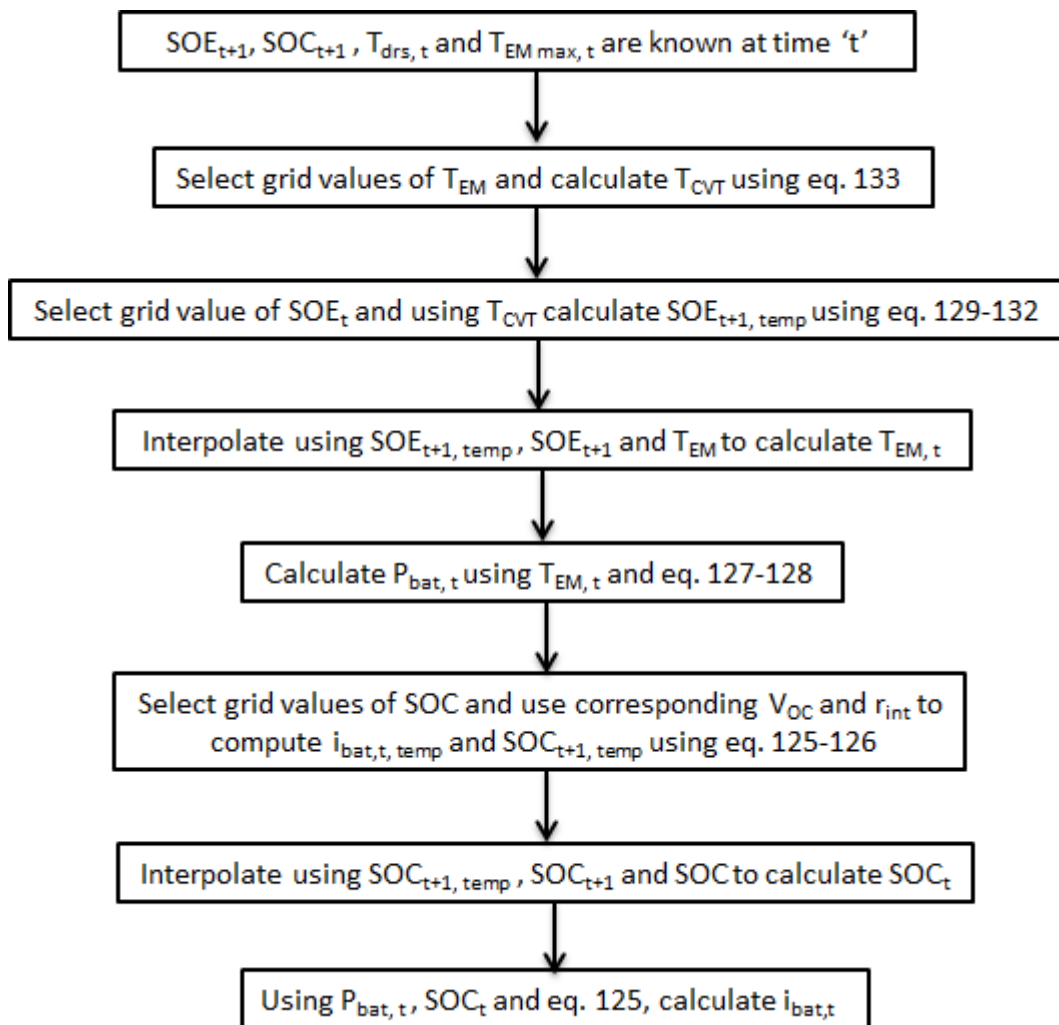


Figure 76 DP process during the mode when vehicle is motoring and clutch A is engaged

The DP is performed on three real world driving cycles which were used in the previous chapter. Firstly the three regime IC PSCVT transmission is used in the model and the DP is run for each of the three cycles. Since in case of FWHV the start SOE of the flywheel can be controlled, the DP is run at intervals of 10 % SOE for the three cycles. Since the SOE is to be

balanced, the DP is run and the control trajectory which gives the SOE balance with the minimum charge consumption for the drive cycle is selected. The Fig. 77 shows the result for the AU cycle. It can be clearly seen that the smallest charge consumption is achieved when the process is started with the smallest initial flywheel SOE. This is expected since the flywheel has to be returned to the same SOE as that at the beginning. Further the same process is repeated for the US06 cycle and LA92 cycle and lowest possible initial SOE is the one with least charge consumption. As expected, it is seen that the LA92 and US06 cycles, require a higher initial SOE than the AU cycle due to the fact that they are relatively higher power cycles. All further DP runs would be done at the initial SOE decided at the previous step for the three concerned cycles.

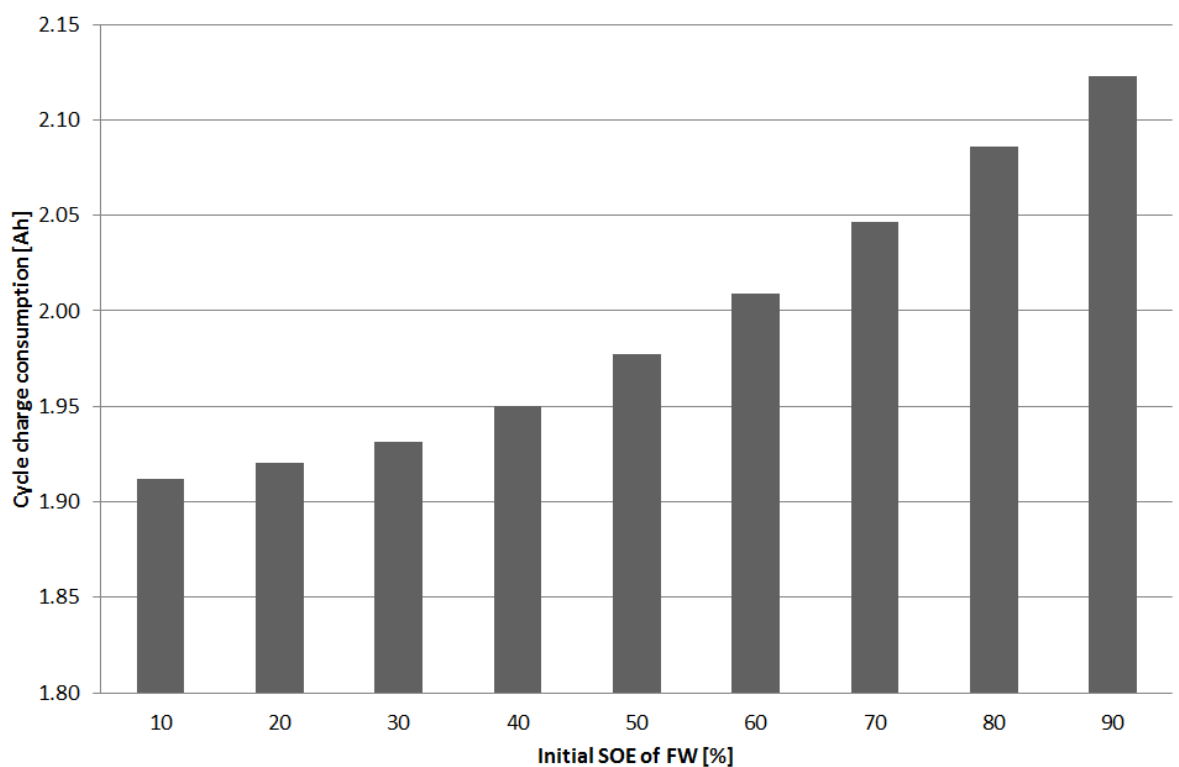


Figure 77 Cycle charge consumption [Ah] for AU cycle for different initial flywheel SOE

As mentioned previously there are two ways of launching the HV. It can be launched via the EM or via the flywheel by slipping the clutch A. To test which one to select, DP is run for both the options. Fig. 78 shows the increase in cycle charge consumption while going from the option of EM based launch to flywheel based launch. The launch via EM is more favourable since it consumes less charge. This is due to the energy lost while the clutch is slipping and the vehicle is launching. The power lost in the clutch can be calculated by multiplying the torque passed through the clutch and the speed difference across it. Another thing to observe is that the increase in cycle charge consumption is highest for the AU cycle and lowest for the US06

cycle which is expected since the AU is a relatively low powered cycle as compared to US06 cycle so the EM power required to launch the vehicle is lower which in turn gives lower battery losses. Again for all further DP runs, it is decided based on the result that the vehicle is to be launched by using the EM.

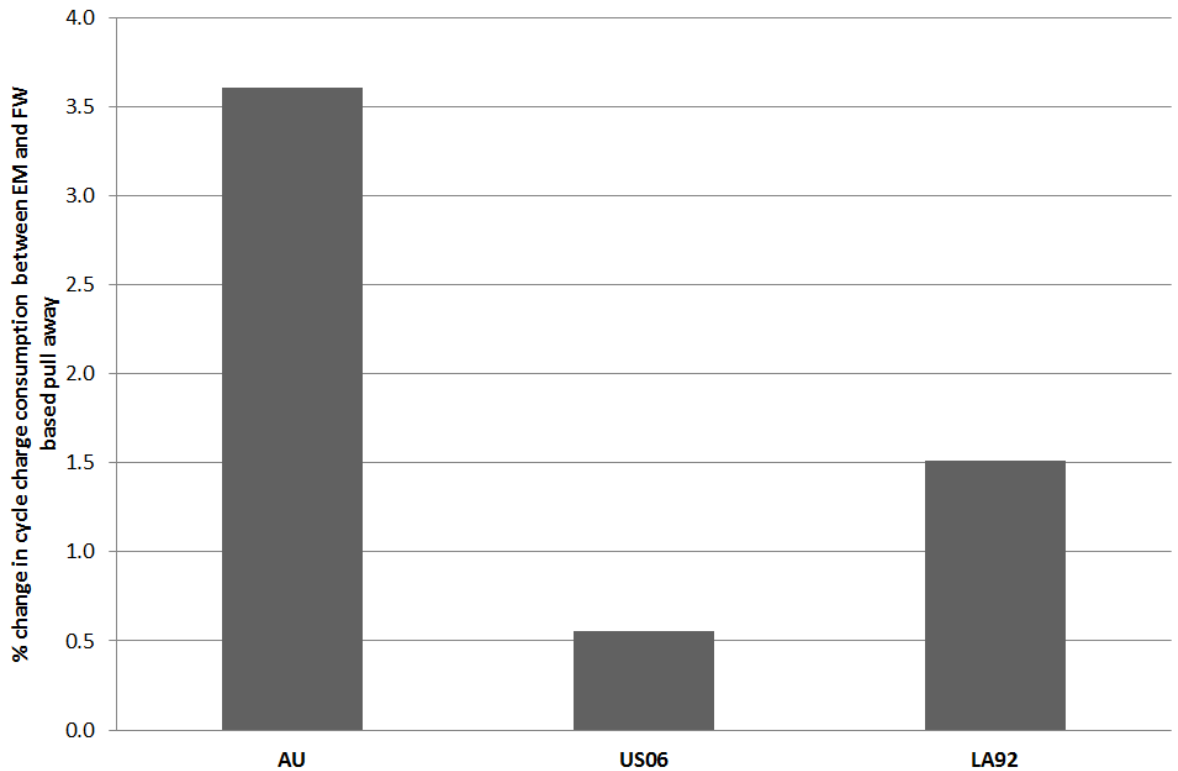


Figure 78 Difference [%] cycle charge consumption between EM and flywheel vehicle launch

The three transmissions designed in the previously are selected and DP is performed on the three cycles with the mode that EM launches the vehicle. As is expected the three regime systems, both IC and OC, give lower charge consumption as compared to the two-regime transmission. This is due to the predominantly lower efficiency of the two regime system in the middle speed ratio area. The three-regime IC PSCVT and OC PSCVT give very similar charge consumption on all the three cycles, with the OC system being just marginally better. For further analysis the three-regime OC PSCVT system is selected.

The calculations up to now have been performed on a time step of 0.5 s so as to save computation time. The next step involves comparing the energy consumption of the HV with that of the base BEV on the three cycles. The original base vehicle model presented in Chapter 3 was a forward simulation model with variable time step built in AVL Cruise [106]. However for this comparison a backward simulation model with fixed time step is created and that is used to compute the energy consumption to compare it with the HV. Further a suitable time step needs to be chosen which would be a compromise between computation time and

accuracy. For this process a smaller time step of 0.1 s is chosen. Applying an average speed of 30 kph for the drive cycles and a torque resolution of 2 Nm for EM torque, the energy handled by the CVT is around 44 J which is roughly equivalent to 0.005 % SOE of the flywheel if losses are neglected. For the further process, flywheel SOE resolution of 0.005% and 2 Nm torque increment are used.

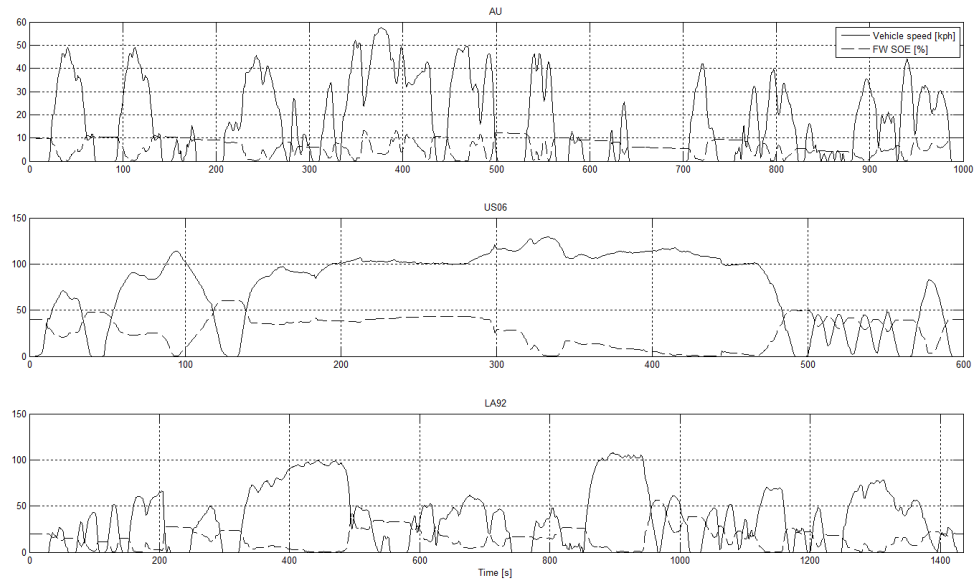


Figure 79 Vehicle speed [kph] and flywheel SOE [%] during drive cycle

5.6 Results and Discussion

In this section the results between the base BEV and the HV are presented and analysed for the three cycles. The start SOC of the battery for the simulations is taken between 85-90% since above 90% regenerative braking is not allowed in the base BEV. The simulations are run steady state at temperature of 25° C. These conditions also represent the best case for BEV since at higher/lower temperatures or at lower SOC; the performance of the battery is expected to be poorer. The Fig. 79 shows the three drive cycles and the variation of flywheel SOE. It can be seen that due to the end constraint in the DP the final SOE converges to the initial value. Fig. 80 shows the torque split in the three drive cycles. It can be seen that the EM torque is much reduced during high driveshaft demand torque and the brake torque demand is provided entirely by the flywheel. Further Fig. 81 shows the energy economy comparison between the base BEV and the HV on the three cycles. It can be seen that the HV has a higher cycle energy economy by 11% and 3.2% as compared to the base vehicle in US06 and LA92 cycles respectively, though it has reduced energy economy by 2% in the AU cycle. Further Table 20 provides the comparison of individual component efficiencies of the drive train and other important results.

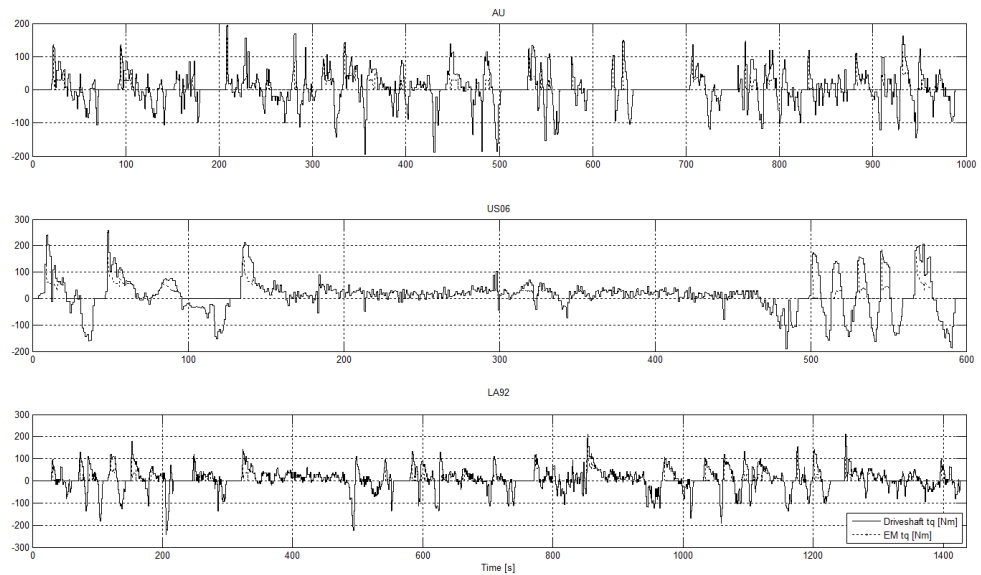


Figure 80 Driveshaft torque [Nm] and EM torque [Nm] during drive cycles

The first thing to observe in Table 20 is that the motoring energy required in the cycle for the HV is higher than that of the base. This is primarily due to the higher weight and inertia in the HV. As has already been shown in Fig. 81, the HV has higher energy economy than the base vehicle in the US06 and LA92 cycles and has a corresponding lower value in the AU cycle. The primary aim of the flywheel in the HES is to protect the battery from high currents to improve its efficiency and life. The improvements in efficiency occur mainly because of the lower battery losses. As can be seen from the Table 20 the battery losses are significantly reduced for the HV as compared to the base vehicle which results in impressive improvements in the battery round trip efficiency.

Further since the EM in the HV is a downsized version of the one in the base vehicle, the operating points on the EM in the HV occur in the higher efficiency regions as compared to the base vehicle. The chapter 3 explored the effect of downsizing the EM on the BEV energy consumption. Due to this fact, a slight improvement in the EM cycle efficiency is observed in the HV as compared to the base. Besides the efficiency improvement, additional benefit is expected in terms of cost due to the downsizing. The CVT efficiency in the cycle is around 90%. Another important advantage of the flywheel in the HV is the drastic reduction of the peak current and peak electric power of the battery as compared to the base vehicle. This reduces the stress on the battery significantly and is expected to improve the life of the battery and lower operating costs. The average battery power is slightly higher in the HV than the base vehicle to take into account the losses in the flywheel and CVT system.

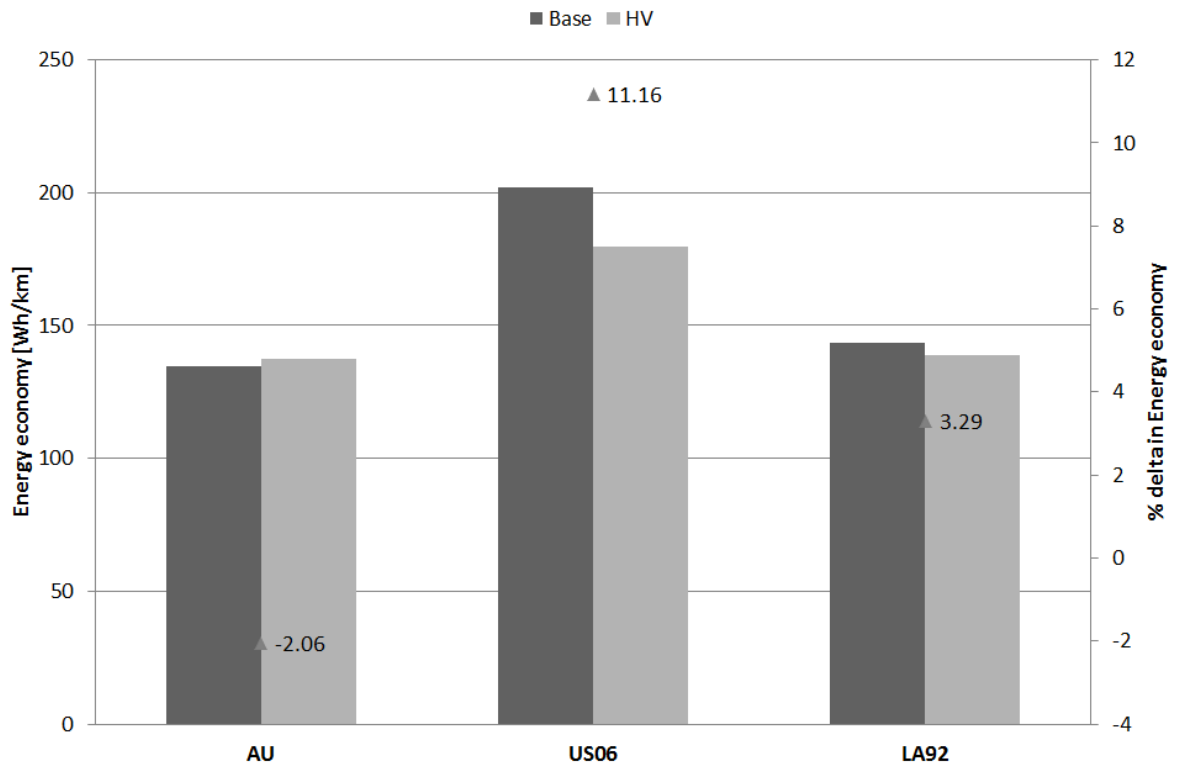


Figure 81 Energy economy [Wh/km] for the drive cycles and difference [%] in energy economy between BEV and HV

Although there are significant benefits obtained in the HV in regards to lower battery peak current and power, the energy consumption in the AU cycle is higher than the base vehicle. It is important to note that though the consumption is higher by 2.06%, the absolute value (13.4 Wh) is quite small. The main reason for this is that the AU cycle is relatively lower power cycle than the US06 and LA92 cycles, and the lower battery losses in the HV are negated by higher required cycle motoring energy and auxiliary losses. The higher auxiliary losses in the HV are due to the fact that it includes the vehicle housekeeping electric loads and transmission pump losses. In the other cycles, these factors have a much lower impact due to the relatively higher power required in these cycles. A check was done to find out if the energy consumption of the HV in AU cycle would improve if it was run as a pure BEV. In this simulation, the clutch A was kept open and the auxiliary power was reduced to the level of the base BEV. It was found that the energy consumption of the HV actually increases by 1.08%.

Table 20 Comparison between BEV and HV

Quantity	AU		US06		LA92	
	Base	HV	Base	HV	Base	HV
Start SOC battery [%]	88.25		86.30		85.77	
Start FW SOE [%]	-	10	-	40	-	20
Motoring energy cycle [Wh]	839.88	891.59	2356.16	2447.37	2486.89	2607.06
Cycle energy consumption [Wh]	655.33	668.80	2603.93	2313.22	2264.75	2190.27
Battery losses [Wh]	103.14	21.04	601.2	211.51	394.54	150.84
Round trip battery efficiency [%]	84.26	96.85	76.90	90.85	82.57	93.11
EM losses [Wh]	159.3	48.4	313.8	157.4	379.8	148.2
EM efficiency [%]	89.17	89.96	90.55	92.13	90.19	91.76
CVT losses [%]	-	95.6	-	148.7	-	212.1
CVT efficiency [%]	-	91.21	-	89.99	-	90.71
FW losses [Wh]	-	33.9	-	31.6	-	60.2
Auxiliary losses [Wh]	82.75	165.5	50	100	119.5	239.1
Peak current [A]	109	64	261	123	177	118
Peak battery power [kW]	46.44	23.17	69.95	40.29	66.6	38.36
Average battery power [kW]	2.0	2.34	12.01	12.61	4.69	5.11
% of FW energy gained from EM [%]	-	0.06	-	2.08	-	0.42

Another interesting point to note is that although there is an option of the flywheel being charged by the EM during the vehicle motoring, this option is almost always avoided by the optimal EMS. The percentage of flywheel energy which is input by the EM is quite low. The bulk of the flywheel energy is gained only by regenerative braking. The highest is about 2% in the US06 cycle, which reflects the fact that it is most high power cycle among the three drive cycles.

This chapter provided the benchmark results and design guidance for the controller, but not a real life implementable controller. This would be explored in the next chapter.

6 Control of the Hybrid Vehicle

This chapter deals with the development of a sub optimal real life implementable controller for the HV. The main aim of the controller results is to get as close as possible to the benchmark results. The controller is first implemented in the quasi-static backward model and results compared to the benchmark simulation. Finally it is implemented in a more realistic forward dynamic model.

6.1 Energy Management Strategy

A major challenge in the design of mechanically connected FWBEV powertrain is the EMS. The performance of the powertrain is highly dependent on the torque split between the two sources of energy in the system i.e. the battery and the flywheel. To get the best performance of the system an optimal EMS is essential. There are various types of control strategies and can be categorised into various groups. Salmasi has explained in detail the various types of control strategies for HEVs [166]. In general there are two types.

- Rule based strategies: These are based on heuristics, intuition and human expertise. The main point of these strategies is that these are easy to implement and are effective in real time though they are usually far from optimal. These strategies apply a set of rules to the instantaneous operating parameters to produce a control and usually do not require a priori knowledge of the drive cycle. These can be further divided into deterministic and fuzzy rule based. An example of deterministic and fuzzy rule based strategy for FWHV is shown in [157] and [167] respectively.
- Optimal strategies: These can be divided into local optimisation and global optimisation strategies. The local optimisation strategies compute instantaneous optimal control depending on the current operation of the vehicle and may use offline driving data and past journey information. On the contrary global optimisation techniques compute global optimal control for the entire drive cycle. These are non-causal in nature and require that the complete drive cycle is known in advance. The two methods which constitute the global optimal control theory i.e. DP and PMP were mentioned in the previous chapter.

Another classification divides energy management strategies based on their dependency of the knowledge of future driving conditions into predictive and non-predictive controllers. Predictive controllers use limited future journey information to optimally use the two energy sources in a HV to reduce fuel consumption. It is well known and has been shown by various authors [168-169, 77] that predictive control in HV has the potential to significantly reduce fuel consumption. This is especially true in case of a FWHV, since the flywheel has relatively small

energy capacity and its SOE changes rapidly as compared to a battery in a HEV. For example in the current case, if the HV is motoring, torque can be supplied both from EM and flywheel if it has sufficient SOE. A non-predictive strategy might use the flywheel immediately to assist the EM whereas if higher torque is required in the near future without any chance of charging the flywheel, the HES might not be optimally used. Thus in the present case it is decided to implement predictive control.

6.2 Predictive control for HV

There are various ways to implement predictive control. Rajagopalan and Washington [169] and Cho [149] implemented predictive control using fuzzy rule based EMS for HEVs. Though a deterministic or fuzzy rule based predictive control is suitable for HEV, it is not suitable for the FWHV due to the smaller capacity and rapid cycling of the flywheel. Thus an optimal controller is needed.

As mentioned before DP and PMP are the two methods of optimisation in classic control, out of which DP guarantees the optimal solution. Although overall optimum is reached, DP has drawbacks to be implemented in real time. First the complete drive cycle has to be known in advance. Secondly the computation time for DP is long and increases with the number of state variables and length of drive cycle. Thirdly the results are specific to the drive cycle on which it is run. Due to these reasons most studies involving DP use the result to provide benchmark for the vehicle [149, 160, 162, 165] and/or provide direction in the design of sub-optimal controllers [170].

More recently some studies have looked at the implementation of global optimisation techniques for real time implementation. One study [171], investigates the application of DP to design a real time control for a HEV for the entire predicted route with a short computation time. The authors assume that the complete driving cycle is known a priori. They show encouraging results for short distance missions. In a similar study [172], a DP-based global optimal power-management scheme for plug-in HEV is presented with the complete future journey created by trip modelling with traffic data. The computation time aspect of this approach is tackled in another related paper by the authors, whereby a two scale DP approach is used for efficient computation [173]. In another study, a combination of DP and classical optimal control theory is used for the EMS of a HEV to optimise the vehicle velocity, gear position and engine power over a preview route segment such that the fuel economy is improved and vehicle completes this route segment within a predefined time length [174]. The computational efficiency is significantly improved compared to the case of using only DP algorithm. A somewhat similar method is suggested in [175]. In the current case a DP based

EMS is implemented for the HV with short computation time intended for real-life implementation. The EMS uses limited future journey information to derive the optimal torque for three real world drive cycles used previously.

6.3 DP based Energy management strategy

In order to implement a predictive controller for the current case, future journey information is needed. Any specific road trip can be broken up into smaller road sections or micro trips where the stop period between any two micro trips can be due to a variety of reasons such as traffic light, stop signs, junctions or roundabouts, though the majority are reported to be due to traffic lights and stop signs [176]. As a result of various telematics technologies and traffic information systems, it is assumed that the vehicle velocity and slope information for the forthcoming micro trip is known a priori at fixed time resolution of 1 s. Thus 1 s would be the time interval for the DP calculation. The three drive cycles on which the controller is to be tested are divided into their micro trips. The AU, US06 and LA92 cycles are divided into 16, 5 and 16 micro trips respectively.

The DP algorithm used in this section is the same as was used for the benchmark simulation from Chapter 5. However in order to make it a realistic option, modification is done on the grid interval for the state variables. In the previous chapter, a fine resolution was taken for the grid of state and control variables in order to achieve maximum accuracy. However a fine grid increases the accuracy at the expense of computation time. The initial resolution for the state variable is taken to be 0.5% and the EM torque increment is taken to be 2 Nm.

The quasi-static vehicle model is run at time step of 0.1 s, since that is the resolution of the benchmark simulation. The initial flywheel SOE and battery SOC for the three drive cycles is taken the same as the benchmark simulation results. The simulation runs till the start of a micro trip is reached which then enables the DP algorithm to run to compute the optimal control variable matrix giving the minimum cost. This matrix is a function of the flywheel SOE and time. After obtaining this matrix the calculation runs further and depending on the current flywheel SOE and time, the optimal EM torque is computed from the matrix and used in operating mode 3. Since the DP algorithm is run at 1 s time step and the simulation runs at 0.1 s, nearest neighbour interpolation is used to compute the optimal EM torque for the in between time. This process is repeated at the start of each micro trip and at the last micro trip, the control tries to achieve flywheel SOE balance by introducing the equality constraint given in equation 138. The simulations were conducted on a 2.5 GHz CPU laptop with 4 GB RAM.

The resolution of the state variable of the DP algorithm strongly affects the computation time of the process. The Fig. 82 shows the normalized cycle energy consumption and normalized

cycle. Naturally as the flywheel SOE resolution is made coarser, the computation time is reduced as well as the accuracy. The decrease in accuracy is less pronounced than the decrease in computation time as the scales of the graph point out. Also as the resolution is made coarser with each step the computation time benefit reduces. A resolution of 0.7% flywheel SOE is seen as a reasonable compromise value between accuracy and computation time and is used in further computations. The Table 21 gives the computation time for the three cycles with 0.7% flywheel SOE resolution and the cycle duration.

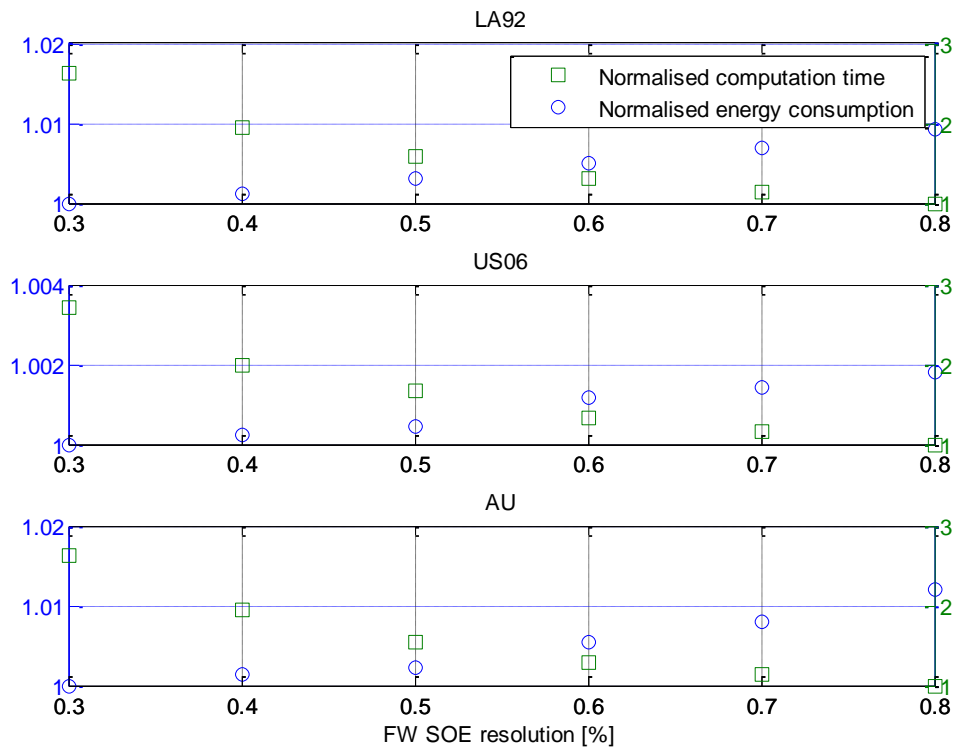


Figure 82 Computation Time vs. Energy Consumption

As can be seen from the Table 21, the computation time is drastically reduced to a matter of few minutes as compared to the usual time it takes to run DP which can go into a number of hours or even days as was the case for the benchmark simulation. In real life implementation, the controller would be able to run the DP algorithm for the forthcoming micro trip during the currently running micro trip, such that it has the optimal control ready when that micro trip actually starts.

Table 21 Computation Time

	AU	US06	LA92
Computation time [s]	114	145	260
Cycle duration [s]	993	600	1435

6.4 Simulation results

In this section the results of the DP based EMS are compared to the benchmark simulation results presented in the previous chapter. The Fig. 83 and 84 show the comparison of results in terms of flywheel SOE and EM torque for the three drive cycles. It can be seen that due to the end constraint in the benchmark simulation results the final SOE converges to the initial value, where as in case of the DP EMS it does not always maintain SOE balance though it generally follows the same trend as the benchmark simulation. Same is the case with EM torque in Fig. 84. Further Table 21 provides the comparison of cycle energy consumption, individual component efficiencies of the drive train and other important results.

Table 22 Comparison between DP EMS and Benchmark

Quantity	AU		US06		LA92	
	DP EMS	Benchmark	DP EMS	Benchmark	DP EMS	Benchmark
Start SOC battery [%]	88.25		86.30		85.77	
Start FW SOE [%]	10		40		20	
Delta FW SOE [%]	1.32	-	5.21	-	0.87	-
Energy economy [Wh/km]	140.98	137.33	185.56	179.48	142.26	138.67
Energy economy difference [%]	2.65		3.38		2.58	
Battery losses [Wh]	18.81	21.04	240.00	211.51	160.29	150.84
Battery efficiency [%]	97.2	96.8	89.9	90.8	92.8	93.1
EM losses [Wh]	55.26	48.4	165.92	157.4	163.54	148.2
EM efficiency [%]	88.99	89.96	91.91	92.13	91.14	91.76
CVT losses [Wh]	100.29	95.6	178.00	148.7	236.12	212.1
CVT efficiency [%]	91.15	91.21	89.81	89.99	90.48	90.71
FW losses [Wh]	36.77	33.9	30.96	31.6	63.73	60.2
Peak current [A]	67	64	164	123	145	118
Peak battery power [kW]	24.21	23.17	51.29	40.29	45.76	38.36

The first thing to observe in Table 22 is that the difference in cycle energy consumption of the DP EMS from the benchmark results is within 2-3% which shows that a good performance can be achieved with this control. AU and LA92 cycles are both around 2.5% from their respective benchmark simulation, whereas the US06 is slightly worse of at 3.3%. This is also reflected in the fact that the delta flywheel SOE in case of the US06 is the worst of the three at 5.2% whereas for the LA92 and AU drive cycles is only about 1%. The battery, EM and CVT efficiencies are very close for both the cases. The flywheel losses, peak current and peak battery power are slightly worse off with the most deviation observed in the US06 cycle. This is probably due to the fact that the US06 is the most aggressive of all the three cycles and Fig. 83-84 show that the benchmark EMS utilizes the flywheel somewhat differently in the first two micro trips and the last micro trip of US06 cycle and its effect is seen in the EM torque as well. In all the result of the DP based EMS would always be sub optimal due to limited future trip information and coarser resolution.

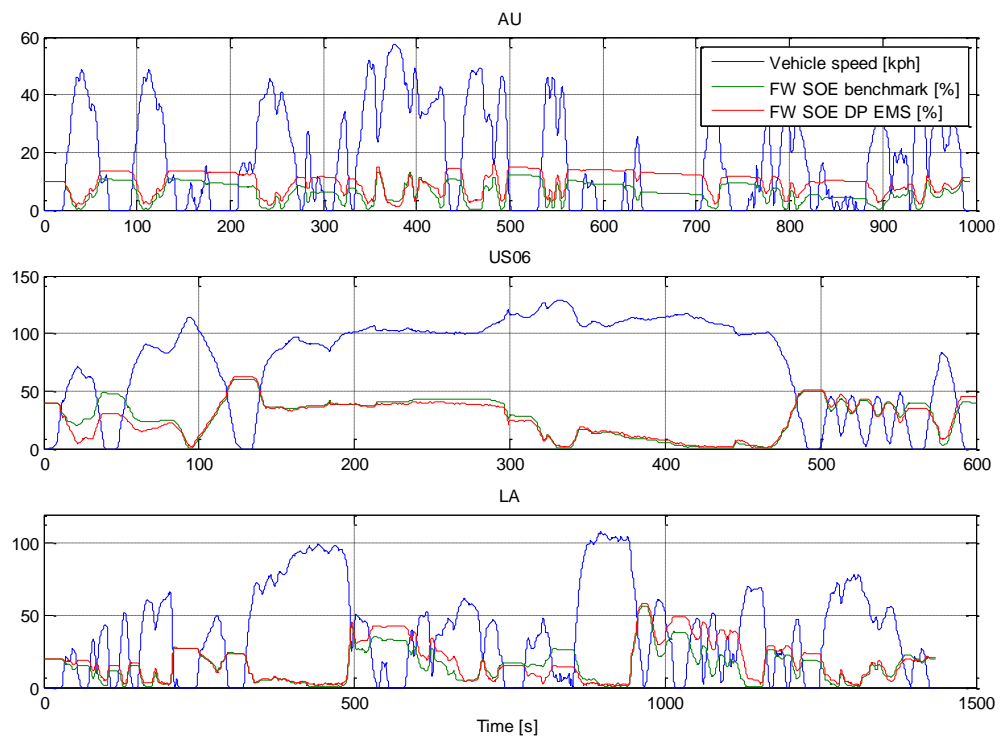


Figure 83 Benchmark vs. DP EMS results for flywheel SOE

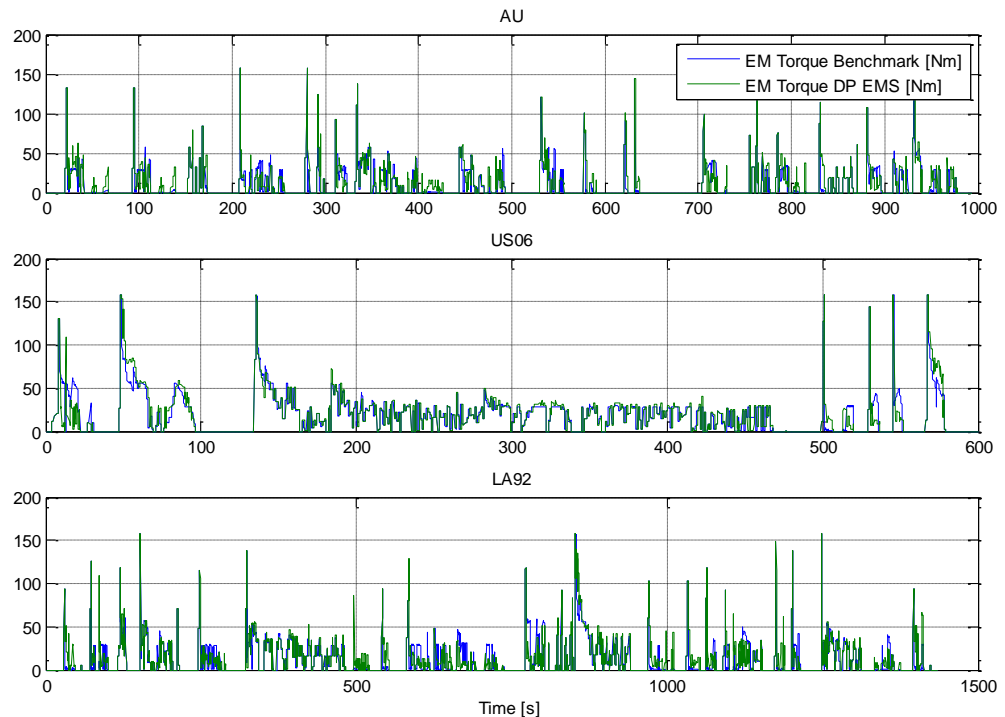


Figure 84 Benchmark vs. DP EMS results for EM Torque

6.5 Forward Simulation

In the previous section the performance of the predictive controller was demonstrated in a quasi-static backward simulation. However the backward model though good for initial design is not realistic as it does not include detailed dynamics of the powertrain and a driver model. To check the suitability of the model for real life implementation it should be tested in a more realistic simulation environment. This section presents a forward dynamic model of the powertrain.

As was the case with the base BEV, the forward dynamic model of the HV is built in AVL Cruise. Although AVL Cruise has a pre-built library of various powertrain components and driver models which can be directly used in modelling, it does not have a flywheel component. In this case the vehicle powertrain and driver model are built in AVL Cruise and the flywheel model and controller are built in Simulink. These are then coupled together to run as co-simulation during which the information is exchanged between the tools at each calculation step and both the tools use their own variable solvers. The drawback of this kind of co-simulation is that it runs at a slow pace.

The Fig. 85 shows the powertrain built in AVL Cruise. Most of the components are self-explanatory. The cockpit module is for the driver. The standard driver model in Cruise handles most situations very well and as such does not need manual tuning. The 'Matlab API' module is

for the interface to Simulink. It contains the signals which are to be exchanged. As in the quasi-static model, the CVT is modelled as lumped output and input inertias and efficiency. The 'Flange' module represents the output of the CVT. A starting speed can be prescribed to it which would of course depend on the initial flywheel SOE. It is torque controlled while the clutch next to it is engaged and speed controlled while it is disengaged. The input inertia of the CVT and flywheel are modelled in Simulink.

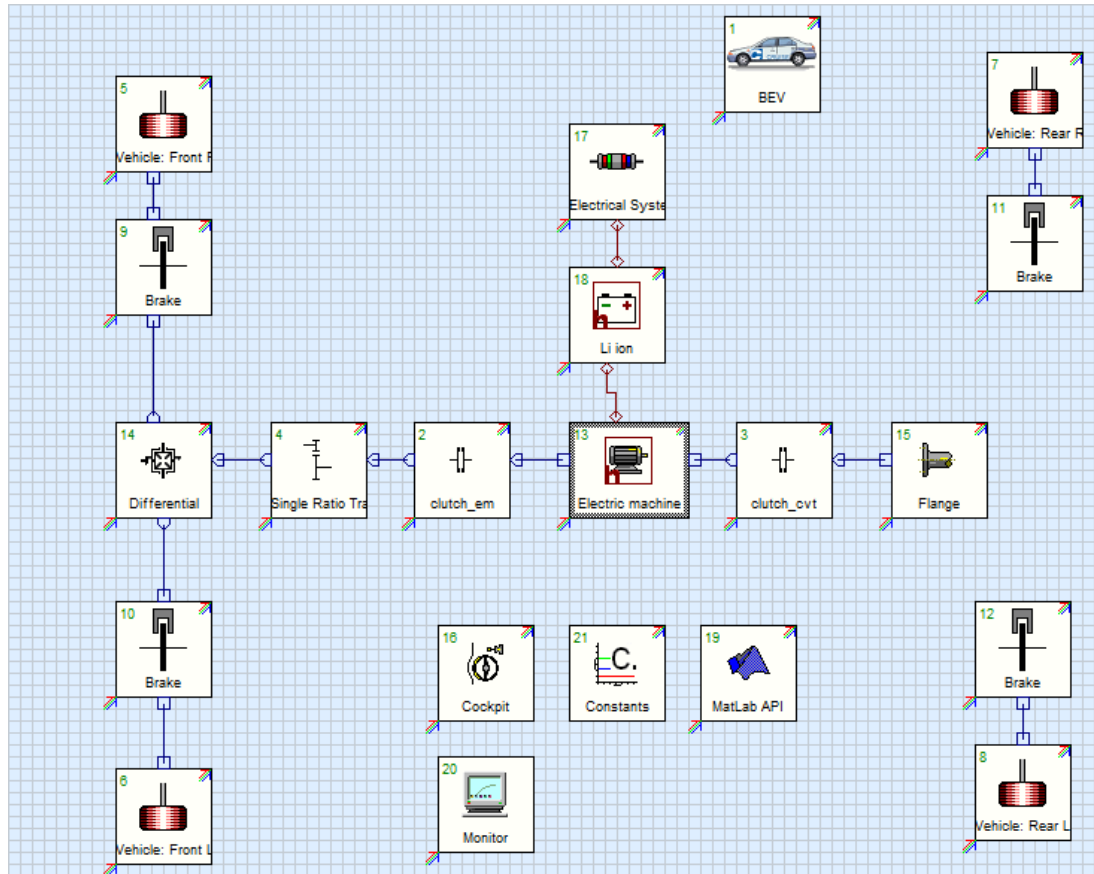


Figure 85 HV model in AVL Cruise

Fig. 86 shows the model in Simulink. The model inputs the load signal, brake pressure, EM speed and flange speed from the Cruise model and outputs EM load, mechanical brake, clutch release of both the clutches, CVT output torque and CVT output speed (only used when the 'clutch_cvt' is disengaged). From the load signal and EM speed signal, a desired torque is calculated. Similarly from the brake pressure a desired brake torque is calculated. The maximum EM torque is calculated from its characteristic map using EM speed. As in the case of the quasi-static model, the optimal EM torque is calculated from its optimal control matrix computed using the DP algorithm by 'nearest neighbour' interpolation. The main controller calculates the desired CVT and EM torque and the desired mechanical brake. Further the flywheel model uses that to calculate flywheel SOE. The 'clutch_em' (or clutch B from backward simulation) remains engaged throughout the simulation and 'clutch_cvt' (or clutch A

from backward simulation) is controlled as mentioned before in the HV operating modes in Chapter 5.

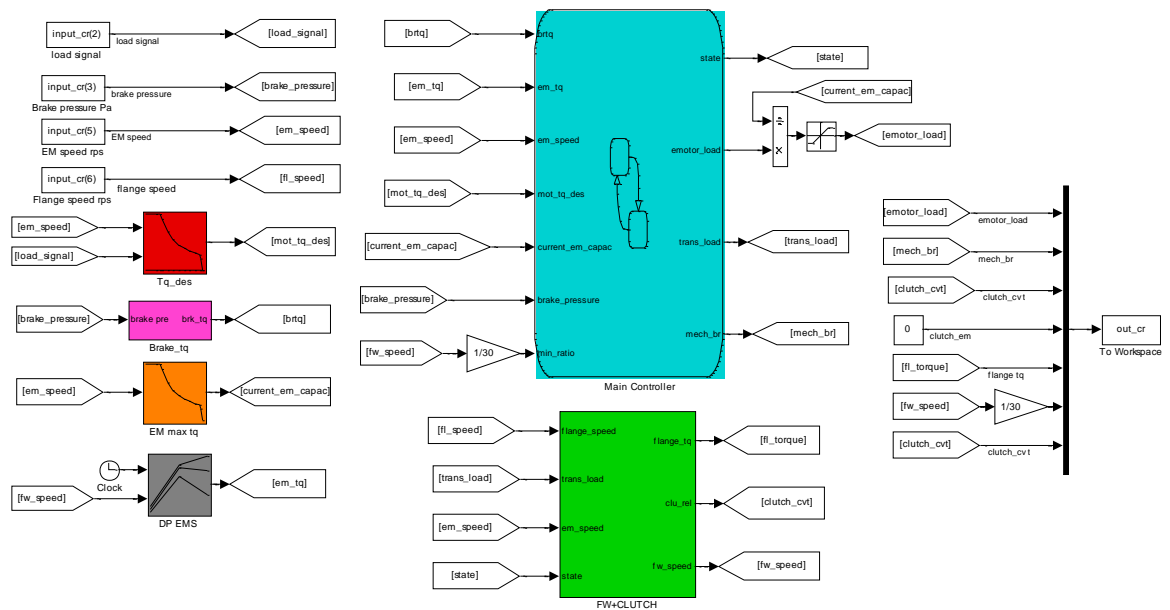


Figure 86 Flywheel and Controller Model in Simulink

6.6 Simulation process and results

The process is similar to the quasi-static one. The simulation is started in AVL Cruise which calls the Simulink model. The Simulink model executes the DP algorithm in Matlab at the start of each micro trip to obtain the optimal control matrix which is used in the calculation. During the simulation the signals are exchanged at each simulation step. The results of the forward simulation are compared with the quasi-static backward simulation. Table 23 presents the comparison.

Table 23 Comparison between FWD and BWD simulation

Drive Cycle	Backward		Forward		Difference Energy Economy [%]
	FW SOE Delta [%]	Energy Economy [Wh/km]	FW SOE Delta [%]	Energy Economy [Wh/km]	
AU	1.32	140.98	3.60	139.05	1.32
US06	5.21	185.56	8.82	184.71	0.45
LA92	0.87	142.26	0.99	140.47	1.25

From Table 23 it can be observed that the difference between the forward and backward simulation in terms of energy economy is relatively small. In terms of flywheel SOE balance the forward simulation is slightly worse off but it does not affect the energy economy. Further Fig. 87 and 88 show the flywheel SOE and EM torque for the comparison. It can be seen that the forward and backward simulation results are well matched in all the three cases. It can therefore be said that the predictive controller in forward simulation environment shows very similar performance as in the quasi-static backward environment and would be suitable for real life implementation.

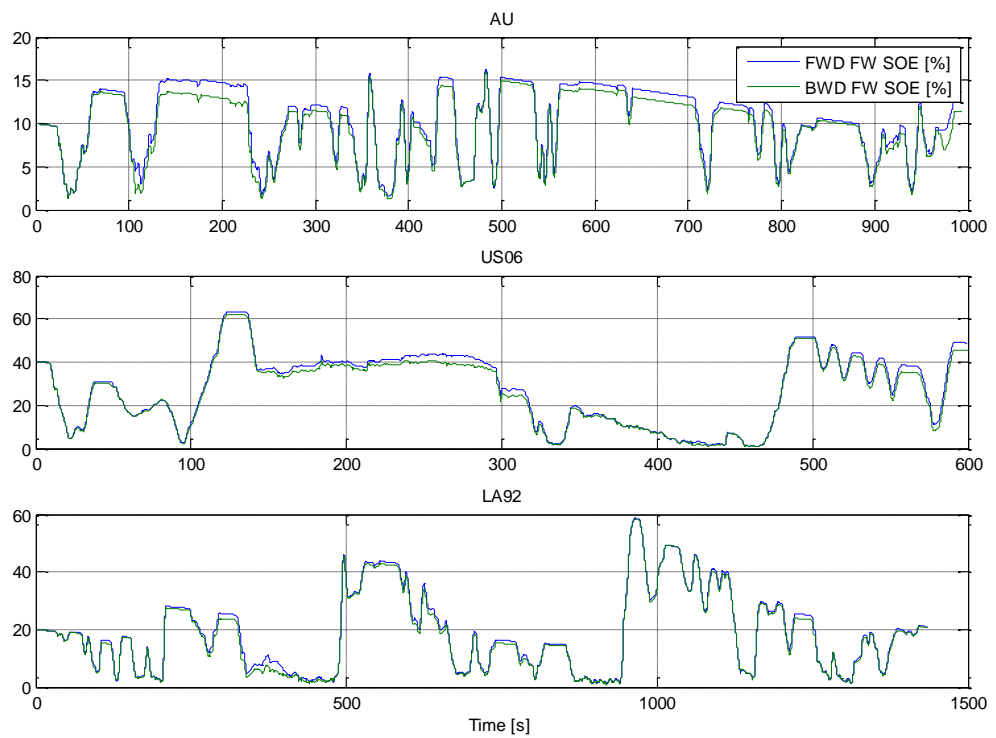


Figure 87 Forward vs. backward simulation for flywheel SOE

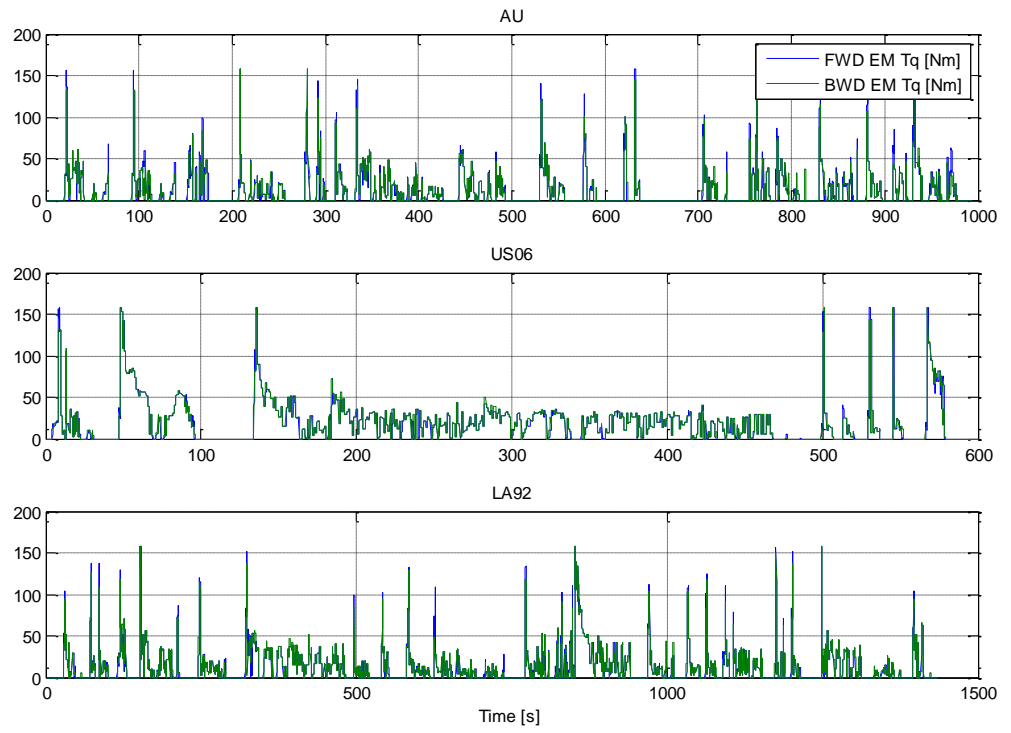


Figure 88 Forward vs. backward simulation for EM Torque

7 Conclusions

This thesis presented the concept and critical appraisal of a mechanically connected FWBEV powertrain for a modern passenger car application. The concept utilized Li-Ion batteries as the main energy source for the BEV and FESS as the main power source. The main aim was to explore the potential improvement in energy efficiency of this system as compared to the base BEV.

7.1 Summary and Findings

Following the introduction in Chapter 1, a detailed literature review was conducted on the hybridisation of energy sources in Chapter 2. After presenting a brief history of BEVs and discussing the presently used batteries, it was concluded that for the BEV to compete with ICEV, hybridisation was one of the potential solutions since none of the ESS could meet all the requirements. After discussing the other options, FESS was deemed to be an attractive secondary storage due to its suitable characteristics and low cost potential. Since the most usual way of changing the energy content of FESS is varying its speed, a suitable transmission is needed. Various transmissions for FESS and other characteristics were discussed. It was concluded that using a mechanical transmission for FESS is beneficial since it avoids energy conversion and is expected to be lower in cost. A detailed review of previous research and applications of FWBEV revealed that most of it carried out in late 1970s and early 1980s and was unsuccessful due to the battery and EM technology at that time such that even with the addition of FESS, the BEV were deemed uncompetitive. Most of the recent research 1990s onwards was focused on implementing the FESS as FWB. Almost all of the existing research used lead-acid batteries in HES, which is not the chemistry of choice for modern BEV. Thus designing a mechanically connected FWBEV powertrain for a modern passenger car application became the main objective of this research.

In the Chapter 3, a detailed discussion of the Li-ion batteries was presented. The various chemistries of Li-ion cells were listed and important properties such as specific energy and specific power were discussed. Specific power and specific energy have trade-offs and one can be increased at the expense of other as the Ragone plot showed. The effect of the cell shape was also discussed. It was noted that for a high power cell a higher surface area is needed whereas for a high energy cell a bigger volume was desired. Due to these reasons a high energy cell was expected to have higher power losses at high loads as compared to high power cells. Further trade-offs such as size and number of cells were also discussed.

Chapter 3 also discussed the various types of battery models. The popular type was the EC model and it could be implemented in three ways namely Rint model, One Time Constant

model and Two Time constant model. Since the battery is a complex system, the Two Time constant model was deemed appropriate for dynamic operation. Further the EV model, its components and control strategy were presented. The forward dynamic model was built in vehicle simulation tool AVL Cruise. The application selected was a C-segment hatchback type car as this is one of the most popular modes of private transport especially in Europe. The BEV had a kerb mass of 1445 kg, a Li-ion battery of 19.2 kWh and EM of 72 kW.

Simulations were carried out using the BEV model on four homologation drive cycles namely the NEDC, FTP-72, JA1015 and HWFET cycles. The obvious effect of regenerative braking improving the energy consumption was observed. The more interesting result was the battery RT efficiency which is a direct measure of battery losses and had values of around 90 % or more on all the four cycles. Statistical analyses of homologation cycles versus real world cycles showed that the homologation cycles have much lower RMS acceleration than real world cycles across the entire speed range as expected. To test the performance of the BEV in different real world conditions AU, LA92 and US06 cycles were chosen to represent urban, extra-urban and motorway conditions.

The results of the real world cycle simulations showed a significant decrease in the battery round trip efficiency ranging from 78-83%. Further when calculations were conducted using average power of the battery from previous simulations, the RT battery efficiency went up to more than 96% for the same energy consumption at the battery terminals. Thus it was concluded that the battery losses could be drastically reduced if low constant power was drawn from it rather than the actual dynamic load. Further the powertrain efficiency from the three cycles was explored for potential efficiency improvements. From the analysis it was found that the EM efficiency which was the major contributor to powertrain efficiency could benefit from a downsized machine at least in the higher speed drive cycles, besides the obvious cost advantage. Thus the addition of a high power secondary storage which could transmit torque directly to the driveline could lead to efficiency improvements of the BEV. Using the mechanically connected FESS would provide this option.

In Chapter 4, the HV and its components were presented. Firstly the FESS capacity and operating characteristics were defined. For this various options were explored and it was decided to size the FESS to have the energy capacity to provide the HV the same 0-100 kph acceleration performance as that of the base BEV. Also the maximum to minimum speed ratio of the FESS was taken to be 2. Thus the FESS was defined to have energy capacity of 250 Wh, minimum speed of 15000 rpm, maximum speed of 30000 rpm and inertia of 0.249 kgm^2 . Real world road usage data was analysed to validate the sizing of the FESS. The data was gathered

from mostly passenger car trips in the US and Europe and constituted about 23000 km. It contained vehicle speed and road elevation from GPS. Analysing the braking events using the data showed that out of total of 69537 events amounting to 746 kWh only 56 events had brake energy dissipation of more than 0.2 kWh per event. Further the maximum change in the KE of the vehicle at intervals of 11 s which is approximately the same as the 0-100 kph acceleration target, was calculated. From the results it was observed that most trips had a maximum change in KE over 11 s less than 167 Wh which is the KE of the vehicle at 100 kph and would have been the ideal capacity of the FESS if losses were disregarded. The analysis concluded that the chosen FESS was sufficiently sized to meet the acceleration and braking requirements.

The next section in Chapter 4 described the analysis of the mechanical CVT needed to connect the flywheel with the driveshaft. The conventional variators like the toroidal and the belt type do not appear to have sufficient speed ratio range to meet the requirements of the FESS. PSCVT have been conventionally used to improve the efficiency of the variators. They can be designed to improve efficiency while achieving high speed ratio range by increasing their complexity. Although there was extensive analysis reported in literature about PSCVT, they were almost exclusively treated either as lossless or one directional systems. Thus a complete analysis in terms of speed ratio, power and efficiency in both directions of power flow was conducted for different types of PSCVT for FESS including power recirculation and multi-regime types. Extending the basic technique presented by Martinez-Gonzales [77], three transmissions namely single regime PSCVT with positive power recirculation, three-regime PSCVT without power recirculation and two-regime PSCVT with negative power recirculation were defined to meet the speed ratio requirements of the FESS derived from the operating speeds of FESS and EM. Further applying the treatise of Pennestri and Freudenstein [127], the ratio of variator to input power and efficiency of the complete PSCVT was derived for both directions of the power flow including the efficiency of all components namely variator, fixed gears and PGS. The resulting simple methodology can be applied to design any PSCVT type for FESS to meet the desired speed ratio requirements and predict its efficiency in both directions of power flow.

Further Chapter 4 focused on selecting a suitable transmission from the previously analysed cases depending upon the variator power capacity in the assumed worst case scenario of using the FESS to propel the HV from 0-100 kph. Three selected transmissions were three-regime IC PSCVT without power recirculation, three-regime OC PSCVT without power recirculation and two-regime IC PSCVT with negative power recirculation. The torque and speed of the variator as well as other parameters of the PSCVT were also briefly discussed. Finally the layout of the

HV is presented. The HV had a downsized EM of 45 kW compared to 72 kW and additional clutches to provide gear neutral and stationary vehicle flywheel charging ability. The HV was 40 kg heavier than the BEV due to differences in EM and addition of clutches, flywheel and CVT system. The only major component of the HV left to be discussed was control strategy.

Chapter 5 focused on providing minimum attainable cycle energy consumption possible with the HV by using global optimal theory. DP was applied to provide benchmark results for the HV on the AU, US06 and LA92 drive cycles and also to provide EMS design direction. The objective of the DP was to provide optimal EMS for minimum cycle energy consumption under system constraints. For this process a quasi-static backward model was created in Matlab and the state and control variables were suitably gridded for efficient computation. Various DP tests were conducted initially to check options such as start SOE of the flywheel, flywheel vs. EM vehicle launch and type of transmission. The start SOE of the flywheel for the three cycles was selected to give lowest energy consumption. Similarly EM launch was found to be more energy efficient than the flywheel launch due to absence slipping clutch losses and three-regime OC PSCVT was selected as the final transmission.

Finally with a finer resolution grid and time step DP was conducted on the HV to compare the results with the base BEV on the three cycles. The battery start SOC was taken to be between 85-90% and the simulations were run steady state at 25° C. This provided the best case for the BEV. The DP was constrained to return the flywheel to the same state as in the beginning of the cycle so no net energy is stored in it. The results showed improved energy consumption for the HV over the BEV by about 11% and 3.2% in the US06 and LA92 cycles respectively, whereas the energy consumption worsened by 2% in the AU cycle predominantly as a result of it being a relatively lower powered cycle. The battery losses were significantly reduced as were the peak battery power and current during all the cycles. This is expected to improve the battery life and lower operating costs. The EM efficiency was also slightly improved.

Chapter 6 focused on designing a real life implementable sub optimal controller for the HV. For this purpose it was decided to implement a predictive control based on global optimisation techniques. The EMS was based on DP and used limited future journey information. For this purpose a given road trip was divided into its constituent micro trips and it was assumed that the vehicle speed and road gradient information for the forthcoming micro trip is known in advance at fixed time intervals using various telematics and traffic information systems. Case studies were conducted to find a compromise between the accuracy and computation time of the DP algorithm by tuning the resolution of the primary state variable. Using a resolution of 0.7% for the flywheel SOE and 1 s time step for the DP algorithm, the computation time for the

three drive cycle simulations was reduced to few minutes as compared to the amount in days it took to run the benchmark simulation. Further the cycle energy consumption with the DP based EMS was within 2-3% of the benchmark simulation results which showed that a good performance can be reached with this type of controller.

Further to test the suitability of the control for real life implementation, a forward dynamic model was run using co-simulation with AVL Cruise and Simulink. The vehicle powertrain was modelled in AVL Cruise and the flywheel and controller were modelled in Simulink and both were linked. The simulation results were compared to the quasi-static backward simulation results and were within 0.5-1.5% of the backward simulation in terms of energy consumption. The flywheel SOE and EM torque followed very similar trends in both the simulations. Thus it is concluded that this type of controller would be practical for a real implementation and beneficial to improve the energy consumption.

7.2 Novel Contributions

- Design of EV propulsion system for a modern passenger car application utilizing a HES combining Li-ion batteries and mechanically connected flywheel.
- Extension of the technique used by Martinez-Gonzales [77] to design single and multi-regime PSCVT for the required speed ratio range.
- Application of the treatise of Pennestri and Freudenstein [127] to derive the equations for ratio of variator to input power and efficiency of the PSCVT in both directions of the power flow including the efficiency of the variator, fixed gears and PGS for power recirculating and multi regime systems.
- Application of DP to find the minimum obtainable energy consumption for the mechanically connected FWBEV in three real world driving cycles.
- Novel DP based EMS for the FWBEV with short computation time using limited future journey information.

7.3 Assumptions and Limitations

The thesis relied on open literature for the required input parameters for the simulations. Due to unavailability for certain data, suitable assumptions were made. Other assumptions were made based on references from literature and where their effect was deemed insignificant.

For the base battery vehicle model, the mass of the battery pack was taken to be double the total mass of the cells which is the case for modern BEVs. The auxiliary load for vehicle housekeeping in the base BEV was taken to be constant 300 W. The motoring and generating performance of the EM was taken to be identical. The minimum vehicle speed and the

maximum battery SOC for allowing regenerative braking in the base BEV are taken to be 10 kph and 90% respectively. Further wheel slip is not considered in the simulations. Also the simulations are performed on deterministic drive cycles and road gradient was not considered.

For the hybrid vehicle, the additional mass of the components is taken to be 40 kg which is a good estimation for road cars. In the road data analysis, it was assumed that the elevation changes linearly in road span of 100 m and maximum road gradient was taken to be 13%. In the transmission analysis the ratio efficiency of the variator in the PSCVT was taken to be constant at 90% and idle losses in the PSCVT were neglected. Single efficiency values were assumed for all fixed gear pairs. The hydraulic pump losses for the CVT were taken to be constant 300 W and the self discharge of the flywheel was taken to be 2% per minute.

During the HV simulation, the energy lost during charging and discharging the flywheel at the start and end of the drive cycle was not considered. For the predictive EMS of the HV, it was assumed that the vehicle velocity and slope information for the forthcoming micro trip is known a priori at fixed time resolution of 1 s.

The limitations of the thesis stems from the previously mentioned assumptions. For example in a real life situation the energy consumption of the HV and the BEV would depend on the vehicle velocity as well as road gradients, which were not considered in the thesis. Further the energy losses in each component of the transmission were not investigated in detail. For example the hydraulic pump losses would be transient in a real life situation but were taken to be constant. The thesis did not investigate various strategies to charge and discharge the flywheel at the beginning and end of the trip. Also the assumption that vehicle velocity is known a priori due to various telematics and traffic information systems would introduce limitation in case such information is unavailable.

7.4 Conclusions

This research analysed the concept of a mechanically connected FWBEV and the benefits it brings in real world energy consumption and battery stress reduction. Li-ion batteries were used in the baseline BEV and as the main energy source in the FWBEV, which is the current battery technology of choice for modern EV, in contrast to previous research on FWBEV which almost always used lead acid batteries. The base vehicle chosen for this application was a C-segment passenger car which is one of the more popular modes of private transport in Europe, to make the research more relevant. Analysis of base BEV showed that the single energy storage cannot meet all the requirements of the BEV and trade-off has to be made in terms of various characteristics especially specific energy vs. specific power. Simulation results showed significant improvements in energy efficiency could be obtained by subjecting the battery to

low average power. The results also showed that EM downsizing would result in lower cost and energy consumption benefit though the latter was expected to be small.

The energy capacity of the FESS was defined by the amount it took for the HV to achieve the 0-100 kph performance of the base BEV. A subsequent road usage data analysis showed that the FESS was sufficiently sized to perform its intended operations. Detailed analysis for the transmission for FESS was conducted which showed various ways of meeting the requirements for PSCVT for FESS. This methodology although concentrated on PSCVT for FESS, can be easily used for designing transmission for other hybrid powertrains that require power flow in both directions of the transmission. The analysis showed that high efficiency PSCVT could be designed by increasing their complexity.

DP was used to obtain the minimum energy consumption and the optimal EMS for the HV. The optimisation problem was complicated by the fact that both energy storage systems have state variables which is not the case with ICE based HEV, and there were slipping of clutches and kinematic constraints to be taken into account. DP was conducted and the results of the HV were compared with the base BEV. The battery was taken at room temperature, since these were the characteristics available and at high SOC which represented the best conditions for battery performance. The results showed that significant energy consumption improvement could be obtained for aggressive drive cycles, though only marginal improvements could be expected on low powered cycles. However the battery would always be protected from high loads. Since the battery is at its best operating condition, greater improvements for the HV are expected in other operating conditions since the battery performance worsens.

To develop a real life sub optimal controller for the HV, predictive control was deemed most suitable since the FESS has relatively small energy capacity and has to undergo frequent charge and discharge to obtain close to optimal performance. A predictive control based on DP was implemented which utilized limited future trip information and had short computation time. The controller performance showed small deviation compared to benchmark simulation and that it was suitable for this type of application. It showed similar performance when tested in forward dynamic simulation.

7.5 Future Work

In this thesis, comparisons in performance of the BEV and HV were done with the battery at room temperature and in the high SOC region, which are the best operating conditions for the battery. In reality the benefit would be much higher if the battery were to operate in low or high temperature or lower SOC regions as the battery performance is expected to be much

poorer. Also in this analysis the same battery was used in the base BEV and HV. In fact, the benefit by use of flywheel in the HV is expected to be higher if the battery is optimised as energy source for the HV since no trade-off has to be made. Analysis of such scenarios is recommended for future work.

Another important parameter is the battery life. It is expected that the battery stress reduction achieved by the addition of flywheel would lead to a substantial increase in battery life and lower operating costs. Quantification of such benefit could also be explored in further research.

Further in the present work, the FESS was defined on the basis of having adequate energy to power the 0-100 kph acceleration of the HV to match that of the base BEV. From the energy capacity of the FESS, the requirements of the transmission were obtained and various PSCVT were developed. However the system performance could be improved by optimisation of the combined flywheel transmission design which could be a subject of further research.

The control of the HV was a DP based EMS with limited future journey information. Future research could focus on various other ways of controlling such a FWBEV to achieve higher energy economy. Other aspects such as consideration of road gradients, and the losses incurred during start of cycle charging and end of cycle discharging of the flywheel could also be investigated in future research.

7.6 List of Publications

- Dhand, A., and Pullen, K., Review of Flywheel based Internal Combustion Engine Hybrid Vehicles, *International Journal of Automotive Technology* 2013; 14(5): 797-804
- Dhand, A., and Pullen, K., Simulation based study of battery electric vehicle performance in real world cycles, *International Journal of Electric and Hybrid Vehicles* 2013; 5(4): 327–343
- Pullen, K., and Dhand, A., Mechanical and electrical flywheel hybrid technology to store energy in vehicles in *Alternative fuels and advanced vehicle technologies for improved environmental performance*, edited by R. Folkson, Woodhead Publishing Limited, 2014
- Dhand, A., and Pullen, K., Characterization of Flywheel Energy Storage System for Hybrid Vehicles, *SAE Technical Paper* 2014-01-1796; 2014
- Dhand, A., and Pullen, K., Analysis of continuously variable transmission for flywheel energy storage systems in vehicular application, *Proceedings of the Institution of*

Mechanical Engineers, Part C: Journal of Mechanical Engineering Science 2015; 229(2): 273-290

- Dhand, A., and Pullen, K., Review of Battery Electric Vehicle Propulsion Systems incorporating Flywheel Energy Storage, International Journal of Automotive Technology 2015;16(3): 487-500
- Dhand, A., and Pullen, K., Optimal energy management for a flywheel assisted battery electric vehicle, Proceedings of the Institution of Mechanical Engineers, Part D: Journal of Automobile Engineering; (accepted) 2014

References

1. UN, Kyoto protocol to the United Nations framework convention on climate change, 1997, United Nations
2. Regulation (EC) No443/2009 of the European Parliament and of the council of 23 April 2009 setting emission performance standards for new passenger cars as part of the Community's integrated approach to reduce CO2 emissions from light-duty vehicles, Official Journal of the European Union, 2009, L 140/1–L 140/15
3. Chan, C. and Chau, K., Modern Electric Vehicle Technology, Oxford University Press, 2001, USA
4. Ehsani, M., Gao, Y., and Emadi, A., Modern Electric, Hybrid Electric, and Fuel Cell Vehicles, Second edition, Taylor and Francis Group, 2010, USA
5. Boulanger, A., Chu, A., Maxx, S., and Waltz D., Vehicle Electrification: Status and Issues, Proceedings of the IEEE, 2011, 99(6), 1116-1138
6. Chau, K., Wong, Y., and Chan, C., An overview of energy sources for electric vehicles, Energy Conversion and Management 1999, 40(10), 1021-1039
7. Dixon, J., Energy Storage for Electric Vehicles, IEEE International Conference on Industrial Technology, 2010
8. Vazquez, S., Lukic, S., Galvan, E., Franquelo, L. et al., Energy Storage Systems for Transport and Grid Applications, IEEE Transactions on Industrial Electronics, 2010, 57(12), 3881-3895
9. Budde-Meiwes, H., Drillkens, J., Lunz, B., Muennix, J. et al., A review of current automotive battery technology and future prospects, Proceedings of the Institution of Mechanical Engineers, Part D: Journal of Automobile Engineering, 2013, 227(5), 761-776
10. Khaligh, A. and Li, Z., Battery, Ultracapacitor, Fuel Cell, and Hybrid Energy Storage Systems for Electric, Hybrid Electric, Fuel Cell, and Plug-In Hybrid Electric Vehicles: State of the Art, IEEE Transactions on Vehicular Technology, 2010, 59(6), 2806-2814
11. Greenwood, C. and Brockbank, C., Formula 1 Mechanical Hybrid Applied to Mainstream Automotive, VDI Getriebe in Fahrzeuge Conference, 2008
12. Chau, K. and Wong, Y., Hybridisation of energy sources in electric vehicles, Energy Conversion and Management, 2001, 42(9), 1059-1069
13. Mikkelsen, K. and Lambert, S., Evaluation of a Hybrid Energy Storage System for EVs, SAE Technical Paper 2011-01-1376, 2011

14. Styler, A., Podnar, G., Dille, P., Duescher, M. et al., Active Management of a Heterogeneous Energy Store for Electric Vehicles, IEEE Forum on Integrated and Sustainable Transportation Systems, 2011, Vienna, Austria
15. Romaus, C., Gathmann, K., and Böcker, J., Optimal Energy Management for a Hybrid Energy Storage System for Electric Vehicles Based on Stochastic Dynamic Programming, IEEE Vehicle Power and Propulsion Conference, 2010
16. Miller, J., Bohn, T., Dougherty, T., and Deshpande, U., Why Hybridization of Energy Storage is Essential for Future Hybrid, Plug-in and Battery Electric Vehicles, IEEE Energy Conversion Congress and Exposition, 2009
17. Wang, J., Li, K., Lv, Q., Zhou, H. et al., Hybrid Energy Storage System Integration For Vehicles, 16th ACM/IEEE international symposium on Low power electronics and design, 2010
18. Miller, J., Energy storage system technology challenges facing strong hybrid, plug-in and battery electric vehicles, IEEE Vehicle Power and Propulsion Conference, 2009
19. Wang, L., Collins, E., and Li, H., Optimal Design and Real-Time Control for Energy Management in Electric Vehicles, IEEE Transactions on Vehicular Technology, 2011, 60(4), 1419-1429
20. Post, R., A new look at an old idea - The electromechanical battery, Science and Technology Review, April 1996, 12-20
21. Calvert, W., Electrical power system, US Patent 3497026, 1970
22. Palti, Y., Electro-mechanical battery, US patent 2010/0282528 A1, 2010
23. Anon., The Oerlikon Electrogyro, Its development and application for Omnibus service, Automobile Engineer, December 1955
24. Clerk, R., The Utilization of Flywheel Energy, SAE Technical Paper 640047, 1964
25. Whitelaw, R., Two new weapons against automotive air pollution: the hydrostatic drive and the flywheel-electric LDV, ASME Paper 72-WA/APC-5, 1972
26. Kugler, G., Electric vehicle hybrid powertrain, SAE Technical Paper 730254, 1973
27. Locker, D. and Miller, H., Flywheel electric vehicle, 4th International electric vehicle symposium, 1976, Dusseldorf
28. Schwarz, R., Four passenger electric vehicle design, 4th International Symposium on Automotive Propulsion Systems, 1977
29. Chang, G., Swisher, J., and Pezdirtz, G., DOE's flywheel program, Flywheel Technology Symposium, 1977
30. Notti, J., Flywheel systems applications, Flywheel Technology Symposium, 1975

31. Rowlett, B., Flywheel drive system having a split electromechanical transmission, US patent 4233858, 1980
32. Anon., The Garrett near-term electric test vehicle (ETV-2), US DOE Information Bulletin No. 403-1, December 1979
33. Chang, M., Computer simulation of an advanced electric-powered vehicle, SAE Technical paper 780217, 1978
34. Ellis, C., Kinetic energy storage system, GB patent 2405129B, 2006
35. Simon, B., Hybrid assembly, a hybrid powertrain and a method for operating a selectively movable assembly, US patent 2010/0304920 A1, 2010
36. Stavropoulou, K., Simulacao em computador de um veiculo hibrido com armazenamento de energia em volante (in Portuguese), Master Thesis, 1981, University of Campinas
37. Lustenader, E., Guess, R., Richter, E., and Turnbull, F., Development of a Hybrid Flywheel/Battery Drive System for Electric Vehicle Applications, IEEE Transactions on Vehicular Technology, 1977, 26(2), 135-143
38. Cornell, E., Turnbull, F., and Barlow, T., Evaluation of a Hybrid Flywheel/Battery Propulsion System for Electric Vehicles, Lawrence Livermore National Laboratory Technical report UCRL-15259, 1980
39. Satchwell, D., An advanced energy storage unit for a US postal service delivery vehicle, Flywheel Technology Symposium, 1977
40. Raynard, A., Advanced flywheel energy storage unit for a high power energy source for vehicular use, Proceedings of the Mechanical and Magnetic Energy Storage Contractors' Review Meeting, 1978
41. Burrows, C. and Barlow, T., Flywheel power system developments for electric vehicle applications, Electric Vehicle Development Group 4th International Conference: Hybrid, Dual Mode and Tracked Systems, 1981, London, United Kingdom
42. Anon., Flywheel Energy Storage Unit Technology Development Program, California Univ., Lawrence Livermore Laboratory Technical report, UCRL-15280, 1980
43. Raynard, A. and Forbes, F., Advanced electric propulsion system concept for electric vehicles, Technical Report DOE/NASA/0081-79/1, 1979
44. Younger, F. and Lackner, H., Study of advanced electric propulsion systems concept using flywheel for Electric vehicles, Technical Report DOE/NASA/0078-79/1, 1979

45. Schwartz, M., Energy storage systems for automobile propulsion: 1979 study, Volume 3, Battery/flywheel electric vehicles using advanced batteries, Lawrence Livermore Laboratory Technical report, UCRL-52841, 1979
46. Loewenthal, S., Advanced Continuously Variable Transmissions for Electric and Hybrid Vehicles, Technical Report DOE/NASA/51044-17, 1980
47. Swain, J., Klausung, T., and Wilcox, J., Design study of steel v-belt CVT for electric vehicles, Technical Report DOE/NASA/0116-80/1, 1980
48. Kumm, E., Design study of flat belt CVT for electric vehicles, Technical Report DOE/NASA/0114-80/1, 1980
49. Raynard , A., Kraus, J., and Bell, D., Design study of toroidal traction CVT for electric vehicles, Technical Report DOE/NASA/0117-80/1, 1980
50. McCoin, D. and Walker, R., Design study of continuously variable roller cone traction CVT for Electric vehicles, Technical Report DOE/NASA/0115-80/1, 1980
51. Parker, R., Loewenthal, S., and Fischer, G., Design Studies of Continuously Variable Transmissions for Electric Vehicles, Technical Report DOE/NASA/1044-12, 1981
52. Secunde, R., Schuh, R., and Beach, R., Electric Vehicle Propulsion Alternatives, Technical report DOE/NASA/51044-33, 1983
53. Wilson, J., The Drive System of the DOE Near-Term Electric Vehicle (ETV-1), SAE Technical Paper 800058, 1980
54. Price, G., An assessment of flywheel energy storage for electric vehicle, PhD Thesis, 1980, University of Sussex
55. Burrows, C., Price, G., and Perry, F., An Assessment of Flywheel Energy Storage in Electric Vehicles, SAE Technical Paper 800885, 1980
56. O'Connell, L., Cooper, J., Miller, A., and Newkirk, H., Utilization of flywheels for the evolution of high performance electric vehicles, Technical Report UCRL-52346, 1977
57. Agarwal, P., Energy Utilization of electric and hybrid vehicles and their impact on US national energy consumption, International Journal of Vehicle Design, 1982, 3(4), 436-449
58. Flanagan, F., Evaluation of a Flywheel Hybrid Electric Vehicle Drive, 25th Intersociety Energy Conversion Engineering Conference, 1990
59. Braess, H. and Regar, K., Electrically propelled vehicles at BMW-experience to date and development trends, SAE Technical Paper 910245, 1991
60. Szumanowski, A. and Brusaglino, G., Analysis of the hybrid drive consisted of electrochemical battery and flywheel, 11th International Electric Vehicle Symposium, 1992

61. Schaible, U. and Szabados, B., A torque controlled high speed flywheel energy storage system for peak power transfer in electric vehicles, IEEE Industry Applications Society Annual Meeting, 1994
62. Anerdi, G., Brusaglino, G., Ancarani, A., Bianchi, R. et al., Technology potential of flywheel storage and application impact on electric vehicles, 12th International Electric Vehicle Symposium, 1994
63. Mellor, P., Schofield, N., and Howe, D., Flywheel and supercapacitor peak power buffer technologies, Electric, Hybrid and Fuel Cell Vehicles, IEE Seminar, 2000
64. Saitoh, T., Ando, D., and Kurata, K., A Grand Design of Future Electric Vehicle with Fuel Economy more than 100 km / liter, SAE Technical Paper 1999-01-2711, 1999
65. Saitoh, T., Yoshimura, A., and Yamada, N., An evaluation of future energy conversion systems including fuel cell, Transactions of the Japan Society of Mechanical Engineers, Part B, 2002, 68(665), 201-208
66. Saitoh, T., Ogasawara, H., and Yamada, N., Study of flywheel energy storage system and application to electric vehicle, Transactions of the Japan Society of Mechanical Engineers, Part B, 2004, 70(697), 2482-2489
67. Saitoh, T., Yamada, N., Ando, D., and Kurata, K., A grand design of future electric vehicle to reduce urban warming and CO2 emissions in urban area, Renewable Energy, 2005, 30(12), 1847–1860
68. Fu, X. and Xie, X., The Control Strategy of Flywheel Battery for Electric Vehicles, IEEE International Conference on Control and Automation, 2007
69. Fu, X., A Novel Design for Flywheel Battery of Electric Vehicles, International Conference on Intelligent System Design and Engineering Application, 2010
70. Briat, O., Vinassa, J., Lajnef, W., Azzopardi, S. et al., Principle, design and experimental validation of a flywheel-battery hybrid source for heavy-duty electric vehicles, IET Electric Power Applications, 2007, 1(5), 665–674
71. Lundin, J., Flywheel in an all-electric propulsion system, Licentiate Thesis, 2011, Uppsala University
72. Wallentowitz, H., Lecture: Alternate vehicle propulsion systems, IKA RWTH Aachen, 1st Edition, 2004, Aachen, Germany
73. Genta, G., Kinetic Energy Storage: theory and practice of advanced flywheel systems, Butterworths, 1985, United Kingdom
74. Rabenhorst, D., Primary Energy Storage and the Superflywheel, APL/JHU Report TG-1081, 1969

75. Hawkins, L., Murphy, B., Zierer, J., and Hayes, R., Shock and vibration testing of an AMB supported energy storage flywheel, 8th International Symposium on Magnetic Bearings, 2002, Mito, Japan
76. Song, L., Gao, J., Zhu, W., and Zeng, Q., Finite element analysis and experimental studies on hybrid magnetic bearing, IEEE Vehicle Power and Propulsion Conference, 2010
77. Martinez-Gonzalez, P., A study on the integration of a high-speed flywheel as an energy storage device in hybrid vehicles, PhD Thesis, 2010, Imperial College London
78. Acarnley, P., Mecrow, B., Burdess, J., Fawcett, J. et al., An integrated flywheel/machine energy store for road vehicles, IEE Colloquium on New Topologies for Permanent Magnet Machines, 1997, London, UK
79. Pichot, M., Kramer, J., Thompson, R., Hayes, R. et al., The flywheel battery containment problem, SAE Technical Paper 970242, 1997
80. Hansen, R. and O’Kain D., An assessment of flywheel high power energy storage technology for hybrid vehicles, Oak Ridge National Laboratory Report ORNL/ TM-2010/280, 2011
81. Strubhar, J., Thompson, R., Pak, T., Zierer, J. et al., Lightweight containment for high-energy rotating machines, IEEE Transactions on Magnetics, 2003, 39(1), 378–383
82. Pullen, K., and Dhand, A., Mechanical and electrical flywheel hybrid technology to store energy in vehicles in *Alternative fuels and advanced vehicle technologies for improved environmental performance*, edited by R. Folkson, Woodhead Publishing Limited, 2014
83. Otaki, H., Some analysis of gyroidal effect and development of a flywheel powered vehicle, SAE Technical Paper 800835, 1980
84. McDonald, A., Simplified Gyrodynamics of Road Vehicles with High-Energy Flywheels, Flywheel Technology Symposium, 1980
85. Moosavi-Rad, H. and Ullman, D.G., A band variable-inertia flywheel integrated-urban transit bus performance, SAE Technical Paper 902280, 1990
86. Van de Ven, J., Fluidic Variable Inertia Flywheel, International Energy Conversion Engineering Conference, 2009
87. Su, H. and Liu, T., Design and Analysis of Hybrid Power Systems with Variable Inertia Flywheel, World Battery, Hybrid and Fuel Cell Electric Vehicle Symposium (EVS25), 2010, Shenzhen, China

88. Beachley, N. and Frank, A., Continuously variable transmissions: theory and practice, Lawrence Livermore Laboratory Report UCRL-15037, 1979
89. Hayes, R., Kajs, J., Thompson, R., and Beno, J., Design and Testing of a Flywheel Battery for a Transit Bus, SAE Technical Paper 1999-01-1159, 1999
90. Thoolen, F., Development of an advanced high speed flywheel energy storage system, PhD Thesis, 1993, Technical University Eindhoven
91. Maeder, K., Continuously variable transmission: Benchmark, status and potentials, 4th International CTI Symposium, 2005, Berlin, Germany
92. Wallentowitz, H., Lecture: Longitudinal dynamics of vehicles, IKA RWTH Aachen, 4th Edition, 2004, Aachen, Germany
93. Anon., MIT Electric Vehicle Team: A Guide to Understanding Battery Specifications, 2008, http://web.mit.edu/evt/summary_battery_specifications.pdf, accessed 3.12.2012
94. Omar, N., Daowd, M., van den Bossche, P., Hegazy, O. et al., Rechargeable energy storage systems for plug-in hybrid electric vehicles – assessment of electrical characteristics, *Energies*, 2012, 5(8), 2952–2988
95. Burke, A. and Miller, M., Performance Characteristics of Lithium-ion Batteries of Various Chemistries for Plug-in Hybrid Vehicles, International Battery, Hybrid and Fuel Cell Electric Vehicle Symposium (EVS24), 2009, Stavanger, Norway
96. Pesaran, A., Kim, G., and Keyser, M., Integration Issues of Cells into Battery Packs for Plugin and Hybrid Electric Vehicles, International Battery, Hybrid and Fuel Cell Electric Vehicle Symposium (EVS24), 2009, Stavanger, Norway
97. Cluzel, C. and Douglas, C., Cost and Performance of EV Batteries, Final Report for The Committee on Climate Change, 2012
98. Zhang, C., Liu, J., Sharkh, S., and Zhang, C., Identification of dynamic model parameters for lithium-ion batteries used in hybrid electric vehicles, International Symposium on Electric Vehicles, 2009, Beijing, China
99. He, H., Xiong, R., Guo, H., and Li, S., Comparison study on the battery models used for the energy management of batteries in electric vehicles, *Energy Conversion and Management*, 64, December 2012, 113–121
100. Singh, P. and Nallanchakravarthula, A., Fuzzy logic modeling of unmanned surface vehicle (USV) hybrid power system, 13th International Conference on Intelligent Systems Application to Power Systems, 2005, Arlington, VA, USA
101. Rahmoun, A. and Biechl, H., Modelling of Li-ion batteries using equivalent circuit diagrams, *Przegląd Elektrotechniczny (Electrical Review)*, 2012, R. 88 NR 7b/2012

102. Antaloae, C., Marco, J., and Assadian, F., A novel method for the parameterization of a Li-ion cell model for EV/HEV control applications, IEEE Transactions on Vehicular Technology, 2012, 61(9), 3881-3892
103. Tang, X., Mao, X., Lin, J., and Koch, B., Li-ion battery parameter estimation for state of charge, American Control Conference, 2011, San Francisco, CA, USA
104. ADVISOR, National Renewable Energy Laboratory, USA, www.nrel.gov
105. PSAT, Argonne National Laboratory, USA, www.anl.gov
106. AVL Cruise, AVL List GmbH, Austria, www.avl.com
107. Van Mierlo, J., Maggetto, G., and Van den Bossche, P., Simulation methodologies for innovative vehicle drive systems, International Power Electronics and Motion Control Conference, 2004, Riga, Latvia
108. Kokam Co. Ltd., www.kokam.com, accessed 15.12.2012
109. Concawe/EU Car, Tank to Wheels Report, Version 3, October 2008
110. Sato, Y., Ishikawa, S., Okubo, T., Abe, M. et al., Development of High Response Motor and Inverter System for the Nissan LEAF Electric Vehicle, SAE Technical Paper 2011-01-0350, 2011
111. Hofman, T. and Dai, C., Energy efficiency analysis and comparison of transmission technologies for an electric vehicle, IEEE Vehicle Power and Propulsion Conference, 2010, Lille, France
112. Guo, J., Wang, J., and Cao, B., Regenerative braking strategy for electric vehicles, IEEE Intelligent Vehicles Symposium, 2009
113. Andre, M., The ARTEMIS European driving cycles for measuring car pollutant emissions, Science of the Total Environment, 2004, Vols. 334–335, 73–84
114. Andre, M., European Development of Hybrid Technology Approaching Efficient Zero Emission Mobility (HYZEM): Driving Patterns Analysis and Driving Cycles, INRETS Report LEN No. 9709, 1997
115. AVL Cruise version, Condensation Description, Edition 11/2010, 2010
116. Kun, L., Wu, J., Jiang, Y., Hassan, Z. et al., Large-scale battery system modeling and analysis for emerging electric-drive vehicles, 16th ACM/IEEE international symposium on Low power electronics and design, 2010
117. Miller, M., Holmes, A., Conlon, B., and Savagian, P., The GM “Voltec” 4ET50 Multi-Mode Electric Transaxle, SAE Technical Paper 2011-01-0887, 2011
118. Barnard, R. and Jefferson, C., Criteria for sizing the prime mover and energy storage capacity in hybrid vehicles, 30th ISATA Conference on Electric and Hybrid Vehicles, 1997

119. Santiago, J., Oliveira, J., Lundin, J., Abrahamsson, J. et al., Design parameters calculation of a novel driveline for electric vehicles, International Battery, Hybrid and Fuel Cell Electric Vehicle Symposium (EVS24), 2009, Stavanger, Norway
120. Gao, Y., Gay, S., Ehsani, M., Thelen, R. et al., Flywheel electric motor/generator characterization for hybrid vehicles, 58th IEEE Vehicular Technology Conference, 2003
121. Cross, D. and Hilton, J., High speed flywheel based hybrid systems for low carbon vehicles, Hybrid & Eco Friendly Vehicles Conference, 2008
122. Diego-Ayala, U., Martinez-Gonzalez, P., and Pullen, K., A Simple Mechanical Transmission System for Hybrid Vehicles Incorporating a Flywheel, Hybrid & Eco Friendly Vehicles Conference, 2008
123. Charge Car, www.chargecar.org, accessed 05.10.2012
124. Fuchs, R., Tamura, T., Mccullough, N. and Matsumoto, K., The Making of the Full Toroidal Variator, JTEKT Engineering Journal English edition, 2009, No. 1006E, 31-36
125. Srivastava, N. and Haque, I., A review on belt and chain continuously variable transmissions (CVT): Dynamics and control, Mechanism and Machine Theory, 2009, 44(1), 19-41
126. White, G., Properties of Differential Transmissions, The Engineer, 1967, 224, 105-11
127. Pennestri, E. and Freudenstein, F., The mechanical efficiency of epicyclic gear trains, Journal of Mechanical Design, 1993, 115(3), 645-651
128. White, G., Multiple-Stage, Split-Power Transmissions, Journal of Mechanisms, 1970, 5(4), 505-520
129. Yu, D. and Beachley, N., On the mechanical efficiency of differential gearing, Journal of Mechanisms, Transmissions and Automation in Design, 1985, 107(1), 61-67
130. Hsieh, L. and Yan, H., On the mechanical efficiency of continuously variable transmissions with planetary gear trains, International Journal of Vehicle Design, 1990, 11 (2), 176-187
131. Yan, H. and Hsieh, L., Maximum mechanical efficiency of infinitely variable transmissions, Mechanism and Machine Theory, 1994, 29(5), 777-784
132. Mangialardi, L. and Mantriota, G., Comments on: maximum mechanical efficiency infinitely variable transmissions, Mechanism and Machine Theory, 1998, 33(4), 443-447

133. Mangialardi, L. and Mantriota, G., Power flows and efficiency in infinitely variable transmissions, *Mechanism and Machine Theory*, 1999, 34(7), 973-994
134. Mantriota, G., Power split continuously variable transmission systems with high efficiency, *Proceedings of the Institution of Mechanical Engineers, Part D: Journal of Automobile Engineering*, 2001, 215(3), 357-368
135. Mantriota, G., Theoretical and experimental study of a power split continuously variable transmission system part 1, *Proceedings of the Institution of Mechanical Engineers, Part D: Journal of Automobile Engineering*, 2001, 215(7), 837-850
136. Mantriota, G., Theoretical and experimental study of a power split continuously variable transmission system part 2, *Proceedings of the Institution of Mechanical Engineers, Part D: Journal of Automobile Engineering*, 2001, 215(7), 851-864
137. Mantriota, G., Performances of a series infinitely variable transmission with type I power flow, *Mechanism and Machine Theory*, 2002, 37(6), 579-597
138. Mantriota, G., Performances of a parallel infinitely variable transmissions with a type II power flow, *Mechanism and Machine Theory*, 2002, 37(6), 555-578
139. Fussner, D. and Singh, Y., Development of Single Stage Input Coupled Split Power Transmission Arrangements and Their Characteristics, SAE Technical Paper 2002-01-1294, 2002
140. Fussner, D. and Singh, Y., Development of Dual Stage Input Coupled Split Power Transmission Arrangements and Their Characteristics, SAE Technical Paper 2002-01-0590, 2002
141. Beachley, N., Anscomb, C., and Burrows, C., Evaluation of split path extended range continuously variable transmissions for automotive applications, *Journal of the Franklin Institute*, 1984, 317(4), 235-262
142. Bottiglione, F. and Mantriota, G., Reversibility of Power-Split Transmissions, *Journal of Mechanical Design*, 2011, 133, Article ID 084503
143. Read, M., Flywheel Energy Storage Systems for Rail, PhD Thesis, 2010, Imperial College London
144. White, G., A two-stage variable-speed transmission for extended speed ranges, *Machine Tool Research*, 1965, 4, 115–120
145. Burke, M., Briffet, G., Fuller, J., Heumann, H. et al., Powertrain Efficiency Optimisation of the Torotrak Infinitely Variable Transmission, SAE Technical Paper 2003-01-0971, 2003
146. Pennestri, E. and Valentini, P., A review of formulas for the mechanical efficiency analysis of two degrees-of-freedom epicyclic gear trains, *Journal of Mechanical Design*, 2003, 125(3), 602-608

147. Yamamoto, T., Matsudaa, K., and Hibi, T., Analysis of the efficiency of a half-toroidal CVT, *JSAE Review*, 2001, 22(4), 565-570
148. Kluger, M. and Long, D., An Overview of Current Automatic , Manual and Continuously Variable Transmission Efficiencies and Their Projected Future Improvements, SAE Technical Paper 1999-01-1259, 1999
149. Cho, B., Control of A Hybrid Electric Vehicle with Predictive Journey Estimation, PhD Thesis, 2008, Cranfield University
150. Van der Sluis, F., Van Dongen, T., Van Spijk, G., Van der velde, A. et al., Efficiency Optimization of the Pushbelt CVT, SAE Technical Paper 2007-01-1457, 1999
151. Brockbank, C. and Greenwood, C., Full-Toroidal Variable Drive Transmission Systems in Mechanical Hybrid Systems – From Formula 1 to Road Vehicles, CTI Symposium and Exhibition: Automotive Transmissions, 2009
152. Pfiffner, R., Guzzella, L., and Onder, C., Fuel-optimal control of CVT powertrains, *Control Engineering Practice*, 2003, 11(3), 329–336
153. Anon., 2011 Nissan Leaf – VIN 0356: Advanced Vehicle Testing – Baseline Testing Results,
http://www1.eere.energy.gov/vehiclesandfuels/avta/pdfs/fsev/2011_nissan_leaf_fs.pdf, accessed 16.1.2013
154. Lechner, G. and Naunheimer, H., *Automotive Transmissions: Fundamentals, Selection, Design and Application*, Springer-Verlag, 1999, Germany
155. Schlurmann, J. and Schr, D., Compensation of Dynamic Torques and Flywheel Start in a CVT Based Hybrid Powertrain, IEEE International Conference on Control Applications, 2006, Munich, Germany
156. Cross, D. and Brockbank, C., Mechanical Hybrid System Comprising a Flywheel and CVT for Motorsport and Mainstream Automotive Applications, SAE Technical Paper 2009-01-1312, 2009
157. Doucette, R. and McCulloch, M., A comparison of high-speed flywheels, batteries, and ultracapacitors on the bases of cost and fuel economy as the energy storage system in a fuel cell based hybrid electric vehicle, *Journal of Power Sources*, 2011, 196(3), 1163-1170
158. Bellman, R., *Dynamic programming*, Princeton University Press, 1957, Princeton, NJ, USA
159. Pontryagin, L., *The Mathematical Theory of Optimal Processes*, English edition, CRC Press, 1987

160. Koot, M., Kessels, J., De Jager, B., Heemels, W. et al., Energy Management Strategies for Vehicular Electric Power Systems, *IEEE Transactions on Vehicular Technology*, 2005, 54(3), 771-782
161. Perez, L., Bossio, G., Moitre, D., and Garcia, G., Supervisory control of an HEV using an inventory control approach, *Latin American Applied Research*, 2006, 36(2), 93-100
162. Pisu, P. and Rizzoni, G., A Comparative Study Of Supervisory Control Strategies for Hybrid Electric Vehicles, *IEEE Transactions on Control Systems Technology*, 2007, 15(3), 506-518
163. Jamzadeh, F. and Frank, A., Optimal Control for Maximum Mileage of a Flywheel Energy-Storage Vehicle, *SAE Technical Paper 820747*, 1982
164. Van Berkel, K., Hofman, T., Vroemen, B., and Steinbuch, M., Optimal Control of a Mechanical Hybrid Powertrain, *IEEE Transactions on Vehicular Technology*, 2012, 61(2), 485-497
165. Dingel, O., Pini, N., Trivic, I., Ross, J. et al., Benchmarking Hybrid Concepts: On-Line vs. Off-Line Fuel Economy Optimization for Different Hybrid Architectures, *SAE Technical Paper 2013-24-0084*, 2013
166. Salmasi, F., Control Strategies for Hybrid Electric Vehicles: Evolution, Classification, Comparison, and Future Trends, *IEEE Transactions on Vehicular Technology*, 2007, 56(5), 2393-2404
167. Huang, Y. and Wang, K., A Hybrid Power Driving System with an Energy Storage Flywheel for Vehicles, *SAE Technical Paper 2007-01-4114*, 2007
168. Johannesson, L., Åsbogård, M., and Egardt, B., Assessing the Potential of Predictive Control for Hybrid Vehicle Powertrains Using Stochastic Dynamic Programming, *IEEE Transactions on Intelligent Transportation Systems*, 2007, 8(1), 71-83
169. Rajagopalan, A. and Washington, G., Intelligent Control of Hybrid Electric Vehicles Using GPS Information, *SAE Technical Paper 2002-01-1936*, 2002
170. Lin, C., Peng, H., Grizzle, J., and Kang, J., Power management strategy for a parallel hybrid electric truck, *IEEE Transactions on Control Systems Technology*, 2003, 11(6), 839-849
171. Mansour, C. and Clodic, D., Optimized energy management control for the Toyota hybrid system using dynamic programming on a predicted route with short computation time, *International Journal of Automotive Technology*, 2012, 13(2), 309-324

172. Gong, Q., Li, Y., and Peng, Z., Trip-Based Optimal Power Management of Plug-in Hybrid Electric Vehicles, *IEEE Transactions on Vehicular Technology*, 2008, 57(6), 3393-3401
173. Gong, Q., Li, Y., and Peng, Z., Trip Based Power Management of Plug-in Hybrid Electric Vehicle with Two-Scale Dynamic Programming, *IEEE Vehicle Power and Propulsion Conference*, 2007, Arlington, Texas, USA
174. Ngo, D., Hofman, T., Steinbuch, M., and Serrarens, A., An Optimal Control-Based Algorithm for Hybrid Electric Vehicle using Preview Route Information, *American Control Conference*, 2010, Baltimore, MD, USA
175. Wahl, H., Bauer, K., Gauterin, F., and Holzaepfel, M., A Real-time Capable Enhanced Dynamic Programming Approach for Predictive Optimal Cruise Control in Hybrid Electric Vehicles, *16th International IEEE Annual Conference on Intelligent Transportation Systems*, 2013, The Hague, Netherlands
176. Karbowski, D., Pagerit, S., and Calkins A., Energy Consumption Prediction of a Vehicle along a User- Specified Real-World Trip, *International Battery, Hybrid and Fuel Cell Electric Vehicle Symposium (EVS26)*, 2012, Los Angeles, California, USA
177. Lawson, L., Applications of kinetic energy storage to transportation systems, *High Speed Ground Transportation Journal*, 1978, 12(3), 1-27
178. Larminie, J. and Lowry, J., *Electric Vehicle Technology Explained*, John Wiley & Sons Ltd, 2003, United Kingdom
179. Oliveira, J., Lundin, J., and Bernhoff, H., Power Balance Control in an AC/DC/AC Converter for Regenerative Braking in a Two-Voltage-Level Flywheel-Based Driveline, *International Journal of Vehicular Technology*, 2011, Article ID 934023
180. Brockbank, C. and Greenwood, C., Fuel economy benefits of a flywheel and CVT based mechanical hybrid for city bus and commercial vehicle applications, *SAE Technical Paper 2009-01-2868*, 2009
181. Planetary gear set, http://www.dacoglu.com/desotocd/11A_ThreeSpeed%20With%20Overdrive/Plymouth%20Bulletin%20-%20Overdrive%20Transmission.htm, accessed 16.4.2013
182. De Guibert, A., Lithium batteries technologies for transportation applications, Keynote address, *International Scientific Conference on Hybrid and Electric Vehicles*, 2011, Rueil-Malmaison, France
183. Kok, D., Design optimisation of a flywheel hybrid vehicle, PhD Thesis, 1999, Technical University Eindhoven
184. Dietrich, P., Eberle, M., and Hörler, H., Results of the ETH – Hybrid III – Vehicle Project and Outlook, *SAE Technical Paper 1999-01-0920*, 1999

8 Appendix

Another way of achieving the required high ratio range needed for the FESS is the so called dual mode CVT or “i2” CVT control [183] where the variator ratio coverage is exploited twice. When the CVT reaches its maximum speed ratio, the input and output shafts are interchanged using clutches and the ratio coverage can be used again. In another variant of this kind of arrangement, instead of the variator, a PSCVT arrangement is utilized and its ratio coverage exploited twice in a similar manner. There are only few examples in literature of this kind of transmission being utilized in a FWHV (Kok [183], Dietrich et al. [184] and Locker and Miller [27]), though the fundamental analysis of this type of transmission has not been discussed. This section analyses this type of transmission using the methodology developed in Chapter 4.

8.1 Variator only Design

This section deals with the basic variator only dual mode design. Fig 89 shows the design which is a variator only design and involves 4 clutches. The power flows through the variator twice to cover the ratio range. In the Fig. 89 G_1 , G_2 and G_3 are fixed gear ratios, which are needed to attain speed synchronization for the mode change as well choose a desired starting minimum speed ratio (This is required to compare results of the two systems discussed in this section). A, B C and D are the four clutches to achieve the dual mode.

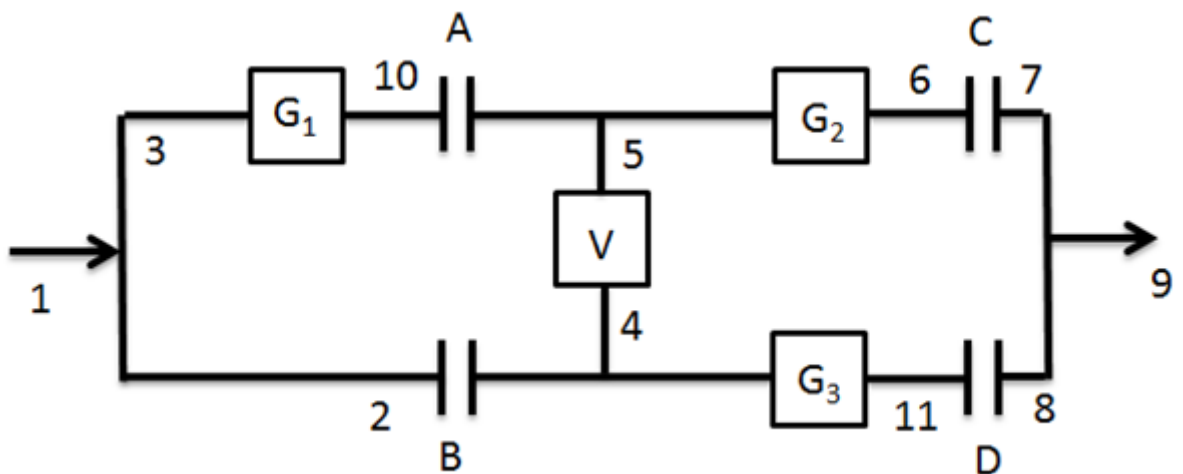


Figure 89 Variator only design

For the above design, equations 143-147 define the various speed ratios.

$$r = \frac{n_9}{n_1} \quad [143]$$

$$V = \frac{n_5}{n_4} \quad [144]$$

$$G_1 = \frac{n_{10}}{n_3} \quad [145]$$

$$G_2 = \frac{n_6}{n_5} \quad [146]$$

$$G_3 = \frac{n_{11}}{n_4} \quad [147]$$

During stage 1, clutches B and C are closed and A and D are open. Equation 148 gives the speed ratio of the stage 1.

$$r = VG_2 \quad [148]$$

To fix a desired start speed ratio of the system (r_{\min}), the equation 149 should be true.

$$G_2 = \frac{r_{\min}}{V_{\min}} \quad [149]$$

For stage 2, clutches A and D are closed and B and C are open. Equation 150 gives the speed ratio of the stage 2.

$$r = \frac{G_1 G_3}{V} \quad [150]$$

For synchronisation, the speed of the shaft 10 ($n_1 \times G_1$) should be equal to the shaft 5 ($n_1 \times V_{\max}$) and the speed of shaft 11 ($n_1 \times G_3$) and 8 (n_9) should be equal at the end of stage 1.

To achieve these conditions the following equations 151-152 should be true.

$$G_1 = V_{\max} \quad [151]$$

$$G_3 = V_{\max} \times G_2 = V_{\max} \times \frac{r_{\min}}{V_{\min}} \quad [152]$$

The ratio range (equation 153) would be equal to square of the variator ratio range since it is being traversed twice.

$$r_t = V_t^2 \quad [153]$$

As mentioned before, V_t of currently available variators is about 6, which would make r_t of this type of transmission 36. This is more than adequate for an FESS application and in fact might be well on the higher side. This high ratio coverage could be utilized in two ways. Either a smaller ratio range variator could be used which would be lower in cost or the operation of the FESS could be narrowed to high efficiency regions of the variator ratio. Though another important consideration is that the complete power flows through the variator at all times, which would cause a drop of efficiency, since it is the least efficient of all the elements and the variator would have to be sized larger to carry the entire power. A variation of this design is the dual mode PSCVT system where both the stages are PSCVT without power recirculation. One of the stage would be Output coupled (OC) and the other Input coupled (IC). This type of design would avoid passing the entire power through variator at all times, leading to a higher efficiency across the speed range. The following section explores this option. Losses are only considered in the gears which are in the path of the power flow from input to output.

8.2 Kinematics of dual mode PSCVT

The Fig. 90 shows this type of design. It involves 4 clutches to achieve the dual mode operation as in the previous case. Further it includes a PGS to constitute the PSCVT.

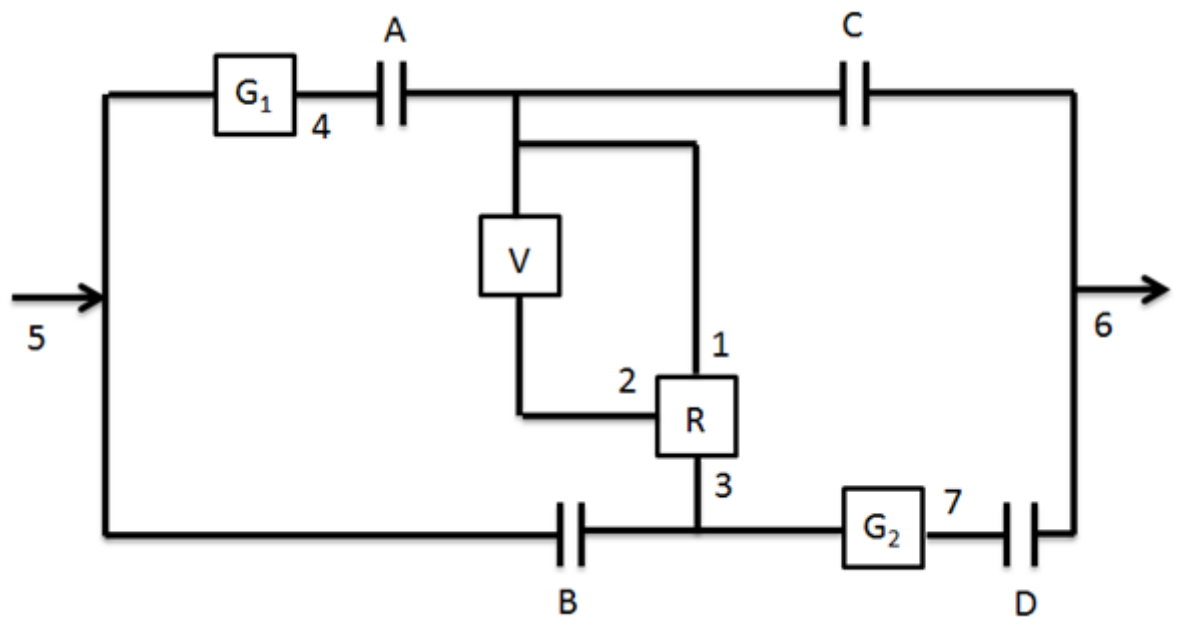


Figure 90 Dual mode PSCVT design

For the above design, equations 154-156 define the various speed ratios.

$$r = \frac{n_6}{n_5} \quad [154]$$

$$V = \frac{n_1}{n_2} \quad [155]$$

$$G_1 = \frac{n_4}{n_5} \quad [156]$$

$$G_2 = \frac{n_7}{n_3} \quad [157]$$

For stage 1, the system is taken as OC PSCVT, though it can easily be the other way around i.e. IC PSCVT by controlling the clutches differently. The clutches B and C are closed, and A and D are open. Equation (20) gives the relation between r , V and R . Fig. 6 (I) shows the power flow during stage 1 marked by dashed lines.

$$r = \frac{V}{VR - R + 1} \quad [158]$$

For stage 2, the system will behave as IC PSCVT. The clutches A and D are closed and B and C are open. Equation 159 gives the relation between r , V and R .

$$r = G_1 \times G_2 \times \left(R + \frac{(1-R)}{V} \right) \quad [159]$$

Again as in the previous case for synchronisation, the speeds of shafts 6 (n_6) and 4 ($n_5 \times G_1$) should be equal at the end of stage 1. Similarly those of shafts 7 ($n_5 \times G_2$) and 6 (n_6) should be equal at the end of stage 1. For this purpose the following equation 160 should be true.

$$G_1 = G_2 = \left(\frac{V_{\max}}{V_{\max} R - R + 1} \right) \quad [160]$$

The advantage of this system over the previous one is that the efficiency will be higher due to the power split and the variator can be sized smaller, however the ratio range will be reduced.

8.3 Efficiency and power flow

In this section the ratio of variator to input power and efficiency for the transmission will be shown separately for the individual stages described previously. For this purpose, applying the methodology described in Chapter 4, Table 24 shows the ratio of variator to input power and efficiency of the transmission.

Table 24 Power flow and Efficiency for the two designs

Parameter	Stage	Variator only	PSCVT
$\frac{P_v}{P_i}$	Stage 1	1	$(1-R)\eta_{1(3-2)} \frac{r}{V}$
	Stage 2	η_{G1}	$\eta_{G1} \left(\frac{\frac{1}{\eta_v V}}{\frac{1}{\eta_v V} + \frac{R\eta_{1(2-3)}}{(1-R)\eta_{2(1-3)}}} \right)$
η	Stage 1	$\eta_{G2}\eta_v$	$rR\eta_{2(3-1)} + \frac{r\eta_v(1-R)\eta_{1(3-2)}}{V}$
	Stage 2	$\eta_{G1}\eta_v\eta_{G3}$	$\frac{r}{\frac{G_1 G_2}{\eta_{G1}\eta_{G2}} \left(\frac{R}{\eta_{2(1-3)}} + \frac{(1-R)}{V\eta_v\eta_{1(2-3)}} \right)}$

8.4 Results and Comparison

To compare the systems numerically, certain values need to be defined as shown in equations 161-166. The equation 165 defines the ratio of ring gear diameter (D_r) to sun gear diameter (D_s) for the PGS and the equation 166 defines the numerical value of R.

$$r_{\min} := 0.47 \quad [161]$$

$$V_{\min} := 0.4 \quad [162]$$

$$V_{\max} := 2.4 \quad [163]$$

$$V_t := 6 \quad [164]$$

$$\frac{D_r}{D_s} := 3 \quad [165]$$

$$R = \frac{D_s}{D_s + D_r} := 0.25 \quad [166]$$

Using the above values and previously derived equations, the speed ratio for the two systems in computed. The Fig. 91 shows a comparison of the two systems using a standard variator

with V_t of 6. The dual stage can easily be seen for both the configurations. For the variator only design the speed ratio varies from 0.47 (r_{min}) to 16.94 (r_{max}) and for the PSCVT from 0.47 (r_{min}) to 6.71 (r_{max}). The speed ratio range for each stage of the variator only design is 6 and for the PSCVT is 3.78. Consequently r_t for the variator only transmission is 36 and for the PSCVT is 14.27. The suitability of the design will of course depend on the nature of the application.

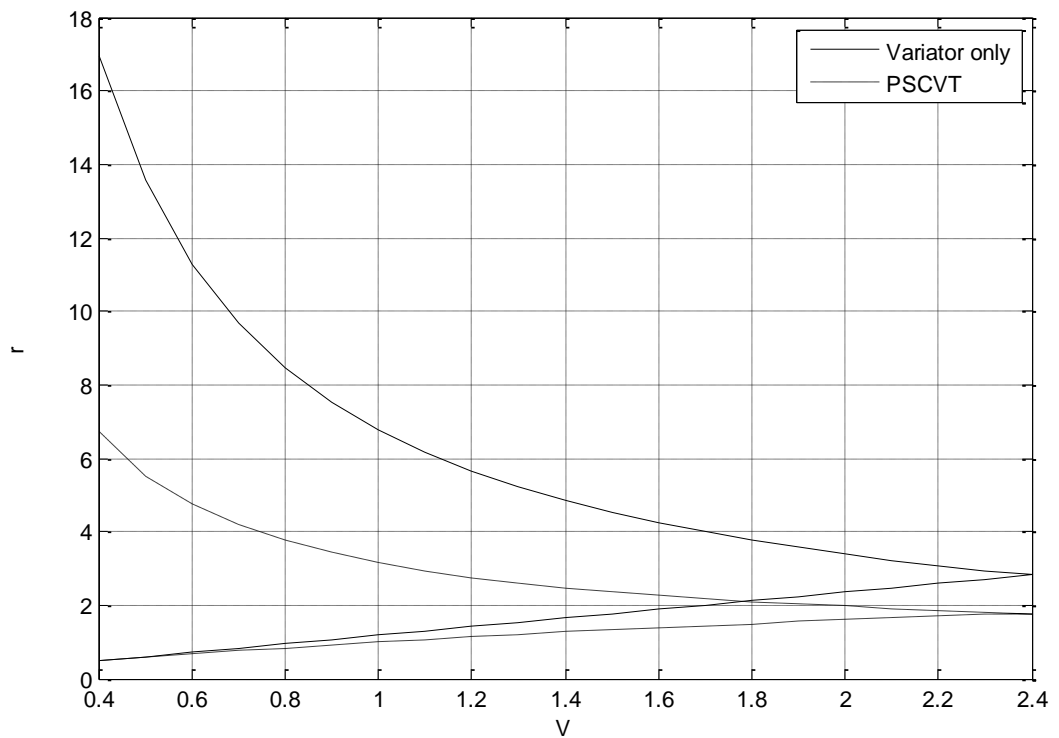


Figure 91 CVT ratio vs. Variator ratio for the two designs